z

Alma Mater Studiorum - Università di Bologna

DOTTORATO DI RICERCA IN

CHIMICA

Ciclo 33

Settore Concorsuale: 03/C1 - CHIMICA ORGANICA

Settore Scientifico Disciplinare: CHIM/06 - CHIMICA ORGANICA

NOVEL CATALYTIC SYSTEMS AND METHODOLOGIES FOR ORGANOCATALYSIS AND PHOTOCATALYSIS

Presentata da: Ada Martinelli

Coordinatore Dottorato

Domenica Tonelli

Supervisore

Claudio Trombini

Co-supervisore

Marco Lombardo
Marco Lucarini

Esame finale anno 2021

Summary

Abstract

In this thesis are reported the main research activities done during the period of my PhD studies, working under the supervision of Prof. Claudio Trombini and Prof. Marco Lombardo. My research has been focused on the study of organocatalysis and photocatalysis. In particular, in the development of new catalysts for organo- and photocatalytic reactions and new photoredox catalyzed transformations.

The thesis is divided into two main parts. In the first one organocatalysis is briefly introduced. Then, the synthesis and characterization of new enantiopure trityl pyrrolidines modified with an ionic tag are described. The synthesized catalysts present a stable scaffold, which could permit to recover it after the performance. All the catalysts are tested in the benchmark Michael addition reaction to prove their activity and stereoselectivity.

In the second part, photocatalysis is first introduced. Then, four different research projects are described.

At first, the construction of a hybrid metal-organo-photoredox catalyst based on the conjugation of an imidazolidinone organocatalyst and $Ir(ppy)_2(bipy)$ (ppy = 2-phenylpyridine, bipy = bipyridine) is described. The introduction of the desired organocatalyst into the bipyridine moiety is quite modular, allowing the preparation of different hybrid photocatalysts, and is realized through a simple click reaction. The hybrid photocatalysts obtained were employed in the benchmark photoredox alkylation of aldehydes. Remarkably, the conjugation of a first-generation MacMillan catalyst produces an active and stereoselective hybrid photoredox catalyst.

Then, the use of visible light and a photocatalytic system for the cyclization of iodoaryl vinyl derivatives to tetrahydroquinoline structures is described. The reaction proceeds under very mild conditions, tolerates different functional groups, and more importantly, the method allows the synthesis of N-free tetrahydroquinolines from N-unprotected starting materials. In addition, the reaction can also be performed using flow-chemistry. Finally, a mechanistic proposal based on some mechanistic studies is described.

Third, a new photoredox catalyzed transformation for the synthesis of 2,3-dihydrofurans is reported. The reaction proceeds under very mild conditions and a wide library of

diversely substituted 2,3-dihydrofurans is developed. Electrophilic radical addition on alkenes and subsequent intramolecular cyclization are exploited. Depending on the involved starting materials, different pathways have arisen. A mechanistic proposal based on reported literatures and experimental data is described.

At last, a new photoredox catalyzed transformation for the synthesis of 2-aminofurans is described. Electrophilic radical addition on allenamides and subsequential intramolecular cyclization are exploited. The reaction proceeds under very mild conditions and in 2-aminofurans are obtained in good to high yield. Also, it represents one of the few applications of allenamides in photoredox catalysis. A mechanistic proposal is described. Finally, preliminary investigations on the applicability of the developed transformation under flow chemistry conditions.

First part: Organocatalysis

Introduction

Nature is asymmetric. Living organisms are not perfectly symmetric, a clear example could be the human brain which his divided into the left and the right sides and each one performs different tasks. Nature is perfectly able to produce a chiral molecule in an enantiopure form. For example, all the natural amino acids in the human body are in the *S* configuration. This Nature ability is essential to life, and it is possible since enantiomers behave identically until they are placed in a chiral environment. Thus, hypothetically, every chiral molecule could be synthesized in an enantiopure form if placed in the perfect reaction environment with perfect tools. For a long time, asymmetric synthesis has been a challenge for the scientific community, a lot of efforts have been focused on it, and different techniques have been developed. All of them exploit the different interactions of the two enantiomers with a chiral compound.

The optical resolution of enantiomers, for example, is a common technique used for the separation of enantiomers from a racemic mixture. With this method, an enantiomer is crystallized from a racemic solution through the formation of a salt with an external chiral agent. Meanwhile, the other enantiomer remains in the solution. It is a very useful technique for the obtainment of both enantiomers, frequently required to test the biological activity. However, it has to be point out that the maximum yield achievable is 50% since both enantiomers are equally present in the original mixture.

Other methods include the use of chiral reactants or chiral auxiliaries in the synthesis. Numerous natural enantiomerically pure molecules can be exploited in different ways to induce chirality in the synthetic product. These techniques can be very effective, but on the other hand, they required a stoichiometric amount of an enantiopure compound: this could get very expensive on a large scale. In addition, the chiral agent is frequently available in only one of his enantiomeric form. Therefore, since the configuration of the product is strictly dependent on the reactant/auxiliar configuration, usually only one enantiomer of the product can be synthesized.

For all these reasons, asymmetric catalysis is considered the most useful tool in asymmetric synthesis nowadays.[1] Indeed, it has been selected by the International Union of Pure and Applied Chemistry (IUPAC) as one of the Top Ten Emerging Technologies in Chemistry. They defined it as one of the emerging advances in the

chemical sciences that hover between the embryonic "eureka" moment at the lab and industrial application.[2]

Asymmetric catalysis is a type of catalysis that involves a chiral enantiopure catalyst that permits to favor the formation of one enantiomer of the product. By definition, the catalyst is not modified at the end of the reaction, thus it can be used in a sub-stoichiometric quantity. Since the late 1960s, a lot of research was focused on asymmetric catalysis involving metal based enantiopure chiral catalyst. Only in the latest 1990s the idea of using chiral enantiopure organic molecules as catalysts spread among the scientific community, and the organocatalytic field rapidly became the most studied one in the development of new synthetic methodologies.[3]

The great spread of organocatalysis is due to the advantages that this methodology could bring to the synthetic field. At first, it permits to develop new synthetic methodologies through different ways of substrate activation. It could also be combined with orthogonal or complementary metal based catalysis. Second, organic molecules are usually insensible to the oxygen contained in the air mixture. This allows to operate with a simple reaction setup and in smooth conditions, avoiding the high cost derived from inert gas atmosphere equipment or dry solvents. Third, numerous chiral enantiopure organic molecules are present in nature and easily accessible. Therefore, the catalyst synthesis could be smooth and relatively cheap. At last, the use of a completely organic catalyst could permit to avoid metals in the synthetic process. Therefore, preventing the presence of metal traces in the process waste and in the final product, lowering the cost of the entire synthesis.

The major limit of organocatalysis is the relatively high turnover number of the catalyst. Usually, the required catalyst loading for organic catalyst is higher than that necessary with metal-based catalysts. On the other hand, the metal-based protocols are frequently more expensive than the organic ones. Thus, organocatalysts are generally cheaper than metal-based catalysts doing the same job, despite the lower TON of the former.

To overcome this disadvantage and enhance the advantages of organocatalysis, numerous solutions have been proposed until nowadays. For example, immobilization of the catalyst over diverse solid supports or recycling of the catalyst under homogeneous condition.[4–7]

Despite its numerous advantages, organocatalysis has been for a long time ignored before being accepted as a new conceptual field, in 2000. The pioneer article involving the use of an enantiopure organic molecule as a catalyst has been published in 1960 by Pracejus. He described a ketene stereoselective reduction catalyzed by the enantiopure O-benzoylquinine.[8] Successively, in 1971 Hajosh and co-workers described an intramolecular aldolic condensation involving enantiopure proline as an organocatalyst.[9] In these two articles has not been pointed out the possible development of a general methodology. Therefore, the organocatalytic field did not arise until the end of 1990s.

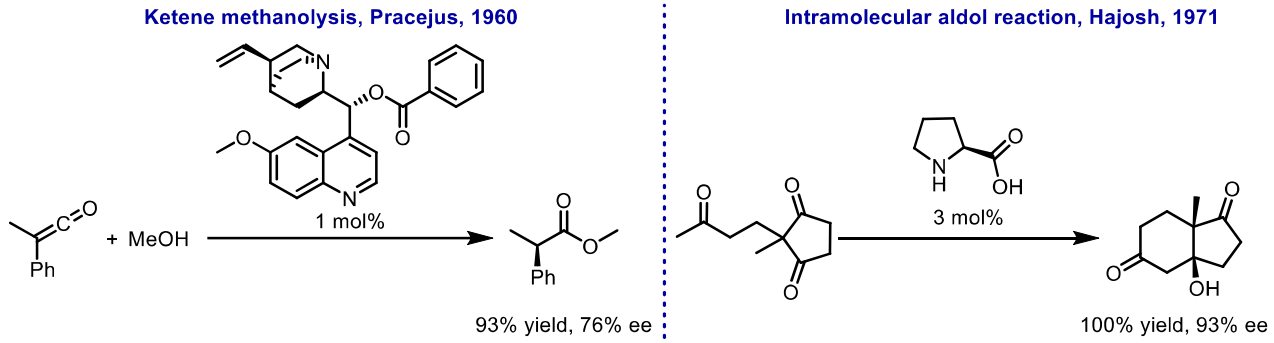

Scheme 1: Ketene methanolysis, Pracejus, 1960; Intramolecular aldol reaction, Hajosh, 1971

In the late 1990s, Corey's group and Jacobsen's group reported two examples of hydrogen bonding organocatalysis in asymmetric Strecker reaction, proving that organocatalysis could be a useful tool for stereoselective syntheses.[10,11]

Finally, the breakpoint in organocatalysis has been established by two articles published in 2000 by the research groups of List and MacMillan.[12,13] The first described a proline catalyzed intermolecular aldol reaction between acetone and benzaldehydes. He proved the generality of Hajosh reported reaction and described the first enamine-type organocatalytic protocol (Scheme 2, left).

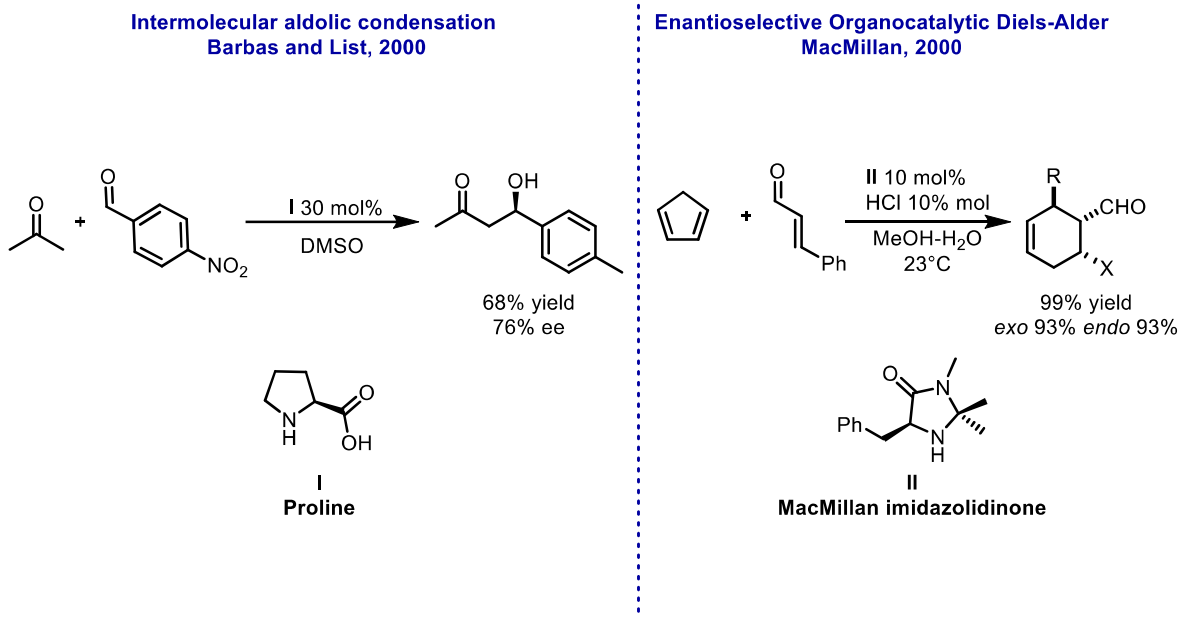

Scheme 2: Intermolecular aldolic condensation Barbas and List, 2000; Enantioselective Organocatalytic Diels-Alder MacMillan, 2000

MacMillan reported an enantioselective Diels-Alder cyclization reaction involving as a catalyst an enantiopure imidazolidine **II** designed in house (Scheme 2, right). In this work, the first iminium-type organocatalytic reaction is described. In addition, MacMillan and co-workers emphasized the high potential of including organocatalysis in the already know asymmetric synthesis field. Since that, a lot of scientists have focused their effort on it causing exponential development.[14–16]

A wide range of organocatalyzed asymmetric transformations has been developed, and numerous organocatalysts have been designed in the last 20 years. Among them, those proposed by Jorgensen group and Hayashi group in 2005 are nowadays considered the most efficient and work-horses in organocatalysis (Figure 1).[17,18] Both the research group designed prolinols derivative and proved their flexibility in numerous stereoselective syntheses.

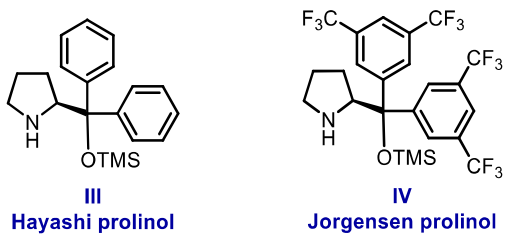

Figure 1: Hayashi and Jorgensen prolinols

Currently, various modes of activation are used in organocatalyzed reactions, depending on the catalyst and the reactants involved in the transformation.[1,16] Here, the different activation modes identified until nowadays, are described. The first two approaches herein described, are the secondary amine catalysis via enamine ion and iminium ion. Two activation modes involving amine catalysis and a covalent bonding interaction between the organocatalyst and the substrate. Other activation modes do not involve covalent bonding interaction. For these last, the interactions between catalyst and substrate are based on non-covalent bond interaction.

Enamine mode covalent organocatalysis

Numerous enamine-type organocatalytic reactions have been developed since 2000, and these processes are now considered the most useful procedures for the α-functionalization of carbonyl compounds.[19] Enamine catalysis is a catalysis by primary and secondary amines of the electrophilic substitution reactions in the α-position of carbonyl compound and related compounds via enamine intermediates.

The catalytic mechanism is based on the reversible condensation of amine **V** on aldehydes **VI** forming imine cationic intermediate **VIII** (Scheme 3, left). Subsequently, the α-carbon is deprotonated, and enamine **IX** is formed. Only one of the two carbon-carbon double bond conformation is favored, because of the catalyst steric hindrance (Scheme 3, right). At this point, the sp^2 α carbon is inclined to an electrophilic attack by an electrophile **E** present in the near environment, and cationic imine **X** intermediate is formed. Depending on the catalyst involved, one enamine face is more favored to be attacked than the other (Scheme 3, right). Ultimately, the catalyst is restored through the cationic imine intermediate hydrolysis and product **XI** is generated. From an electronic point of view, the enamine-type catalysis exploits the HOMO-raising activation of carbonyls and adjacent α-carbon. The newly formed enamine has sufficient p-electron density to react in nucleophilic addition with numerous different electrophiles.

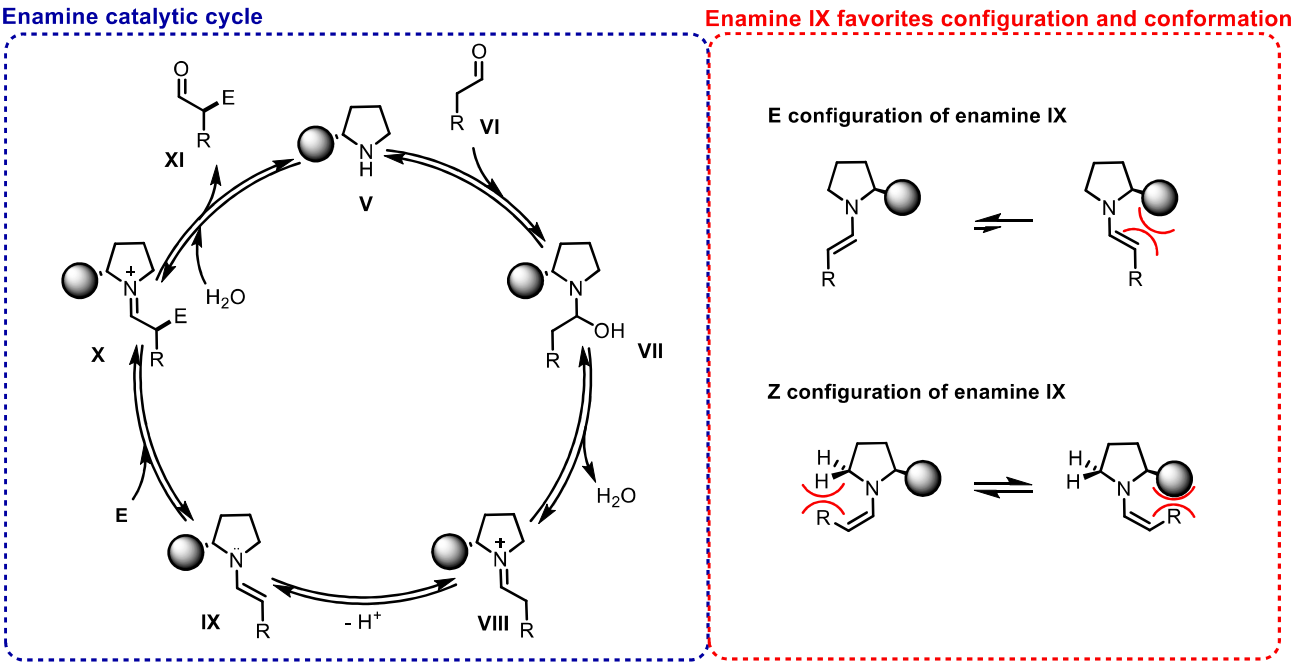

Scheme 3: Enamine organocatalysis catalytic cycle

The stereoselectivity of the process depends on the type of catalyst and its absolute configuration. In 2000, List described the stereoselectivity of a proline catalyzed reaction.[12] In this case, the enamine is formed between acetone and the catalyst with the double bond on the opposite side of the proline carboxylic group. (Scheme 4, right). In the meantime, an H-bond is formed between the carbonyl oxygen of the aldehyde and the hydroxyl group of the catalyst, activating the electrophile for the attack on the double bond. The *Re*-facial attack is, therefore, more favored than the *Si*-face attack. Thus, the synthesis is stereoselective versus the respective enantiomer. In the reaction involving prolinol derived catalysts, like the one designed by Jorgensen in 2005, the stereoselectivity operates with a different approach (Scheme 4,left).[20] As in the previous type, the enamine double bond is formed on the opposite side of the bulky group, but then the electrophilic attack occurs on the *Si*-face. This time, the *Re*-face is completely hindered, and no H-bond are formed between the enamine bulky group and the electrophile. For these reasons, the attack on the *Si*-face is favored, hence it is also the derived enantiomer.

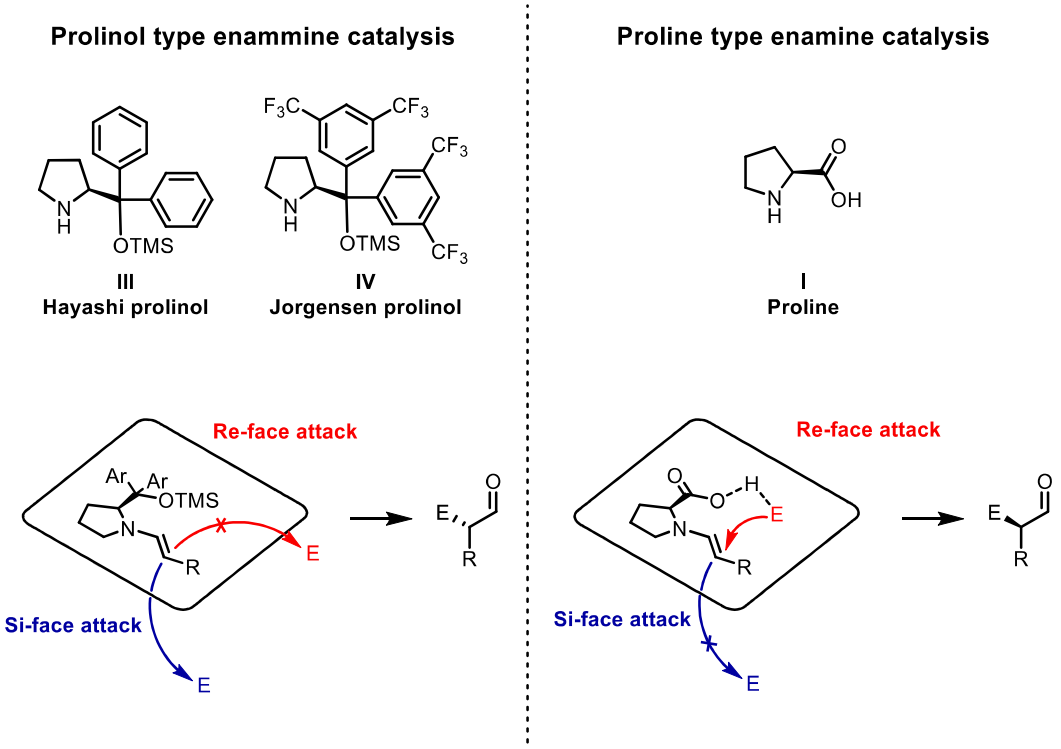

Scheme 4: Enamine organocatalysis stereoselection

Enamine type catalysis has been applied in numerous different well-known reactions. For example, aldol condensation and Mannich reaction, but also in the development of new procedures for the α-functionalization of aldehydes with a wide range of electrophiles.[19]

Iminium mode covalent organocatalysis

The second covalent bond mode of activation is the catalysis via iminium ion. Iminium catalysis is based on the condensation of a chiral secondary amine with an enal to form an iminium ion (Scheme 5).[21] The LUMO orbital of the iminium species is lowered in energy. It can now interact with suitable coupling partners either through pericyclic reactions or by conjugate addition. In 2000, MacMillan and co-workers reported the first enantioselective iminium type organocatalyzed synthesis. They developed an enantioselective organocatalyzed Diels Alder reaction.[13] The involved catalyst was imidazolidinone **II** designed in MacMillan laboratory. The catalytic mechanism is based on the reversible formation of iminium ion **XIV** formation. At first, the iminium ion **XIV** is formed between an enal **XII** and the aminic organocatalyst **V**. The ß-carbon of **XIV** is now electrophile, therefore inclined to a nucleophilic attack. Subsequently to the nucleophilic addition, enaminic intermediate **XV** is formed in enantioenriched

configuration on the carbonyl ß-carbon. Finally, intermediate **XVI** is hydrolyzed by a water molecule, forming product **XVII**, and regenerating the initial aminic catalyst **V**. From an electronic point of view, the iminium type catalysis is opposed to the enamine type, indeed the activation mode is based on lowering the LUMO energy.

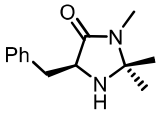

II

MacMillan imidazolidinone organocatalyst

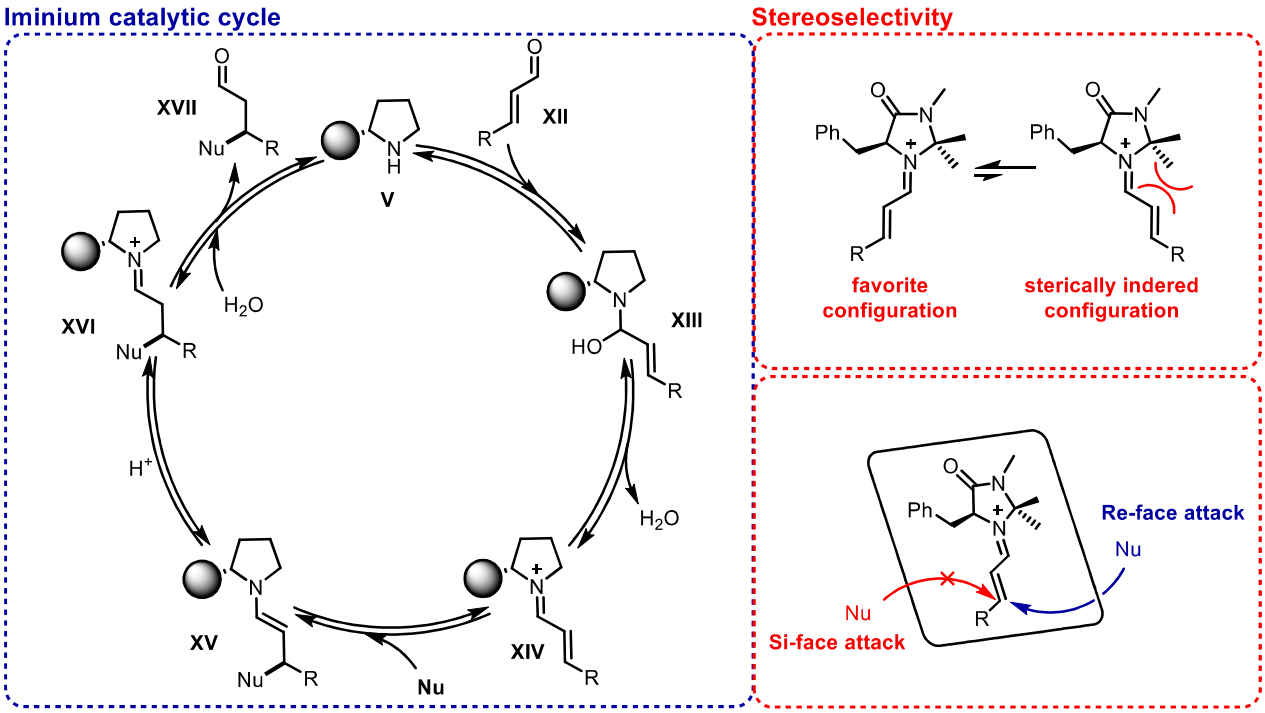

Scheme 5: Iminium organocatalysis

As in the enamine type catalysis, the diastereoselectivity of the iminium methodology is derived from the preferred form of the iminium ion **XIV** with the double bond opposed to the catalyst bulky group, to minimize the steric effect (Scheme 5, left). Meanwhile, the enantioselectivity depends on the prochiral face attacked by the nucleophile, which as mentioned before is the one not shielded by the catalyst bulkier group. In the example, MacMillan imidazolidinone is used as a catalyst. Thanks to the presence of two methyl substituents on the imidazolidinone ring, the iminium ion is formed selectively with *E*-geometry. Moreover, the *Si*-face is completely shielded by the benzyl group. Thus, the nucleophilic attack on the Re-face and the enantioselective formation of the corresponding enantiomer are promoted (Scheme 5, left).

In the last 20 years, the iminium-mode organocatalysis has been widely explored. Numerous enantioselective transformations such as cycloaddition, Friedel Crafts alkylation, and Michael addition to α,ß-unsaturated aldehydes or ketones, have been developed.[21] In addition, several organocatalysts have been designed to achieve new transformation or to improve the already known ones, both via enamine and iminium ion.

Phase transfer organocatalysis

The first no covalent activation mode described is the phase transfer catalysis (PTC).[22] PTC is based on the use of a biphasic reaction system where an ionic catalyst Q^+X^-, generally a quaternary ammonium or phosphonium salt, acts as a shuttle of an anionic reagent from the aqueous phase to the organic apolar phase (aliphatic or aromatic hydrocarbon). (Scheme 6). PTC is usually based on three fundamental steps.

i) the anionic reactant Nu^- is transported from the aqueous to the organic one as the Nu^-Q^+ ion pair.

ii) The reaction occurs in the organic phase where the Nu^- anion displays its highest nucleophilicity being a desolvated species. The SN2 reaction is ten orders of magnitude faster than in polar protic solvents. The reaction can occur both in the organic phase or at the interface between the two different phases

iii) Eventually, the catalyst goes back to the aqueous phase and a new catalytic cycle starts. A lot of factors influence the reaction performance, the catalyst steric hindrance, hydrophilicity, and counter anion are fundamental.[23]

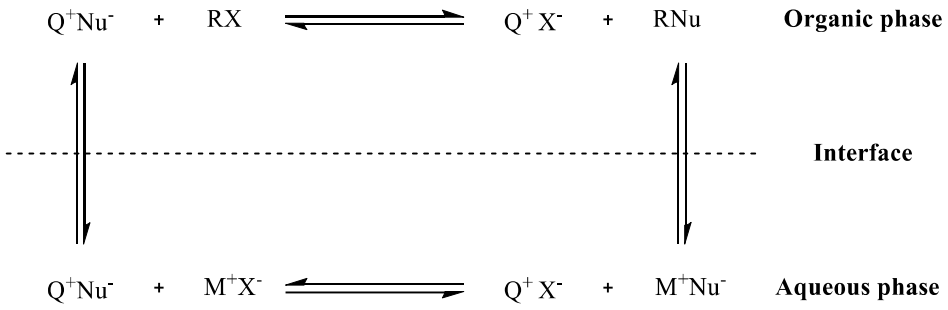

Scheme 6: Phase transfer organocatalysis

The most common catalysts involved in the asymmetric version of PTC are the quaternary ammonium salts derived from cinchona alkaloid **XVIII**[24,25] and the

binaphthyl-modified quaternary phosphonium salts **XIX** proposed by Maruoka and co-workers (Figure 2).[26]

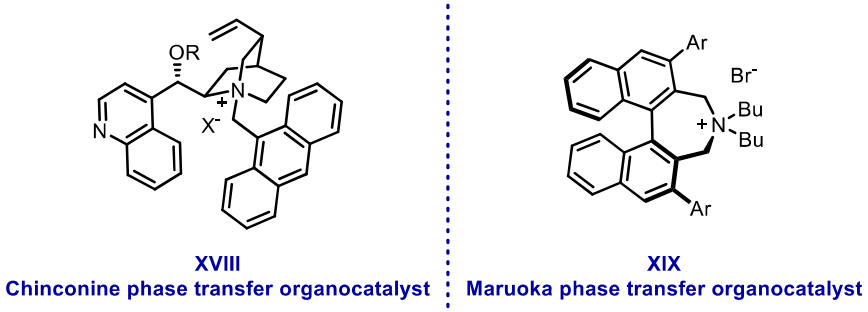

Figure 2: Chinconine phase transfer organocatalyst; Maruoka phase transfer organocatalyst

Chinchona derived organocatalysts are not expensive and available in both pseudo-enantiomeric forms (cinchonine vs. cinchonidine, and quinidine vs. quinine). Phase transfer catalysis main advantage is based on mild conditions and simple experimental protocols required.[27]

Hydrogen bond donor organocatalysis

A second version of non-covalent organocatalysis relies on the substrate activation through the formation of intermolecular hydrogen bonds with the catalyst.[28] This complexation is similar to the Lewis acid activation mode, but instead metal salts, low molecular weight enantiopure H-donors are used as catalysts. The stereocontrol of the process is controlled by the organocatalyst chirality, since once formed the H-bond complex between the chiral catalyst and the starting material, the nucleophilic attack is preferentially occurring towards a defined enantio-face or diastereoface.

The first examples of hydrogen bond asymmetric catalysis were reported by both Corey[10] and Jacobsen[11] respectively in 1999 and 1998. Later, in 2002, Jacobsen showed how thioureas could be used as organocatalysts for different synthetic purposes, defining the hydrogen bond donor catalysis as a new organocatalytic activation mode. (Figure 3).[29] Numerous H-bond donor organocatalysts have been devised to date, with different structures and acidities.[28] However, they all share a fundamental design scaffold: an H-bond donor site flanked by other moieties for secondary interactions with substrates (for example a basic functionality, acidic functionality, or hydrogen bond acceptor). In addition to the already mentioned Jacobsen thiourea **XX**, some of the most common typologies of catalyst for the H-bond activation mode are the squaramide based organocatalysts **XXIII** (Figure3).[30] These are similar to the thiourea ones for both

structure moieties and mode of action. The squaramide site presents two NH-bond donor sites, as thioureas do. However, they differ in terms of spacing between the two N-H moieties and the acidity of them. Other important types of catalysts for this catalytic activation mode, are for example chiral diols derivatives **XXI**[31,32] or the phosphoric acid derivatives **XXII**[33] (Figure 3).

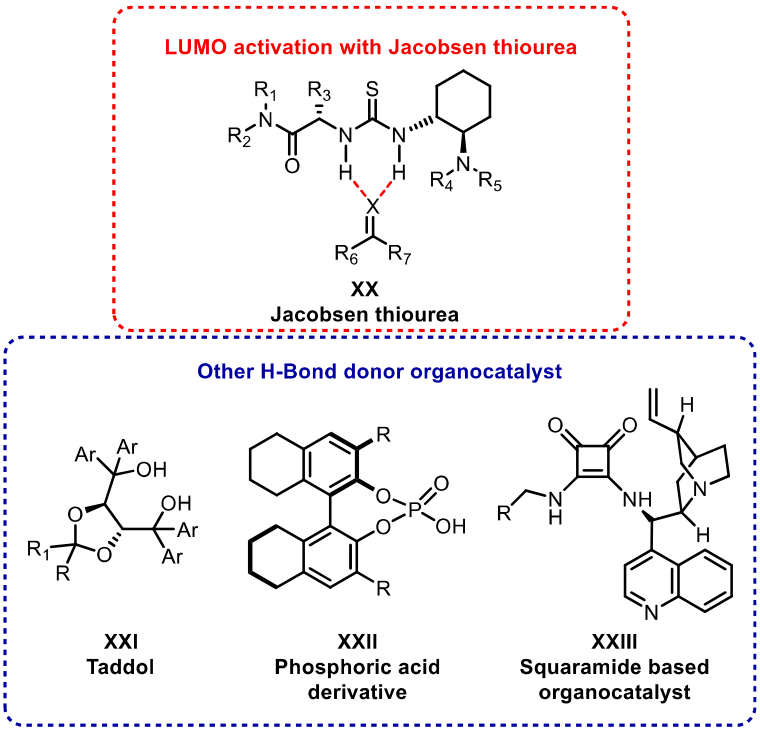

Figure 3: Hydrogen bond donor organocatalysis

SOMO catalysis

The last developed activation was again introduced by MacMillan in 2006.[34] It relies on the one electron oxidation of an electron rich enamine **IX**, and the subsequent generation of reactive radical **XXIV** with three π-electrons and a single occupied molecular orbital (SOMO) (Scheme 7).

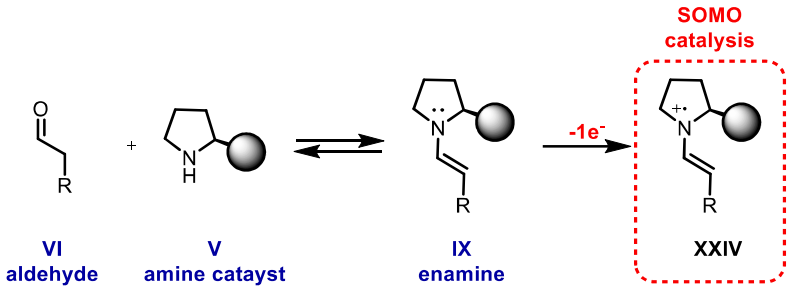

Scheme 7: SOMO organocatalysis via single electron oxidation of a transiently formed enamine

The electrophilicity of the SOMO orbital of the newly formed **XXIV**, allows to perform new stereoselective transformations not accessible with the previously reported activation modes. Initially, inorganic chemicals were involved as oxidant agents. In 2008 MacMillan proved that enamine oxidation can be achieved via light irradiation in the presence of a photosensitizer. Thereby, opening the productive research field of photoredox catalysis.[35] Thus, the α-alkylation of carbonyl compounds has been developed in the last years and a completely new catalytic field started to be investigated.[34,36–39] This last mode of activation will be further described in the second part of this thesis.

Catalyst recycle and sustainable processes

Organocatalysis has several advantages compared to metal catalysis. First of all, metals are not used, avoiding the problem of metal traces in the wastes, metal contamination of the product. A severe problem when pharmaceutically active products are the target and the use of hazardous reactants. In addition, the general robustness of organocatalyzed transformations toward the presence of air and water allows to perform reactions using simple glassware and practical conditions, with no need for anhydrous solvents or inert atmosphere. At last, neither heating nor cooling is generally required, thus reducing the process cost. Nevertheless, during the last twenty years, many efforts have been done to render organocatalysis even more sustainable,[40] for example focusing on catalyst recycling. It is noteworthy that most of the commonly used organocatalysts, the Hayashi prolinol[17], the cinchona alkaloids[24], and the L-proline[12] are relatively cheap. However, they are often used in relatively high catalytic loading, and generally are not recovered once the reaction has completed, raising the amount of waste derived from the transformations. Therefore, efficient and smoothly catalyst recycling would improve the process' sustainability. The various solutions reported until now can be divided into two main categories, reactions under homogeneous and heterogeneous conditions. In the case of the homogeneous processes, reactants and catalyst meet in the same phase. On the contrary, in the heterogeneous approach, reactants and catalyst reside in a different phase, for example with catalysts anchored on solid supports. In this last case, the catalyst is usually less active or stereoselective since the active catalytic site is less accessible compared to the homogeneous conditions. However heterogeneous conditions favor the separation of the catalyst from the reactants and

products, therefore favoring the recycling.[7,41–44] Diverse functionalized catalyst for homogeneous organocatalysis have been developed in the last decade.

A recent example of supported homogeneous covalent organocatalysis has been published by our research group.[45] Inspired by a recently reported trityl pyrrolidine, designed by Maruoka research group,[46,47] a new recyclable organocatalyst has been developed. The synthesized catalyst **XXV** was composed by a derivative of Maruoka trityl pyrrolidine connected to [60]fullerene (C_{60}) through a flexible linker (Figure 4).

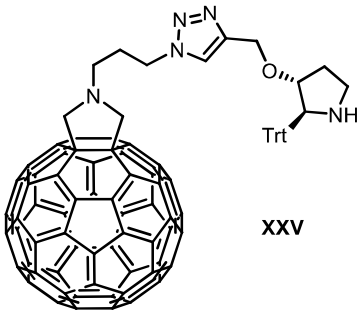

XXV

Figure 4: [60]fullerene organocatalyst hybrids

Some examples of [60]fullerene organocatalyst hybrids were previously reported.[48–50] Besides acting as a platform covalently binding a catalytically active species, fullerene, as well as carbon-nanotubes (CNTs) and graphene, exert their effects as catalysts.[51–53] In addition to the catalyst recycling, we were interested in investigating the possible participation of intrinsic redox properties of C_{60} as well as the effect of π- stacking interaction between C_{60} and conjugate planar substrates. The aim was to develop a supported recyclable organocatalyst anchored to a moiety that could improve the catalytic activity, and not affect it. Catalyst **XXV** revealed itself robust catalyst storable intact for months under an inert atmosphere. As benchmark reaction for catalysis investigations, Michael addition reaction of dimethyl malonate to cinnamaldehyde was selected.[18] The chosen transformation is an iminium type organocatalytic reaction. It is noteworthy that the few investigation involving trityl pyrrolidine in organocatalysis have been essentially limited to enamine type chemistry.[46,47,54]

After an optimization of the reaction conditions, the [60]fullerene hybrid **XXV** proved high activity and stereoselectivity in the involved transformation. Permitting to apply the developed protocol to various cinnamaldehydes and malonates.

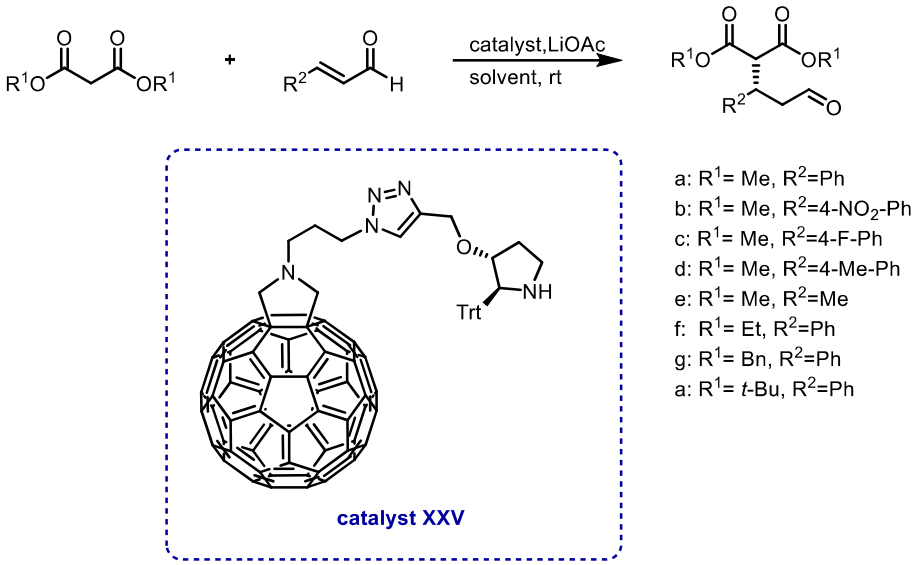

Scheme 8: Michael addition reaction with catalyst **XXV**

Successively, catalyst **XXV** recycling has been analyzed. Thanks to the insolubility of the catalyst in methyl *ter*-butyl ether, this solvent added to the reaction mixture after completion of the reaction, allowed to extract selectively the product and residual starting material from the reaction mixture. The residual solid catalyst could be dried under vacuum and reused in a successive organocatalyzed reaction. Conversion slightly decreased after the second cycle, probably due to a limited catalyst leaching during the extraction phase. Noteworthy, the enantioselectivity was preserved virtually unchanged over the six runs. The reported example is one of the numerous attempts to render well known organocatalytic transformation more sustainable.

In addition to catalyst recycling, another way to improve sustainability involves the exploitation of economic catalysts using green solvents and avoiding additives and co-catalysts. Moreover, the necessary reaction workup has to be considered. The development of a simple and efficient purification protocol, indeed, avoids the use of a large amount of organic solvents with an economic benefit.

An example of a more sustainable process for the proline-catalysed asymmetric aldol reaction was recently reported by our research group.[55] L-proline is stable, inexpensive, non-toxic, and easily available. Given its characteristic, we thought to improve its performance by exploring new experimental conditions in the well-known aldol reaction. Despite the large number of publications concerning this organocatalyzed reaction, the use of unmodified proline (without additives) forced to choose polar aprotic solvents to

obtain acceptable yields and selectivities. Polar aprotic solvents are characterized by several undesirable features (toxicity, high production cost, high environmental impact, high boiling points, and difficult product recovery).[56]

The use of unmodified proline can be also combined with additives[57], such as water[57,58], acids[57,59], diols[60,61], amine[57], or thioureas[62–64]. In these cases, the additive can tune the solubility, the reactivity, and/or the stereoselectivity of native proline, making the asymmetric aldol process more efficient. Nevertheless, the achieved performance is not optimal yet, some drawbacks are still present, such as high proline loadings and long reaction times. With the reported protocol, the use of polar aprotic solvents and additives were avoided, to develop an efficient and sustainable organocatalyzed aldol condensation protocol, which could be interesting from a scale-up and industrial point of view. In particular, the goals were the following: (1) a reduction of the costs associated to solvents and reagents, purification and waste disposal; and (2) an improved reactivity Despite a plethora of studies focused on the use and the role of water (as solvent, co-solvent, or additive), very few authors extended their investigations to alcohols, discouraged by the generally observed poor diastereo- and enantioselectivity. Only when proline was used in combination with metal salts as additives, the use of methanol as solvent or co-solvent afforded acceptable results. In the developed protocol, the impact of methanol (MeOH) in the L-proline catalyzed aldol reaction was deeply investigated (Scheme 9).

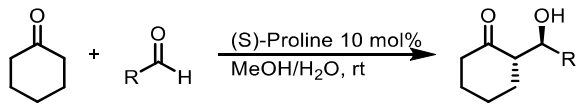

Scheme 9: L-proline catalyzed aldol reaction in methanol and water mixture

During the protocol optimization, water proved to have a crucial role in the enantioselectivity of the process but at the expense of reactivity, very poor, while ethanol ensured high reaction rates but with poor stereocontrol. Combining the two solvents in a 2/1 V/V mixture we observed the same rates obtained in pure methanol and almost the same ee_s (enantiomeric excesses) and good dr_s (diastereomeric ratios) obtained in pure water. Nicely, doubling the methanol volume (4/1 V7V MeOH/Water), the conversions significantly improved with all the tested aldehydes, while maintaining an excellent to a remarkable level of enantiocontrol.

The developed protocol for the L-proline catalyzed aldol reaction proved to produce high conversion and excellent *ee* values even diminishing the acetone quantity to 2 equivalents. A large excess of ketone (5 equivalents) only enhanced the initial reaction rate, but it was not necessary for the achievement of an excellent final performance. The robustness of the procedure on a 100 mmol scale was demonstrated too. Finally, work-up was investigated. Among the tested work-up approaches, one method reached 86% of proline recovery using an acceptable volume of diethyl ether (Et_2O) to precipitate the catalyst.

Ionic tagged organocatalysts

At last, the use of ionic tagged organocatalyst is described. Among the diverse methodologies developed for recycling, liquid-liquid multiphase homogeneous catalysis has emerged in the last decade. The key strategy to this approach is the immobilization of the homogeneous catalyst onto a liquid phase in which the reaction takes place under homogeneous conditions. At the end of the reaction, the catalyst and the product are separated into two mutually immiscible phases in which they present high and complementary partition coefficients. Therefore, both the products and the catalyst could be separately recovered from the reaction mixture.[5] To develop an efficient organocatalyst recycle protocol, the catalyst structure and the solvents have to be carefully selected. The functionalization of catalysts with ionic tags has been explored in the last ten years exploiting liquid-liquid multiphase homogeneous conditions. Indeed, the presence of the ionic tag would provide a particular solubility profile to the catalyst, allowing the catalyst recovery by a careful choice of solvents. Because of their ionic character, ion-tagged catalysts are usually insoluble in non-polar, organic solvents, such as hexane or diethyl ether. On the other hand, they are usually soluble in polar, organic solvents, like acetonitrile, dimethylformamide, methanol, and halogenated solvents, such as chloroform or dichloromethane. The solubility in water can be tuned depending on the nature of the ionic tag. Numerous organocatalysts functionalized with an ionic tag have been developed in the last decade.[6,65–69] All the developed catalysts consist of three elementary elements: the tag, containing the solvent recognition moiety, the linker connecting the tag to the catalyst frame, and the catalyst active site. (Figure 5).

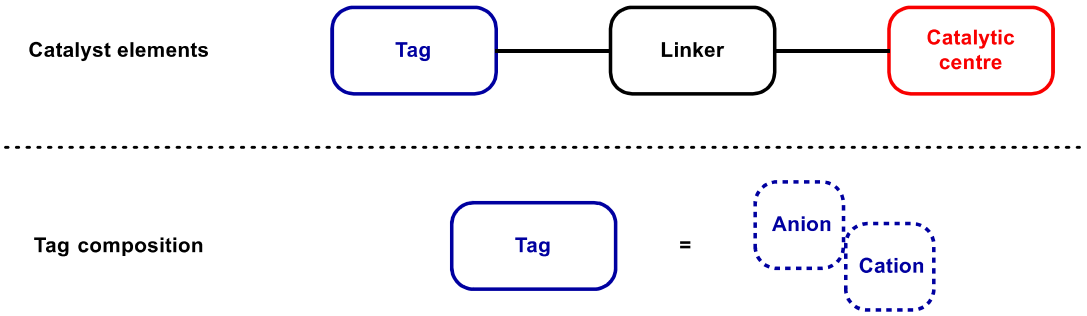

Figure 5: Ionic tagged catalysts components

The tag is composed of both a cation and an anion, which are usually chosen depending on the desired properties. For example, using counter ions like PF_6^- or NTf_2^- (bis(trifluoromethanesulfonyl)imide) permits to obtain a hydrophobic catalyst. Concerning the cationic element on the tag, usually ammonium, phosphonium, and nitrogen containing heterocycle salts are commonly involved, in particular, imidazolium and pyridinium ions. In addition to the catalyst recovery, the functionalization with an ionic tag can enhance the reactivity. With an accurate choice of the linker structure, it could stabilize the charges developed along the reaction coordinated, lowering the free-energy barrier by complementing charge separation in a dipolar transition state. As a consequence, better results could be obtained with lower catalytic loading and time, compared to an analogous catalyst without the ionic tag. Moreover, the presence of the ion pair also determines new steric interactions, that could affect the stereoselectivity of the asymmetric organocatalyzed transformation. This stabilization effect of the transition states has been defined by our research group as "electrosteric stabilization".[6] In addition, this electrosteric stabilization could affect the stereoselectivity of the process, too. Usually, parallel reaction pathways leading to stereoisomeric products are accessible. The electrosteric interactions can favor one path, influencing the final enantiomerically purity of the product. However, it is tough to anticipate the global impact on the catalytic process, especially if the free-energy differences involved are low. The designing of an ionic tag functionalized organocatalyst with a stable backbone, general catalytic activity and stereoselectivity and smoothly recoverable, is not effortless. But it would permit the development of numerous sustainable enantioselective organocatalyzed processes.

New enantiopure trityl pyrrolidine modified with an ionic tag

Aim of the project

During the last decades, the organocatalysis has been widely studied. Particularly, covalent organocatalysis has been deeply explored in order to develop efficient and stereocontrolled constructions of carbon-carbon and carbon-heteroatoms bonds.[19,21] Among the wide range of catalysts designed, the family of α,α-diarylprolinol silyl ethers[17,20] proved to be the most active and enantioselective one for most of these reactions. However, α,α-diarylprolinol silyl ethers are usually not recovered after the isolation of the target products because the silicon-oxygen bond is easily hydrolyzed. Therefore, the development of a stable, recoverable and stereoselective catalyst it is still an issue. In this project, new chiral trityl pyrrolidines functionalized with an ionic moiety have been synthesized (Figure 6). Inspired by Maruoka's recent works[46,47], and our previous studies[6,45] , trityl pyrrolidine was chosen as a catalyst. It presents a stable substituent on the pyrrolidine ring and is able to efficiently catalyze both enamine type and iminium type transformations. Imidazolium salt was chosen as cationic component of an anionic tag bis triflimide (NTf_2^-) as counter anion enhances the catalyst hydrophobicity. Exploiting the ionic tag and with a careful choice of the organic solvents, these catalysts could potentially be recycled and used in successive enantioselective syntheses. Finally, the ionic tag moiety could affect the reaction rate permitting to obtain more efficient process.[70]

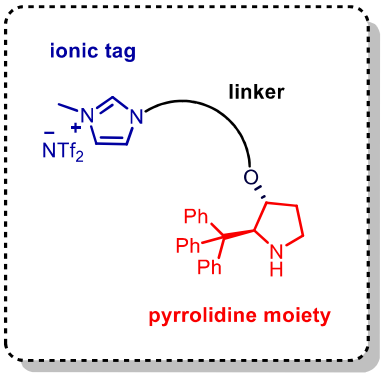

Figure 6: Ionic tag functionalized trityl pyrrolidine organocatalyst

The designed catalysts were tested in the organocatalyzed Michael addition of malonates to cinnamaldehydes,[17] a benchmark reaction selected for covalent bond

iminium type organocatalysis, and in the enantioselective α-benzoylation of aliphatic aldehydes,[46] our benchmark reaction for covalent bond enamine organocatalysis.

Discussion and results

Initially, the synthetic routes to catalyst **1a** and **1b** have been designed. Trityl pyrrolidine **2** was chosen as starting material. His preparation has been recently reported by our research group in the above mentioned design of a 2-trityl pyrrolidine anchored to fullerene. (Scheme 10).[45]

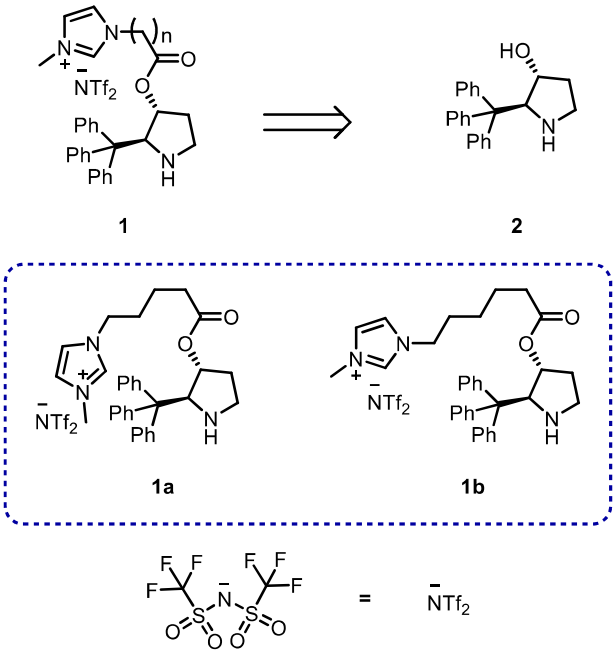

Scheme 10: Retrosynthesis of catalyst **1a** and **1b**

In this project, **2** has been first protected with benzyl chloroformate (Cbz) and triethylammine (TEA) to obtain the *N*-protected 2-trityl pyrrolidine **3** in a 90% yield.

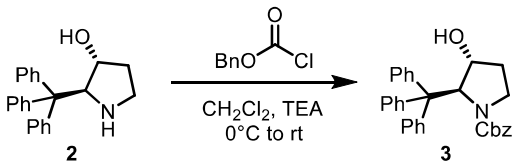

Scheme 11: Protection of trityl pyrrolidine **2** with benzyl chloroformiate

Successively, Steglich esterification reaction[71] has been performed on **3.** Stoichiometric amount of *N,N'*-dicicloesilcarbodiimmide (DCC) and catalytic amount of dimethylamino pyridine (DMAP) were used as reagents. (Scheme 12). ω-Bromo valeric acid and ω-bromo hexanoic acid were used to produce pyrrolidine **4a** and pyrrolidine **4a,**

respectively. Both the esters were smoothly obtained in high yield (83% yield for **4a** and 89% yield for **4b**).

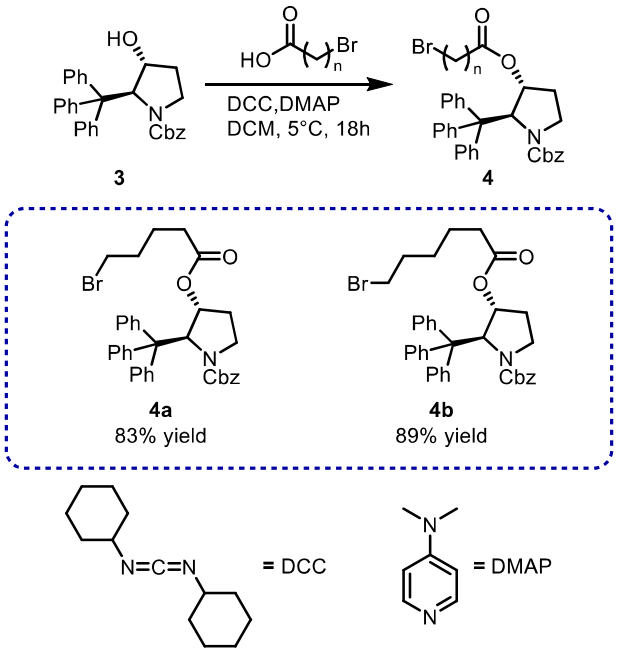

Scheme 12: Steglich esterification reaction

A nucleophilic substitution has then been performed on **4** to insert the ionic tag portion on the trityl pyrrolidine scaffold. (Scheme 13). The nucleophilic nitrogen on the imidazole ring attacks the electrophilic carbon (in α position respect the bromine), generating an imidazolium bromide tag. Thanks to the presence of the ionic tag, both product **5a** and **5b** were easily separated from the residual imidazole through washes with diethyl ether. No further purification was needed; therefore, they were directly used in the subsequent step.

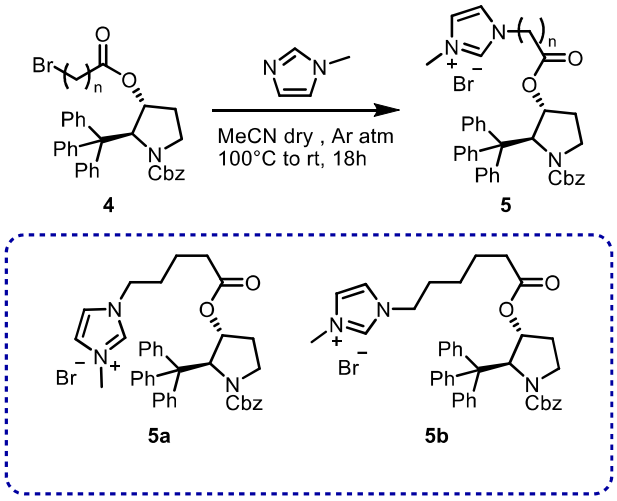

Scheme 13: Nucleophilic substitution for the synthesis of ionic tagged pyrrolidines **5a** and **5b**

Both pyrrolidines **5a,b** were subjected to a counterion exchange with bistriflimide (NTf_2^-), chosen for its stability and the enhanced solubility of the organocatalyst in apolar solvents. (Scheme 14). The ionic exchange proceeded efficiently. . According to the HSAB theory (hard and soft acids and bases) bistriflimide is a soft nucleophile due to the high charge delocalization, while the bromide ion is a hard nucleophile. Therefore, the softer imidazolium has a preference for the softer NTf_2^-, meanwhile the harder Li^+ prefers the harder Br^-. In addition, once formed, LiBr salt precipitates out from the reaction mixture. Consequently, the thermodynamic equilibrium is shifted towards product **6**. Even for this synthetic step, no further purification was needed. Both ionic tagged pyrrolidine **6a** and **6b** were obtained in good yields over two synthetic steps (59% yield for **6a** and 78% yield for **6b**).

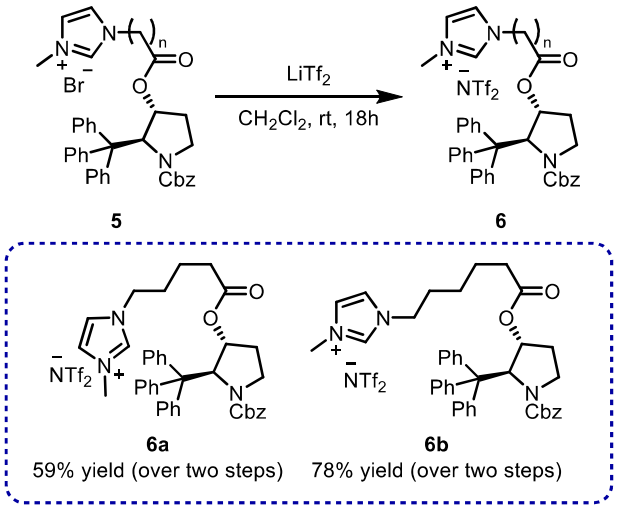

Scheme 14: Counterion exchange for the synthesis of **6a** and **6b**

The last synthetic step required the pyrrolidine nitrogen deprotection achieved using palladium adsorbed on carbon under hydrogen atmosphere (1 atm). (Scheme 15). The deprotection permit to obtain organocatalyst **1a** and **1b** with 90% yield and 83% yield, respectively.

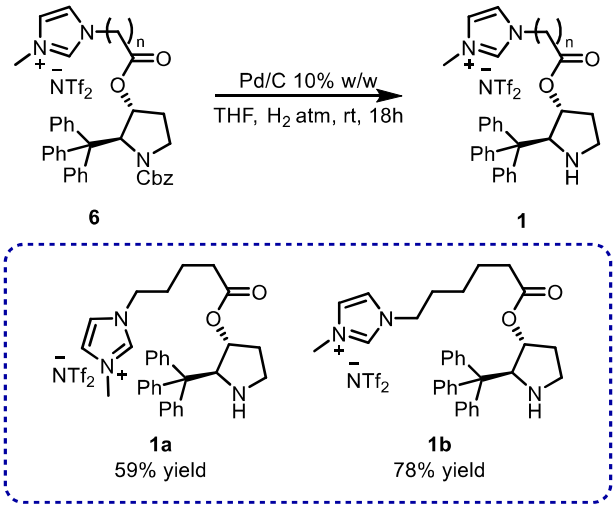

Scheme 15: Nitrogen deprotection for the obtainment of organocatalysts **1a** and **1b**

Catalytic tests were then conducted to investigate the activity and stereoselectivity of the new catalysts. The asymmetric Michael addition of malonate to cinnamaldehyde was chosen as benchmark reaction in covalent bond iminium ion organocatalytic reactions.[18]

In our previous project, the 2-trityl pyrrolidine scaffold displayed a high activity and stereoselectivity in the Michael addition, using a mixture of dichloromethane (DCM) and ethanol as solvents.[45] In addition, in 2010 Flescher and Pfaltz reported the enhancement in the reaction rate adding benzoic acid (BzOH).[72] Indeed, acid can accelerate the formation of the initial iminium ion intermediate as well as the conversion of the product enamine to the corresponding iminium salt. Based on these reasons, the first screening was conducted involving 15 mol% of BzOH and a 1:1 mixture of DCM and EtOH (Table 1). The Hayashi prolinol catalyst **III**[17] was involved in the screening too, for a comparison with our designed catalysts. Kinetic studies were developed as well with the intention of study the different reaction rates (Figure 7).

Table 1: Preliminary catalytic test

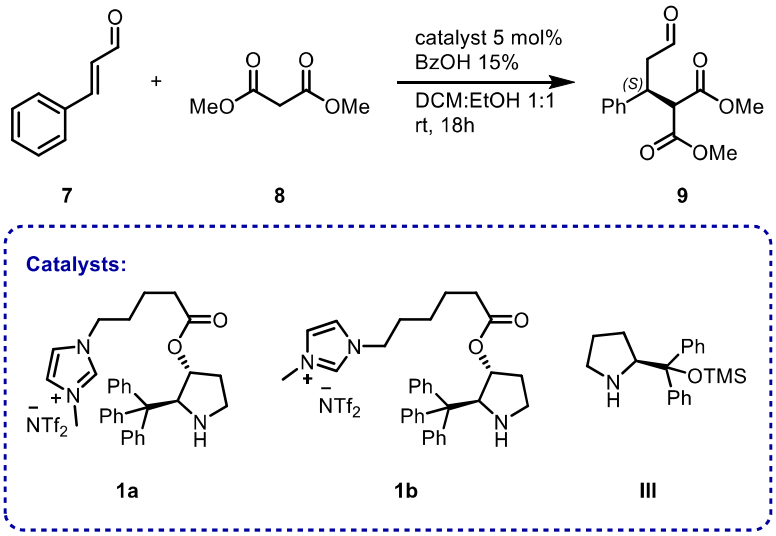

Entry[a]	Catalyst	Conversion[b]	*ee* %[c]
1	1a	75	95
2	1b	59	95
3	III	85	89

[a] Reaction conditions: cinnamaldehyde (0.1 mmol), dimethylmalonate (0.3 mmol) in 200 µl of DCM:EtOH mixture 1:1; [b] Calculated trough analysis on ^{1}H-NMR on the crude mixture, referring to aldehyde **7**; [c] calculated by means of chiral stationary phase HPLC after witty reaction derivatization.

Figure 7: Kinetics analysis on preliminary test[a]

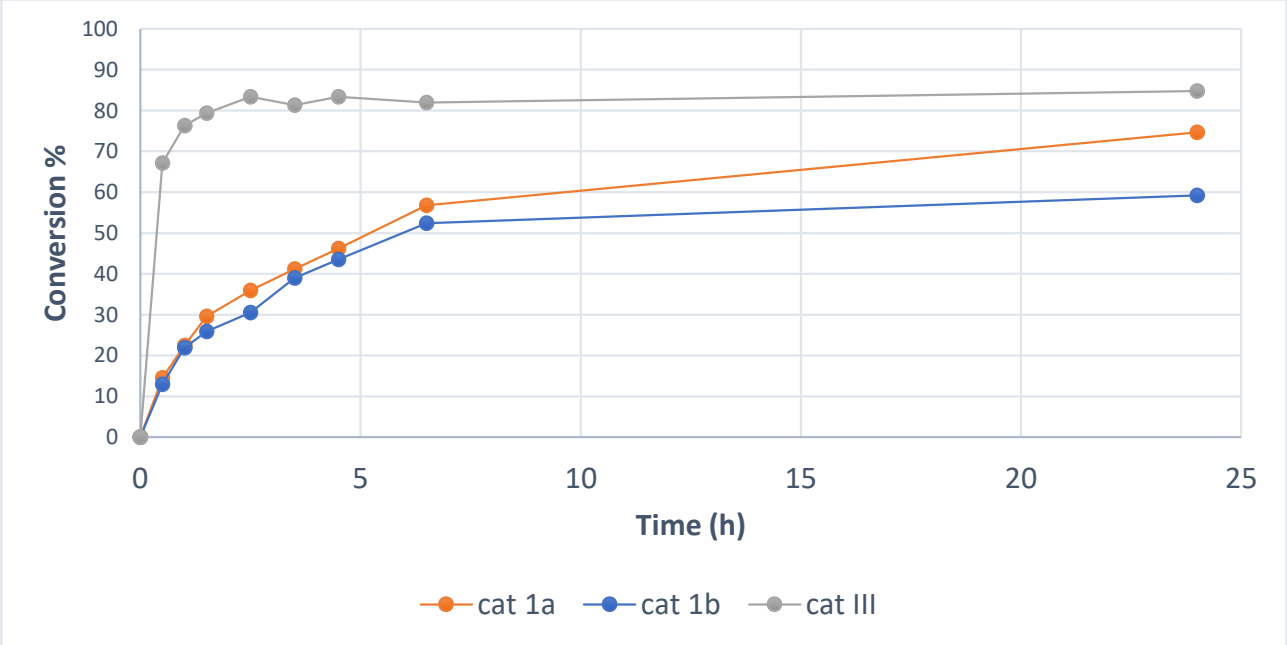

[a] Reaction conditions: cinnamaldehyde (0,1 mmol), dimethylmalonate (0,3 mmol), catalyst (0,05 mmol), BzOH (0,015 mmol) in 200 µl of DCM:EtOH mixture 1:1, stirred at room temperature for the indicated time.

It resulted clear the higher reaction rate obtained with the prolinol Hayashi catalyst under the chosen reaction conditions (85% conversion was reached in 6 hours reaction time, Entry 3, Table 1). Catalysts **1a** and **1b** proved slower activity, but at the same time major enantioselectivity since 95% enantiomeric excess (*ee*) was reached with both. Meanwhile, lower 89% *ee* was detected with Hayashi prolinol catalyst. Among the two ionic tagged trityl pyrrolidine, **1a** demonstrated higher reaction rate: 75% conversion was reached over 18 hours reaction time with **1a** (Entry 1, Table 1), meanwhile a lower 59% conversion with **1b** (Entry 2, Table 1). On the other hand, no differences were observed in the stereoselectivity of the transformation. **1a** was consequently chosen for further investigations.

Various solvent mixtures were tested in the Michael addition reaction with catalyst **1a** with the intention of improve the reaction performance (Table 2).

Table 2: Solvent optimization for the Michael addition of dimethylmalonate to cinnamaldehyde

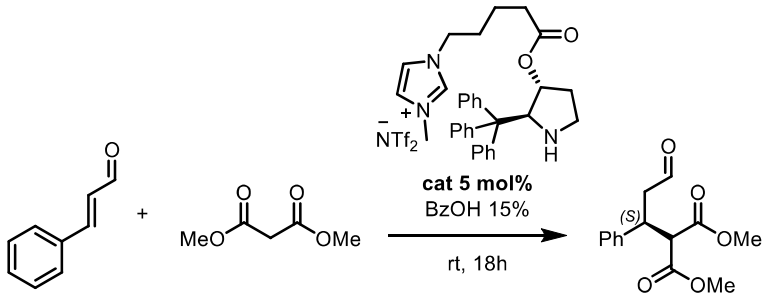

7 8 9

Entry[a]	Solvents mixture	H_2O	Conversion[b]	*ee* %[c]
1	1:1 DCM:EtOH	No	75	95
2	30:70 DCM:EtOH	No	95	94
3	EtOH	No	100	92
4	1:1 DCM:EtOH	2eq	87	95
5	30:70 DCM:EtOH	2eq	96	94
6	EtOH	2eq	100	93

[a] Reaction conditions: cinnamaldehyde (0.1 mmol), dimethylmalonate (0.3 mmol) in 200 µl of the correspondent solvent mixture; [b] calcolated trough analysis on ^{1}H-NMR on the crude mixture, referring to aldehyde **7**; [c] calculated by means of chiral stationary phase HPLC after witty reaction derivatization

Figure 8: Kinetics analysis on the solvent optimization

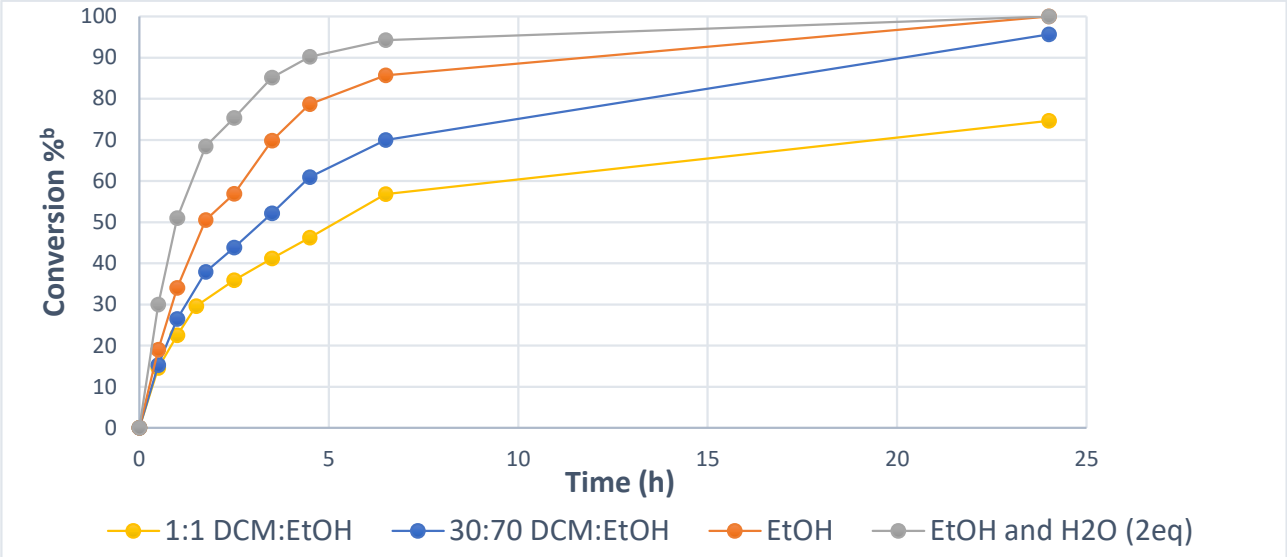

[a]Reaction conditions: cinnamaldehyde (0.1 mmol), dimethylmalonate (0.3 mmol), catalyst **1a** (0.05 mmol), BzOH (0.015 mmol) in 200 µl of solvent mixture, stirred at room temperature for the indicated time. [b] calcolated trough analysis on ^{1}H-NMR on the crude mixture, referring to aldehyde **7**.

It was apparent the favorable effect of protic solvents on the reaction rate. Raising the amount of ethanol compared to dichloromethane, led to a higher conversion. 95% Conversion was reached with a 3:7 DCM:EtOH mixture in 18 hours and 100% conversion utilizing only EtOH. (Entry 2 vs Entry 3). In contrast, the protic solvent seemed to slightly lower the stereoselectivity of the process. The enantiomeric excess on product **6** diminished from 95% (1:1 DCM:EtOH, Entry 1, Table 2) to 92% (EtOH, Entry 3, Table 2). In 2010 Flescher and Pfaltz, along with the positive effect of BzOH, demonstrated the positive influence of a little amount of water in Michael addition transformation (2 equivalent) utilizing prolinol type catalysts.[72] Due to this report, for each one of the tested solvent mixtures, the influence of water was analyzed. In general, water enhanced reaction kinetics since higher conversion were reached under all the tested conditions. It could seem that the higher is the amount of ethanol, the lower is the water effect. Indeed, no substantial differences were observed after 18 hours reaction time with 30:70 DCM:EtOH (Entry 2, Table 4) mixture as well as with 100% EtOH (Entry 3, Table 4). As far as concerning the enantiomeric excess, no water influence was detected in the product formation.

For this reasons, 30:70 DCM:EtOH was selected as solvent mixture for further analysis on the catalyst activity. It represented the better compromise between activity and stereoselectivity for the obtainment of product **6**. (Scheme 16).

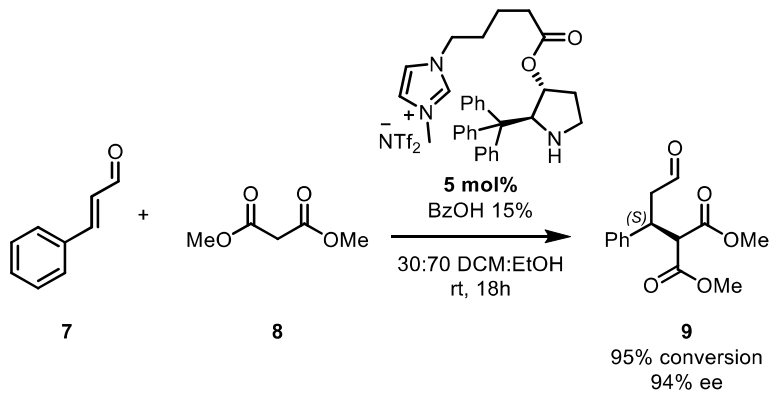

Scheme 16: Optimized conditions for the Michael addition of malonates to cinnamaldehydes catalyzed by ionic tag trityl pyrrolidine **1a**

The α-benzoylation of aliphatic aldehydes has then been investigated to ascertain the catalytic activity of **1a** and **1b** in an enamine type organocatalyzed reaction This specific reaction has been chosen since Maruoka demonstrated the high activity and enantioselectivity of his trityl pyrrolidine **XXVI** and **XXVII** in it.[46,47] With a comparative aim, α-benzoylation of aliphatic aldehydes was performed with catalyst **1a** and **1b** under the same reaction conditions optimized by Maruoka (Table 3).

Table 3: α-benzoylation of aliphatic aldehydes

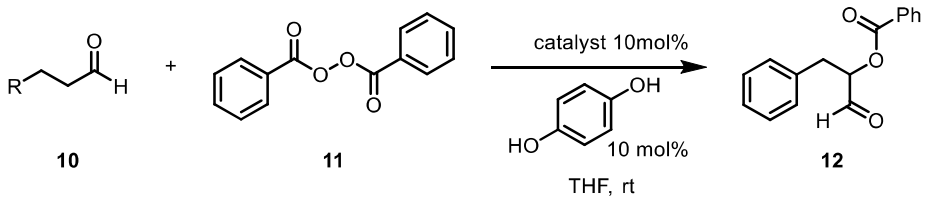

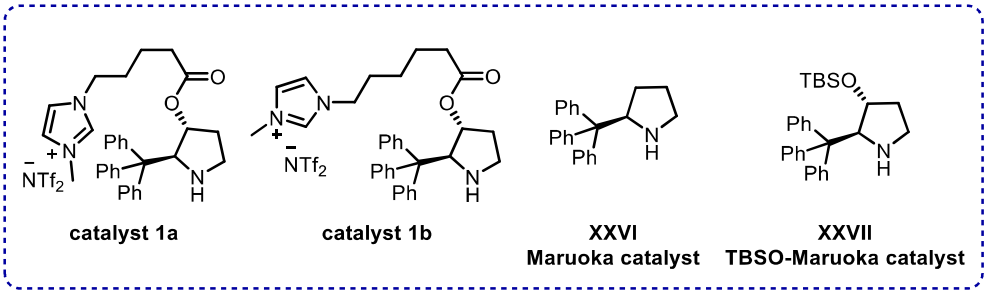

Entry[a]	Catalyst	Catalyst mol %	R	T (h)	Conversion %[b]	*ee* %[c]
1	**1a**	10	Ph	6	100	94
2	**1b**	10	Ph	6	80	93
3	**1a**	5	Ph	24	77	92
4	**1a**	10	$-CH_2CH_3$	2	>95	92
5	**XXVI**	10	Ph	2	72	93
6	**XXVII**	10	Ph	24	77	94

[a] Reaction conditions: 0,1 mmol aldehyde and 0,11 mmol of BPO in THF (0,500 μL); [b] Calculated through ^{1}H-NMR on the crude reaction mixture, referring to aldehyde **10**; [c] Calculated by means of chiral stationary phase HPLC after witty reaction derivatization

Once again, catalyst **1a** demonstrated to be more active compared to **1b**. (Entry 1 vs Entry 2, Table 3). Indeed, 100% conversion was reach with **1a** after 6 hours, meanwhile 80% conversion with **1b**. Again, no difference on the process stereoselectivity was outlined (94% ee with **1a** and 93% with **1b**). From the performed reaction, the similar reactivity of ionic tag trityl pyrrolidine **1a** and Maruoka's trityl pyrrolidines **XXVI** and **XXVII** rose clear.

In both the analyzed enamine and iminium type reactions, the ionic tag catalysts did not enhance the reactivity compared to the un-tagged reference organocatalysts.

A first preliminary recycle attempt has been performed, involving catalyst **1a** in the Michael addition reaction (Table 4). Thanks to the presence of the ionic tag, the functionalized pyrrolidine is insoluble in some solvents, as for example diethyl ether.[6,73] For this reason it could be recycle simply adding diethyl ether to the crude reaction

mixture, causing the precipitation of the catalyst itself meanwhile the other species remain solubilized. From the initial attempt, we could observe that the enantiomeric excess value did not decrease during the recycling cycles (94-95 *ee*), while the conversion decreased. Indeed, a 10% conversion loss was observed after each recycle.

Table 4: Preliminary recycle attempt with catalyst **1a**

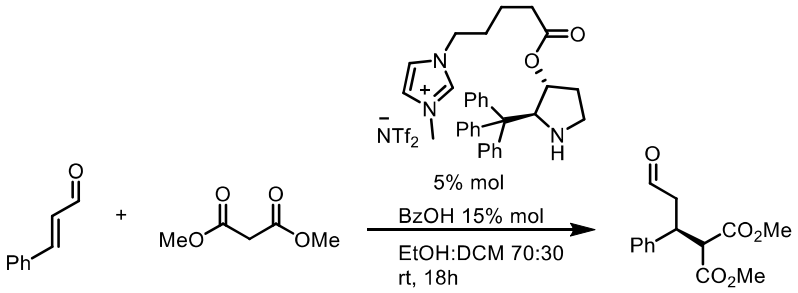

Entry[a]	Conversion%[b]	*ee* %[c]
1st cycle	90	94
2nd cycle	80	95
3rd cycle	70	95

[a] Reaction conditions: cinnamaldehyde (0.1 mmol), dimethylmalonate (0.3 mmol) in 200 µl of the correspondent solvent mixture; [b] calcolated trough analysis on ^{1}H-NMR on the crude mixture, referring to aldehyde **7**; [c] calculated by means of chiral stationary phase HPLC after witty reaction derivatization

This reduced reactivity could reflect a physical loss of the catalyst during the recycle. Another reason of the reduced activity could be due to the ester group on the catalyst **1a** an **1b.** Indeed, it could be hydrolyzed, cleaving the ionic tag functionality from the aminic one.[74] In the absence of the ionic tag, the catalyst loses his particular solubility profile, invalidating the recycling protocol.

With the intention to improve the stability of the catalyst and investigate the influence of the ester moiety on the catalyst activity, a new catalyst has been designed, bearing an ether linker instead of the ester. The ether linkage is much more stable than a ester, no risk of hydrolysis existing under the selected reaction conditions. (Figure 9).

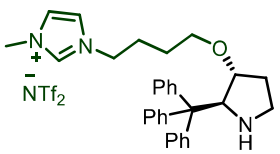

Figure 9: Catalyst **1c**

A new synthetic route was then devised to obtain catalyst **1c.** Even for this catalyst, pyrrolidine **2** was chosen as starting material, and again its nitrogen was preliminarily protected with benzyl chloroformiate (Cbz) to obtain **3**. (Scheme 17).

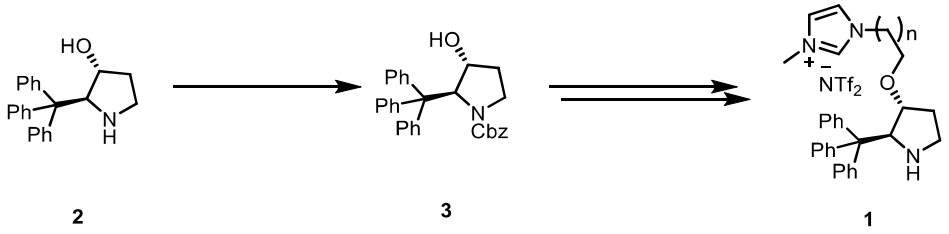

Scheme 17: Designed synthesis for catalyst **1c**

Alkylation was performed on pyrrolidine **3** to obtain the alkylated pyrrolidine **4c** (Scheme 18). As expected from our previous investigation, the alkylation reaction resulted very challenging. Due to the spatial proximity of the trityl group, the steric hindrance on the hydroxyl moiety highly affects the alkylation yield. Numerous strategies and alkylating agents have been tested, but unfortunately no positive results were obtained. Finally, the allylic bromide (*Z*)-1,4-dibromobut-2-ene proved to be suitable for the project purpose. Due to the allylic position of the bromine, it shows high reactivity compared to other alkyl halides.

To avoid dialkylation of (*Z*)-1,4-dibromobut-2-ene, 2.5 equivalents of **3** and 3.5 equivalents of NaH has been utilized in the alkylation reaction. The complete conversion was not reached to completely avoid the formation of product **13** and recycle the remaining starting material **3**. Pyrrolidine **4c** has therefore be obtained in 58% yield. Under the optimized reaction conditions, no formation of dimeric product **13** was detected.

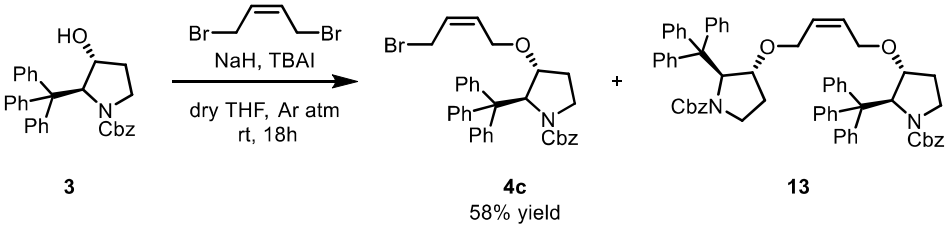

Scheme 18: Alkylation reaction for the synthesis of **4c**

The successive synthetic steps were analogous to those developed for catalyst **1a** and **1b**. Therefore, the nucleophilic substitution with imidazole led to trityl pyrrolidine **5c**. (Scheme 19).

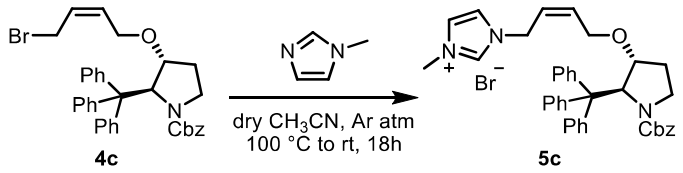

Scheme 19: Nucleophilic substitution for the synthesis of **5c**

Subsequently, counterion exchange afforded **6c** in quantitative yield over two synthetic steps. (Scheme 20)

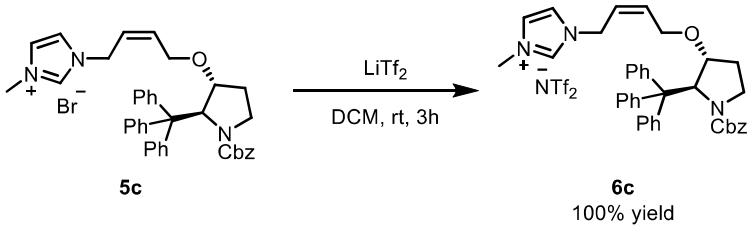

Scheme 20: Counterion exchange for the synthesis of **6c**

At last, catalyst **1c** is obtained in 76% yield after CBZ removal under hydrogen atmosphere catalyzed by palladium adsorbed on charcoal in THF solvent (Scheme 21).

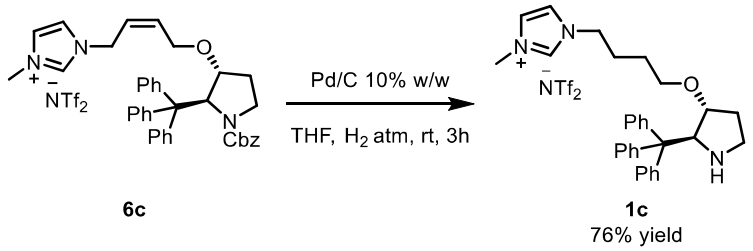

Scheme 21: Nitrogen deprotection for the synthesis of catalyst **1c**

As for catalysts **1a** and **1b**, catalyst **1c** activity and stereoselectivity have been investigated on our standard Michael addition reaction. (Table 5).

Table 5: Optimization for the Michael addition of dimethylmalonate to cinnamaldehyde catalyzed by caalyst **1c**

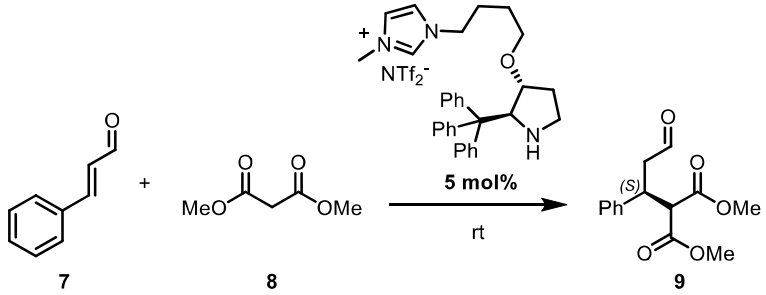

Entry[a]	Solvent	BzOH mol %	t (h)	Conversion %[b]	*ee* %[c]
1	3:7 DCM:EtOH	15	6	92	96
2	EtOH	15	6	95	95
3	EtOH	No	6	100	96
4 [d]	EtOH	No	6 (18)	52 (70)	97
5 [e]	EtOH	No	18	100	93
6 [f]	EtOH	15	3 (18)	70 (100)	96
7	H_2O	15	18	80	95

[a] Reaction conditions: cinnamaldehyde (0.1 mmol), dimethylmalonate (0.3 mmol) and catalyst **1c** (0.05 mmol) in 200 µl of the correspondent solvent mixture; [b] Calculated trough analysis on ^{1}H-NMR on the crude mixture, referring to aldehyde **7**; [c] calculated by means of chiral stationary phase HPLC after witty reaction derivatization; [d] The reaction has been conducted with 2.5 mol %; [e] the reaction has been conducted with 0.1 mmol of cinnamaldehyde and 0.15 mmol of dimethylmalonate; [f] the reaction has been conducted with 0.2 mmol of cinnamaldehyde and 0.1 mmol of dimethylmalonate.

Promising results were obtained performing the reaction under the same condition optimized for **1a** and **1b** (Entry 1, Table 5). Indeed, 92% was reached in 6 hours reaction time and product **9** was obtained in 96% enantiomeric excess. Utilizing only ethanol as solvent, an increased conversion was recorded after the same reaction time. Also, it seemed not to affect the enantioselection of the process, the contrary of what happened with **1a** and **1b** (Entry 2, Table 5). In addition, avoiding the use of the benzoic acid additive, did not diminish the catalytic performance of **1c**. Complete conversion was reached after 6 hours in 96% enantiomeric excess on product **9** (Entry 3, Table 5). Given the high performance demonstrated by this last catalyst, an attempt to diminish the catalytic loading (2,5 mol%) was run. The result was a decrease of the reaction rate. Indeed, 52% and 70% conversion were reached after 6 and 18 hours, respectively (Entry 4, Table 5). On the other hand, the enantioselection slightly enhanced, even if the obtained value is comparable with the one obtained using 5 mol% catalytic loading. The effect of changing the reactants equivalents has been then analyzed for comparison

with other catalysts reported in literatures.[18,45,72,73] Diminishing the excess of malonates, resulted in lower conversion and enantiomeric excess (Entry 5, Table 5). Meanwhile, performing the reaction with an excess of aldehyde, the opposite to our standard conditions, satisfactory results were still achieved (Entry 6, Table 5). Even the enantioselection was not affected under these conditions. At last, a test utilizing water as solvent has been performed to test the efficiency of the new catalyst even in this reaction media.[75] An 80% conversion and 95% enantiomeric excess were successfully achieved, proving the applicability of catalyst **1c** in water reaction media (Entry 7, Table 5). Even for this catalyst, kinetic curves of some catalytic test were analyzed (Figure 10).

Figure 10: Kinetics analysis on Michael addition catalyzed by catalyst **1c**

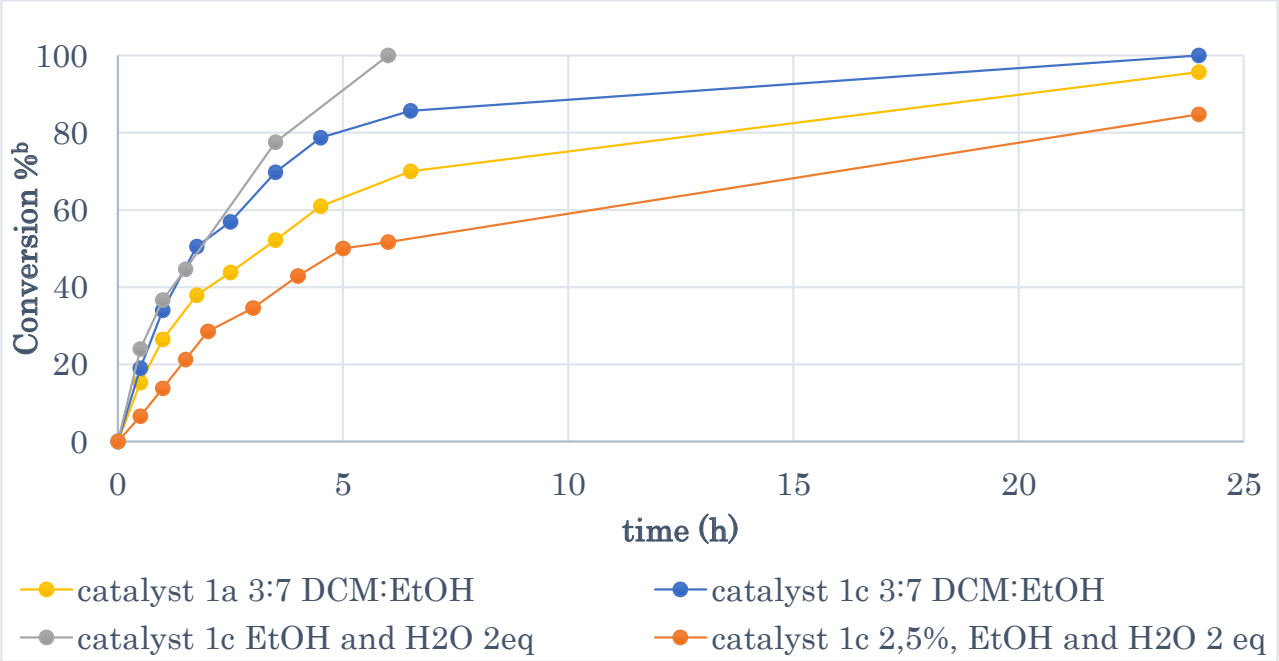

[a]Reaction conditions: cinnamaldehyde (0.1 mmol), dimethylmalonate (0.3 mmol), catalyst **1c** (0.05 mmol), BzOH (0.015 mmol) in 200 µl of solvent mixture, stirred at room temperature for the indicated time. [b]Calculated trough analysis on ^{1}H-NMR on the crude mixture, referring to aldehyde **7**

Even with catalyst **1c**, increasing in the relative amount of a protic solvent, the average reaction rate increases (blue line vs grey line). Moreover, the difference between the activity of **1a** and **1c** is highlighted by the kinetic diagrams. Performing the reaction in DCM:EtOH 3:7 solvent mixture involving **1a** (yellow line) or **1c** (blue line), the kinetic curve is divided in two stages, a first one with the highest reaction rate, that is reaches of a plateau. The second stage starts with the achievement of the plateau. It is noticeable that catalyst **1c** allows to reach the plateau at higher conversion (blue line) compared to

1a (yellow line). From the kinetic diagram it can also be confirmed that decreasing the catalytic loading, the reaction rates drastically drop, delaying the product formation. In summary, the better conditions for catalyst **1c** involve EtOH as solvent, 5 mol % catalytic loading with no additive at room temperature for 6 hours (Scheme 22).

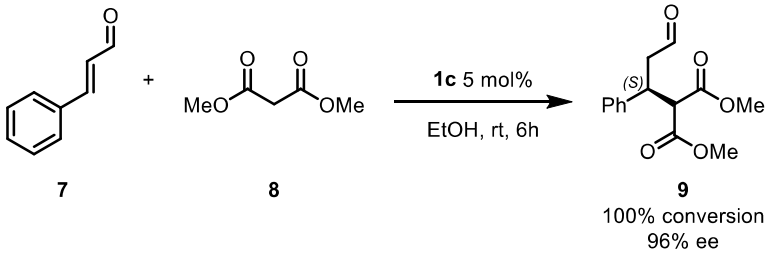

Scheme 22: Optimized conditions for Michael addition of diethylmalonate to cinnamaldehyde organocatalyzed by **1c**

Recycle attempts were performed under different conditions. On the basis of literature reports[73,76], a mixture of diethyl ether and hexane was chosen to separate the ionic tagged catalyst from the reaction crude mixture. In none of the attempts, the recycling of **1c** seemed to work efficiently. Even after 24 hours reaction time, no promising results were obtained. Even after 24 hours reaction time, no promising results were obtained. Two tests were conducted in ethanol, they were the most promising (Entry 1 and 2, Table 6). However, considering the extension of the reaction time and the obtained conversion, the recycle resulted inefficient. Supposing that a non complete solubilization of the catalyst in the reaction media could favor the recycling, an attempt utilizing water as reaction media has been conducted.[77] Poor results were obtained even in this reaction media (Entry 3, Table 6).

Table 6: Catalyst recycle attempt

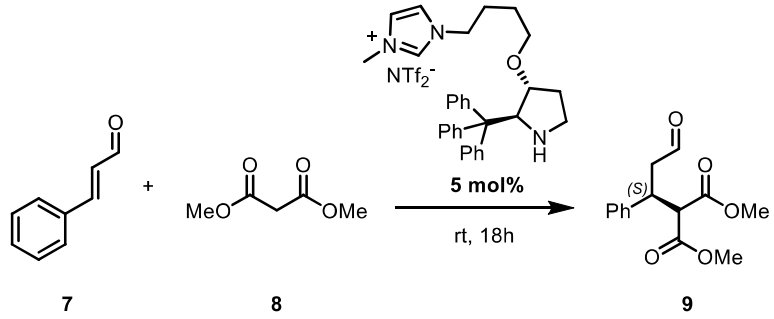

7 8 9

Entry[a]	Solvent	7 (mmol)	8 (mmol)	BzOH (mol %)	Conversion % [b] 1st	Conversion % [b] 2nd
1	EtOH	0,1	0,3	No	100	80
2	EtOH	0,2	0,1	15	100	67
3	H_2O	0,1	0,3	15	>95	10

[a] Reaction conditions: catalyst **1c** (0.05 mmol) and the corresponding amount of BzOH, cinnamaldehyde, and dimethylmalonate in 200 µl of the correspondent solvent; [b] calcolated trough analysis on ^{1}H-NMR on the crude mixture, referring to aldehyde **7**.

The poor recycling results could be due to a difficult precipitation of the catalyst from the extraction mixture. When only diethyl ether was used to separate the catalyst from the crude reaction mixture, a homogeneous solution was obtained, therefore no separation was achieved. On the contrary, when adding only hexane, no extraction of the product was observed. For this reason, a mixture of the two solvents was used in the recycling protocol, unfortunately with poor results. Once confirmed the insolubility of the ionic tagged pyrrolidine **1c** in diethyl ether and hexane, the selective extraction of Michael product **9** revealed troublesome, even with the mixture of diethyl ether and hexane. Several extractions had to be performed to recuperate most of **9**. Thus, this methodology was not suitable for the catalyst recycling. It may be possible the laboratory scale used in the recycling to be too low for an efficient recovery of the catalyst. Working in little scale, few milligrams of catalyst are involved in each reaction, a minimal loss during the recycling protocol could results in a significant drop in the product formation. Operating with higher quantity could permit a major tolerance in catalyst leaching. In addition, an easier precipitation of the catalyst in the anti-solvent mixture could be achieved with higher quantity of catalyst involved. Bigger scale investigation could be conducted to overcome this recycling problem.

Additionally, a change in the catalyst counterion could be studied for the same purpose. A different interaction among the imidazole cation and his counterion could results in a change on the catalyst physical properties, first on his solubility in organic and aqueous media. Also, catalyst **1c** present itself has a gummy solid, a more crystalline solid could result in a more efficient precipitation, therefore in a more efficient recycling.

Despite the negative recycling results, catalyst **1c** showed a high activity and stereoselectivity in the Michael addition reaction of malonate to cinnamaldehyde. Comparing **1c** with **1a** and **1b**, it could be confirmed that the ionic tag highly affects the catalyst activity. The more flexible linker on **1c** could reduce the distance of the ionic tag, therefore leading to possible higher stabilization of dipolar transition states. In order to obtain this stabilization, the linker between the ionic tag and the pyrrolidine scaffold must be sufficiently flexible to avoid substantial distortion of bond angles and distances.[6] Probably, the ester linker of **1a** and **1b**, does not permit a high influence of the ionic tag in the reaction catalytic cycle.

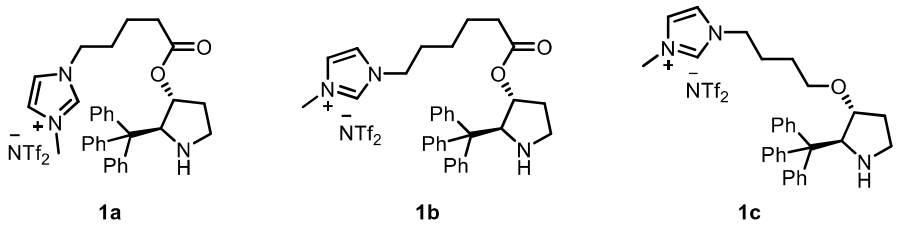

Figure 11: Synthesized ionic tag organocatalysts **1a,b,c**

Evaluating the catalytic performance of catalyst **1c** with some of the numerous organocatalysts developed in the last twenty years, it results clearly promising.[18,67,72,73,78–80] In our work, utilizing catalyst **1c**, high activity and stereoselectivity were achieved even without the aid of those additive and with only 5% of catalyst loading (100% conversion, 96% *ee*, rt, 6h). However, there are not enough data on trityl pyrrolidine derivatives in the literature to make a direct comparison with prolinol derived catalysts and determine the specific reason of the high performance showed by **1c**. The described protocol represents the first example of Michael addition of malonate to cinnamaldehyde catalyzed by a trityl pyrrolidine derivatives without additives. The only example of the involvement of trityl pyrrolidine derivative in the asymmetric Michael addition reaction was recently reported by our research group, and there, additives resulted fundamental for the transformation efficiency.[45]

An analysis of the trityl substituent effect on the pyrrolidine scaffold was recently developed by Mayr.[81,82] In his work he determined a lower basicity and nucleophilicity for the Maruoka 2-trityl-pyrrolidine, compared to different functionalized pyrrolidines. He rationalized his data with a negative hyperconjugative effect of the trityl group with the pyrrolidine nitrogen. According to Mayr, the trityl substituent acts as electron withdrawing group, reducing the enamine electrophilicity. On the other hand, this electronic effect could enhance the electrophilicity of the corresponding iminium ion, therefore favoring iminium type organocatalytic reaction. The same electronic effect was also observed for the -$CPh_2(OSiMe_3)$ group in Hayashi-Jorgensen catalyst, even slightly increased compared to the trityl one. Therefore, the two diverse groups exert similar electronic effects on the enamine and iminium intermediates of organocatalytic reactions. He allocated the different stereoselectivity of the two catalyst into the different steric hindrance caused by the two different C-2 substituents, without empathizing a major difference in the theoretical catalytic activity.

Surely, an effect of the ionic tag on the catalyst backbone was observed in the reported project. The diverse catalytic activity of catalyst **1c** from catalyst **1a,b** is clear, the only difference among these catalysts residing in the spacer connecting the ionic tag and the pyrrolidine scaffold.

A specific performance comparison could be done with the ionic tagged catalyst designed by Zlotin and co-workes in 2009.[73] They developed the synthesis of ionic tag functionalized prolinol derivatives **XXVIII** and tested the catalyst in the Michael addition of malonates to cinnamaldehydes (Scheme 23). Performing the reaction at 4°C, the Michael addition products were formed with excellent yields and stereoselectivities in 24-72 hours involving 10 mol% of the organocatalyst. Even in this case, no additives were necessary, but 10 mol% of catalyst and low temperature were necessary. In addition, Zlotin catalyst backbone resulted not to be resistant, since showed hydrolysis of the silyl ether site. In our protocol, employing catalyst **1c**, room temperature and 5 mol% of catalyst are sufficient to obtain **9** with comparable results. In addition, catalyst **1c** presents a robust backbone with no hydrolysable sites.

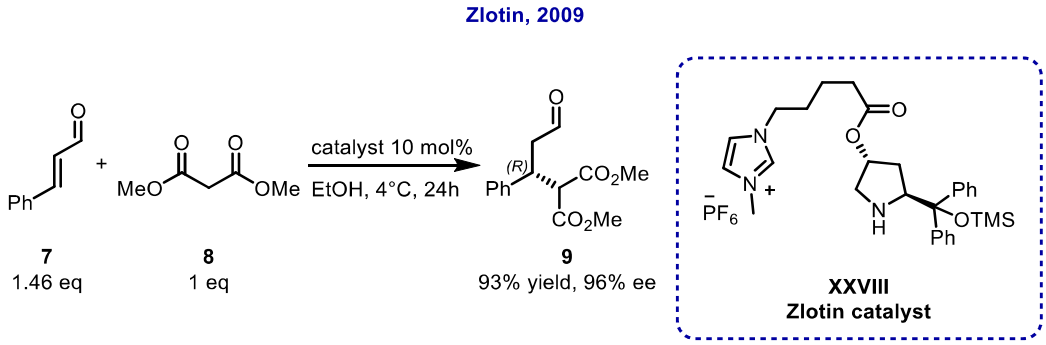

Scheme 23: Zlotin, 2009

One last advantage of ionic tag trityl pyrrolidine **1c** relies on the absolute configuration induced to the product. Most of the designed pyrrolidine organocatalysts present a C-2 chiral center in an absolute configuration, that shields the *Si* face of the iminium ion and thus leads to the synthesis of the product in *R* - enantioenriched configuration. On the contrary, in catalyst **1c**, the C-2 chiral center is enantiopure in the S configuration. Thus, the R face of the iminium is hindered by the trityl bulky group, and the Michael addition product is formed in the *S*– enantioenriched configuration. Due to their diverse interactions in biologic systems, the synthesis of both the enantiomers of the same molecule is often requested.

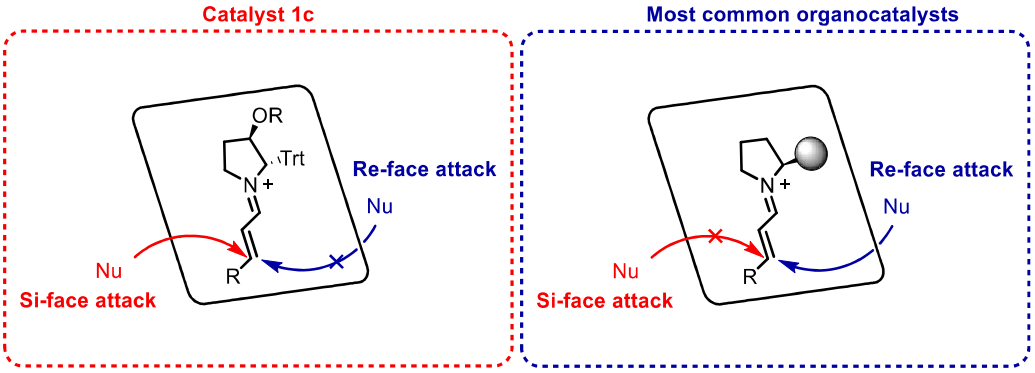

Figure 12: Diverse stereoselectivity for diverse catalysts

Conclusions

In conclusion, three different ionic tag functionalized enantiopure trityl pyrrolidines were synthesized (**1a-c**).

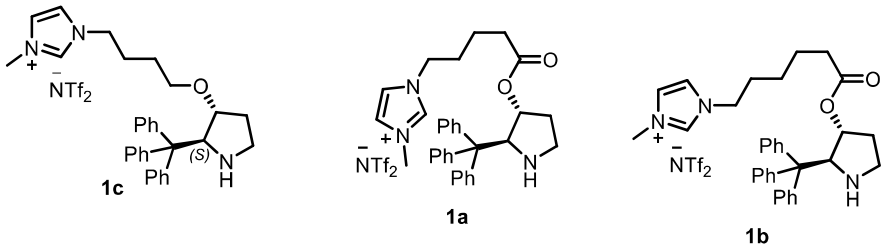

Figure 13: Synthesized organocatalysts

Their catalytic activity and stereoselectivity were investigated in the same Michael reaction. The collected data showed a different influence of the ionic tag moiety depending on the linker structure. We could deduce that the ether linked on **1c** positively affected the reaction outcome. Indeed, the Michael product was obtained as only product and in highly enantioenriched form. Meanwhile, the ester linker present inn **1a** and **1b** did not seem to favor the product formation. Catalyst **1c** provided the most promising results: no trityl pyrrolidine derivatives gave so far so efficient results in the Michael addition of malonate to cinnamaldehydes, but poor results were obtained in iminium-type organocatalyzed reactions.

An efficient procedure for the catalyst recovery from the reaction mixture has still to be developed, since good results were not achieved with the performed attempts.

In the future, different reaction involving **1c** as catalyst will be analyzed to test the scope of **1c** applicability. Investigation concerning the catalyst recycle will be carried out to find a suitable protocol. Finally, diverse functionalized organocatalysts derived from 3-hydroxyl-2-trityl pyrrolidine **2** will be designed. The developed alkylation procedure could permit numerous different applications of 3-hydroxyl-2-trityl pyrrolidine in asymmetric synthesis.

General procedures and products characterization

Material and methods

^{1}H-NMR spectra and ^{13}C-NMR were recorded on Varian Inova 400 NMR instrument with a 5 mm probe. Chemical shifts (δ) are reported in ppm, relative to the residual peaks of deuterated solvent signals. HPLC-MS analyses were performed on an Agilent Technologies HP1100 instrument coupled with an Agilent Technologies MSD1100 single-quadrupole mass spectrometer. CSP-HPLC analyses were performed on an Agilent Technologies Series 1200 instrument using chiral columns and n-hexane/2-

propanol (n-Hex/IPA) mixtures. The enantiomeric compositions were checked against the corresponding racemic products, obtained under the same reaction conditions using pyrrolidine as the catalyst. Flash chromatography purifications were carried out using Merck Geduran® Si 60 silica gel (40-63 µm particle size). Thin layer chromatography was performed on Merck 60 F254 plates. Commercial reagents were used as received without additional purification.

Synthesis of 3

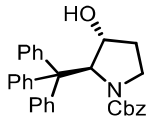

In a round bottom flask, pyrrolidine **2** (10 mmol), dry DCM (40 mL) and triethyl amine (20 mmol, 2 eq) are added sequentially. Subsequently, benzyl carbonochloridate (20 mmol, 2eq) is dropped at 0°C into the reaction mixture. The reaction mixture is stirred at room temperature overnight. Then, the organic phase is washed with water and evaporated in vacuum. Pyrrolidine **3** is thus obtained in 90% yield.

^{1}H-NMR (401 MHz, Chloroform-*d*) δ 7.50 – 7.41 (m, 6H), 7.35 – 7.27 (m, 4H), 7.25 – 7.13 (m, 10H), 5.82 (s, 1H),), 5.09 (d, *J* = 12.6 Hz, 1H), 4.79 (bs, 1H), 4.44 (d, *J* = 5.1 Hz, 1H), 3.61 (dt, *J* = 10.8, 9.3 Hz, 1H), 3.02 (td, *J* = 10.7, 2.3 Hz, 1H), 1.27 (td, *J* = 9.9, 4.9 Hz, 1H), 0.04 (ddt, *J* = 19.8, 10.0, 5.1 Hz, 1H).

^{13}C-NMR (101 MHz, cdcl$_3$) δ 157.92, 144.56, 136.86, 130.82, 128.49, 127.83, 127.55, 127.07, 126.22, 76.06, 73.38, 66.97, 60.78, 49.39, 31.85.

$[\alpha]_D^{25}$= -49 (c=1.04, $CHCl_3$); white solid Tf=56.9-58.7°C; HPLC-MS (ESI): 464 [M+H$^+$].

Synthesis of 4a

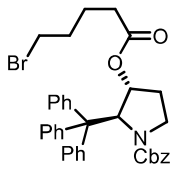

In a round bottom flask, pyrrolidine **3** (0.431 mmol) and CH_2Cl_2 (2 mL) are added. Then, bromovaleric acid (0.647 mmol, 1.5 eq), DCC (0.647 mmol, 1.5 eq) and DMAP (0.064 mmol, 0.15 eq) are added to the solution. The reaction mixture is stirred at 5°C for 18 hours, then the precipitate is filtered off and washed with CH_2Cl_2. The organic extract is evaporated and the crude mixture purified by column chromatography on silica gel

(95:5 Cy:AcOEt to 8:2 Cy:AcOEt). Pyrrolidine **4a** is obtained as a white solid with 83% yield.

^{1}H-NMR (401 MHz, Chloroform-*d*) δ 7.41 (d, *J* = 7.1 Hz, 6H), 7.31 (t, *J* = 4.0 Hz, 3H), 7.25 – 7.13 (m, 11H), 5.98 (s, 1H), 5.32 (d, *J* = 5.4 Hz, 1H), 5.12 (d, *J* = 12.5 Hz, 1H), 4.86 (bs, 1H), 3.50 (q, *J* = 9.5 Hz, 1H), 3.43 (t, *J* = 6.6 Hz, 2H), 2.93 (td, *J* = 10.6, 2.7 Hz, 1H), 2.60 – 2.22 (m, 2H), 2.04 – 1.88 (m, 2H), 1.88 – 1.72 (m, 2H), 1.36 (ddd, *J* = 15.0, 9.2, 2.7 Hz, 1H), 0.19 (dtd, *J* = 15.2, 9.8, 5.4 Hz, 1H).

^{13}C-NMR (401 MHz, cdcl$_3$) δ 172.14, 157.23, 143.95, 136.87, 130.46, 128.41, 127.81, 127.54,127.52, 126.31, 79.42, 69.88, 66.89, 60.81, 48.71, 33.56, 32.84, 31.95, 30.00, 23.67. $[\alpha]_D^{25}$= -84 (c=0.16, $CHCl_3$); white solid Tf=56.9-58.7°C; HPLC-MS (ESI): 626 [M+H$^+$], 628 [M+H$^+$] (pattern Br).

Synthesis of 5a

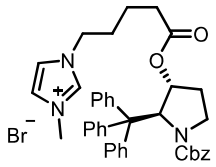

A mixture of pyrrolidine **3a** (0.748 mmol) and 1-methyl-1H-imidazole (1.5 mmol, 2 eq) in dry CH_3CN (3.7 mL) is heated for 10 minutes as 100°C under argon atmosphere, then the reaction is cooled to room temperature and stirred overnight. Subsequently, CH_3CN in evaporated and the crude is washed three time with Et_2O. Due to its high hygroscopicity, pyrrolidine **5a** is used for the next synthetic step without further purification.

^{1}H-NMR (401 MHz, Chloroform-*d*) δ 10.35 (s, 1H), 7.42 (s, 1H), 7.38 (d, *J* = 8.0 Hz, 7H), 7.28 (t, *J* = 6.6 Hz, 3H), 7.17 (dq, *J* = 13.7, 7.1 Hz, 11H), 5.92 (s, 1H), 5.29 (d, *J* = 5.3 Hz, 1H), 5.08 (d, *J* = 12.6 Hz, 1H), 4.84 (bs, 1H), 4.35 (t, *J* = 7.0 Hz, 2H), 4.04 (s, 3H), 3.47 (q, *J* = 9.6 Hz, 1H), 2.90 (t, *J* = 9.9 Hz, 1H), 2.58 – 2.36 (m, 2H), 1.99 (p, *J* = 7.4 Hz, 2H), 1.67 (p, *J* = 6.8, 6.3 Hz, 2H), 1.34 (dd, *J* = 14.0, 9.0 Hz, 1H), 0.16 (dtd, *J* = 15.1, 9.9, 5.9 Hz, 1H).

Synthesis of 6a

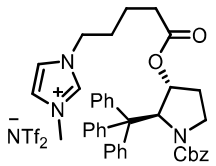

Pyrrolidine **5a** (0.655 mol), CH_2Cl_2 (14 mL) and lithium bis(trifluoromethanesulfonyl)imide (0.982 mol, 1.5 eq) are added in a round bottom flask. The reaction mixture is stirred a room temperature for 18 hours. Then water is added, and the mixture stirred for 1 hour at room temperature. The organic phase is afterward washed 3 times with water. The organic solvent is evaporated in vacuum and the reaction crude purified with a chromatographic column on silica gel (98:2 CH_2Cl_2:MeOH). Product **6a** is obtained with 59% yield over two synthetic steps.

^{1}H-NMR (401 MHz, Chloroform-*d*) δ 8.89 (s, 1H), 7.39 (dt, *J* = 6.1, 1.4 Hz, 6H), 7.30 (d, *J* = 5.1, 3.9, 2.3 Hz, 4H), 7.25 – 7.13 (m, 12H), 5.94 (s, 1H), 5.32 (d, *J* = 5.3 Hz, 1H), 5.10 (d, *J* = 12.6 Hz, 1H), 4.87 (bs, 1H), 4.16 (t, *J* = 7.4 Hz, 2H), 3.94 (s, *J* = 1.7 Hz, 3H), 3.49 (q, *J* = 9.6 Hz, 1H), 2.93 (td, *J* = 10.5, 2.6 Hz, 1H), 2.59 – 2.34 (m, 2H), 1.95 (p, *J* = 7.4

Hz, 2H), 1.65 (p, *J*= 7.5, 6.9 Hz, 2H), 1.36 (dd, *J*= 15.1, 9.0 Hz, 1H), 0.19 (dtd, *J*= 15.1, 9.7, 5.4 Hz, 1H).

^{13}C-NMR (101 MHz, cdcl$_3$) δ 171.80, 157.33, 143.89, 136.85, 136.19, 130.39, 128.42, 127.82, 127.54, 127.30, 126.34, 123.60, 122.28, 121.38, 118.19, 79.45, 69.88, 66.87, 60.78, 49.70, 48.67, 36.36, 33.22, 29.66, 29.25, 21.26. 26

$[\alpha]_D^{25}$= -40 (c=0.61, $CHCl_3$); gummy solid; HPLC-MS (ESI): 628 [M-NTf_2^-].

Synthesis of 1a

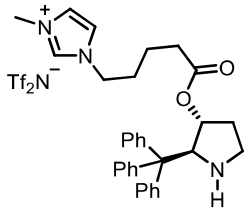

In a round bottom flask is added pyrrolidine **6a** (0.440 mmol) under argon atmosphere. Subsequently, THF (2 mL) and Pd/C (0.10 % w/w, 0.044 mmol, 0.10 eq) are added. The reaction is stirred at room temperature for 18 hours. Then, the reaction mixture is filtered through celite. The organic phase is evaporated, and the crude is purified by means of chromatographic column on silica gel (9:1 CH_2Cl_2:MeOH). The product is obtained as a gummy solid in 90% yield.

^{1}H-NMR (401 MHz, Chloroform-*d*) δ 8.82 (s, 1H), 7.42 – 7.15 (m, 17H), 5.14 (d, *J*= 5.8 Hz, 1H), 5.01 (s, 1H), 4.21 (t, *J*= 7.3 Hz, 2H), 3.91 (s, 3H), 2.93 (td, *J*= 10.7, 5.9 Hz, 1H), 2.77 (t, *J*= 8.9 Hz, 1H), 2.42 (t, *J*= 7.1 Hz, 2H), 2.07 (s, 1H), 1.94 (p, *J*= 7.3 Hz, 2H), 1.66 (p, *J*= 7.2 Hz, 2H), 1.48 (dd, *J*= 14.0, 5.5 Hz, 1H), 0.84 – 0.65 (m, 1H).

^{13}C-NMR (101 MHz, cdcl$_3$) δ 172.09, 135.88, 129.82, 127.78, 126.30, 123.66, 122.28, 121.36, 118.18, 78.58, 68.73, 60.75, 49.61, 45.03, 36.20, 33.70, 33.28, 29.19, 21.17.

$[\alpha]_D^{25}$= -33 (c=1.01, $CHCl_3$); gummy solid; HPLC-MS (ESI): 494 [M-NTf_2^-], 247 [M-NTf_2^- +H^+].

Synthesis of 4b

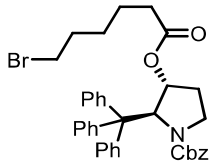

In a round bottom flask, pyrrolidine **2** (0.200 mmol) and CH_2Cl_2 (2 mL) are added. Then, bromohexanoic acid (0.300 mmol, 1.5 eq), DCC (0.300 mmol, 1.5 eq) and DMAP (0.030 mmol, 0.15 eq) are added to the solution. The reaction mixture is stirred at 5°C for 18 hours, then the precipitate is filtered off and washed with CH_2Cl_2. The organic extract is evaporated and the crude mixture purified by column chromatography on silica gel (95:5 Cy:AcOEt to 8:2 Cy:AcOEt). Pyrrolidine **4b** is obtained as a gummy solid with 89% yield.

^{1}H-NMR (401 MHz, Chloroform-*d*) δ 7.45 – 7.38 (m, 6H), 7.37 – 7.28 (m, 3H), 7.25 – 7.13 (m, 11H), 5.97 (s, 1H), 5.31 (d, *J* = 5.4 Hz, 1H), 5.19 – 5.08 (m, 1H), 4.86 (bs, 1H), 3.49 (q, *J* = 9.6 Hz, 1H), 3.43 (t, *J* = 6.7 Hz, 2H), 2.93 (td, *J* = 10.6, 2.7 Hz, 1H), 2.52 – 2.25 (m, 2H), 1.90 (p, *J* = 6.9 Hz, 2H), 1.69 (pd, *J* = 7.1, 2.3 Hz, 2H), 1.52 (p, *J* = 7.4 Hz, 2H), 1.36 (ddd, *J* = 14.8, 8.9, 2.2 Hz, 1H), 0.18 (dtd, *J* = 15.2, 9.8, 5.1 Hz, 1H).

^{13}C-NMR (101 MHz, cdcl$_3$) δ 172.45, 157.23, 143.95, 136.89, 130.48, 128.40, 127.80, 127.53, 127.49, 126.30, 79.28, 69.91, 66.85, 60.79, 48.72, 34.30, 33.45, 32.33, 27.59, 24.20, 1.03.

$[\alpha]_D^{25}$ = -57 (c=1.01, $CHCl_3$); gummy solid; HPLC-MS (ESI): 642 [M+ H^+], 640 [M+H^+].

Synthesis of 5b

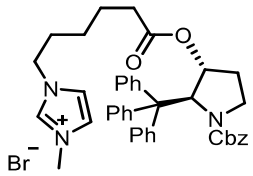

A mixture of pyrrolidine **4b** (0.173 mmol) and 1-methyl-1H-imidazole (0.260 mmol, 1.5 eq) in dry CH_3CN (1 mL) is heated for 10 minutes as 100°C under argon atmosphere, then the reaction is cooled to room temperature and stirred overnight. Subsequently, CH_3CN in evaporated and the crude is washed three time with Et_2O. Due to its high hygroscopicity, pyrrolidine **5b** is used for the next synthetic step without further purification.

^{1}H-NMR (401 MHz, Chloroform-*d*) δ 10.14 (s, 1H), 7.43 (d, J = 1.3 Hz, 2H),7.34 (d *J*= 7.5 Hz, 6H), 7.30 – 7.20 (m, 3H), 7.20 – 7.07 (m, 11H), 5.90 (s, 1H), 5.24 (d, *J*= 5.3 Hz, 1H), 5.05 (d, *J*= 12.6 Hz, 1H), 4.80 (bs, 1H), 4.29 (t, *J*= 7.4 Hz, 2H), 3.99 (s, 3H), 3.44 (q, *J*= 9.7 Hz, 1H), 2.87 (td, *J*= 10.7, 2.6 Hz, 1H), 2.48 – 2.15 (m, 2H), 1.91 (p, *J*= 7.6 Hz, 2H), 1.64 (p, *J*= 7.2 Hz, 2H), 1.38 (p, *J*= 7.9 Hz, 2H), 1.36 – 1.24 (m, 1H), 0.11 (dtd, *J*= 15.3, 9.7, 5.5 Hz, 1H).

Synthesis of 6b

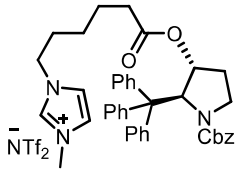

Pyrrolidine **5b** (0.175 mol), CH_2Cl_2 (2 mL) and lithium bis(trifluoromethanesulfonyl)imide (0.263 mol, 1.5 eq) are added in a round bottom flask. The reaction mixture is stirred a room temperature for 18 hours. Then water is added, and the mixture stirred for 1 hour at room temperature. The organic phase is afterward washed 3 times with water. The organic solvent is evaporated in vacuum and the reaction crude purified with a chromatographic column on silica gel (98:2 CH_2Cl_2:MeOH). Product **6b** is obtained as a gummy solid in 78% yield over two synthetic steps.

^{1}H-NMR (401 MHz, Chloroform-*d*) δ 8.86 (s, 1H), 7.39 (d, *J*= 6.8 Hz, 6H), 7.29 (t, *J*= 7.0 Hz, 4H), 7.25 – 7.12 (m, 12H), 5.94 (s, 1H), 5.31 (s, 1H), 5.10 (d, *J*= 12.7 Hz, 2H), 4.85 (bs, 1H), 4.18 (t, *J*= 7.4 Hz, 2H), 3.90 (s, 3H), 3.48 (q, *J*= 9.5 Hz, 1H), 2.93 (td, *J*= 10.2, 1.8 Hz, 1H), 2.54 – 2.26 (m, 1H), 1.90 (p, *J*= 7.6 Hz, 2H), 1.69 (p, *J*= 7.4, 6.9 Hz, 2H), 1.41 (p, *J*= 9.6, 8.7 Hz, 2H), 1.35 (dd, *J*= 24.3, 1.8 Hz, 1H), 0.18 (ddd, *J*= 18.6, 9.3, 4.2 Hz, 1H).

^{3}C-NMR (101 MHz, cdcl$_3$) δ 172.24, 157.19, 143.85, 136.77, 135.97, 130.35, 128.33, 127.72, 127.46, 127.22, 126.26, 123.58, 122.17, 121.32, 118.13, 79.19, 69.81, 66.75, 60.71, 53.37, 49.64, 48.63, 36.16, 33.76, 29.57, 25.31, 23.89

$[\alpha]_D^{25}$= -41 (c=0.89, $CHCl_3$); gummy solid; HPLC-MS (ESI): 642 [M+ H^+].

Synthesis of 1b

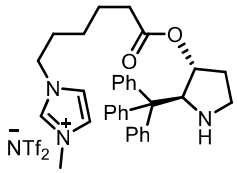

In a round bottom flask is added pyrrolidine **6b** (0.135 mmol) under argon atmosphere. Subsequently, THF (1.5 mL) and Pd/C (0.10 % w/w, 0.0135 mmol, 0.10 eq) are added. The reaction is stirred at room temperature for 18 hours. Then, the reaction mixture is filtered through celite. The organic phase is evaporated, and the crude is purified by means of chromatographic column on silica gel (9:1 CH_2Cl_2:MeOH). The product is obtained as a gummy solid in 83% yield.

^{1}H-NMR (401 MHz, Chloroform-*d*) δ 8.72 (s, 1H), 7.33 (s, 6H), 7.29 – 7.13 (m, 11H), 5.10 (d, *J* = 5.6 Hz, 1H), 4.97 (s, 1H), 4.15 (t, *J* = 7.4 Hz, 2H), 3.84 (s, 3H), 2.89 (td, *J* = 10.7, 5.6 Hz, 1H), 2.73 (t, *J* = 8.8 Hz, 1H), 2.35 (t, *J* = 7.4 Hz, 2H), 1.89 (p, *J* = 7.6 Hz, 2H), 1.67 (p, *J* = 7.6 Hz, 2H), 1.44 (dd, *J* = 14.2, 5.3 Hz, 1H), 1.37 (t, *J* = 7.2 Hz, 2H), 0.71 (tq, *J* = 11.3, 6.8 Hz, 1H).

^{13}C-NMR (101 MHz, cdcl$_3$) δ 172.45, 136.09, 129.49, 127.80, 126.32, 123.57, 122.21, 121.35, 118.16, 78.34, 68.73, 60.72, 49.71, 45.05, 36.24, 33.94, 33.63, 29.64, 25.40, 23.92. $[\alpha]_D^{25}$= -15 (c=0.66, $CHCl_3$); gummy solid; HPLC-MS (ESI): 508 [M+ H^+], 254 [M+ $2H^+$].

Synthesis of 4c

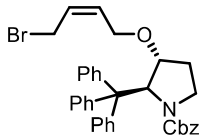

In a round bottom flask 2.5 mL of dry THF, NaH (60% w/w, 3.02 mmol, 3.5 eq) and tetrabutyl ammonium iodide (0.043 mmol, 0.05 eq) are added under argon atmosphere. The reaction mixture is stirred at 0°C for 5 minutes, then (Z)-1,4-dibromobut-2-ene (0.863 mmol, 1 eq) is added. Subsequentially, a solution of pyrrolidine **3** (0.863 mmol, 2.5 eq) in THF (2.5 mL) is dropped into the round bottom flask and the reaction is stirred a room temperature. After 18h, NH_4Cl is poured in the reaction mixture and the aqueous phase is washed three times with EtOAc. The combined organic phases are evaporated and the crude mixture is purified on a silica gel chromatographic column (gradient from 95:5 Cy:EtOAc to 80:20 Cy:EtOAc). The product is obtained as a white solid in 58% yield.

^{1}H-NMR (401 MHz, Chloroform-*d*) δ 7.44 (d, *J*= 6.9 Hz, 6H), 7.35 – 7.26 (m, 3H), 7.24 – 7.12 (m, 11H), 5.96 – 5.84 (m, 2H), 5.78 (dt, *J*= 11.4, 6.2 Hz, 1H), 5.09 (d, *J*= 12.6 Hz, 1H), 4.12 – 4.03 (m, 2H), 4.01 – 3.93 (m, 3H), 3.54 (q, *J*= 9.6 Hz, 1H), 2.97 (td, *J*= 10.7, 2.6 Hz, 1H), 1.49 (dd, *J*= 12.3, 3.7 Hz, 1H), -0.13 (dtd, *J*= 14.9, 9.8, 5.1 Hz, 1H).
^{13}C-NMR (101 MHz, cdcl$_3$) δ 157.27, 144.38, 136.96, 131.08, 130.64, 128.33, 128.14, 127.65, 127.50, 127.37, 126.10, 83.51, 72.00, 66.72, 63.08, 60.95, 49.19, 26.38, 26.26.
$[\alpha]_D^{25}$= -46 (c=0.27, $CHCl_3$); white solid Tf=147°C; HPLC-MS (ESI): 628 [M-Br$^-$].

Synthesis of 5c

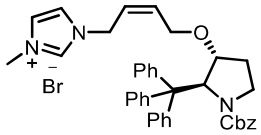

A mixture of pyrrolidine **5c** (0.502 mmol) and 1-methyl-1H-imidazole (1.76 mmol, 3.5 eq) in dry CH_3CN (2.5 mL) are heated for 10 minutes as 100°C under argon atmosphere. Then the reaction is cooled to room temperature and stirred for 18h. Subsequently, CH_3CN is evaporated and the crude is washed three time with Et_2O. Due to its high hygroscopicity, pyrrolidine **5c** has not been isolated and is used for the next synthetic step without further purification.
^{1}H-NMR (401 MHz, Chloroform-*d*) δ 10.14 (s, 1H), 7.37 (d, *J*= 7.7 Hz, 7H), 7.29 – 7.19 (m, 3H), 7.15 (dt, *J*= 21.7, 7.2 Hz, 12H), 6.02 (dt, *J*= 11.4, 5.6 Hz, 1H), 5.89 – 5.75 (m, 2H), 5.08 – 4.94 (m, 3H), 4.74 (s, 1H), 4.18 (dd, *J*= 13.2, 5.7 Hz, 1H), 4.03 (d, *J*= 4.7 Hz, 1H), 3.95 (s, 4H), 2.95 (t, *J*= 10.6 Hz, 1H), 2.54 (s, 1H), 1.56 (dd, *J*= 14.3, 9.3 Hz, 1H), -0.14 (ddt, *J*= 18.9, 9.2, 5.1 Hz, 1H).
N-methyl imidazole
^{1}H-NMR (401 MHz, Chloroform-*d*) δ 7.45 (s, 1H), 7.05 (s, 1H), 6.88 (s, 1H), 3.69 (s, 3H).

Synthesis of 6c

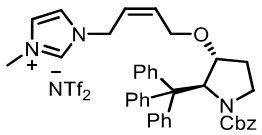

In a round bottom flask, pyrrolidine **5c** (0.500 mmol), CH_2Cl_2 (5 mL) and lithium bis(trifluoromethanesulfonyl)imide (0.750 mmol, 1.5 eq) are added. The reaction mixture is stirred at room temperature for 3h. The organic phase is afterward washed 3 times with water. The organic solvent is evaporated in vacuum and the reaction crude purified with a chromatographic column on silica gel (98:2 CH_2Cl_2:MeOH). Pyrrolidine **6c** has been obtained as a gummy solid in quantitative yield.

^{1}H-NMR (401 MHz, Chloroform-*d*) δ 8.61 (s, 1H), 7.45 – 7.36 (m, 6H), 7.33 – 7.14 (m, 15H), 7.09 (s, 1H), 6.08 (dt, *J* = 11.1, 5.5 Hz, 1H), 5.86 (s, 1H), 5.80 (q, *J* = 8.0 Hz, 1H), 5.05 (d, *J* = 12.8 Hz, 1H), 4.85 (qd, *J* = 14.5, 7.6 Hz, 3H), 4.17 (dd, *J* = 14.0, 5.6 Hz, 1H), 4.07 (d, *J* = 5.0 Hz, 1H), 3.99 (dd, *J* = 13.5, 5.1 Hz, 1H), 3.85 (s, 3H), 3.50 (q, *J* = 9.5 Hz, 1H), 3.02 (td, *J* = 10.7, 2.5 Hz, 1H), 1.61 – 1.49 (m, 1H), -0.08 (dtd, *J* = 14.8, 9.9, 5.0 Hz, 1H).

^{13}C-NMR (101 MHz, cdcl$_3$) δ 157.59, 144.26, 137.05, 135.70, 133.96, 130.41, 128.43, 127.79, 127.52, 127.15, 126.33, 123.63, 123.05, 122.13, 121.41, 118.22, 84.16, 77.45, 77.13, 76.81, 72.05, 66.63, 64.34, 60.75, 49.17, 46.69, 36.22, 26.52

$[\alpha]_D^{25}$= -39 (c=0.45, $CHCl_3$); gummy solid

Synthesis of 1c

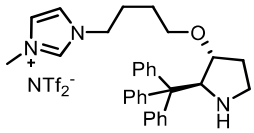

In a round bottom flask, pyrrolidine **6c** (0.568 mmol), THF (6 mL) and Pd/C (10% w/w, 0.056 mmol, 0.10 eq) are added. The reaction is stirred for 3h at room temperature under H_2 atmosphere. Then, it is filtered through celite and the filter washed with CH_2Cl_2. The crude mixture is purified through silica gel chromatography (CH_2Cl_2:MeOH 98:2) and the product is obtained as a gummy solid in 76% yield.

^{1}H-NMR (401 MHz, Chloroform-*d*) δ 8.69 (s, 1H), 7.37 (d, *J* = 7.7 Hz, 6H), 7.29 (d, *J* = 10.4 Hz, 3H), 7.26 – 7.15 (m, 8H), 5.05 (s, 1H), 4.21 (t, *J* = 7.5 Hz, 2H), 3.84 (s, 3H), 3.77 (d, *J* = 4.8 Hz, 1H), 3.56 (bs, NH), 3.42 (dt, *J* = 9.0, 6.0 Hz, 1H), 3.24 (dt, *J* = 9.0, 5.6 Hz,

1H), 3.03 (td, *J*= 11.9, 11.3, 5.8 Hz, 1H), 2.86 (t, *J*= 8.9 Hz, 1H), 2.02 (p, *J*= 7.7 Hz, 2H), 1.70 – 1.53 (m, 3H), 0.25 (tdd, *J*= 12.9, 7.9, 5.0 Hz, 1H).

^{13}C-NMR (101 MHz, cdcl$_3$) δ 135.83, 129.51, 128.06, 126.62, 123.63, 122.35, 121.33, 118.15, 82.79, 71.17, 67.93, 60.42, 49.93, 45.39, 36.12, 29.61, 27.41, 26.50.

HPLC-MS (ESI): 747 [M+H$^+$], 466 747 [M-NTf$_2^-$], 233.8 [M-NTf$_2$+H$^+$]; $[\alpha]_D^{25}$= -38.45 (c=0.38, CHCl$_3$); gummy solid

General procedure for the Michael reaction addition with catalyst 1a e 1b

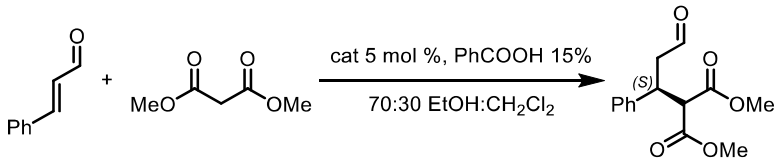

In a 2 mL vial, cat **1a-b** (0.005 mmol), EtOH (0.140 mL), CH_2Cl_2 (0.060 mL), cinnamaldehyde (0.1 mmol) and benzoic acid (0.015 mmol) are added. Then, dimethyl malonate (0.3 mmol) is added to the mixture, and the reaction is stirred at room temperature. After 18 hours, the reaction is quenched with saturated aqueous solution of NH_4Cl (0.200 mL). The aqueous phase is washed three times with CH_2Cl_2. The organic phases are then evaporated and the crude mixture is purified through silica gel chromatography (9:1 Cy:AcOEt). The product is obtained as a yellowish oil.

^{1}H-NMR (401 MHz, Chloroform-*d*) δ 9.59 (t, *J*= 1.7 Hz, 1H), 7.34 – 7.26 (m, 2H), 7.25 – 7.19 (m, 3H), 4.02 (td, *J*= 9.6, 9.2, 5.6 Hz, 1H), 3.79 – 3.71 (m, 4H), 3.50 (s, 3H), 3.08 – 2.66 (m, 2H). AM157

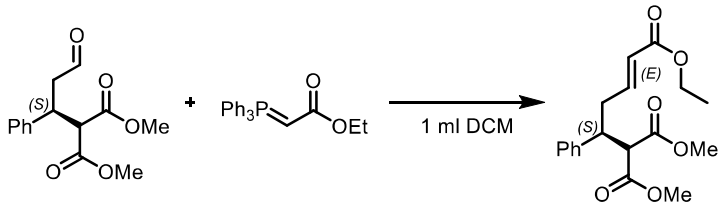

In order to permit the evaluation of the enantiomeric excess by means of a chiral stationary phase HPLC, the Michael addition product is derivatize with a Wittig reaction. Dimethyl (S)-2-(3-oxo-1-phenylpropyl)malonate (0,1 mmol), CH_2Cl_2 (1 mL) and ethyl 2-(triphenyl-l5-phosphaneylidene)acetate (1.1 eq) are added in a 5 mL vial. The reaction mixture is stirred at room temperature overnight, then the organic solvent is evaporated in vacuum. The crude is purified through a silica gel chromatography (CH_2Cl_2).

^{1}H-NMR (401 MHz, Chloroform-*d*) δ 7.32 – 7.24 (m, 2H), 7.24 – 7.13 (m, 3H), 6.68 (dt, *J* = 15.6, 7.4 Hz, 1H), 5.71 (dt, *J* = 15.6, 1.4 Hz, 1H), 4.11 (q, *J* = 7.1 Hz, 2H), 3.76 (s, 3H), 3.71 (d, *J* = 10.3 Hz, 1H), 3.56 (td, *J* = 9.8, 4.7 Hz, 1H), 3.45 (s, 3H), 2.70 – 2.51 (m, 2H), 1.22 (t, *J* = 7.1 Hz, 3H).

IC 80:20 hexane:*i*-PrOH T=40°C flux: 0.5 mL/min t'=19.5 t''=29.5'

General procedure for the α-benzoilation of aliphatic aldehyde

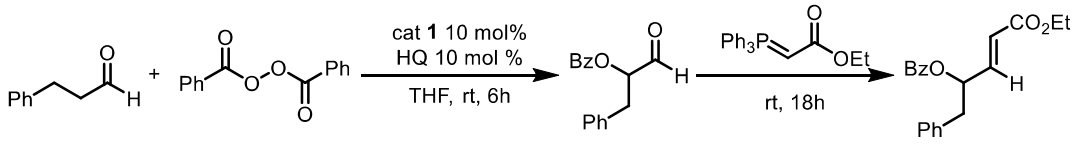

In a 2 mL vial, catalyst **1** (0.010 mmol, 0.1 eq), THF (0.500 mL), 3-phenylpropanal (0.1 mmol, 1 eq) and hydroquinone (0.010 mmol, 0.1 eq) are added. Last, benzoic peroxyanhydride (0.110 mmol, 1.1 eq) is added and the reaction mixture is stirred at room temperature for 6 hours. Then, the reaction is quenched with aqueous saturated NH_4Cl and the aqueous phase washed with EtOAc. The crude mixture is purified through silica gel chromatographic column (4:1 Cy:AcOEt).

In order to permit the evaluation of the enantiomeric excess by means of a chiral stationary phase HPLC, 1-oxo-3-phenylpropan-2-yl benzoate is derivatize by means of a wittig reaction. Ethyl 2-(triphenyl-l5-phosphaneylidene)acetate (1.1 mmol, 1.1 eq) is directly added to the reaction mixture, the reaction is stirred for 1 hour at room temperature. Then, the organic solvent are evaporated in vacuum, and the crude mixture purified through silica gel chromatography (9:1 Cy:AcOEt).

^{1}H-NMR (401 MHz, Chloroform-*d*) δ 8.03 (d, *J* = 6.9 Hz, 0H), 7.59 (td, *J* = 7.3, 5.4 Hz, 1H), 7.51 – 7.41 (m, 1H), 7.32 – 7.18 (m, 2H), 6.99 (dd, *J* = 15.7, 5.1 Hz, 0H), 5.99 (dd, *J* = 15.7, 1.6 Hz, 0H), 5.88 (qd, *J* = 6.8, 5.9, 1.6 Hz, 0H), 4.18 (q, *J* = 7.1 Hz, 1H), 3.16 (dd, *J* = 13.9, 7.1 Hz, 0H), 3.08 (dd, *J* = 13.9, 6.3 Hz, 0H), 1.30 (t, *J* = 6.4 Hz, 1H).

AD 95:5 1ml/min 40°C 210 lamda t'=8.3' t''=9.3'

Second part: Photocatalysis

Introduction

The sunlight is an inexhaustible source of energy that every day arrives on the Earth's crust. Due to the presence of ozone, oxygen, and of the other atmospheric components, the radiation that gets to the Earth is for the most composed of blue, green, and red wavelengths radiation (λ = 400-650). In nature, plants use sunlight energy to perform photosynthesis. Therefore, convert raw materials (CO_2 and water) into more complex molecules (carbohydrates). Fascinated by Nature, scientists have been tried to exploit solar radiation energy to permit chemical transformation since the early decade of the 18th century.[39] In 1790 the British chemist Joseph Priestley observed the photoinduced production of NO_2 from a solution of nitric acid. He observed that the yellow solution turned to red if exposed to sunlight and this is considered the pioneering experiment in the field of photochemistry. He also described the basic principle of photosynthesis, starting with the idea that sunlight could influence the plants' behavior. In the 19th century, several scientists focused their research on the discovering of light ability to permit chemical transformation. In particular, the German chemist Lieberman, performed the first [2+2] cycloaddition, being the first one to use artificial light to permit the reaction. The Italian founder of photochemistry is considered to be Alessandro Sestini, which faced the problem of light in the santonin reaction. Among Stanislao Cannizzaro they have been investigated this santonin photoreaction for more than 20 years. A student of them, Giacomo Ciamician was the first one to establish photochemistry as a science field of its own. He emphasized the importance of the future application of photochemistry in organic synthesis reactions and of light as important tools for the fuels industry.[39]

Light radiation is a primary energy source which permits to avoid harsh reaction conditions such as high temperature. Photons can provide enough energy to achieve the desired reactivity. Exploiting photocatalyzed methodologies, less reactive low-energy reagents could be activated with high chemoselectivity and functional group tolerance. It is a powerful tool for the development of a new shorter and green synthetic route.[83]

Until a few years ago, most of the reported researches were focused on the direct photoexcitation methodology. In the direct photoexcitation, the photoexcited molecule is a reactant or an intermediate. Therefore, the photoexcited species is the same one

that is subjected to a chemical transformation. To permit it, the involved organic molecule must be able to absorb light. Most of the organic compounds do not absorb at the available solar radiation wavelengths (λ = 400-650). Usually, they absorb at lowers wavelengths (λ = 250-300) which usually are filtered by atmospheric components. Also, the molecule must absorb light efficiently, to exploit as much as possible of the involved radiation. These two characteristics severely restrain the number of substrates that could be involved. This way, the development of new procedures is limited.

The photocatalytic process, instead, exploits the presence of a molecule which is photoexcited at the available solar radiation wavelengths (λ = 400-650). It catalyzes the chemical transformation regenerating itself, and it is named photocatalyst. As far as nowadays knowledge, the excited photocatalyst can promote the reaction in three different ways:[84]

- photosensitization (PS): physical energy is transferred from the excited species to an acceptor.
- Atom transfer (AT): the excited species can abstract an atom from a donor, often is a hydrogen atom transfer (HAT).
- photoinduced electron transfer (PET or SET): the photoexcited molecule can act both as oxidant and reductant, depending on the reaction environment.

Photocatalytic strategy permits to develop of a broad scope of photoinduced chemical reactions. In 2008, MacMillan and co-workers reported the photocatalyzed asymmetric alkylation of aldehydes, involving $[Ru(bpy)_3]Cl_2$ as a photocatalyst (Scheme 24, left).[35] Simultaneously Yoon and co-workers described an [2+2] enone cycloadditions photocatalyzed by $[Ru(bpy)_3]Cl_2$ (Scheme 24, right).[85]

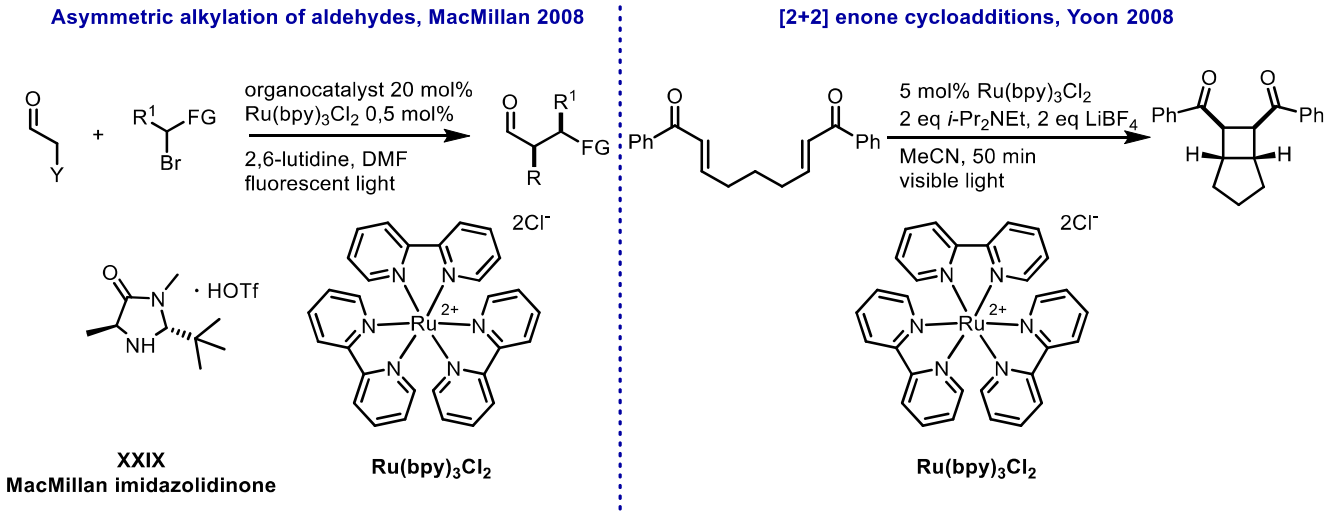

Scheme 24: Asymmetric alkylation of aldehydes, MacMillan 2008 [2+2]; Enone cycloadditions, Yoon 2008

Inspired by those two works, numerous photocatalyzed reactions have been developed since then.[86,87] These reactions are usually high regioselective and sometimes the final products can be obtained in the diastereoselective and enantioselective form. [88] In this chapter, photophysical processes that occur in a photoinduced reaction are concisely described. In detail, the attention is focused on the single electron transfer methodology (SET), since it is the one involved in this work of thesis.

Jablonski diagram[89]

The main photophysical processes that happen when a molecule is irradiated can be explained utilizing the Jablonski diagram (Figure 14).

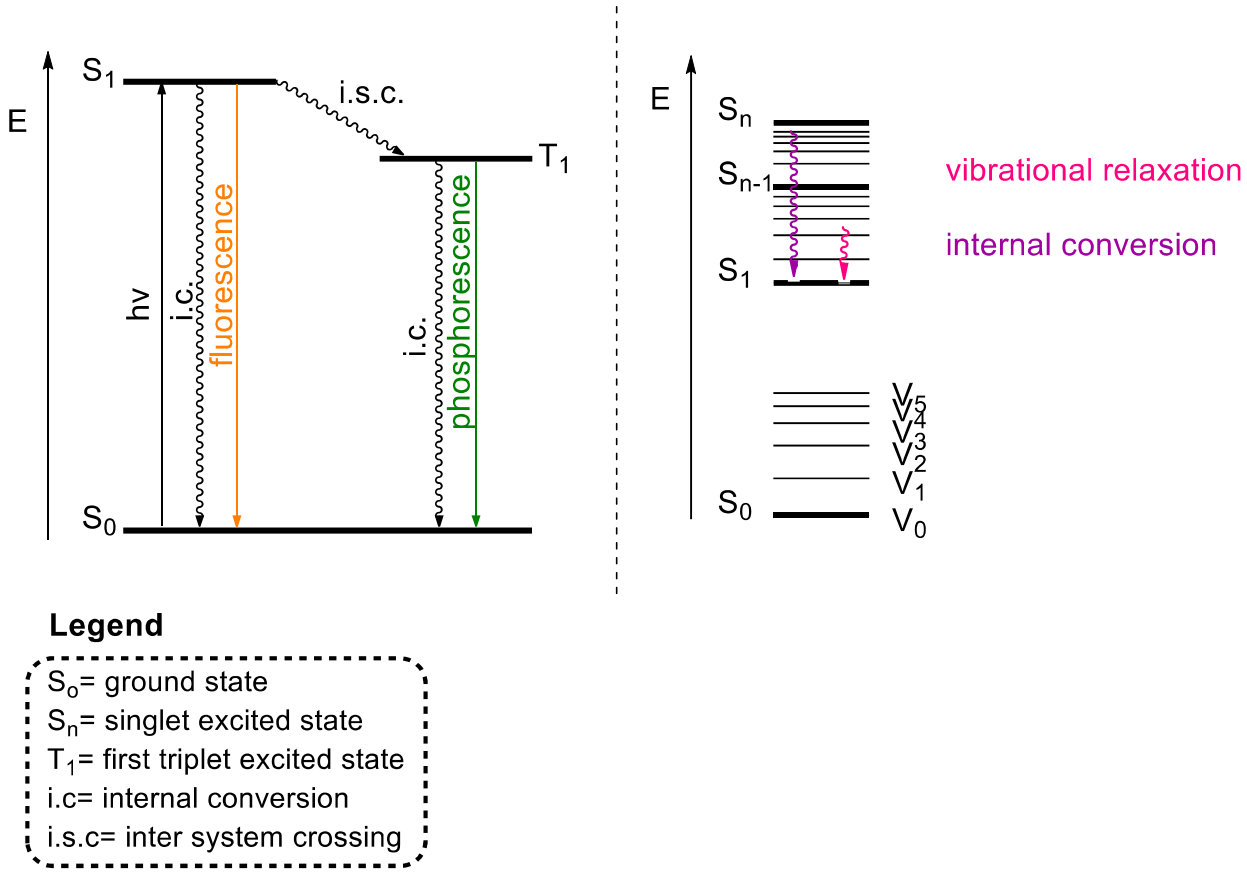

Figure 14: Jablonski diagram

When a molecule is irradiated with light of the required energy ($h\nu$), it absorbs energy and shifts from its electronic ground state ($\mathbf{S_0}$) to an electronic singlet excited state ($\mathbf{S_N}$). In this process, the radiation energy must at list correspond to the energetic difference between the ground state ($\mathbf{S_0}$) and the first electronic singlet excited state ($\mathbf{S_1}$).

Depending on the radiation energy, the molecule can reach different electronic excited states. However, the lifetimes of the excited states higher than $\mathbf{S_1}$ are short due to vibrational relaxation of the molecule itself. Therefore, the energy of $\mathbf{S_1}$ is usually the highest energy available to be exploited in the reaction. Vibrational relaxation is the fastest method for a molecule to dissipate the absorbed energy (Figure 14, right). It is a non-radiative process, in which the absorbed energy is converted into kinetic energy through vibrational modes. The dissipated energy can stay within the molecule itself or be transferred to other molecules in the environment. It is a very fast process that occurs between different vibrational levels in the same electronic state.

However, the excited electron could also be transferred from a vibrational level in $\mathbf{S_n}$, to another vibrational level in $\mathbf{S_{n-1}}$ through dissipation of kinetic energy. In this case, the

process is called internal conversion (i.c.), a spin-allowed non-radiative process (Figure 14, right). The higher is the energy of the electronic level, the higher is the probability of internal conversion to occurs. Usually, the energy gap between S_1 and S_0 is high. Thus internal conversion among these two electronic states is less probable and the excited state lifetime longer.

In addition to vibrational relaxation and internal conversion, other radiative or no radiative processes can undergo from S_1. The quickest radiative transition that may happen is the fluorescence (Figure 14, left). It is a spin-allowed process in which a photon is emitted from the molecule to dissipate the energy absorbed. It often occurs between the S_1 and the S_0 since at higher excited states the energy is often dissipated through internal conversion and vibrational relaxation. The energy of the photon emitted is as high as the difference between S_0 and S_1.

Another possible route is the intersystem crossing (i.s.c.), a spin-non-allowed no radiative process (Figure 14, left). Through it, the excited electron goes from the singlet state S_1 to the triplet state T_1. Basing on the electronic selection rules, this transition is forbidden. However, under some special vibrational and electronic circumstances, it is slightly permitted.

At last, the energy can be dissipated through a spin-non-allowed radiative transition, the phosphorescence (Figure 14, left). In this latter process, the excited electron goes from the T_1 to S_0 and the energy is dissipated through photon emission. In this case, the energy of the photon emitted is as high as the difference between S_0 and T_1.

The molecule used as a photocatalyst must have a long-lived excited state (triplet or singlet). In this way, it could be quenched by another species and catalyze the chemical transformation. Moreover, its absorption spectra must not overlap with those of reactants and products, thus avoiding their degradation in the reaction media.

Photosensitization (PS)[90]

As above mentioned, three different ways are possible to catalyze a photochemical transformation,PS, PET and HAT. It should however be outlined that most of the photocatalysts could act both via energy transfer process and electron via transfer

process. Thus, it not always easy to understand the true mode of action of a new transformation.

The PS catalytic process involves an energy transfer from a donor (**D**) to an acceptor (**A**).

$$D^* + A \rightarrow D + A^*$$

The donor is always the excited species (photosensitizer). Through the energy transfer **D*** is deactivated to a lower or ground energy state. At the same time, the acceptor is exited to a higher energy state (S_1). As described by the Jablonsky diagram (Figure 14)[91], the excited species could now return to its ground state S^0 via internal conversion or fluorescence, or could undergo intersystem crossing to its triplet state T^1. This triplet state has a relatively long life since the radiative emission is spin-forbidden and the non-radiative decay slows (see Jablonski diagram paragraph). At this stage, two different energy transfer mechanisms are possible: the Foster and the Dexter ones (Scheme 25).

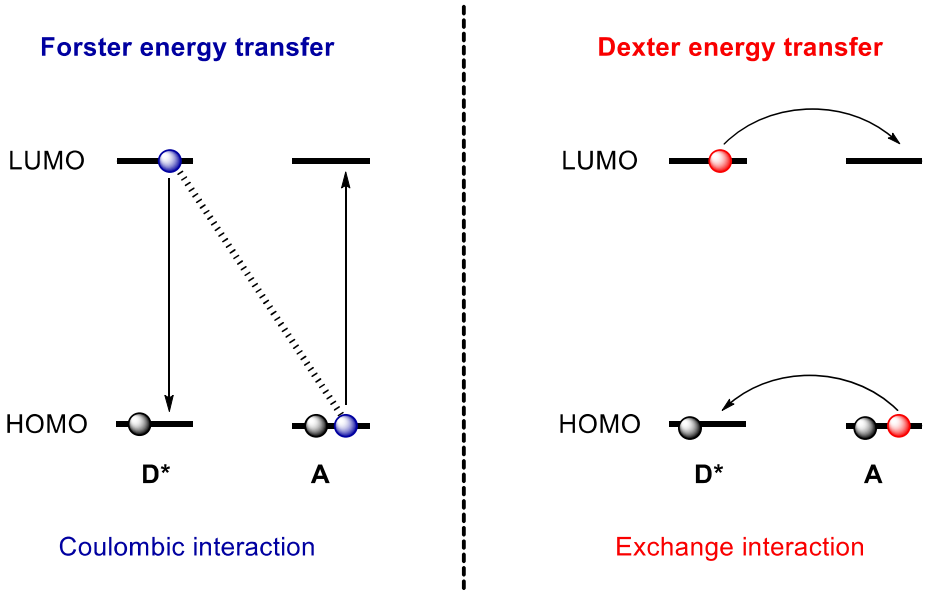

Scheme 25: Foster energy transfer; Dexter energy transfer

The Forster energy transfer (Figure 25, left) process proceeds through coulombic interactions (dipole-dipole) via a transmitter antenna mechanism.[92] The excited state oscillation of **D*** causes a dipole and conseguently electronic oscillation in the ground state of **A** by creating electronic repulsion. This resonant interaction could lead to the desired energy transfer. By this way, **A** is promoted to his excited state **A*** and **D*** returns in ground state **D**. There is no exchange of electrons in this process. However,

the Foster mechanism would involve two different spin reversal processes, which would violate Wigner's spin conservation rules. Therefore, it is unlikely to happen in photocatalytic transformation.

The second mechanism is the Dexter process (Figure 25, right), in which a mutual exchange of electron occurs after the photosensitizer excitation.[93] This second pathway is strongly dependent on the spatial proximity between the donor **D*** and the acceptor **A**. Here, intimate physical contact between **A** and **D*** is required. Indeed, a collision complex is formed among the two species, and the process efficiency depends on numerous factors (Scheme 26).

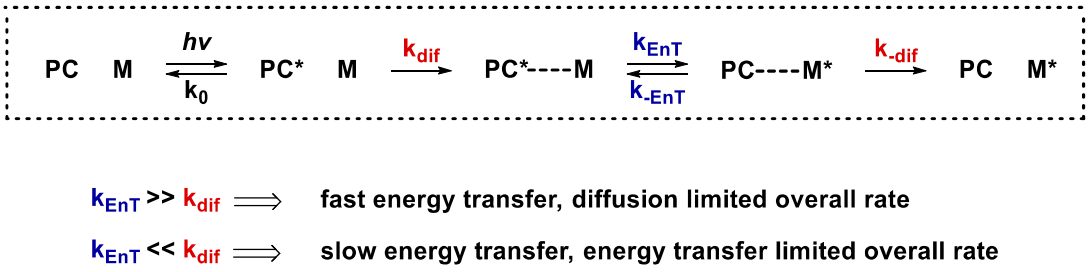

Scheme 26: Dexter energy transfer mechanism

The steric repulsion between **D*** and **A** orbitals, strongly affects the energy transfer kinetics (k_{EnT}), therefore the process efficiency.[94] Also, the spectral overlap integral in D* and A emission/absorption spectra is fundamental. It represents the number of T_1-S_0 transitions of **D*** which can energetically induce a S_0-T_1 transition in **A**. Consequently, major is the overlap, major is k_{EnT}.

When considering the Dexter mechanism, the diffusion rate constant of **D*** and **A** in the reaction media has to be considered to calculate the efficiency of the overall process. Depending on k_{EnT}, the diffusion contribution (k_{dif}) could be approximated or not. Fastest is the energy transfer in the collision complex, lower will be the influence of diffusion in the overall rate.

Certainly, a lot of variables have to be taken into account when considering the energy transfer process. On the other hand, numerous organic transformations have been developed exploiting it, and it is considered a useful tool for future development in the organic field.

Hydrogen atom transfer photocatalysis (HAT)[95]

The hydrogen atom transfer photocatalysis involves the concerted movement of a proton and an electron between two substrates in the same kinetic step. The photocatalyst is responsible for the generation of an active intermediate through the homolytic rupture of an A-H bond. Thus, the newly formed **A•** radical species is activated to perform chemical transformations.

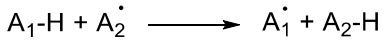

The developed HAT transformation could be divided into two categories depending on the mode of activation: direct activation or indirect activation.

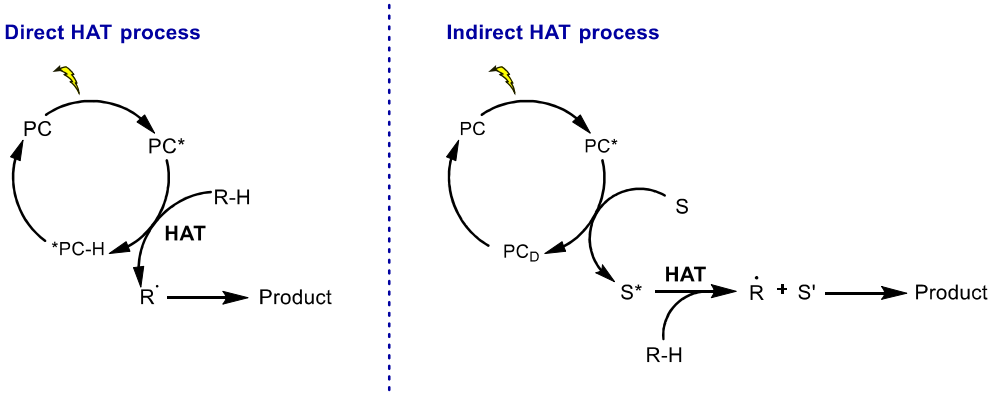

***Scheme 27**: HAT direct and indirect activation*

The direct activation is based on the ability of the photoexcited catalyst **PC*** to directly cause the homolytic cleavage of an R-H bond by hydrogen atom abstraction (Scheme 27). The newly generated activate species **R•** is now able to reach with other species to form the desired product. Finally, **•PC-H** retrodonates the hydrogen radical **H•** to an intermediate of the reaction mechanism. Hence, **PC** is restored, and the catalytic cycle is closed. However, so far, the number of photocatalysts able to promote direct activation is strictly limited.[96]

Due to the few photocatalysts able to catalyze a direct HAT activation, the indirect HAT activation has been deeply investigated in the last years (Scheme 27). This approach exploits a species able to promote the hydrogen atom transfer process upon activation by the photocatalyst **PC**. This way, various photocatalysts can be involved in the process, since the HAT is performed by the additive **S**. The HAT photocatalysis permit the

generation of a large library of radical in mild conditions. However, most of the developed transformations include the formation of nucleophilic radicals.

Photoinduced single electron transfer reaction (PET or SET)

The single electron transfer methodology involves the exchange of an electron from a species in its excited state to a species in the ground state (Figure 15). As previously mentioned, when a molecule is irradiated and absorbs light energy, it goes from its ground electronic ground state $\mathbf{S_0}$ to one of its excited states $\mathbf{S_n}$. This means that one electron goes from its ground state orbital to one at higher energy. Within this process, a change in the electronic proprieties of the molecule is made. Its ionization potential value is lowered, and its electronic affinity is enhanced.

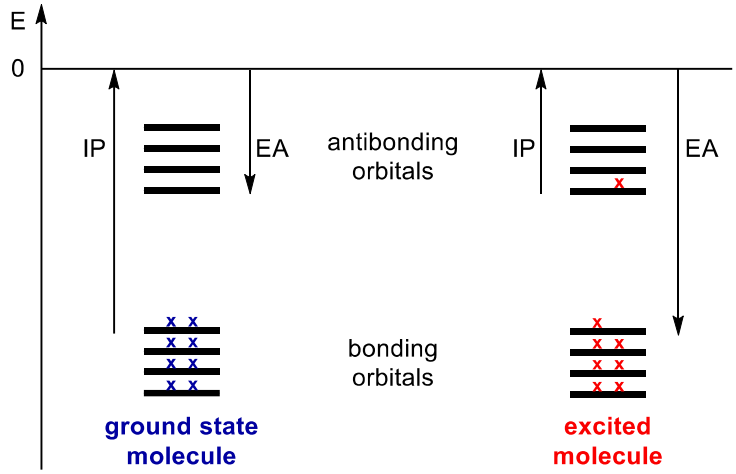

Figure 15: Difference between electronic properties of ground state molecule and excited state molecule

Therefore, its redox properties drastically change, and the molecule becomes both a better electron donor and electron acceptor.[38]

The excited state redox potentials can be calculated employing the Rehm-Weller equation:

$$(1) \quad E^0(A^+/A^*) = E^0(A^+/A) - E_{00}(A^*/A)$$
$$(2) \quad E^0(A^*/A^-) = E^0(A/A^-) + E_{00}(A^*/A)$$

Equation 1: Rehm-Weller equations

In this equation, E_{00} (A*/A) represents the potential corresponding to the electronic energy of the excited state. It can be calculated from the emission spectra of the irradiated molecule. Meanwhile, E^0 (A/A^-) and E^0 (A^+/A) correspond to the redox potential of the compound in its ground state. To elucidate the equation meaning and

the changes in the redox properties of the molecule, an example is described (Scheme 28).

$[Ru(bpy)_3]^{2+}$ is one of the most extensively used photocatalysts for organic synthesis reactions (Scheme 28). Taking inspiration by MacMillan[35] and Yoon's[85] researches, a lot of studies involving $[Ru(bpy)_3]^{2+}$ as photocatalyst has been published in the following years.[39,86] Thus, this Ru complex has been widely studied in all its chemical and physical properties. In Scheme 28 are summarized the electronic potential of $[Ru(bpy)_3]^{2+}$ in its different states and the correlation between them.[38]

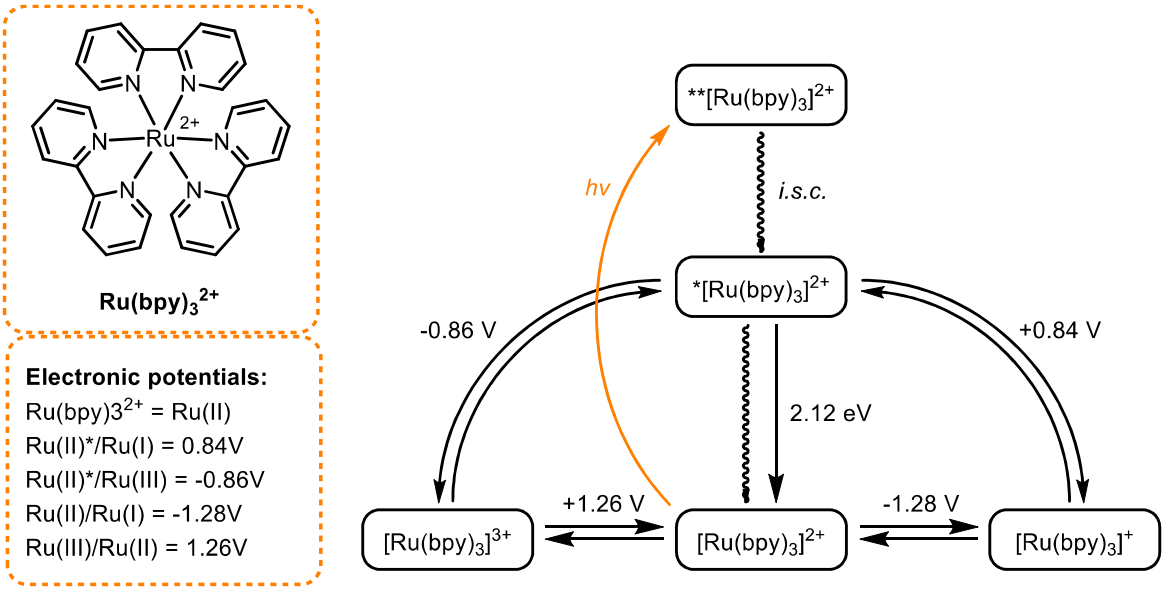

Reduction potentials are referred to NHE. bpy=2,2'-bipyridine.

Scheme 28: $[Ru(bpy)_3]^{2+}$ reduction potentials[38]

Once **$[Ru(bpy)_3]^{2+}$** is irradiated with 452 nm wavelength radiation, it achieves its singlet excited state **$^{**}[Ru(bpy)_3]^{2+}$**. This is a short-lived state. Intersystem crossing occurs rapidly to bring the complex to its triplet excited state **$^{*}[Ru(bpy)_3]^{2+}$**. Here the complex could return to its ground state through radiative or not processes. However, **$^{*}[Ru(bpy)_3]^{2+}$** lifetime is long enough for it to be quenched from a different molecule presents in the nearest environment. The reported data shows that the energetic difference among the ground state (**$[Ru(bpy)_3]^{+}$**) and **$^{*}[Ru(bpy)_3]^{2+}$** is 2.12 eV (Scheme 28. This value represents the equation addend E_{00} (A*/A). From Scheme 28, the differences between redox potential in the excited state and the ground state are outlined.

It is common knowledge that the change in the Gibbs free energy in a thermodynamically feasible reaction must be minor to zero. Photoredox reactions are not an exception to this rule. Thus, it must be applied in the development of a SET synthesis. The Gibbs free energy value depends on the redox potential of the reaction partners (E_{OX} and E_{RED}) and the coulombic interactions between the two radical ions (ΔC) (Equation 2). ΔC depends on the solvent of the reaction and, at first approximation, can be ignored. Therefore, in the case of a reaction that involves the oxidation of D and the reduction of A*, the oxidation potential of D should be lower than the reduction potential of A* ($E_{OX}(D)<E_{RED}(A^*)$).

$$A^* + D \rightarrow A^- + D^+$$

$$\Delta G = E_{OX}(D) - E_{RED}(A^*) + \Delta C$$

$$E_{OX}(D) < E_{RED}(A^*)$$

Equation 2: Gibbs energy in irreversible transformation

Photocatalytic cycles for SET transformations

Numerous catalytic cycles for the photoinduced single electron transfer catalysis (SET) have been developed in recent years, involving different pathways. However, all the already reported cycles can be divided into two main categories. The ones that exploit the reductive quenching of the catalyst (Scheme 29, left) and the ones that involve oxidative quenching (Scheme 29, right).

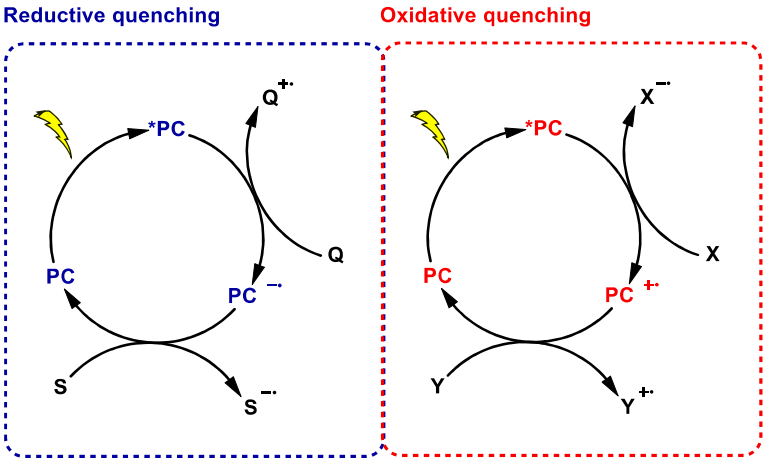

Scheme 29: General scheme for the photoredox reductive quenching and oxidative quenching catalytic cycles

In the reductive quenching (Scheme 29, left), the reaction mixture is irradiated, and consequently, the photocatalyst shifted to its excited state ***PC**. An electron donor **Q** is

involved, and a SET occurs to reduce the excited photocatalyst ***PC** and form **PC$^{-\bullet}$**. In the meantime, **Q** is oxidized to form **Q$^{+\bullet}$**. Ultimately, an electron acceptor **S** is employed to regenerate the original form of the catalyst **PC** and close the cycle.

In the oxidative quenching (Scheme 29, right), a SET occurs among the excited photocatalyst ***PC** and electron acceptor **X**. The catalyst remains in his oxidized form **PC$^{+\bullet}$**. Meanwhile, **X** is reduced to **X$^{\bullet-}$**. Thus, **PC*** is quenched in an oxidative manner. At this point, an electron donor **Y** is involved to restore the original form of the catalyst and close the catalytic cycle.

Both this category can be developed in different manners. In some cases, a sacrificial agent could be utilized to restore the photocatalyst original form and to close the catalytic cycle (Scheme 30, left). In other situations, the sacrificial agent is not necessary (Scheme 30, right). Two examples are described for better comprehension.

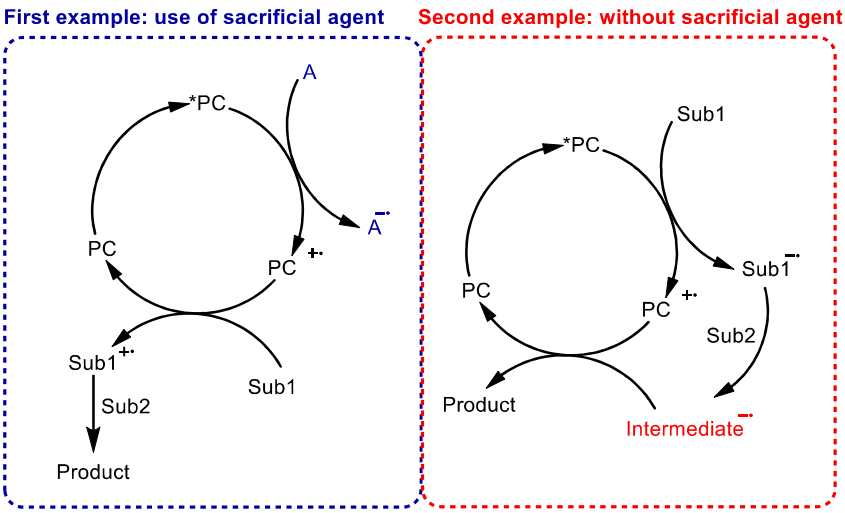

Scheme 30: Photoredox catalytic cycles with the use of a sacrificial agent (left) or without (right)

The first example is an oxidative quenching type which exploits a sacrificial oxidant molecule **A**. Indeed, ***PC** is oxidized by **A** to form **PC$^{+\bullet}$** (Scheme 30, left). Then, a SET occurs among **PC$^{+\bullet}$** and the substrate **Sub1.** Radical cation **Sub1$^{+\bullet}$** is thus generated and catalyst original form **PC** restored. **Sub1$^{+\bullet}$** reacts with a second substrate **Sub2** to obtain the desired product. Through this pathway, the initial form of the photocatalyst is restored and the cycle can start again. The involved sacrificial agent does not directly participate in the final product construction. But it is fundamentally to permit the catalyst regeneration. The species produced from its reduction is considered a waste and it diminishes the reaction total (atom) economy. Frequently, the sacrificial agent needs

to be used in a stoichiometric amount. It must be inexpensive and easily available. Additionally, it must not affect product formation.

The second example is still an oxidative quenching type, yet in this case, no sacrificial agents are involved (Scheme 30, right). Indeed, the catalyst **PC** is irradiated and photoexcited to form ***PC**. Then it is oxidized by a first substrate. This way the oxidized **$PC^{+\bullet}$** and a reactive radical anion **$Sub1^{-\bullet}$** are generated. The last one reacts with a second substrate **Sub2** to produce a radical ion intermediate. At this point, a SET occurs among **$Intermediate^{-\bullet}$** and **$PC^{+\bullet}$** to form the final product and restore the catalyst. Theoretically, in this mechanism, there are no wasted molecules. The atom economy of the reaction should be higher than the one in which the sacrificial agent is involved.

In conclusion, these are only two of the numerous kinds of photocatalytic cycles that can be designed for a photoredox reaction. Each one of them can be useful for the synthesis of important building blocks or final products.

Efficient photocatalyst for SET transformations

In single electron transfer photoredox catalysis, the efficiency of the photocatalyzed process depends on various stages:[94]

(i) **PC** has to be excited by photons absorption (k_0).

(ii) **PC*** and the substrate **M** have to form a precursor complex **PC*-M** (k_d).

(iii) The excited stated photocatalyst could be quenched by the substrate and return to his ground state (**PC-M***) (k_q).

(iv) The two species have to diffuse apart to avoid a retrodonation (k_{esc}).

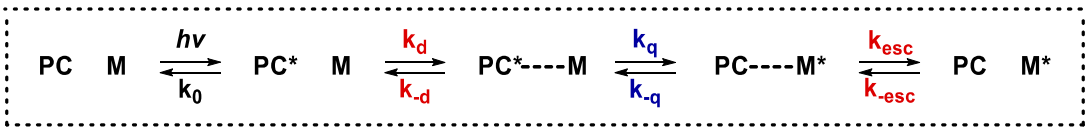

Scheme 31: Mechanism of photocatalyst quenching

Fundamental for the success of the photocatalytic transformation is the use of the correct photocatalyst.[97] The involved photocatalyst should:

(i) Have good absorption.

(ii) Absorb at different wavelengths compared to the involved substrates.

(iii) Have a high yield in the formation of the excited state upon photon absorption.

(iv) Photochemical and electronic reversible behavior is necessary.

(v) It should not degrade in absence of a quencher.

(vi) The excited it should live long enough for the substrate to diffuse and complex it.

(vii) Ideally, the electronic properties of the catalyst should be easily tunable by little modifications on the molecular structure. This way numerous different transformations could be achieved with the same catalyst's scaffold.

During the last decade, numerous photosensitizers have been applied to the photoredox catalyzed organic synthesis. Among the high number of photocatalysts designed, it is necessary to mention the polypyridyl complexes of iridium metal (Figure 16). They strongly absorb visible light, rendering easy their selective excitation in an organic reaction mixture. Indeed, usually organic substrates do not absorb at visible light wavelengths. Their excitation efficiency is about 100% and the lifetimes of the excited states are long enough to permit them to be quenched by the organic substrate.[38,97,98] Moreover, they are stable toward chemical and thermal decomposition and exhibit reversible electrochemical properties. At last, depending on ligands structure, complex electrochemical properties can be easily tuned.[99–101] Generally, lowering the electron density on the metal, the oxidative power of the complex in the excited state increases. Conversely, increasing the electron density on the metal, the reductive power of the complex increases (Figure 16).

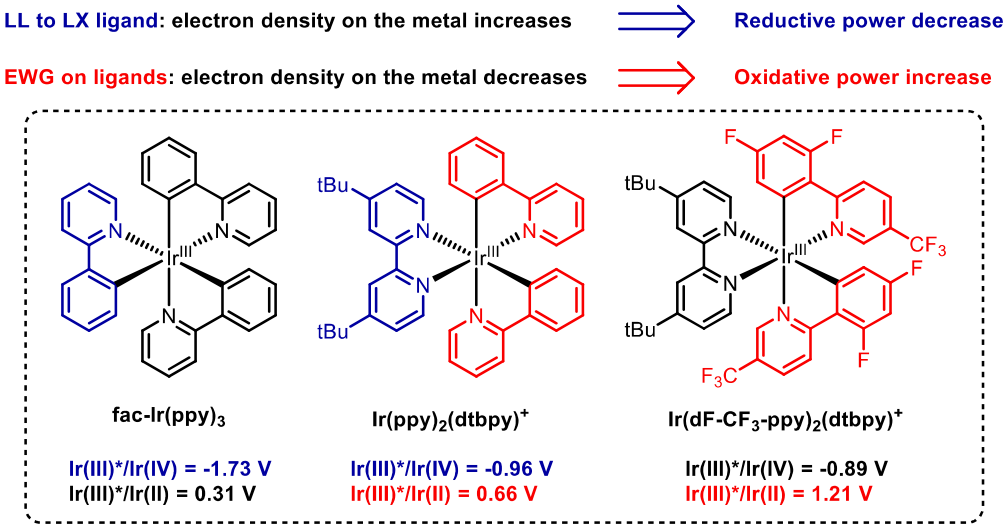

Figure 16: Common Iridium complex photocatalysts and the correspondent potentials

Photocatalyzed microflow technology

The conversion of the photocatalytic approach from a laboratory scale to a larger industrial scale has been the focus of various researches.[102] Since irradiation is mandatory for reaction performance, an efficient irradiation system has to be constructed. The entire reaction mixture should be equally irradiated. According to Lambeer-Beer law (Equation 3), there is a decrease in photonic energy profile along the path length due to the absorption of the photons.

$$A = \varepsilon l c$$

Equation 3: Lambeer-Beer law

Lambeer-Beer law calculates the absorbance (A) depending on the absorptivity (ε), which is specific to the attenuating species, the optical length (l), and the concentration of the involved species (c). The absorbance represents the quantity of light that is absorbed by a specific amount of a species in a determined optical length. The major is the absorbance, the minor will be the transmittance (T). Transmittance represents the ratio of the transmitted intensity (I) over the incident intensity (I_0). Thus, minor will be the intensity of the radiation that reaches the considered distance.

$$A = -\log T$$

$$T = I/I_0$$

Equation 4: Definition of Absorbance and transmittance

Therefore, in a batch system, only the external molecule will receive much of the irradiation. Meanwhile, no photon will arrive in the center of the reaction vessel. This effect eliminates the possibility of increasing the reaction scale to an industrial scale.

To overcome this problem, the number of photons irradiated could be raised. But then, this would diminish the irradiation efficiency. In addition, too powerful photon source could promote different reaction pathways. This would affect the process selectivity or provoke an overheating in the reaction mixture. The reactant concentration could also be lowered. This would cause a decrease in process productivity and at the same time an increase in the solvent volume. The best way to overcome the problem is to apply photocatalyzed microflow technology.[103–106] Employing the flow technology. The diameters of the involved reaction apparatus are minimized, and so it is the pathway o

the light radiation. Consequently, the irradiation in the reaction mixture is uniform and the efficiency of the irradiation is maximized. This way, the necessary reaction time could be reduced compared to batch technology and productivity increased.[107] Uniform light irradiation on all the reaction media could permit to use of lower catalytic loading without affecting the transformation yield.

In addition, the mixing efficiency is well defined by the high volume/surface ratio and reaction time controlled by the specified flow rate. Hence, a major control on those parameters is achieved.[108] A more homogeneous solution could improve the process yield toward the preferred product, avoiding other undesired reaction pathways and so increasing the procedure selectivity.

Performing the reaction in flow conditions could also be an advantage from a safety point of view since reactors with high amount of solvent are avoided. A small reactor size would bring to less severity in case of accidents. [109] Furthermore, mass and heat transfer rates are higher in flow technology compared to the batch one. Thanks to the lowest reactor volume and high surface, thermal control on the reactor easier achieved increasing the safety of the process.

For these reasons, flow technology in photocatalyzed transformation is considered the most powerful tool for the application of laboratory developed methodology to an industrial scale. Thanks to the continuous development in the photocatalytic field and the concerned light technologies, the applicability of this approach is day by day wider. In the future, it may be possible to exploit sunlight irradiation to perform various photocatalyzed transformation.[106]

A supramolecular bifunctional iridium photoaminocatalyst for the enantioselective alkylation of aldehydes[110]

In 2008, MacMillan reported the first photoredox catalyzed asymmetric α-alkylation of aldehydes.[35] The reported transformation represented the first synergistic system of organocatalysis and photoredox catalysis. Both ruthenium photosensitizer $Ru(bpy)_3^{2+}$ and MacMillan imidazolidinone **XXIX** organocatalyst actively catalyzed the reaction. The asymmetric α-alkylation of aldehydes and ketones has become rapidly an attractive topic for synergistic photoredox catalysis, and diverse dual catalytic systems based on other photocatalysts (metal complexes[111], semiconductors[112,113], and organic dyes[114]) were developed. In the development of the synergistic catalyzed transformation, he started from the newly SOMO (Single Occupied Molecular Orbital) organocatalytic activation mode.[34,36,37]

The merging of SOMO organocatalysis and photoredox activation permitted to avoid the use of stoichiometric oxidant reactants. The transformation mechanism is described in Scheme 32. The dual catalyzed transformation relies on the photoexcitation of $Ru(bpy)_3^{2+}$ to populate the $*Ru(bpy)_3^{2+}$ excited state. At this point, the excited species $*Ru(bpy)_3^{2+}$ oxidize a sacrificial quantity of the *in situ* formed enamine **XXX** to provide the reductant species $Ru(bpy)_3^{+}$ (–1.33 V versus SCE in CH_3CN). At this point, $Ru(bpy)_3^{+}$ reduces the phenacyl bromide **XXXI** (–0.49 V versus SCE in CH_3CN). Hence, the corresponding electron deficient radical **XXXII** is generated, and $Ru(bpy)_3^{2+}$ is restored. The alkylation step is thus formed through the addition of the SOMOphilic enamine **XXX** to radical **XXXII**. This coupling would create an electron-rich α-amino radical **XXXIII**, a single electron species with low barrier to oxidation (–0.92 to –1.12 V versus SCE in CH_3CN). A SET between the oxidant $*Ru(bpy)_3^{2+}$ and **XXXII** permits then to obtain the iminium species **XXXIV**, which is subsequently hydrolyzed to restore organocatalyst **XXIX** and obtain enantioenriched α-alkylated **XXXV**. The stereoinduction of the process depends on the organocatalyst involved in the reaction, in this case the second generation imidazolidinone catalyst **XXIX**.

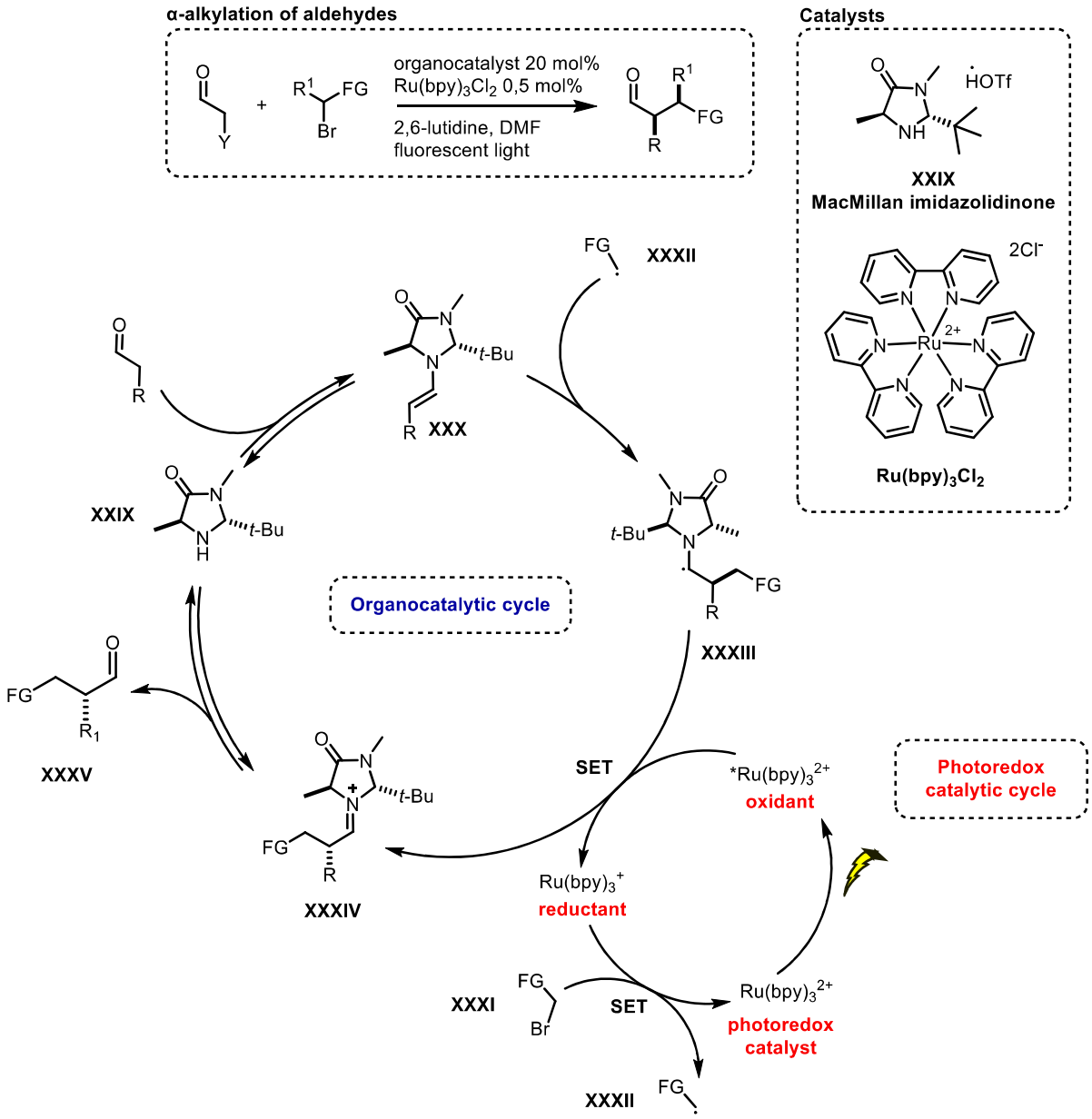

Scheme 32: Mechanism of the photo- organocatalyzed α-alkylation of aldehydes

The developed approach avoids the use of heating or cooling apparatus and a stoichiometric amount of metal reactants. Moreover, it involves commercially available components.

It is also worth mentioning that the chiral enamine, transiently formed during the catalytic cycle, can behave as an effective photocatalyst able to promote the α-alkylation of aldehydes.[115] However, the nucleophilicity of enamines[116] seems to be relevant to these applications, and as imidazolidinones are forming less nucleophilic enamines[117], the possibility of employing these organocatalysts without the presence of an active photocatalyst has not yet been demonstrated.

Recently, Alemán and co-workers reported the development of a general photo-organocatalyst for the α-alkylation of aldehydes (Scheme 33).[118] They studied the design of an effective bifunctional photoaminocatalyst, capable of performing the photoredox process and forming an active enamine intermediate simultaneously. In the designed photoaminocatalyst **XXXVI**, the two different moieties (photosensitizer and aminic one) act in accordance with the original mechanism proposed by MacMillan. It is noteworthy that the nature of the substitution on the imidazolidinone scaffold proved to be determinant for the success of the enantioselective α-alkylation. Indeed, poor results were obtained modifying the *tert*-Butyl substituent. In addition, as with the MacMillan 2nd generation imidazolidinone catalyst, the epimer of the successful catalyst (*cis* form) resulted in scarce formation and enantioselection on the product.

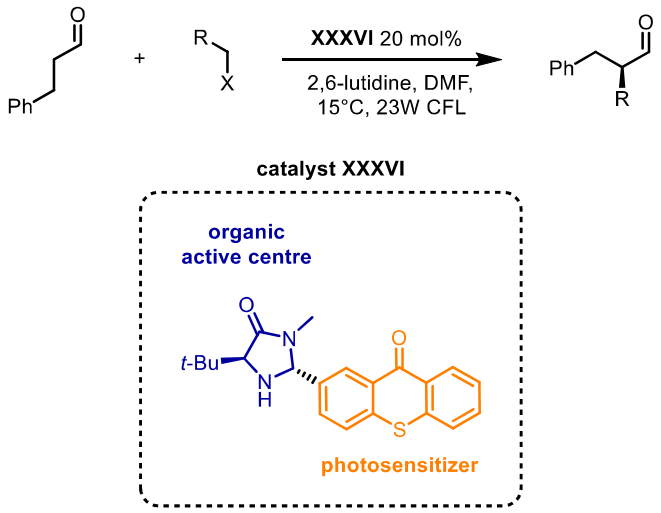

Scheme 33:Alemàn photoaminocatalyst

As far as our knowledge, this was the first example of a bifunctional photoaminocatalyst involved in this type of dual catalyzed transformation.

Aim of the project

The aim of the developed project is the synthesis and characterization of a bifunctional photoaminocatalyst and the comparison of the catalytic activity of this hybrid system with the classic dual catalytic system[35]. The proximity of the metal photosensitizer to the organic catalyst could permit new transformations or improve the already described ones. For the design of the new iridium photoaminocatalyst, various issues have been considered. As a primary instance, a long-lived excited state iridium photocatalyst had to be chosen to be incorporated in the hybrid metal-organo-catalyst. Secondly, the

chosen organic chiral scaffold had to be able to form reactive enamines and to induce stereoselection in the final reaction product. Finally, a facile system for the conjugation of the metal photosensitizer and the chiral amino organocatalyst in the same supramolecular system had to be developed. So, a versatile and modular approach could be further tuned. Different photoaminocatalysts have been synthesized and characterized to study the influence of different amino group in the photochemical properties and the photocatalytic activity.

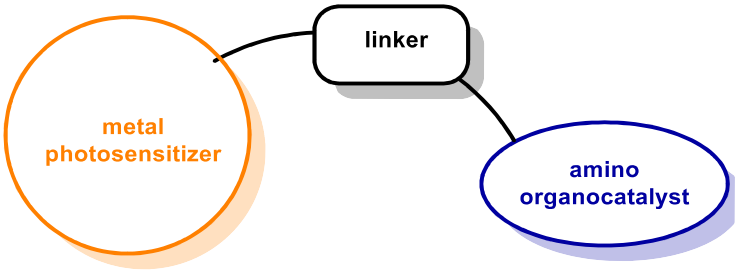

Figure 17: Elements of the designed supramolecular bifunctional iridium photoaminocatalyst

Successively, the catalysts have been tested in the enantioselective α-alkylation of aldehydes, benchmark reaction for the dual catalytic system secondary amine-photosensitizer. The activities of the developed hybrid metal-organic-catalysts have been compared with the dual catalytic ones optimized by MacMillan and co-worker in 2008.[35]

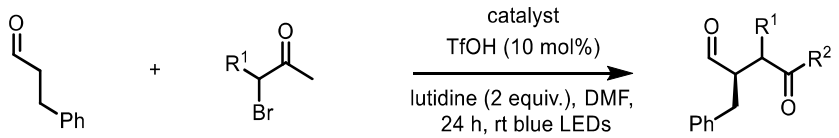

Scheme 34: Enantioselective α-alkylation of aldehydes

Finally, a mechanistic investigation has been performed to better understand the difference between the designed catalysts and to comprehend the photocatalytic reaction catalytic cycles.

Discussion and results

Inspired by a recent work on the preparation of artificial photosynthetic dendrimers[119], we decided to bind the azido-substituted iridium photo-sensitizer **13** to some suitably functionalized representative organocatalysts, exploiting a click-chemistry approach. The general synthetic strategy used for the preparation of iridium bifunctional photoaminocatalyst **13** through CuAAC (Copper-catalysed azide-alkyne cycloadditions)

is outlined in Scheme 35 Due to the requirement of mild reaction conditions, CuAACs have been largely used to couple different groups onto ruthenium(II) polypyridyl-type sensitizers[120]. Three different enantiopure secondary amines have been chosen as reaction partners: two different MacMillan oxazolidinones derivatives (**14a** and **14b**)[13] and a pyrrolidine derived from Maruoka 2-triphenylmethyl pyrrolidine (**14c**)[46,47].

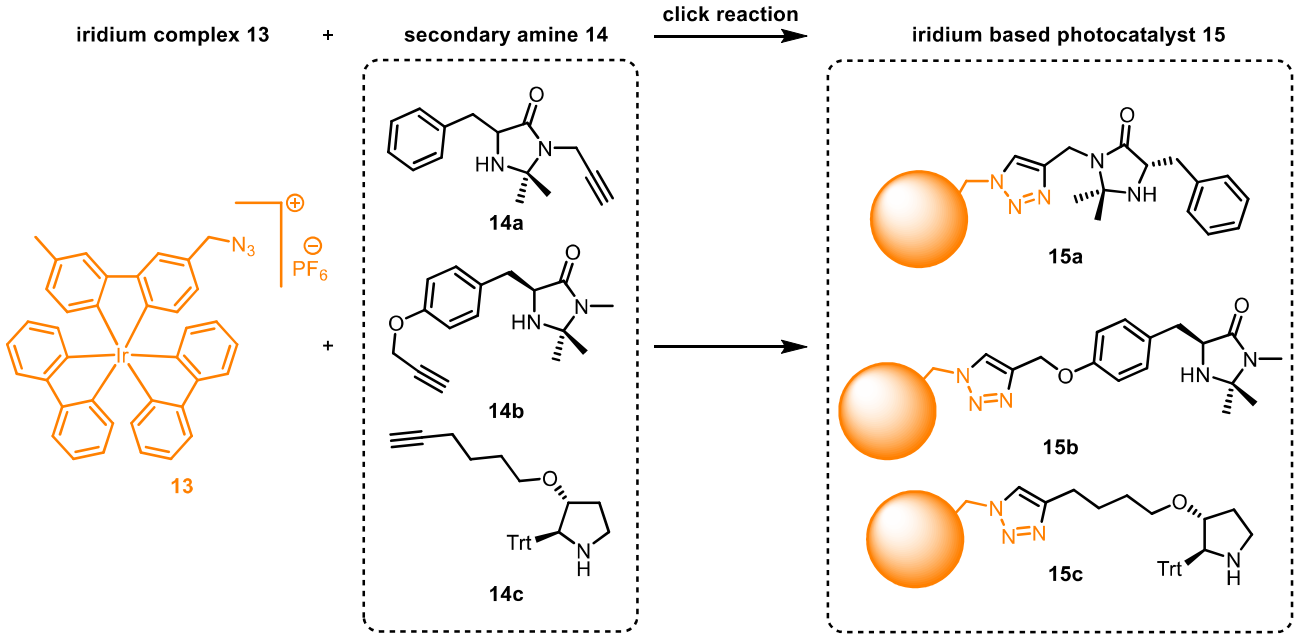

Scheme 35: strategy for the synthesis of supramolecular iridium based photoaminocatalyst

At first, the selected iridium complex has been synthesized following the procedure reported in 2015 by Zhang and coworkers (Scheme 36).[119] The bipyridine ligand has been obtained in a three steps route. In the first step, 4,4'-dimethyl-2,2'-bipyridine **16** was oxidized with selenium dioxide in 1,4-dioxane as a solvent, and successively reduced with $NaBH_4$ in MeOH. The desired mono oxidized product **17** was obtained in 50% yield. Due to the high possibility of a successive oxidation on the mono oxidized product **17** itself, a little percentage of the bis-oxidized undesirable product **17'** was always detected in the crude reaction mixture. The longer was the reaction time, the higher was the **17'** percentage. A lower reaction time was thus preferred to higher ones. For this reason, the complete conversion is never reached, leading to a maximum of 50% yield. This oxidation was therefore considered the most crucial step in the overall synthesis of the metal complex. Once synthesized (4'-methyl-[2,2'-bipyridin]-4-yl)methanol **17**, a nucleophilic substitution was performed and 4-(bromomethyl)-4'-methyl-2,2'-bipyridine **18** was smoothly obtained with 85% yield. Finally, azide **19** was efficiently synthesized

in 87% yield utilizing NaN_3 in a mixture of dimethylformamide and water (10:1) at 70°C for 24 hours.

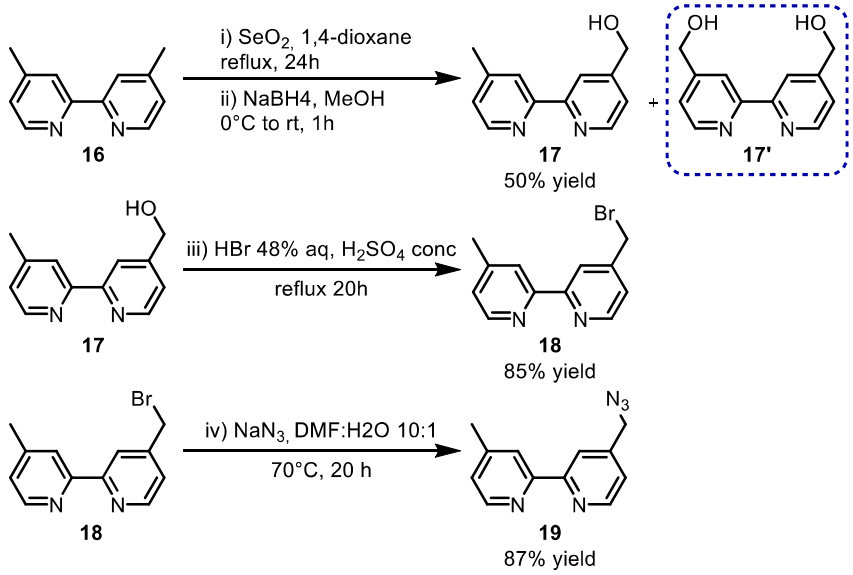

Scheme 36: Synthetic route to bipyridine ligand for the Iridium complex

With**19** in hands, iridium complex **20** has been synthesized basing on a reported procedure.[119] Iridium photosensitizer **20** was finally achieved with a 59% yield over two synthetic steps (Scheme 37).

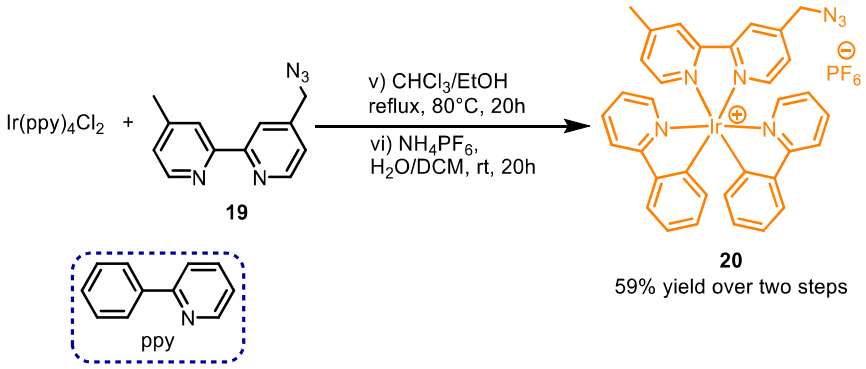

Scheme 37: Synthesis of iridium photosensitizer **20**

Successively, the three alkyne-functionalized amino organocatalyst **14a,b,c** have been synthesized. The two different MacMillan imidazolidin-4-ones derivatives have been obtained starting from the corresponding enantiopure amino acid, respectively the *L*-phenylalanine for **14a** (Scheme 39) and *L*-tyrosine for **14b** (Scheme 38). A CuAAC involving *L*-phenylalanine-derived imidazolidin-4-one **14a** was recently performed for the preparation of a recyclable magnetic nanocatalyst, employed in asymmetric 1,3-dipolar cycloadditions.[121] Similarly, *L*-tyrosine-derived imidazolidin-4-one **14b** was used to synthesize a recyclable pentaerythritol supported catalyst, exploited in enantioselective Diels–Alder reactions[122] and in the immobilization of the catalyst on

siliceous mesocellular foam.[123] Both the alkyne-functionalized imidazolidin-4-ones **14a** and **14b** were smoothly obtained in a two steps route.

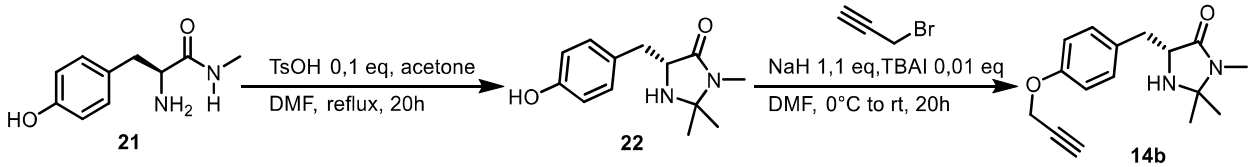

Scheme 38: Synthetic route to alkyne functionalized imidazolidin-4-one **14b**[121]

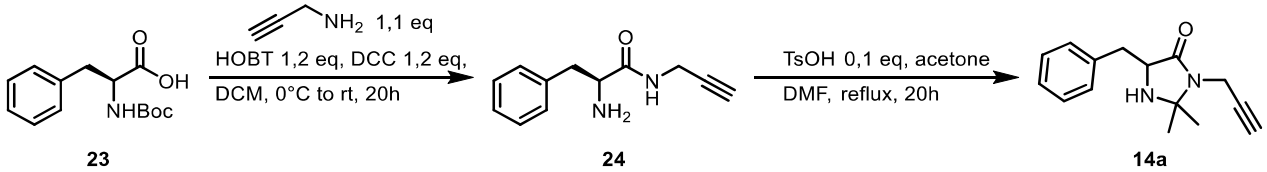

Scheme 39: Synthetic route to alkyne functionalized imidazolidin-4-one **14a**[122]

The synthetic procedure for the third alkyne-functionalized amino organocatalyst **14c** resulted to be more complicated than the ones used for **14a** and **14b**. Two different alkyne-functionalized trityl pyrrolidine (**14c** and **14c1**) have been synthesized. The propargyl derivative of (2*S*,3*R*)-3-hydroxy-2-triphenylmethyl-pyrrolidine **2** was recently used by our research group in a CuAAC to prepare a recyclable [60]fullerene-hybrid catalyst.[45] According to that procedure, the nitrogen of trityl pyrrolidine **2** has been protected with di-*tert*-butyl dicarbonate (Boc_2O) to obtain compound **25**. (Scheme 40) Successively, the propargylation of the hydroxyl group has been performed: tetrahydrofuran (THF) has been used as a solvent and sodium hydride (NaH) as a base. *N*-Boc-Propargylated trityl pyrrolidine **26** and *N*-Boc-Alkylated trityl pyrrolidine **27 are** thus obtained (Scheme 40). For this molecule, the alkylation reaction resulted challenging. The high steric hindrance caused by the trityl group on the C-2 position could affects the efficiency of alkylation. After some different alkylation attempts, a strong dependence of the reaction conversion from the dryness of the solvent and the aging of NaH was observed. Next to an optimization of the reaction partners equivalents, the alkylated pyrrolidine **27** has been obtained with a 40% yield. Eventually, both the *N*-protected pyrrolidine **26** and **27** have been deprotected and the synthesis of alkyne-functionalized amino organocatalysts **14c'** and **14c** accomplished (Scheme 40).

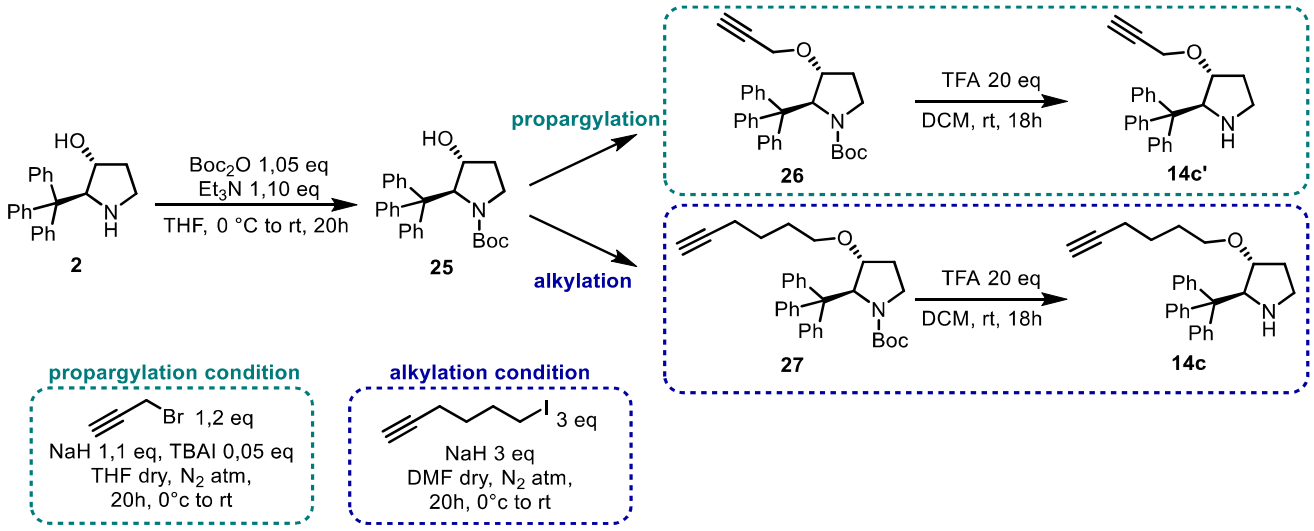

Scheme 40: Synthesis of alkyne-functionalized trityl pyrrolidine **14c** and **14c'**

At last, CuAAC has been performed to connect the iridum complex **13** to each organic counterparts **14a,b,c,c'** and complete the synthesis of bifunctional iridium photoaminocatalysts **15a,b,c,c'** (Scheme 41). The click chemistry reactions were performed using 25 mol% of the tetrakis(acetonitrile)copper(I) hexafluorophosphate catalyst in DCM at room temperature for 48 h. Reactions involving alkyne-functionalized organocatalysts **14,a,b,c** proceeded smoothly allowing us to obtain the desired iridium bifunctional photoaminocatalysts **15a,b,c** from good to very high isolated yields (**15a**: yield =75%, **15b**: yield = 97%, and **15c**: yield = 90%).

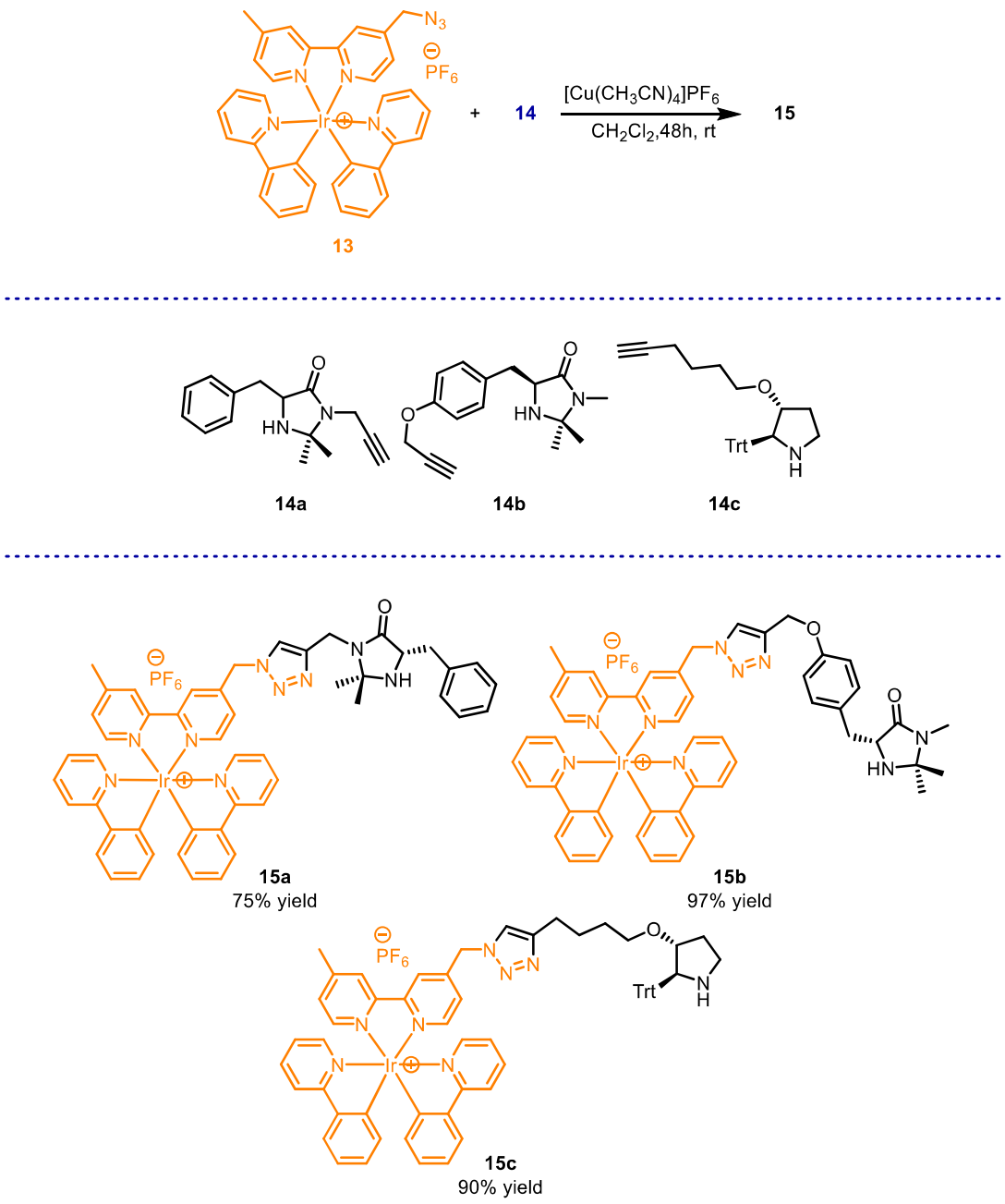

Scheme 41: Synthesis of supramolecular iridium based photoaminocatalyst **15a,b,c**

On the other hand, the click chemistry reaction performed involving **13** and **14c'** led to the production of the amine derivative **28** with a 45% yield. Since the desired photoaminocatalyst **15c'** has been isolated with only a 15% yield, it was not considered useful for the project purpose. Therefore, it was neither photochemical characterized nor used in the following catalytic test.

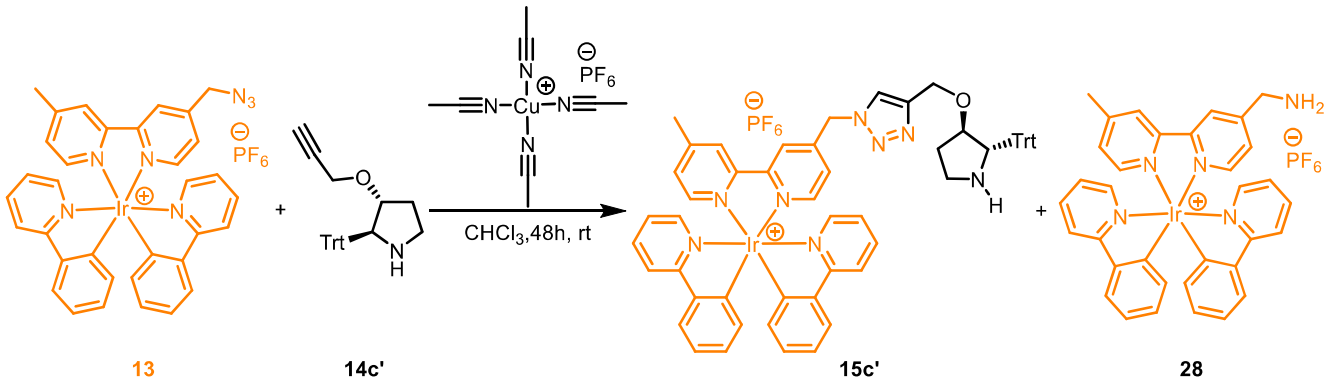

Scheme 42: Click reaction among iridium complex **13** and pyrrolidine **14c'**

Photophysical analyses on photocatalysts **15a,b,c** have been carried out (Table 7). From the data obtained, the three photocatalysts showed very similar photophysical properties (absorption and emission) in both acetonitrile and DMF solutions. Moreover, the phosphorescence lifetime, measured in air equilibrated DMF solution at room temperature, is ca. 110 ns for all of them (Table 7), similar to the value of 124 ns recorded for the model $[Ir(ppy)_2(dtbbpy)]PF_6$ under the same experimental conditions. Therefore, it could be deduced that the photophysical properties of supramolecular bifunctional iridium photoaminocatalyst **15a,b,c** are dominated by the $Ir^{(III)}$ complex moiety, the functionalization of the photosensitizer with organocatalysts does not affect the photophysical properties of the metal complex, which are comparable with those of $[Ir(ppy)_2(dtbbpy)]PF_6$.[124]

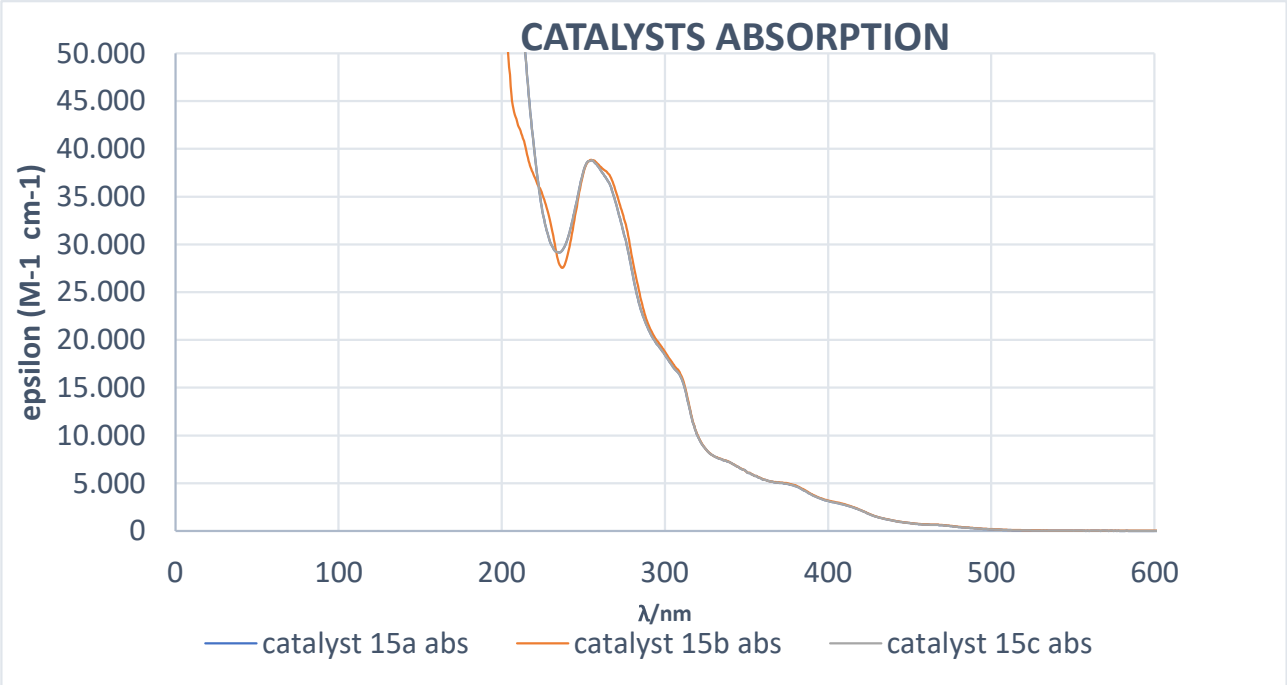

Figure 18: Absorption of photoaminocatalysts **15a,b,c**

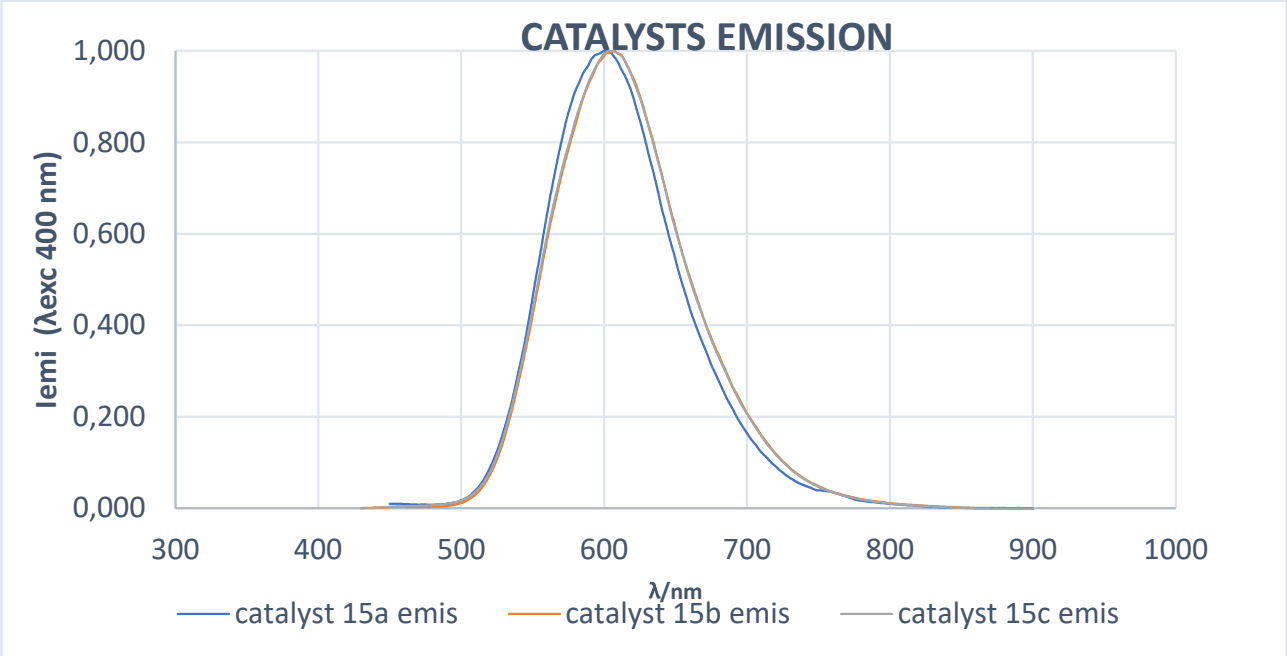

Figure 19: Emission of photoaminocatalysts **15a,b,c**

Table 7: Photophysical analysis on the photocatalysts **15a,b,c**

	Absorption		**Emission**	
	λ/nm	ε/10^{-4} M^{-1} cm^{-1}	λ/nm	τ[a] (ns)
3a	255	3.38	600	108
	311	1.41		
	387	0.43		
15b	255	3.88	604	110
	311	1.56		
	387	0.45		
3c	255	3.89	606	114
	311	1.59		
	387	0.46		
Ir[b]	257	2.53	581[c]	124
	299	1.16		
	381	0.26		

[a] Value estimated in air-equilibrated DMF solution, 298 K. [b] Ir = $[Ir(ppy)_2(dtbbpy)]PF_6^-$

The three photoaminocatalysts **15a,b,c** have been tested in the enantioselective α-alkylation of aldehydes under the standard reaction conditions developed by MacMillan (Table 8).[35] Hydrocinnamaldehyde **29** and bromo derivatives **30a,b** were chosen as model substrates. The reaction has been performed under blue LED irradiation using DMF as a solvent in the presence of 2 equivalents of 2,6-lutidine, 10 mol% of the catalyst, and 10 mol% of trifluoromethanesulfonic acid (TfOH) to promote the enamine formation.

Table 8: Catalytic test for the enantioselective α-alkylation of aldehydes

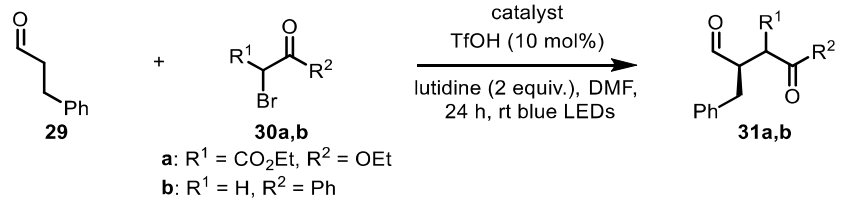

Entry[a]	Catalyst	Product	Conversion % of 29 [b] (yield % of 31)[c]	ee[d]
1	**15a**	**31a**	26	30
2	**15b**	**31a**	>99 (84)	70
3	**15b**[e]	**31a**	28	70
4	**15c**	**31a**	22	n.d.
5[f]	**15b**	**31a**	64 (57)	59
6[g]	**15b**	**31a**	<5	n.d.
7	**15a**	**31b**	26	57
8	**15b**	**31b**	>99 (77)	80
9	**15c**	**31b**	0	-
10[f]	**14b**	**31b**	9	n.d.

[a] Reactions were performed with 0.05 mmol of **29** in DMF (0.5 mL); [b] Determined by ^{1}H-NMR analysis of the reaction crude using the internal standard method; [c] Determined after chromatographic purification; [d] Determined by HPLC analysis of the chiral stationary phase of the reaction crude; [e] The reaction was performed with **5** mol% of **15b** and TfOH; [f] 2 mol% of $[Ir(ppy)_2(dtbbpy)]PF_6$ was used as the photoredox catalyst in the reaction; [g] Reaction performed in the absence of $[Ir(ppy)_2(dtbbpy)]PF_6$; n.d. = not determined.

Iridium complex **15b** proved to be the most effective catalyst, giving the alkylation products in good yields and with satisfying enantiomeric excesses with both bromo derivative **30a** and **30b** (Table 8, entries 2 and 8). On the other hand, imidazolidinone catalyst **15a** (Table 8, entries 1 and 7), carrying the iridium complex moiety on the amide nitrogen, gave poor results in terms of yield and enantioselectivity. Similar results were obtained with the pyrrolidine based catalyst **15c** (Table 8, entries 4 and 9), which resulted the worst under the tested conditions: no conversion was observed using

bromide **30b** and only 22% conversion involving bromide **30a**. An attempt to reduce the catalytic loading has been performed with catalyst **15b** (5 mol%). It affected drastically the reaction conversion, only 28% conversion was reached after 24 hours. Noteworthily, lowering the catalytic loading did not affect the enantiomeric excess of the desired product. The supramolecular approach, which combines the photosensitizer and the organocatalyst in the same supramolecular molecule system, resulted in a significant improvement in the catalytic performance. This is apparent by comparing the reactions involving separated components, imidazolidinone **14b** and $[Ir(ppy)_2(dtbbpy)]PF_6$ (Entry 5 and 10). The reactions lead to the formation of product **31a** with 57% yield and 59% enantiomeric excess, and poor results were obtained upon using **30b** as a bromo derivative. The lower performances achieved compared to those observed with the supramolecular photocatalyst **15b**, demonstrate how the spatial proximity of the two functions improves the synergy of the entire process, in terms of both yield and enantioselectivity. To exclude that the transient enamine, formed during the catalytic cycle, was able to promote the α-alkylation of aldehydes behaving as an effective photocatalyst[125], a test using chiral imidazolidinone **14b** in the absence of an iridium complex was performed (Table 7, entry 6). Only traces of product **31a** were observed after 24 h of irradiation with blue LEDs, excluding these reaction pathways.

The scarce results in terms of yield and enantioselectivity obtained with catalyst **15a** could be attributed to the presence of the bulky N-2 substituent that inhibits the enamine formation and competes with the benzyl group for the stereocontrol of the process.[69]

The inefficiency of catalyst **15c** in the photocatalytic process could be ascribed to the presence of the bulky trityl group on the C-2. However, the trityl pyrrolidine **XXVI** was introduced in 2009 by Maruoka as an effective organocatalyst for the enamine and iminium type organocatalysis[46]. In addition, it has been proved by the same research group the *anti* 4-*ter*butyl dimethyl-3-trityl-pyrrolidine efficiency too.[46,47,126] Moreover, our research group recently demonstrated that the *anti* 2-benzyl-3-trityl-pyrrolidine **XXVII** works as an efficient organocatalyst even for iminium type organocatalytic transformation.[45] Although the bulky trityl group may block the approach of the electrophile to enamine, the lack of reactivity could be explained by a stereoelectronic effect caused by the trityl substituent and pointed out by Mayr.[81] He stated that the negative hyperconjugative interaction of the trityl group with the lone pair of the

enamine nitrogen causes a reduction of the nucleophilicity of the enamine. Also, he reported Brønsted basicities pKaH (i.e., pKa of the conjugate acids) of pyrrolidines and imidazolidinones, as well as their nucleophilicities, determined by the kinetic investigation of the reactions with benzhydrylium ions (Ar_2CH^+) and structurally related quinones.[82] Among all the pyrrolidines studied, pyrrolidines bearing in the α-position a trityl group were found the less nucleophilic ones. However, all the mentioned studies were related to the interaction of polar groups (electrophiles) with the enamine, meanwhile, it is well known that the photoredox stereoselective alkylation of aldehydes is a radical process.[127]

Since the malonyl radical **32** is involved in our process, some investigations of the reactivity of enamines with **32** have been carried out, to shed some light on the factors that could determine the catalysts' activity. A series of preliminary DFT calculations have been conducted (Scheme 44).

In particular, the addition pathways of the dimethyl-malonate radical **32** to the enamines (**33b,c**) have been modeled. The simulated enamines (**33b,c**) were derived from propanal with simplified catalysts, in which the photoactive side-chain of **15b** and **15c** has been replaced with a hydrogen atom and with a benzyl group, respectively (Figure 43). The first simplified catalyst is the 1st generation MacMillan catalyst II[21], while the second one is the trityl-pyrrolidine **XXXVII**, which synthesis has been recently reported by our research group.[45]

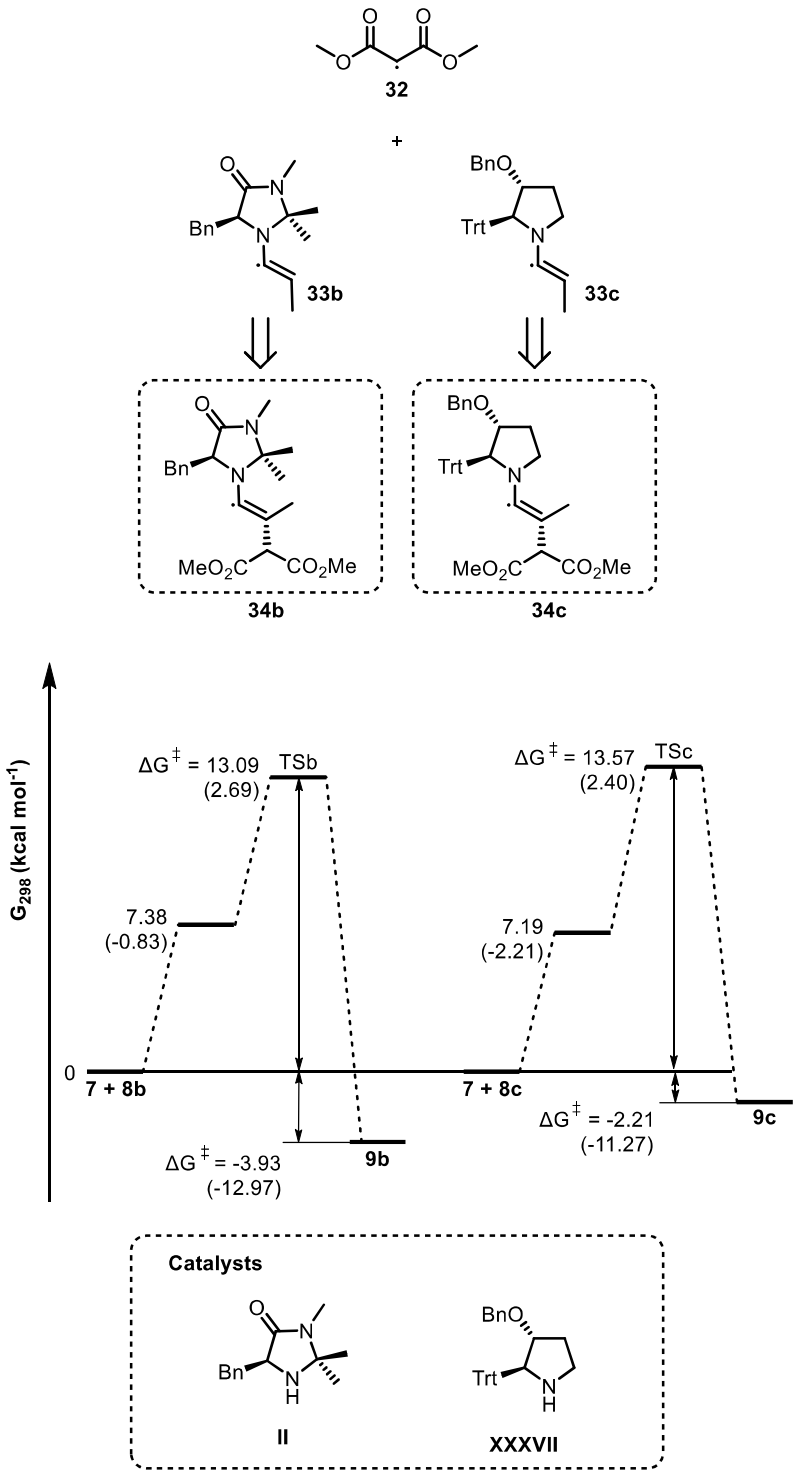

Scheme 43: DFT calculation

As shown in Scheme 43, the energy profiles relative to the addition of the malonate radical to enamines **33b** and **33c** resulted very similar, both in the gas-phase and using DMF as the solvent, clearly excluding a contribution of the radical addition step for determining the lack of reactivity of the analyzed trityl-derived catalysts.

The lack of reactivity showed by the hybrid catalyst **15c** could be more related to the stereo-electronic properties of the substituted pyrrolidine. In a recent article, Wennemers and coworkers highlighted the importance of the pyramidalization direction of the enamine nitrogen in the reactivity of chiral enamine derived from cyclic amines.[128] Cyclic amines with different ring sizes revealed that the endo-pyramidalized enamines (Figure 20, left). are significantly more reactive compared to exo-pyramidalized (Figure 20, right).

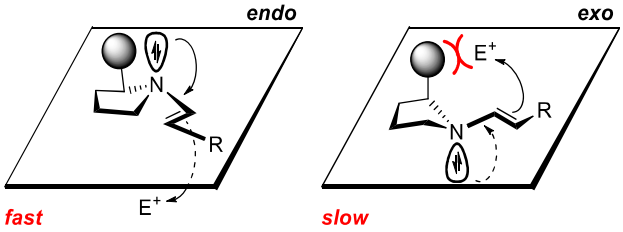

Figure 20: Pyramidalization direction of the enamine nitrogen in the reactivity of chiral enamine

In the enamines with an *endo* pyramidalization, the N orbital is on the same side of the C-2 substituent. On the contrary, in the enamines with an *exo* pyramidalization, the N orbital is on the opposite side of the C-2 substituent. For this reason, in the enamines with the *exo* pyramidalization, the incoming electrophile is subjected to higher steric hindrance compared to the *endo* pyramidalized ones. Therefore, they react slower. The enamine derived from catalyst **15c** present bulky substituents both in the α (C-2) and in the ß (C-3) positions. If the enamine derived from **15c** preserves an endo-pyramidalization, the presence of the substituent in the ß-position could hinder the electrophilic attack, diminishing the efficiency of the radical attack.

Finally, given the long alkyl linker between the photoredox center and the organocatalyst in **15c**, the benefits from spatial proximity in this bifunctional catalyst may be quite limited, resulting in a low reactivity.

The major finding of our investigation relies on the remarkable reactivity observed with the supramolecular photo-organocatalyst formed with **II** MacMillan imidazolidinone catalyst (**15c**). It is important to mention that the effective catalyst used in the alkylation of aldehydes is **XXIX** MacMillan imidazolidinone catalyst (Figure 21).[35]

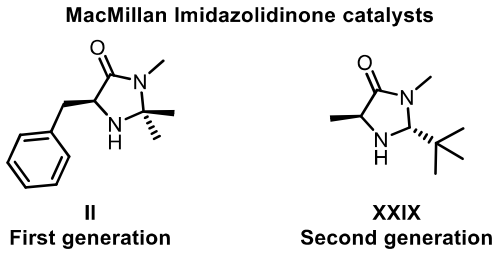

Figure 21: MacMillan imidazolidinone catalysts

The same catalyst was used in different processes mediated by different photocatalysts.[111–113,129] It is also worth of note that, although these processes appear very similar, the photoredox mechanism involved is rather different. When $[Ru(bpy)_3]^{2+}$ was employed by MacMillan as a photocatalyst[35] the process did occur via a reductive quenching forming $[Ru(bpy)_3]^{+}$, able to reduce the bromomalonate and form the malonyl radical. In other processes an oxidative quenching of the photocatalyst by using the bromomalonate is operative.[111,129] In the mentioned examples the effective organocatalyst is **XXIX**. It is capable of forming the chiral enamine responsible for the stereoselective transformation. Other imidazolidinone catalysts, and in particular **II** were proved to be less reactive and selective under the same reaction conditions. **XXIX** is not quite stable and its *cis* form gives worse results than the *trans* form.[130] Remarkably, **II** was found effective in the enantioselective α-benzylation of aldehydes,[131] based on the mechanistic principle of the spin-center shift recently reported by MacMillan, using alcohols as alkylating agents.[130] Surprisingly, in the same work, **XXIX** was found ineffective. In some photoredox reactions, it was reported that the aminal group in the C-2 position on the imidazolidinone framework was susceptible to H-atom abstraction, therefore, leading to a decreased efficiency of the catalyst due to these decomposition pathways.[132] The first generation imidazolidinone catalyst **II** appears more robust and less prone to such decompositions.

To get further insight into the reaction mechanism, quenching experiments were performed. Upon addition of each reaction component (at the same concentration under the optimized reaction conditions) to a DMF solution of complex **15b**, no quenching of the photocatalyst phosphorescence was observed. (Figure 22 and 23)

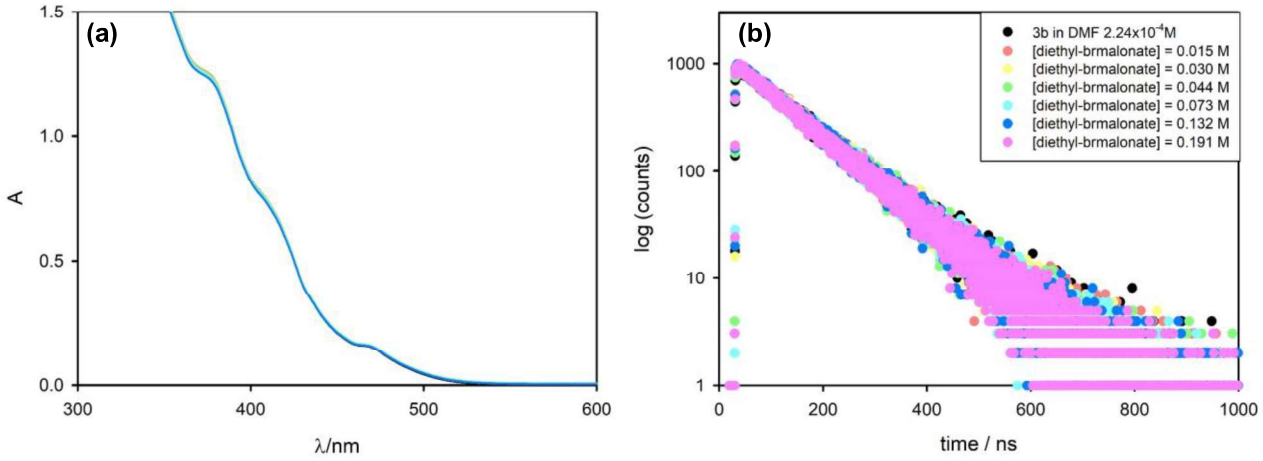

Figure 22:(a) Absorption spectrum of **15b** in air-equilibrated DMF solution (2.24 x 10^{-4} M) with an increasing amount of diethylbromomalonate up to 0.191 M and (b) the corresponding lifetime decay (excitation 405 nm). Optical path length 1 cm.

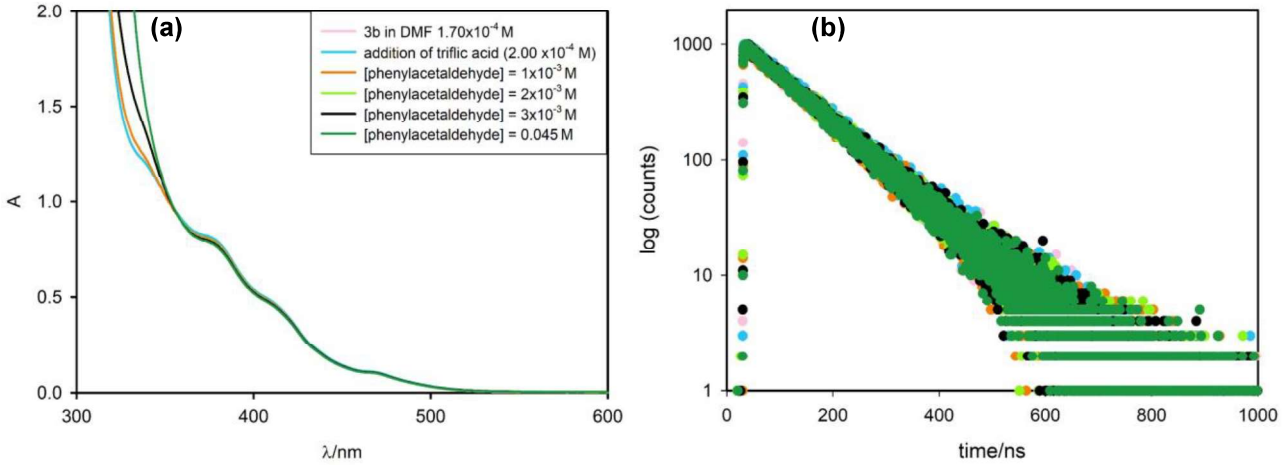

Figure 23: (a) Absorption spectrum of **15b** (1.70 x 10^{-4} M) and equimolar triflic acid in air equilibrated DMF solution with an increasing amount of phenylacetaldehyde up to 0.045 M and (b) the corresponding lifetime decays (excitation 405 nm). Optical path length 1 cm.

Since the photophysical behavior of complex **15b** is not affected by the reagents, the role of the enamine transiently formed on the photocatalyst was then examined. Enamine derived from phenylacetaldehyde and **15b** catalyst was chosen for these studies due to its stability versus hydrolysis. The enamine can be generated by in situ adding an excess of phenylacetaldehyde to a **15b** solution in the presence of triflic acid or can be separately prepared and isolated. In the first case, after 24 hours from the addition of phenylacetaldehyde to a **15b** solution in the presence of triflic acid, the emission decay of the solution showed two lifetime components of 102 and 8.3 ns. (Figure 24)

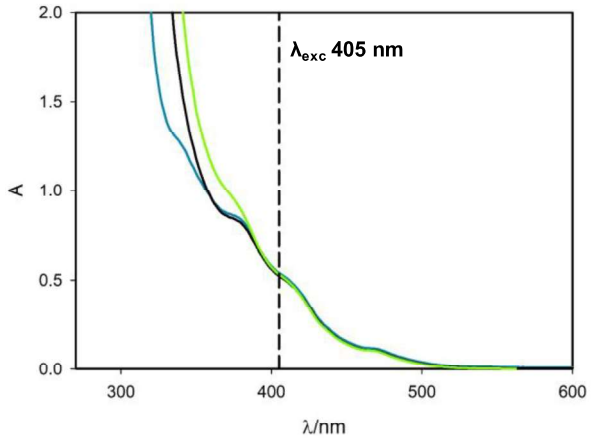

Figure 24: Absorption spectrum of **15b** (1.70 x 10^{-4} M) and equimolar triflic acid in air-equilibrated DMF solution (blue line), upon addition phenylacetaldehyde 0.045 M (black line) and after one day (green line).

The long component is attributed to the unreacted **15b** photocatalyst with a close similarity of the lifetime (110 ns). The short component is attributed to the intramolecular quenching of the Ir complex by the formed enamine with a quenching constant of 1.1×10^8 s^{-1} and a quenching efficiency as high as 92%. The enamine was also prepared and isolated, but due to the presence of both the iridium photocatalytic moiety and the reactive enamine, the product was not stable enough to be fully characterized. In any case, the photophysical analysis performed using the freshly isolated enamine showed similar results to the ones obtained with in situ prepared enamine. The emission decay of the solution containing the isolated enamine derived from **15b** showed two lifetime components: a long one, 99 ns, and a short one of 8.4 ns. (Figure 25)

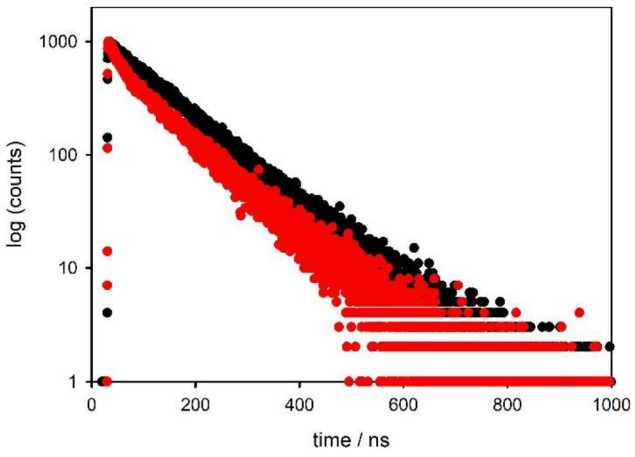

Figure 25: Emission intensity decay of **15b** (1.70 x 10^{-4} M) and equimolar triflic acid (black dots) and isolated enamine (red dots) in air-equilibrated DMF solution. Excitation at 405 nm.

Based on the photophysical evidence and MacMillan original literature[35], a reaction mechanism is proposed and illustrated (Scheme 44).

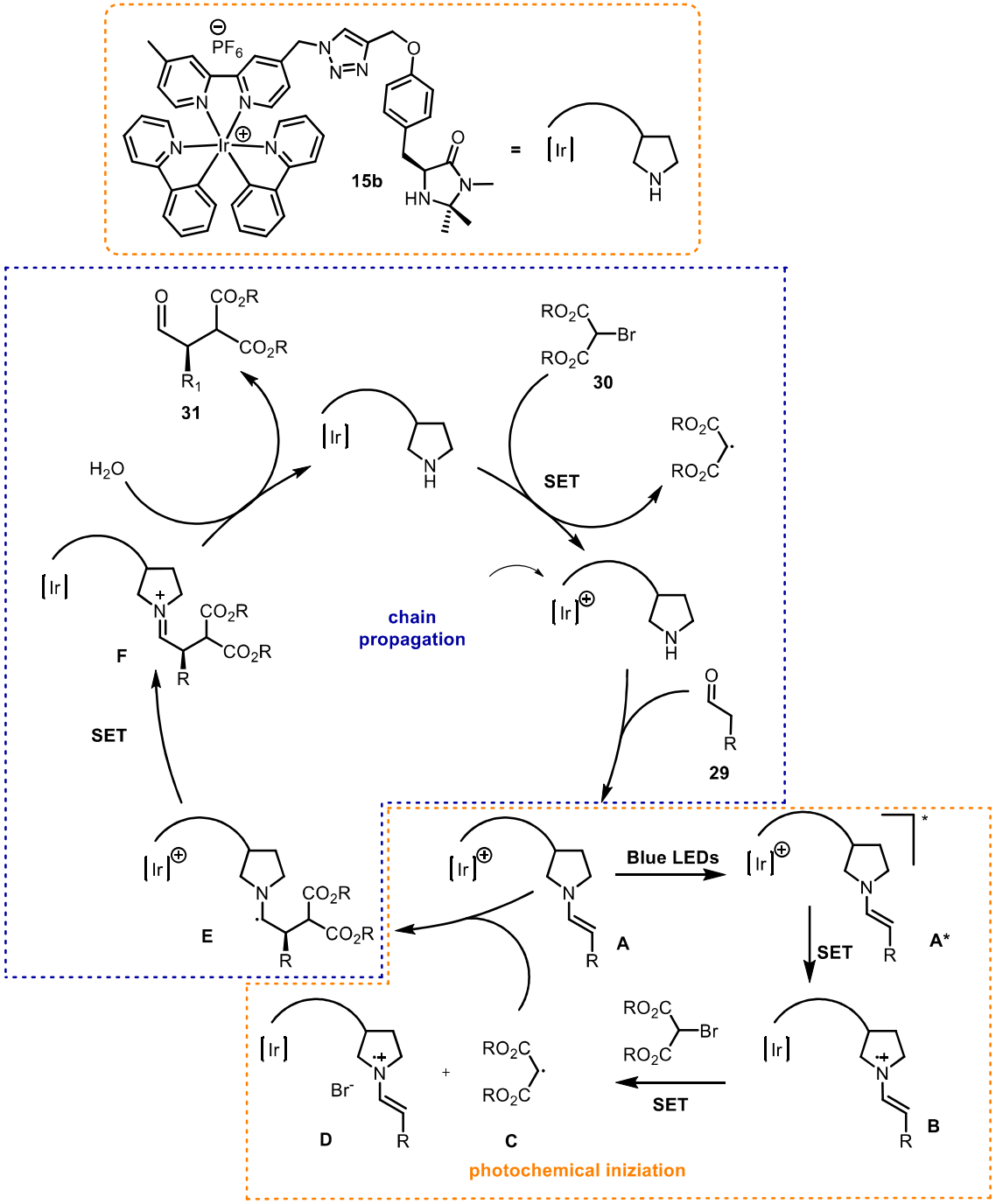

Scheme 44: Mechanism of the α-alkylation of aldehydes catalyzed by the supramolecular iridium bifunctional photoaminocatalyst **15b**

At first enamine, **A** is formed by the condensation of bifunctional iridium photoaminocatalyst **15b** and hydrocinnamaldehyde **29**. Subsequently, the iridium complex is photoexcited and, an intramolecular reductive quenching takes place. The iridium excited state is reduced by the newly formed enamine **A**, which in turn is

oxidized. As a result, the reduced photosensitizer is generated. The process is thermodynamically allowed, based on the excited state reduction potential of the Ir(III) photosensitizer of +0.95 V vs. SCE and estimated potential for enamine oxidation of +0.85 V vs. SCE.[133] Photosensitizer **B** is a strong reductant able to generate the alkyl radical **C** from **30**. This process triggers the photoredox cycle as suggested by MacMillan[35]. Radical **C** attaches enamine **A**. Consequently, α-amino radical **E** is formed and is easily oxidized through a SET transformation to form the iminium ion **F**. Hydrolysis of **F** would reconstitute the original iridium photoaminocatalyst **15b** and deliver the enantioenriched α-alkylated aldehyde **31**. It is not verified the effective nature of the SET transformation caused by the **E** oxidation. This species could engage a SET with the bromo derivative **30** to directly form radical **E** or participate in an inter or intramolecular SET with the iridium complex to form iminium ion **IV**. In the latter case, the reduced iridium complex formed is itself capable of generating a new alkyl radical and restoring the initial bifunctional iridium photoaminocatalyst **15b** form. It is noteworthy that there is no experimental evidence about the fate of the sacrificial enamine after its oxidation, namely if it could be restored to the original catalyst. Probably, as demonstrated by Yoon, the reaction is a radical chain, but we do not have enough evidence to sustain this hypothesis. However, in our reaction irradiation with visible light is mandatory.

Conclusion

In this study, three supramolecular systems composed of an Ir(III) photosensitizer and secondary amine organocatalyst have been synthesized (Figure 26).

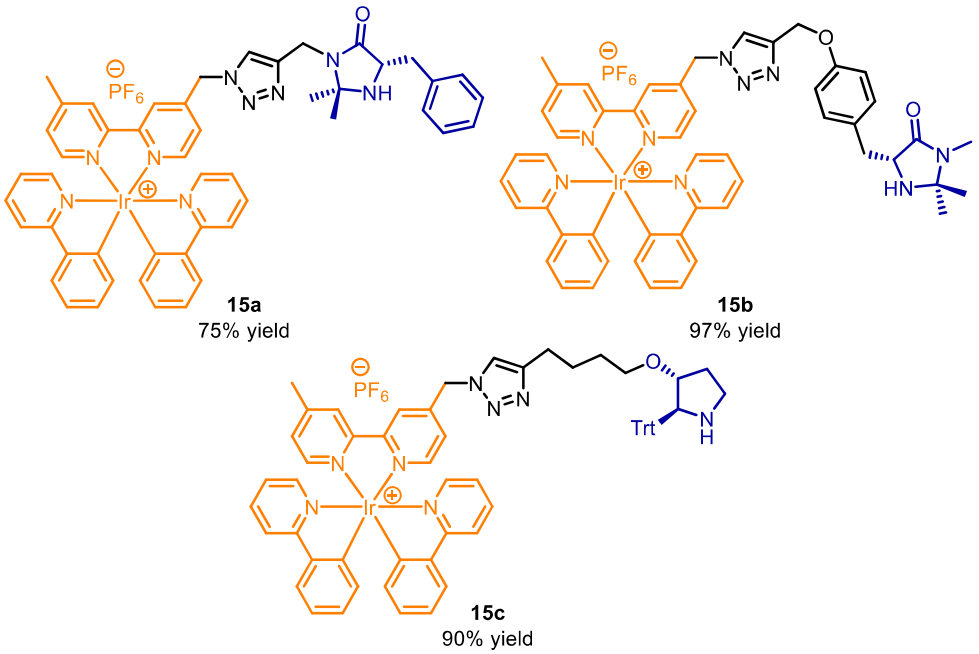

Figure 26: Catalyst **15a,b,c**

Preliminary reactivity and selectivity have been investigated in the benchmark α-alkylation reaction of aliphatic aldehydes for each one of the synthesized catalysts. Among the three catalysts tested, the supramolecular iridium based photoaminocatalyst bearing a MacMillan imidazolidinone **15b** proved good reactivity and selectivity for the tested reaction. Mechanistic photophysical studies revealed a fast and very efficient (92%) intramolecular reductive quenching of the iridium photosensitizer by the in situ formed enamine. The resultant reduced iridium catalyst was able to form, from bromo derivatives, alkyl electron poor radicals, therefore, to promote the α-alkylation reaction of aliphatic aldehydes. Moreover, the bifunctional organo-photocatalyst **15b** proved to be considerably more efficient and selective as compared to the catalytic system formed by mixing the single separated components. Differently from previous investigations, the typical second generation MacMillan imidazolidinone trans catalyst used in many transformations is avoided, and a simple and more stable organocatalyst can be employed. The conjugation of the organocatalyst gives a system that could be further implemented and could allow the immobilization of this type of catalyst for flow applications. Future studies will also be aimed at the replacement of the phosphorescent iridium photosensitizer with fluorescent organic dyes. Indeed, the supramolecular approach relieves the constraint of the long-lived excited state by taking advantage of the proximity of the photosensitizer and organocatalyst which results in a fast and efficient intramolecular quenching process.

General Procedures and Products Characterization

Materials and methods

All commercial chemicals and dry solvents were purchased from Sigma Aldrich, Alfa Aesar or TCI Chemicals and used without additional purification. 1H and 13C-NMR spectra were recorded on a Varian Inova 400 NMR instrument with a 5 mm probe. All chemical shifts (δ) are referenced using deuterated solvent signals; chemical shifts are reported in ppm from TMS and coupling constants (J) are reported in Hertz. Multiplicity is reported as: s = singlet, d = doublet, t = triplet, q = quartet, hept = heptet, and m = multiplet. HPLC-MS analyses were performed using an Agilent Technologies HP1100 instrument coupled with an Agilent Technologies MSD1100 single-quadrupole mass spectrometer using a Phenomenex Gemini C18 3 µm (100 × 3 mm) column; mass spectrometric detection was performed in a full-scan mode from m/z 50 to 2500, with scan time 0.1 s in a positive ion mode, ESI spray voltage 4500 V, nitrogen gas 35 psi, drying gas flow rate 11.5 mL min−1, and fragmentor voltage 30 V. HRMS was performed using Waters Xevo G2-XS QT with, ESI+, cone voltage 40 V, Capillary 3 kV, and source temperature 120 °C. CSP-HPLC analyses were performed with an Agilent Technologies Series 1200 instrument using chiral columns. The enantiomeric compositions were checked against the corresponding racemic products. Flash chromatography purifications were carried out using VWR or Merck silica gel (40–63 µm particle size). Thin-layer chromatography was performed with Merck 60 F254 plates.

4-(azidomethyl)-4'-methyl-2,2'-bipyridine 19, **iridium photosensitizer 20**, **alkyne functionalized imidazolidinone 14b**, **alkyne functionalized imidazolidinone 14a** have been synthesized according to a reported literature procedure.

Photochemical reactions set-up

Reaction set-up and emission spectrum of 23W blue LEDs used for the irradiation of the reaction mixture.

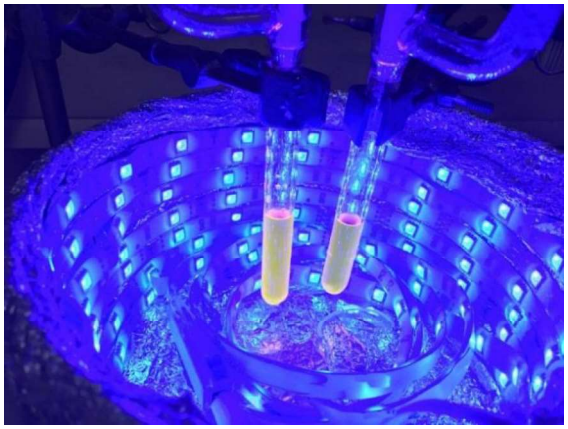

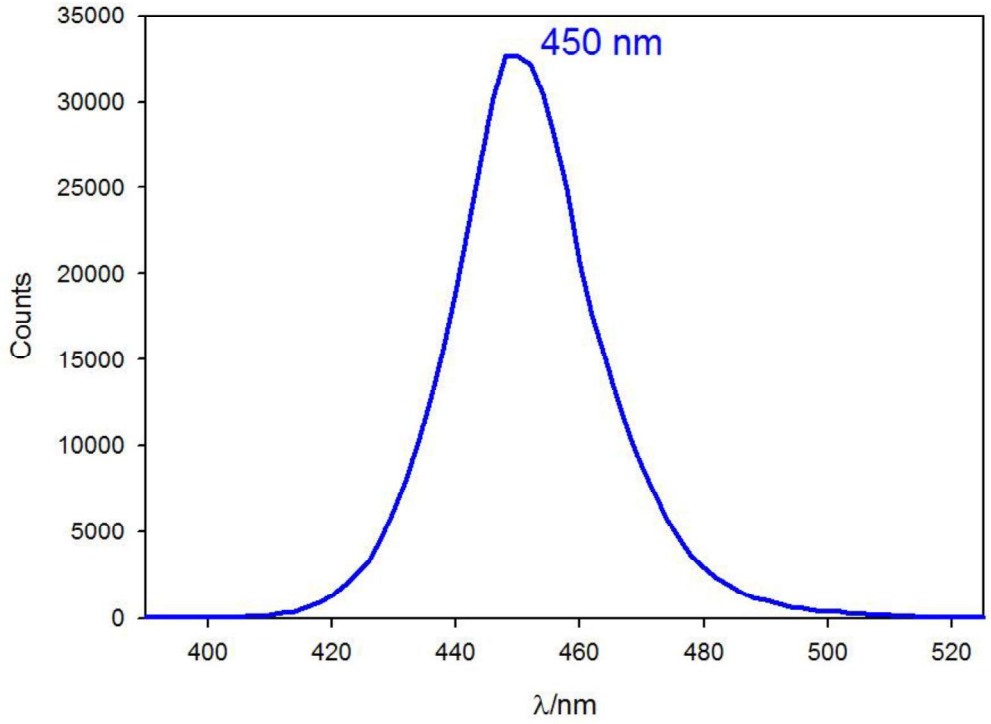
450 nm
35000
30000
25000
20000
15000
10000
5000
0
Counts
400
420
440
460
480
500
520
λ/nm

Preparation of Enamine from catalyst 15b and hydrocinnamaldehyde 29.

The enamine deriving from iridium catalyst **15b** and stoichiometric 2-phenylacetaldehyde **29** was prepared and isolated by column chromatography (0.01 mmol scale), adapting the procedure reported by Mayr and Lakhdar for the simple imidazolidinone organocatalyst.[117] Due to the presence of both the iridium photocatalytic moiety and the reactive enamine, the product was not stable enough to be fully characterized and was used as soon as possible in photochemical trials. The formation of the enamine was determined by investigation of the ^{1}H-NMR spectrum of the crude reaction mixture. A new doublet appeared in the expected chemical shift region, relative to the ß-proton of the desired (*E*)-configured enamine (5.73 ppm, d, J = 14.7 Hz). Moreover, analogously to what observed by Mayr for the corresponding enamine of imidazolidinone, we also noticed both a significant shielding of one of the diastereotopic methyl groups of the aminal group in the spectrum of the enamine, as well as a shielding of the other (Δδ = 0.56 ppm vs 0.65 ppm reported by Mayr). In the free catalyst **15b**, only a single singlet signal was registered for the methyl groups, thus evidencing the considerably lower conformational mobility of the benzyl group in the corresponding enamine.

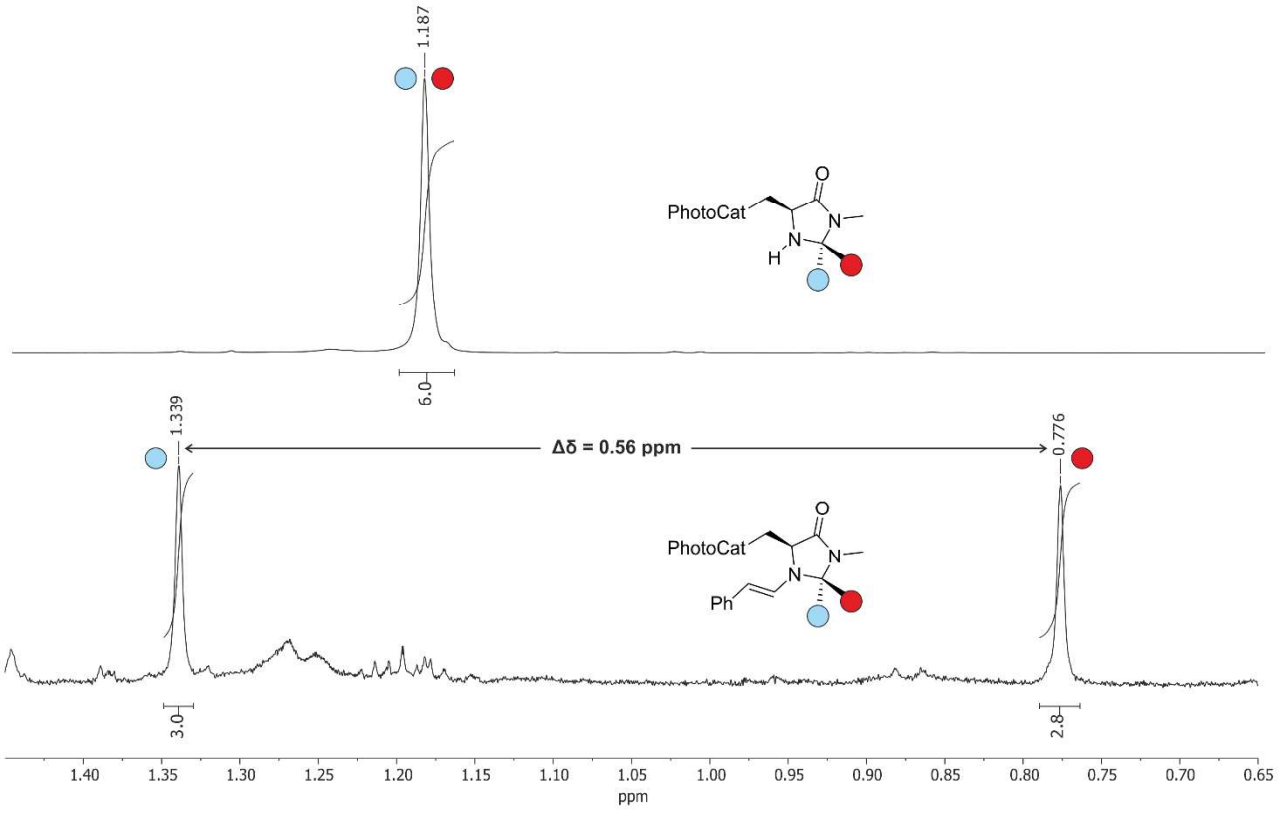

Electrochemical investigations

The electrochemical experiments were carried out in argon-purged CH_3CN (Hi-Dry anhydrous solvent) solution at 298 K. In the cyclic voltammetry (CV) the working electrode was a glassy carbon electrode (0.08 cm^2), the counter electrode was a Pt spiral. The potentials reported are referred to SCE and Ferrocene was used as standard. The concentration of the compounds examined was of the order of $5x10^{-4}$ M; tetraethylammonium hexafluorophosphate ($TEAPF_6$) 0.05M was added as supporting electrolyte. Cyclic voltammograms were obtained with scan rates in the range 0.01–1 V s^{-1}. The estimated experimental error on the $E_{1/2}$ value is ± 10 mV.

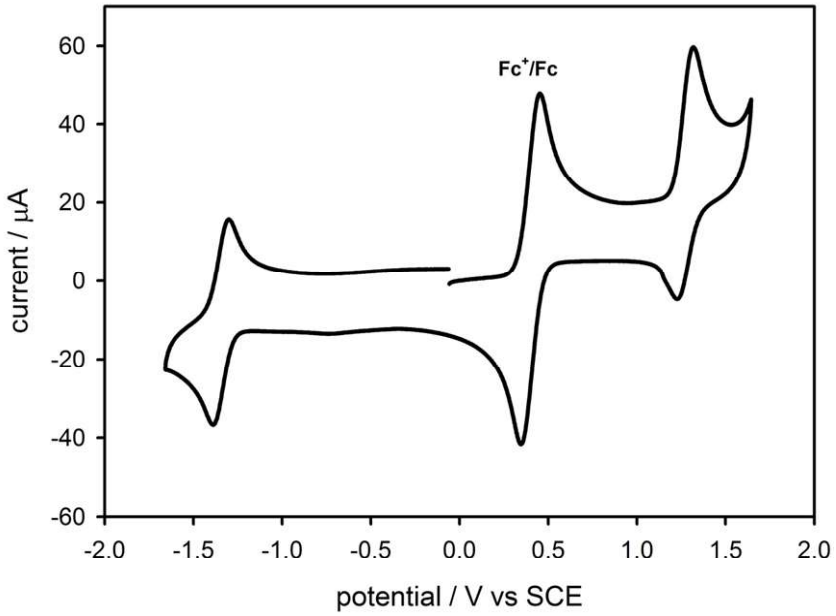

Cyclic voltammetry of an argon purged solution of **15b** (0.5 mM) in CH_3CN in the presence of 0.05 M tetraethylammonium hexafluorophosphate ($TEAPF_6$). Scan rate=0.5 V s^{-1}; working electrode: glassy carbon. Ferrocene (Fc) was used as internal standard.

	$E_{1/2}^{red}$ (V vs SCE)	$E_{1/2}^{ox}$ (V vs SCE)
Iridium complex **15b**	-1.35	+1.26
Excited state iridium complex **15b**	+0.95	-1.04

Redox potentials estimated from cyclic voltammetry performed in argon purged CH_3CN solution with tetraethylammonium hexafluorophosphate ($TEAPF_6$). Working electrode: glassy carbon. The estimation of the excite state potential is based on the energy of the fluorescent excited state of **15b** (E00 = 2.30 eV).

Photochemical investigation

Photochemical experiments were carried out at room temperature in air-equilibrated solutions (CH_3CN and DMF Uvasol®), in a quartz cuvette (optical pathlength 1 cm). All absorption spectra were recorded with a spectrophotometer Varian Cary 300 UV-Vis. Phosphorescence spectra were recorded with Perkin Elmer LS 50 spectrofluorometers equipped with Hamamatsu R928 photomultiplier. Lifetime decays measurements were performed using an Edinburgh FLS920 spectrofluorimeter equipped with a TCC900 card for data acquisition in time-correlated single-photon counting experiments (0.5 ns time resolution) with LDH-P-C-405 pulsed diode laser.

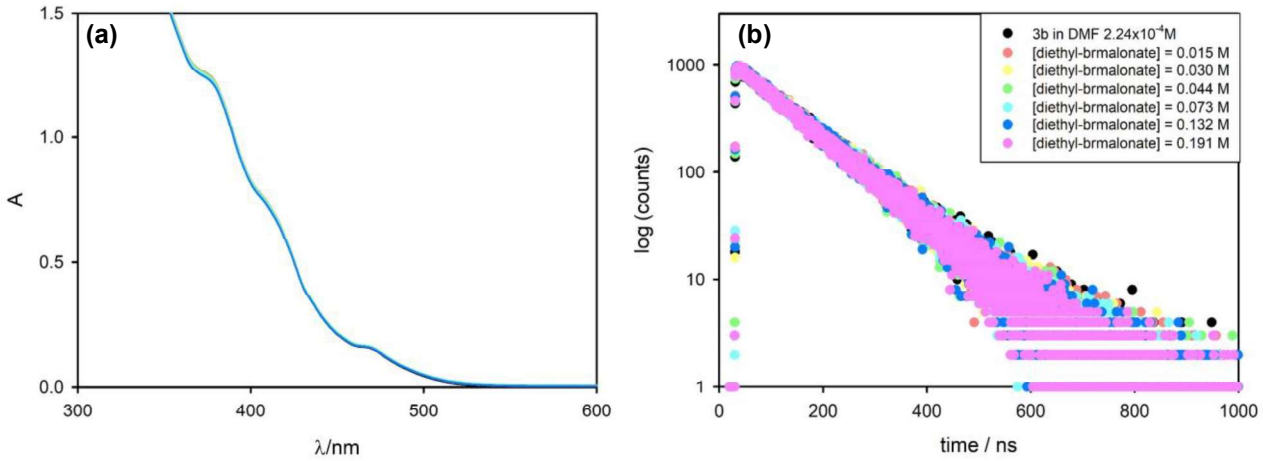

(a) Absorption spectrum of **15b** in air-equilibrated DMF solution (2.24 x 10^{-4} M) with increasing amount of diethylbromomalonate up to 0.191 M and (b) the corresponding lifetime decay (excitation 405 nm). Optical path length 1 cm.

Immediately after the addition of phenylacetaldehyde to a **15b** solution in the presence of triflic acid, no quenching was observed.

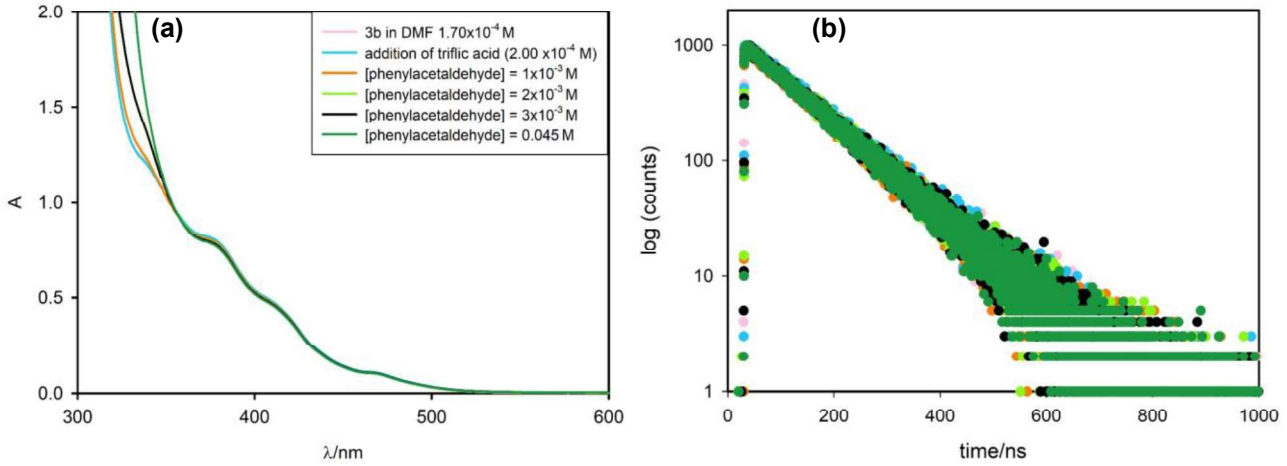

(a) Absorption spectrum of **15b** (1.70 x 10^{-4} M) and equimolar triflic acid in air equilibrated DMF solution with increasing amount of phenylacetaldehyde up to 0.045 M and (b) the corresponding lifetime decays (excitation 405 nm). Optical path length 1 cm.

The concentration of **15b** along with that of aldehyde and triflic acid were decreased by a factor of 50 with respect to the reaction conditions, in order to have value of absorbance suitable to perform photophysical measurements.

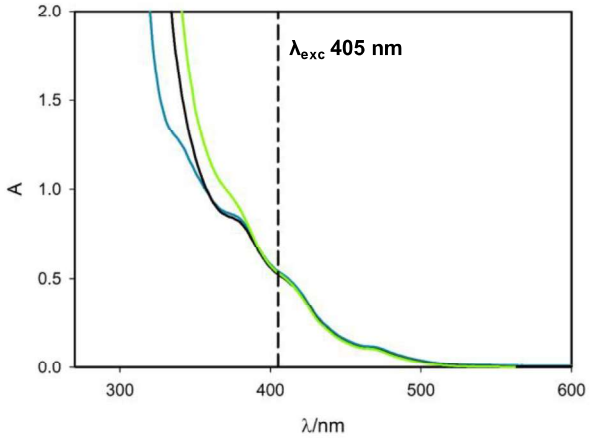

Absorption spectrum of **15b** (1.70 x 10^{-4} M) and equimolar triflic acid in air-equilibrated DMF solution (blue line), upon addition phenylacetaldehyde 0.045 M (black line) and after one day (green line).

The emission decay of the solution containing the isolated enamine derived from **15b** showed two lifetime components: a long one, 99 ns and a short one of 8.4 ns. The values are comparable with those obtained with the generation of the same enamine *in situ*. Also in that case, the short component is attributed to the intramolecular quenching of the Ir(III) complex by the enamine; the longer lifetime is comparable with the one measured for 15**b** in solution (110 ns).

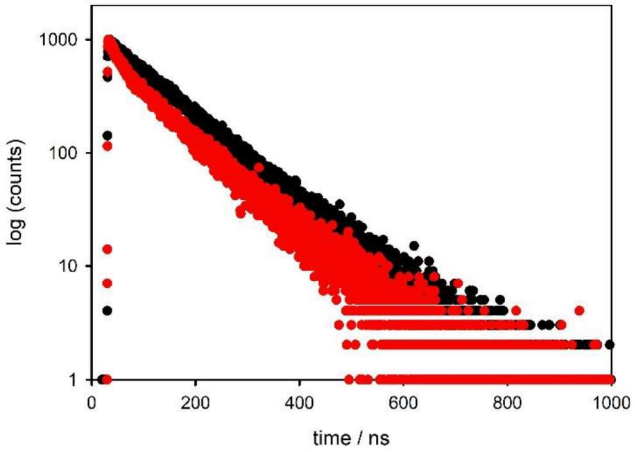

Emission intensity decay of **15b** (1.70×10^{-4} M) and equimolar triflic acid (black dots) and isolated enamine (red dots) in air-equilibrated DMF solution. Excitation at 405 nm.

The formation of the enamine was followed with spectrofluorimetric kinetic: an emission spectrum of the solution containing **15b**, triflic acid and an excess of phenylacetaldehyde was collected each hour for 2 days. The trend of the emission intensity with time shows a decrease of intensity, compatible with the concomitant increasing amount of the enamine formed.

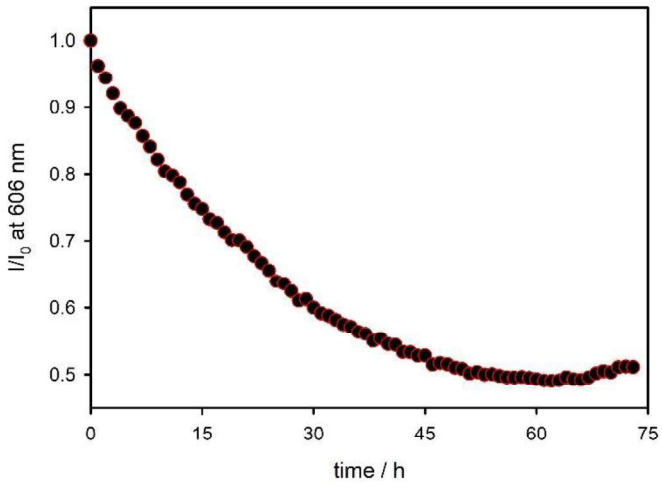

Normalized emission intensity changes at 606 nm as a function of time of a solution containing **15b** (1.70×10^{-4} M), equimolar amount of triflic acid, phenylacetaldehyde 0.045 M in air-equilibrated DMF. λ_{exc} at 405 nm.

The constant kq of the intramolecular quenching process occurring within the supramolecular photocatalyst **15b'** comprising the Ir(III) photosensitizer and the formed enamine can be evaluated according to the following equation:

$$k_q = \frac{1}{\tau} - \frac{1}{\tau^0}$$

where τ and τ^0 are the lifetime of the Ir(III) complex in **15b'** and **15b**.

The corresponding quenching efficiency is evaluated by the following equation:

$$n_q = \left(1 - \frac{\tau}{\tau^0}\right)$$

Synthetic procedures and product characterizations

tert-Butyl-(2S,3R)-3-(hex-5-yn-1-yloxy)-2-tritylpyrrolidine- 1-carboxylate (N-Boc-14c)

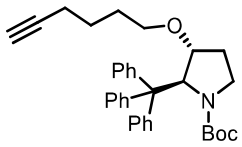

NaH (3 mmol, 0.12 g, 60% in mineral oil) was added to a solution of tert-butyl (2*S*,3*R*)-3-hydroxy-2-tritylpyrrolidine-1-carboxylate (1 mmol, 0.43 g)[45] in DMF (5 mL) at 0 °C and the reaction mixture was stirred at 0 °C for 1 h. 6-Iodo-hex-1-yne (3 mmol, 0.4 mL) was added dropwise at 0 °C and the reaction mixture was stirred at room temperature for 18 h. The reaction mixture was quenched with aqueous NH_4Cl and diluted with ethyl acetate and the organic phase was washed with aqueous 5% LiCl. The organic phase was dried (Na_2SO_4) and concentrated under vacuum and the crude mixture was purified by flash chromatography on silica (cyclohexane/ethyl acetate 9/1), affording N-Boc-**14c** as a gummy solid (0.155 g, 0.3 mmol, 30%).

^{1}H-NMR (400 MHz, $CDCl_3$) δ 7.51–7.39 (m, 6 H), 7.29–7.08 (m, 9 H), 5.81 (s, 1 H), 3.91 (d, J = 5.2 Hz, 1 H), 3.41 (m, 2 H), 3.22 (m, 1 H), 2.89 (td, J = 10.6, 2.6 Hz, 1 H), 2.27 (dt, J = 6.7, 3.2 Hz, 2 H), 1.96 (t, J = 2.6 Hz, 1 H), 1.75–1.66 (m, 4 H), 1.43 (ddd, J = 14.0, 10.2, 2.9 Hz 1 H), 1.34 (s, 9 H), −0.12–0.30 (m, 1 H). ^{13}C-NMR (100 MHz, $CDCl_3$) δ 157.2, 144.8, 130.7, 127.3, 125.9, 84.3, 83.7, 71.2, 68.4, 67.2, 65.8, 60.9, 49.5, 28.9, 28.2, 26.7, 25.5, 18.2. $[\alpha]^{25}_D$ = −80.1 (*c* = 0.24, $CHCl_3$). HPLC-MS (ESI): 532 [M + Na^+] 454 [M − *t*Bu + 2H^+] 1042 [2M + H^+ + Na^+]; calcd for ($C_{34}H_{39}NO_3$: 509.69): C, 80.12; H, 7.71; N, 2.75; found: C, 79.75, H, 7.69; N, 2.74.

(2S,3R)-3-(hex-5-yn-1-yloxy)-2-tritylpyrrolidine (14c)

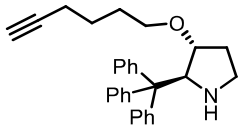

Trifluoroacetic acid (20 mmol, 1.53 mL,) was added to a solution of N-Boc-**14c** (1 mmol, 0.51 g) in DCM (2 mL) and the reaction mixture was stirred at room temperature for 18 h. The organic solvents were removed under vacuum, and the solid residue was diluted

with ethyl acetate and treated with aqueous $NaHCO_3$. The aqueous phase was extracted with ethyl acetate (3 × 5 mL), and the combined organic phases were dried (Na_2SO_4) and evaporated under vacuum to give pure **2c** as a gummy solid (0.37 g, 0.9 mmol, 90%). ^{1}H-NMR (400 MHz, $CDCl_3$) δ 7.40 (d, J = 7.6 Hz, 6 H), 7.29–7.12 (m, 9 H), 4.84 (s, 1H), 3.63 (d, J = 5.0 Hz, 1 H), 3.45 (dtd, J = 8.8, 6.4, 5.6, 3.2 Hz, 1H), 3.15 (dt, J = 8.1, 5.5 Hz, 1 H), 2.93 (ddd, J = 11.8, 9.0, 5.4 Hz, 1 H), 2.75 (t, J = 8.2 Hz, 1 H), 2.27 (hept, J = 2.6 Hz, 2 H), 1.98 (t, J = 2.6 Hz, 1 H), 1.81–1.64 (m, 5 H), 1.53 (dd, J = 13.1, 5.4 Hz, 1 H), 0.29 (tdd, J = 12.6, 7.5, 5.1 Hz, 1 H). ^{13}C-NMR (100 MHz, $CDCl_3$) δ 130.2, 127.5, 125.9, 84.3, 83.2, 77.3, 77.0, 76.7, 70.9, 68.5, 68.1, 60.9, 44.8, 30.2, 29.2, 25.6, 18.3, 1.0. $[\alpha]^{25}_D$ = −97.16 (*c* = 0.33, $CHCl_3$). HPLC-MS (ESI): 410 [M + H^+]; calcd for ($C_{29}H_{31}NO$: 409.57): C, 85.04; H, 7.63; N, 3.42; found: C, 85.30, H, 7.66; N, 3.43.

Synthesis of catalysts 15a–c, general procedure

Tetrakis(acetonitrile)copper(I) hexafluorophosphate (0.023 mmol, 8.9 mg, 0.25 equiv.) was added to a mixture of [Ir(N_3-CH_2bpy)(ppy)$_2$]PF_6 (**1**, 83.1 mg, 0.095 mmol) and the desired organocatalyst (**14a–c**, 0.095 mmol) in dichloromethane (0.5 mL) and the reaction mixture was stirred at room temperature for 48 h. The crude mixture was poured on top of a silica gel flash-chromatography column and directly purified by eluting first with dichloromethane and then with dichloromethane/methanol 9 : 1.

15a.

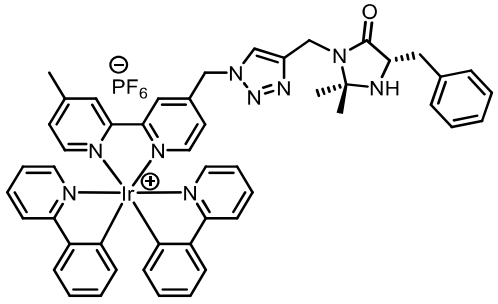

Yellow solid, Y = 75%. ^{1}H-NMR (400 MHz, CD_3CN, two stereoisomers) δ 8.31 (d, J = 4.1 Hz, 1 H), 8.23 (dd, J = 9.2, 1.5 Hz, 1 H), 8.04 (dd, J = 8.3, 5.5 Hz, 2 H), 7.93 (d, J = 5.7 Hz, 1H), 7.87–7.72 (m, 6 H), 7.65 (d, J = 1.7 Hz, 1 H), 7.62–7.51 (m, 2H), 7.33 (d, J = 5.8 Hz, 1 H), 7.23–7.10 (m, 4 H), 7.09–6.95 (m, 5H), 6.90 (tdd, J = 7.4, 2.4, 1.3 Hz, 2 H), 6.27 (td, J = 7.2, 1.3 Hz, 2 H), 5.72 (s, 2 H), 4.52 (dd, J = 15.8, 2.0 Hz, 1 H), 4.36 (dd, J =15.8, 3.0 Hz, 1 H), 3.74 (ddd, J = 8.0, 4.3, 1.4 Hz, 1 H), 3.04 (ddd, J = 14.2, 4.2, 2.8 Hz, 1 H),

2.78 (ddd, J = 14.0, 7.9, 3.5 Hz,1 H), 2.53 (s, 3 H), 1.193 and 1.186 (s, 3H), 1.15 and 1.14 (s, 3H).

^{13}C-NMR (100 MHz, CD_3CN, two stereoisomers) δ 175.10 and 175.08, 168.9, 168.8, 157.91 and 157.89, 156.32 and 156.31, 153.6, 152.35 and 152.33, 151.8, 151.7, 151.4, 150.52 and 150.51, 150.54, 150.0, 147.1, 145.5, 145.4, 139.97 and 139.95, 139.8, 139.7, 133.01 and 132.91, 131.81 and 131.79, 131.00 and 130.98, 130.0, 129.62, 129.59, 127.93, 127.88, 127.80, 127.77, 126.99 and 126.97, 126.97 and 126.95, 126.33 and 126.31, 125.4, 125.0, 124.90 and 124.89, 124.14 and 124.13, 123.96 and 123.94, 121.3, 77.5, 60.23 and 60.20, 53.2, 38.92 and 38.86, 36.57 and 36.56, 29.01 and 28.99, 27.16, 21.92. HPLC-MS (ESI): 968 $[M - PF_6]^+$, 484 $[2M - PF_6 + H]^+$. HRMS (ESI/Flow Injection): calcd for $C_{49}H_{45}IrN_9O$ 968.3376; found 968.3379.

15b.

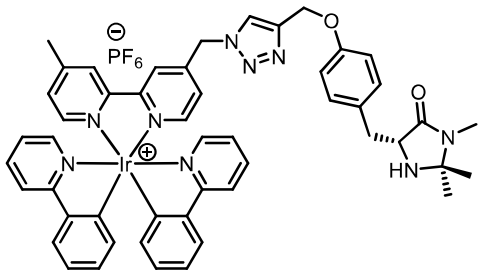

Yellow solid, Y = 97%. ^{1}H-NMR (400 MHz, CD_3CN, two stereoisomers) δ 8.42 (s, 1 H), 8.35 (s, 1 H), 8.04 (dd, J = 8.1, 3.1 Hz, 2 H), 7.98 (s, 1 H), 7.92 (d, J = 5.7 Hz, 1 H), 7.88–7.73 (m, 5 H), 7.60 (t, J = 6.8 Hz, 1 H), 7.32 (d, J = 5.6 Hz, 1 H), 7.20 (d, J = 5.7 Hz, 1 H), 7.16 (d, J = 8.4 Hz, 2 H), 7.07–6.97 (m, 4 H), 6.94–6.84 (m, 4 H), 6.27 (dd, J = 6.8, 5.3 Hz, 2 H), 5.74 (s, 2 H), 5.13 (s, 2 H), 3.63 (s, 1 H), 3.02 (dd, J = 14.2, 3.8 Hz, 1 H), 2.72–2.61 (m, 4 H), 2.52 (s, 3 H), 1.95 (dt, J = 5.0, 2.5 Hz, 1 H), 1.20 (s, 6 H). ^{13}C-NMR (100 MHz, CD^3CN, two stereoisomers) δ 174.3, 168.42 and 168.35, 157.9, 157.5, 155.9, 153.1, 151.9, 151.31 and 151.25, 150.9, 150.13 and 150.09, 149.1, 145.2, 145.06 and 144.98, 139.53 and 139.50, 132.55 and 132.46, 132.2, 131.4, 131.35 and 131.33, 130.3, 127.8, 126.6, 125.87 and 125.85, 125.76, 124.49 and 124.45, 124.3, 123.51 and 123.48, 120.85 and 120.83, 115.6, 76.5, 62.4, 60.4, 52.8, 37.8, 27.6, 25.5, 25.3, 21.5. HPLC-MS (ESI): 998 $[M - PF_6]^+$, 499 $[2M- PF6 + H]^+$. HRMS (ESI/Flow Injection): calcd for $C_{50}H_{47}IrN_9O_2$ 998.3482; found 998.3476.

15c.

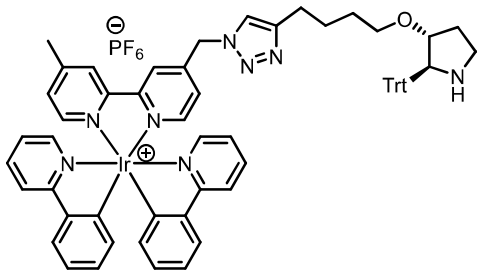

Yellow solid, Y = 90%. ^{1}H-NMR (400 MHz, $CDCl_3$, two stereoisomers) δ 8.59–8.36 (m, 2 H), 7.91–7.79 (m, 4 H), 7.82–7.70 (m, 4 H), 7.70–7.60 (m, 2 H), 7.54–7.47 (m, 2 H), 7.47–7.31 (m, 6 H), 7.24–7.18 (m, 6 H), 7.18–7.12 (m, 4 H), 7.06–6.96 (m, 4 H), 6.94–6.22 (m, 2 H), 6.30–6.22 (m, 2 H), 5.76 (s, 1 H) and 4.97–4.84 (m, 1H), 4.77 (s, 1 H), 3.70–3.60 (m, 1 H), 3.46–3.73 (m, 1 H), 3.21–3.10 (m, 1 H), 3.01–2.83 (s, 1 H), 2.84–5.69 (m, 1 H), 2.58 and 2.54 (s, 3 H), 2.30–2.24 (s, 1 H), 2.00–1.96 (s, 1 H), 1.77–1.63 (m, 4 H), 1.59–1.50 (m, 1 H), 0.20–0.35 (m, 1 H). ^{13}C-NMR (100 MHz, CD_3CN, two stereoisomers) δ 168.47 and 168.41, 157.4, 156.0, 153.1, 151.9, 151.29 and 151.22, 150.9, 150.1, 149.6, 145.05 and 144.99, 139.54 and 139.49, 139.51, 132.56 and 132.47, 131.4, 130.3, 128.6, 128.3, 127.7, 126.6, 125.9, 124.46 and 124.43, 123.5, 120.9, 52.7, 32.7, 30.4, 30.2, 30.0, 27.0, 26.0, 23.4, 22.3, 21.5, 19.3. HPLC-MS (ESI): 1135 $[M - PF_6]^+$, 568 $[2M - PF6 + H]^+$. HRMS (ESI/Flow Injection): calcd for $C_{63}H_{58}IrN_8O$ 1135.4363; found 1135.4359.

Photocatalytic alkylation of aldehydes, general procedure

In a Schlenk tube with a rotaflo stopcock under an argon atmosphereat r.t., catalysts **15a–c** (0.005 mmol, 0.01 equiv.), a solution of trifluoromethanesulfonic acid (0.1 M in DMF, 0.005 mmol, 50 µL, 0.01 equiv.) and DMF (0.45 mL) were sequentially added. After 15 minutes, bromo derivatives **30a–b** (0.05 mmol), 4 (20 µL, 0.15 mmol, 3 equiv.) and 2,6-lutidine (12 µL, 0.1 mmol, 2 equiv.,) were then added. The reaction mixture was carefully degassed via freeze-pump thaw (three times), and the vessel was refilled with argon. The mixture in the Schlenk tube was stirred and irradiated with blue LEDs. After 24 h of irradiation, aq. HCl 1 M (2 mL) was added and the mixture was extracted with AcOEt (4 × 5 mL). The organic phase was dried (Na_2SO_4) and concentrated under vacuum and the crude mixture was purified by flash-chromatography on silica.

31a. diethyl (R)-2-(1-oxo-3-phenylpropan-2-yl)malonate[35]

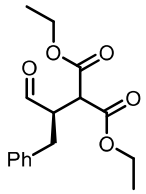

The title compound was isolated by flash column chromatography (SiO2, cyclohexane/EtOAc 95/5) as colorless oil. Y =84%, ee = 60%. ee before column purification was 70%. ee was determined by chiral HPLC analysis using a Daicel Chiralpak®IC column: hexane/i-PrOH 90/10, flow rate 1.00 mL min^{-1}, 30 °C, λ = 210 nm: t_{major} = 18.9 min, t_{minor} = 14.7 min; 1H-NMR and 13C-NMR were consistent with those reported in the literature.

31b. (R)-2-benzyl-4-oxo-4-phenylbutanal[35]

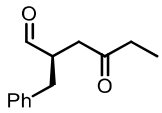

The title compound was isolated by flash column chromatography (SiO2, cyclohexane/EtOAc 97/3) as colorless oil. Y = 77%, ee = 77%. ee before column purification was 80%. ee was determined by chiral HPLC analysis using a Daicel Chiralpak®IC column, hexane/i-PrOH 90/10, flow rate 1.00 mL min^{-1}, 30 °C, λ = 210 nm: t_{major} = 17.8 min, t_{minor} = 14.9 min; ^{1}H-NMR and ^{13}C-NMR were consistent with those reported in the literature.

Visible Light Photocatalytic Synthesis of Tetrahydroquinolines Under Batch and Flow Conditions[134]

The synthesis of tetrahydroquinolines is of special interest since they are heterocyclic structures present in natural and unnatural compounds with interesting biological properties.[135–138] For example, tetrahydroquinolines display anti-HIV activity,[139] antifungal properties against Cladosporium cladosporioides, yeasts, hialohyphomycetes and dermatophytes.[140,141] In addition, they show antitumor[142] as well as antidepressant activities.[143]

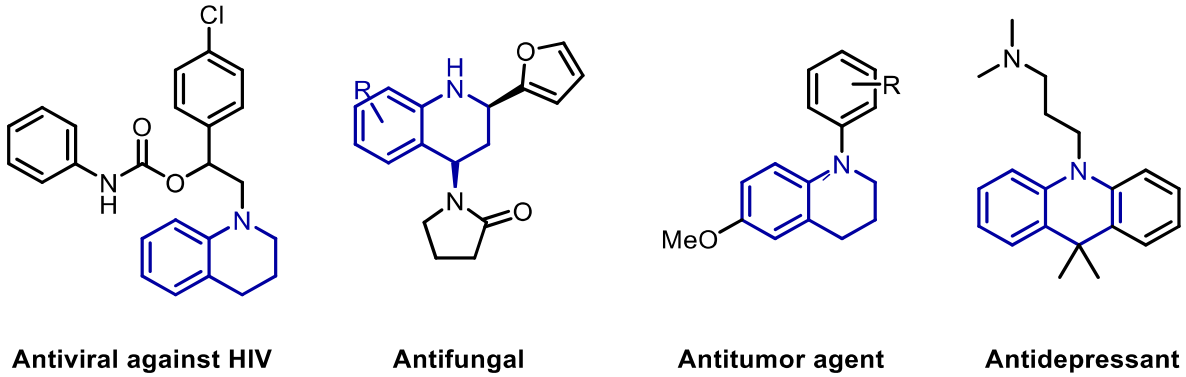

Figure 27: Bioactive molecule containing pyrrolidine heterocycle

Therefore, new approaches and strategies for the synthesis of this class of molecules are main objectives of the modern synthetic chemistry.[135]

In this regard, among all the synthetic methods available for preparing tetrahydroquinolines, radical chemistry has proven to be a straightforward methodology with a good functional group tolerance. In fact, different synthesis of tetrahydroquinolines have been reported under radical conditions, most of them using tin sources as hydrogen donor and AIBN as initiator (Scheme 45).[144–149] In these methodologies, given the harsh reaction conditions (usually 80–100 °C) required, the control in the regioselectivity of the reaction (6 exo-trig vs 7 endo-trig cyclization) is not very predictable, normally giving a mixture of products. Moreover, the protection of the starting material is usually needed, making tedious the synthesis of these derivatives because of the protection and deprotection protocols at the nitrogen atom. All these

characteristics have limited the expansion and applicability of radical chemistry for the synthesis of tetrahydroquinolines.

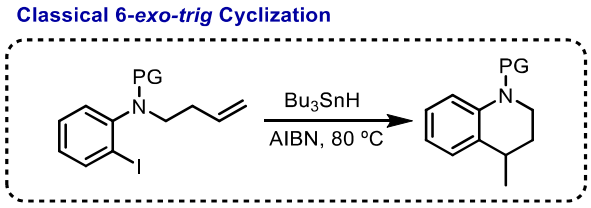

Scheme 45: Classical 6-exo-trig Cyclization

Visible light photoredox catalysis has received significant attention over the last years due to the possibility of achieving new bond constructions that are not possible using other methodologies.[39,108] The generation of radicals through SET reactions can substitute the reagents and harsh conditions of classical radical strategies. The fast development achieved in the photoredox catalytic field has paved the way for the discovery of new reactivities such as the reduction of aryl halides. Indeed, in 2012, Stephenson and co-workers demonstrated the feasibility of the photoredox catalyzed reduction of aryl halides utilizing $Ir(ppy)_3$ as photocatalyst (Scheme 46).[150] In this methodology, the reduced aryl halide underwent cyclization to five membered ring heterocyclic rings.

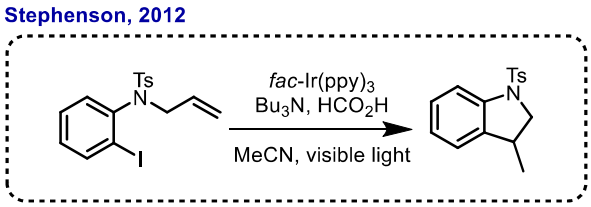

Scheme 46: Stephenson, 2012

In the same year, Lee developed a visible-light-induced photocatalytic reductive transformation of organohalides involving iridium photocatalyst ($[Ir(ppy)_2(dtbbpy)]PF_6$). In his work, too, the reduced species was subjected to an intramolecular cyclization to produce five membered heterocycles (Scheme 47).[151]

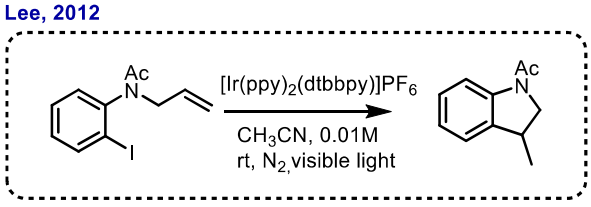

Scheme 47: Lee, 2012

Both the above-mentioned examples demonstrated the selectivity of the reduction of the carbon iodide bond compared to other carbon halogen bond. These protocols required the use of protected amino groups in the starting material molecule. However, the synthesis of tetrahydroquinolines using photocatalytic mediated conditions has not been reported yet.

Aim of the project

Given the abundance of tetrahydroquinolines in natural and unnatural compounds with interesting biological properties, the development of a practical synthetic methodology for the synthesis of these heterocyclic structures would be nowadays an important achievement. The development of a methodology eliminating toxic and hazardous reagents and performing the reaction under mild conditions, therefore avoiding heating/cooling requirement, would render the tetrahydroquinolines synthesis more accessible. Moreover, tolerance on deprotected nitrogen could facilitate the successive functionalization of the obtained tetrahydroquinolines toward the synthesis of bioactive compounds. Since common mild conditions and functional group tolerance are the major advantages of photoredox catalyzed methodologies, a new transformation involving that approach is designed and developed.

Inspired by Lee[151] and Stephenson[152] works, we envisaged that the reduction of ortho-iodo homoallylic anilines **35** under visible light photocatalysis could form aryl radical intermediates, which after intramolecular cyclization would construct tetrahydroquinolines in one-step.

In this work, the synthesis of tetrahydroquinolines under visible light irradiation and smooth conditions is developed. Moreover, a protocol for the flow photocatalytic conditions is established. Finally, a mechanistic proposal is described based on some experimental assays.

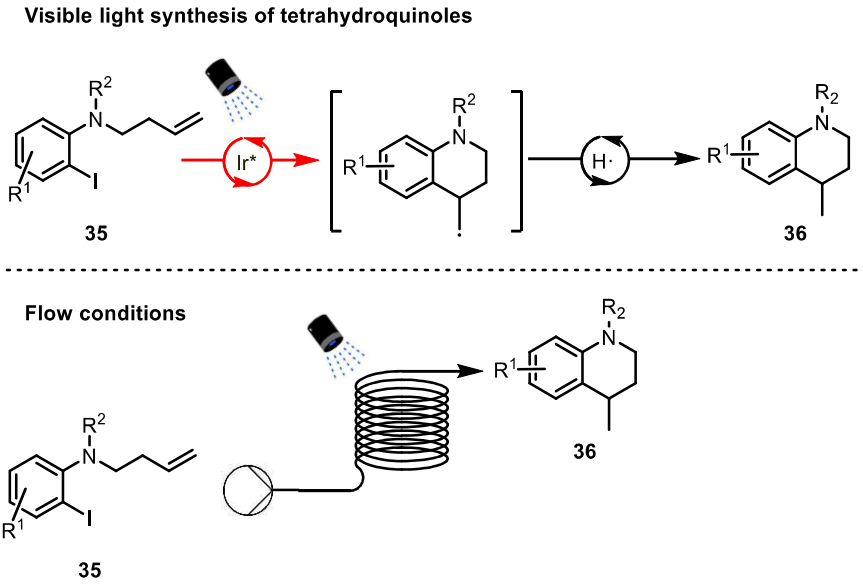

Scheme 48: Visible light photocatalytic synthesis of tetrahydroquinolines under batch and flow conditions

Discussion and results

Initially, 2-iodoaniline derivative **35a** has been synthesized and chosen as starting material for the optimization of the reaction conditions. At first, different catalysts were tested, using MeCN (0.1 M) and DIPEA (N,N-Diisopropylethylamine) as solvent and base, respectively.

Table 9: Catalysts screening

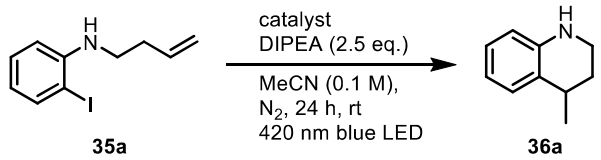

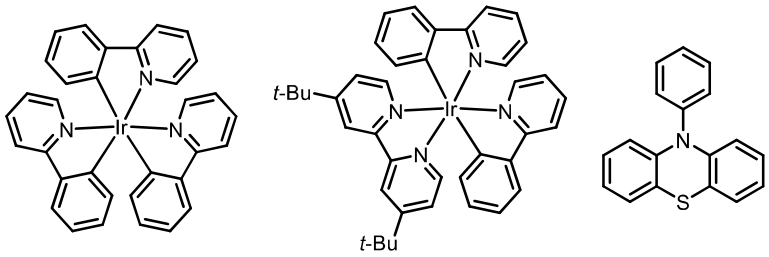

Entry[a]	Catalyst	Molarity	Catalyst mol%	Conversion %[b]	Yield %[b]
1	PTH	1	5	42	nd
2	$[Ir(dtbbpy)(ppy)_2]PF_6$	1	2	28	nd
3	$Ir(ppy)_3$	1	2	65	nd
4	$Ir(ppy)_3$	0.5	2	75	62

[a] Reaction conditions: **35a** (0.05 mmol), DIPEA (0.125 mmol) and the corresponding amount of photocatalyst in MeCN (0.5 mL, 0,5 M) were irradiated under blue LED (410 nm, 15 W) for 24 h. [b] Conversions and yields were determined by ^{1}H-NMR using CH_3NO_2 as internal standard. nd: Not determined.

The organic photocatalyst 10-phenylphenothiazine (PTH) was tested first. Its high reduction potential (E*red = –2.1 V vs. SCE)[153] would permit the reduction of aromatic halides such as **35a**.[152,154] Tetrahydroquinoline **36a** was obtained with a 42% conversion in 24 hours. The hydrodehalogenation product derived from **35a** was also observed in the reaction mixture. According to reported data,[155] $[Ir(dtbbpy)(ppy)_2]PF_6$ appeared a suitable candidate for our photoredox transformation. Therefore, it was tested too. However, only 28% conversion was reached after 24 hours. Successively, $Ir(ppy)_3$ was evaluated, even in this case the reduction potential of the catalyst would permit the reduction of aryl halides (E*red = –1.7 V vs. SCE).[153] Under the same reaction conditions, the use of this photocatalyst provides a 65% conversion with selectivity toward desired tetrahydroquinoline **36a**. This last iridium photocatalyst was selected for further optimization. Due to the low solubility of this photocatalyst in acetonitrile solvent, a reaction under more dilute conditions has been performed. This dilution permit to raising the conversion to 75%. For this experiment, the reaction yield has been

calculated from the ^{1}H-NMR using nitromethane as the internal standard. Nicely, a 62 % yield was detected, proving the high selectivity of the studied transformation.

The reaction solvent and base have then been analyzed. Among the tested solvent, MeCN confirmed itself the more suitable for our purpose, since no reaction occurred with dichloromethane (DCM), and poor conversion and selectivity were achieved with DMF. Even changing the involved base did not improve product **36a** yield.

Table 10: Solvents and bases screening

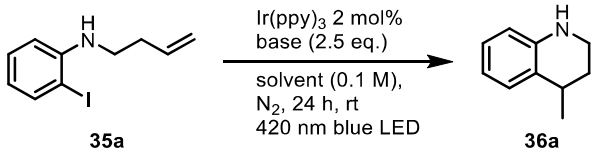

Entry[a]	Solvent	Base	Conversion %[b]	Yield %[b]
1	MeCN	DIPEA	75	62
2	DMF	DIPEA	30	nd
3	DCM	DIPEA	0	0
4	MeCN	TEA	58	42

[a] Reaction conditions: **35a** (0.05 mmol), DIPEA (0.125 mmol) and the corresponding amount of photocatalyst in MeCN (0.5 mL, 0,5 M) were irradiated under blue LED (410 nm, 15 W) for 24 h. [b] Conversions and yields were determined by ^{1}H-NMR using CH_3NO_2 as internal standard. nd: Not determined.

Afterward, the remaining reaction conditions were evaluated. Reduction of catalyst loading to 1 mol% had a positive outcome since a 78% conversion and a 70% yield were achieved. Whereas a further decrease on it (0.5 mol%) did not improve the result.

Successively, reaction concentration has been diluted up to 0.025 M, obtaining the highest conversion (90 %) and 78 % of **36a** yield. At last, reaction time was extended to 36 hours to reach complete conversion, but it led to worst results compared to 24 hours (65% yield). It could be justified by a possible degradation of product **36a** under extended time in the reaction mixture.

Table 11: Various reaction conditions screening

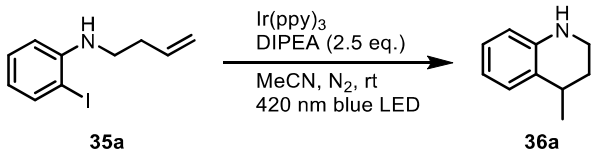

Entry[a]	Concentration (M)	Mol% catalyst	Time (h)	Conversion %[b]	Yield %[b]
1	0.05 M	2	24	75	62
2	0.05 M	1	24	78	70
3	0.05 M	0.5	24	71	60
4	0.025 M	1	24	90	78
5	0.025 M	1	36	87	65

[a] Reaction conditions: **35a** (0.05 mmol), base (0.125 mmol), and the corresponding amount of $Ir(ppy)_3$ and MeCN were irradiated under blue LED (410 nm, 15 W) for 24 h. [b] Conversions and yields were determined by ^{1}H-NMR using CH_3NO_2 as internal standard.

Reactions without light, DIPEA, or photocatalyst were carried out. In all those cases, the reaction did not proceed, confirming the key role of each component and the photocatalytic nature of the reaction.

The optimized reaction conditions were then defined. Comparing to the initial conditions, $Ir(ppy)_3$ was selected as photocatalyst and catalyst loading lowered to 0,5 mol%. DIPEA was kept as base, and acetonitrile has a solvent, even if the reaction concentration was lowered to 0.025 M.

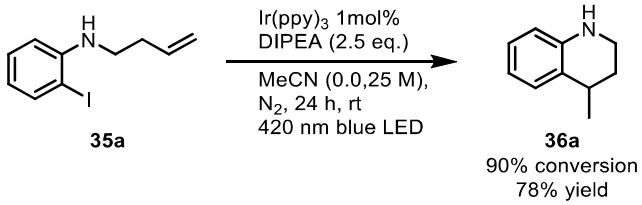

Scheme 49: Optimized reaction conditions for the photocatalyzed synthesis of tetrahydroquinolines

With the optimized conditions in hand, the scope of the reaction was then evaluated. Although the tetrahydroquinoline **36a** was considered the most interesting product from a synthetic point of view, the influence of other nitrogen substituents has been analyzed.

Thus, the N-alkyl derivatives **35b** or **35c** led to the corresponding **36b** or **36c** in good yields (63 % and 80 %, respectively). Interestingly, protecting the aniline with an acetyl group, a common protecting group for analogous substrates,[155] strongly affects the selectivity of the reaction. The almost complete conversion was observed after 24 hours,

but a complex ^{1}H-NMR spectrum showed the presence of **36d** in only a 37% yield. From the analyzed substrates, it could be deduced that electron donating protecting groups on the nitrogen favors the photocatalytic transformation. On the other hand, electron attractors deeply penalize it. The double bond substitution resulted fundamental in the investigated reaction. When the reaction was performed with 2-iodoaniline **35e** carrying a triple substituted double bond, cyclization products **36e** and **36e'** were afforded with 25% and 30% yield, respectively. Both the products observed derive from the intramolecular cyclization of **35e**, but in this case, the post-cyclization formed radical is stabilized by the two adjacent methyl group. Therefore, it can be oxidized to carbocation which undergoes E1 elimination to **36e'**.[144]

Scheme 50: Scope of the photocatalyzed synthesis of tetrahydroquinolines

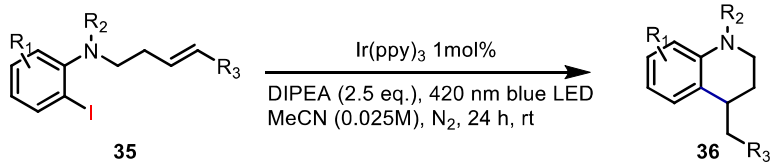

Substrates

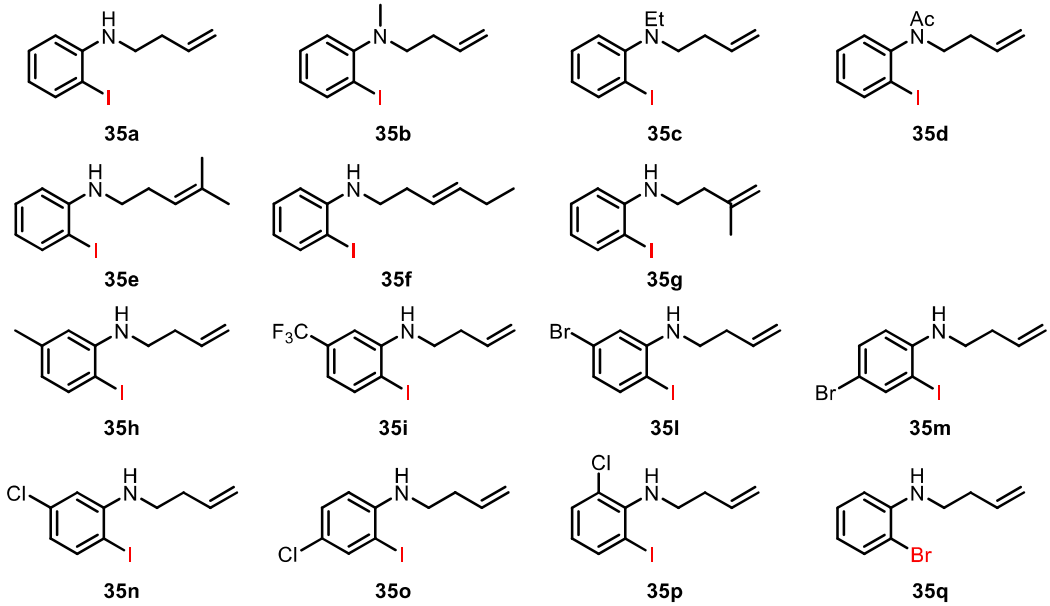

Tetrahydroquinolines

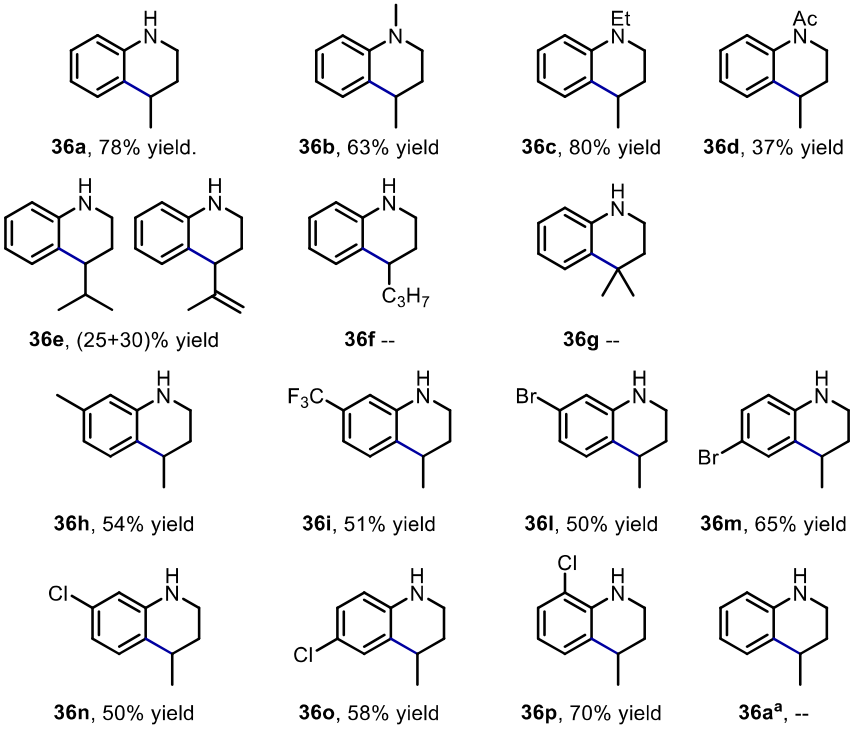

[a] Reaction with **35q** as starting material

The heterocyclization step was not observed using both **35f** and **35g**, probably due to the steric hindrance imposed by those substituents.

Next, we studied the influence of substituents at the aromatic ring of the 2-iodoaniline derivative. The introduction of a methyl group (**35h**), as well as electron withdrawing (CF_3) group (**35i**) in meta-position with respect to the amino moiety, afforded the corresponding tetrahydroquinolines **36h-i** in good yields (50–54 %). The moderate yields obtained for some examples are due to the detection of the dehalogenation product along with the cyclized product **36**. Tetrahydroquinolines having bromine substituents are interesting compounds in the medicinal chemistry area, as they can be further functionalized via transition metal coupling reactions to easily generate derivatives. Thus, bromo-substituted anilines **35l** and **35m** having bromine at 7- and 6-position, respectively, were tested under the reaction conditions. Pleasantly, they reacted to obtain tetrahydroquinolines **36l** and **36m** in 50 and 65 % yield, correspondingly. It is important to mention that the reduction of the iodide group was the only pathway observed and the possible reduction of the bromine was not detected for those cases. Furthermore, the chemoselectivity of the reduction process was confirmed by when a chlorine atom is present at ortho-, meta-, and para-positions with respect to the amino group of the aromatic ring. In all cases, the corresponding heterocycles **36n-p** have been successfully isolated in good yields (50– 70 %). As a authentication of the observed trend, bromo derivative **35q** could not give any reaction, probably due to its high reduction potential (for analogous bromo-benzene derivatives, Ered = –2.05 to –2.57 vs. SCE).[154]

Successively, the reductive cyclization of **35a** at 0,2 mmol scale, which was the largest quantity allowed by the utilized batch photoreactor. At this reaction scale, the heterocycle **36a** was obtained in low yield (36% yield). Different well-known reasons such as the low concentration of the reagents and low penetrability of light (Lambert–Beer law) among others render batch conditions not suitable for scaling up purposes with our devices.[106,156] Considering the importance of developing a scalable procedure for the synthesis of tetrahydroquinolines, a photocatalytic flow methodology was designed. Thus, the flow of the reaction mixture through a fine channel increases the surface/volume ratio as well as the radiation efficiency of the light. In addition, the development of the reaction in flow chemistry allows to scale up processes even though

the concentration of the reaction is not very high. For all the reasons, the reductive cyclization procedure under photocatalytic flow conditions was studied.

A continuous flow microreactor was then assembled. Initially, the assembled flow apparatus consisted of a syringe pump connected to a coil reactor (7 mL) made of perfluoroalkoxy (PFA) capillary tubing (1/16" OD; 0.80 mm ID; 14 m length), wrapped around a Pyrex beaker (80 mm diameter; 140 mm height) and irradiated with a 15W blue LEDs system. Different reaction parameters have been optimized. At first residence time was investigated, 10 minutes residence time led to poor yield in product **36a** formation (Entry 1). Thus, a longer time was analyzed, after 1 hour a 45% yield was pleasingly achieved (Entry 2). On the other hand, a further increase of the involved time did not improve the efficiency of the developed transformation (45% yield, Entry 6). Degassing the reaction mixture before the injection in the flow reactor, permit to reach a 60% yield, confirming the data collected under batch conditions (Entry 3, Table 12). A decrease in the reaction concentration affects product formation (Entry 4, Table 12). At last, the effect of lowering temperature was studied. Even in this case, no improvement was achieved (Entry 5, Table 12).

Table 12: Optimization of the photocatalyzed synthesis of tetrahydroquinolines in flow chemistry technology

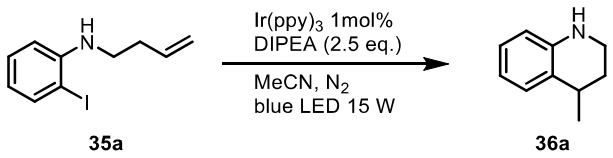

35a **36a**

Entry[a]	Flow rate (µL / min)	t_R (min)	Concentration	T (°C)	Yield %[b]
1	675	10	0.025	30	10
2	112.5	60	0.025	30	45
3 [c]	112.5	60	0.025	30	60
4 [c]	112.5	60	0.015	30	44
5 [c]	112.5	60	0.025	0 to 30	40
6 [c]	56.25	120	0,025	30	45

[a] Reaction conditions: **35a** (0.0625 mmol), DIPEA (0.16 mmol), Ir(ppy)3 (1 mol%) and MeCN (2.5 mL). [b] Yields determined by ^{1}H-NMR using CH_3NO_2 as internal standard. [c] Degasified sample.

Under optimized conditions (t_R = 60 min; [**35a**] = 0.025 M; T = 30 °C), tetrahydroquinoline **36a** was obtained in 60% yield (throughput = 4.6 x 10-4 mmol/min). Giving these promising results, flow system volume was increased to achieve higher

throughput. The second flow system apparatus consisted of a syringe pump connected to a coil reactor (18 mL) made of PFA capillary tube (1/8" OD; 1.60 mm ID; 9 m length), wrapped around a Pyrex beaker (80 mm diameter; 140 mm height). This setup was irradiated with a blue LED spot (Kessil A160WE; 40 W) placed at the top of the coil reactor. A fan (90 mm diameter) was set at the top of the system to dissipate heat generated by the light source. The second flow photoreactor allowed us to increase flow rate up to 0.3 mL/min, yielding **36a** (0.045 mmol; 72%) in 60 min residence time, corresponding to a 1.45 times productivity enhancement (throughput = 6.6 x 10-4 mmol/min) in comparison with the first flow photoreactor.

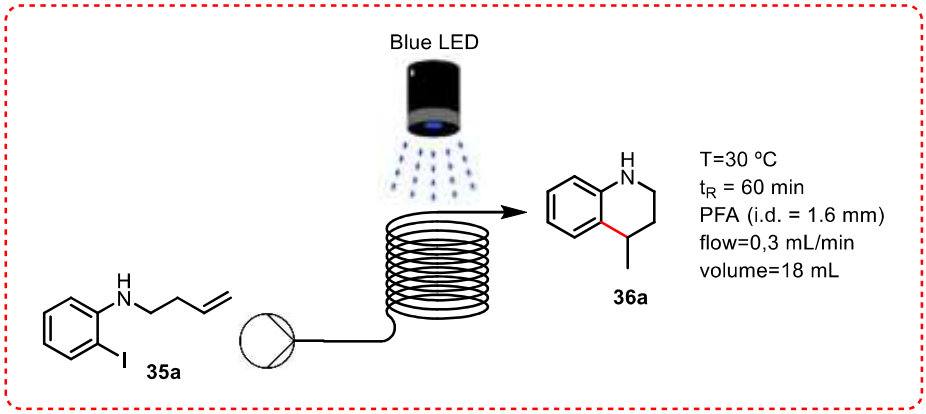

First flow photoreactor
coil (7 mL) made of 1/16' PFA tubing

Second flow photoreactor
coil (18 mL) made of 1/8' PFA tubing

Figure 28: Flow chemistry apparatus

The optimized flow conditions worked quite well for most of the substrates **35** studied, obtaining similar yields to batch conditions for heterocycles **36a**, **36c**, **36h,** and **36j**. It has to be outlined that each substrate has been tested under two hours of residence time. However, no significant differences from 1 hour residence experiments time were observed. Moreover, consistently higher yields for products **36i** and **36k** were detected.

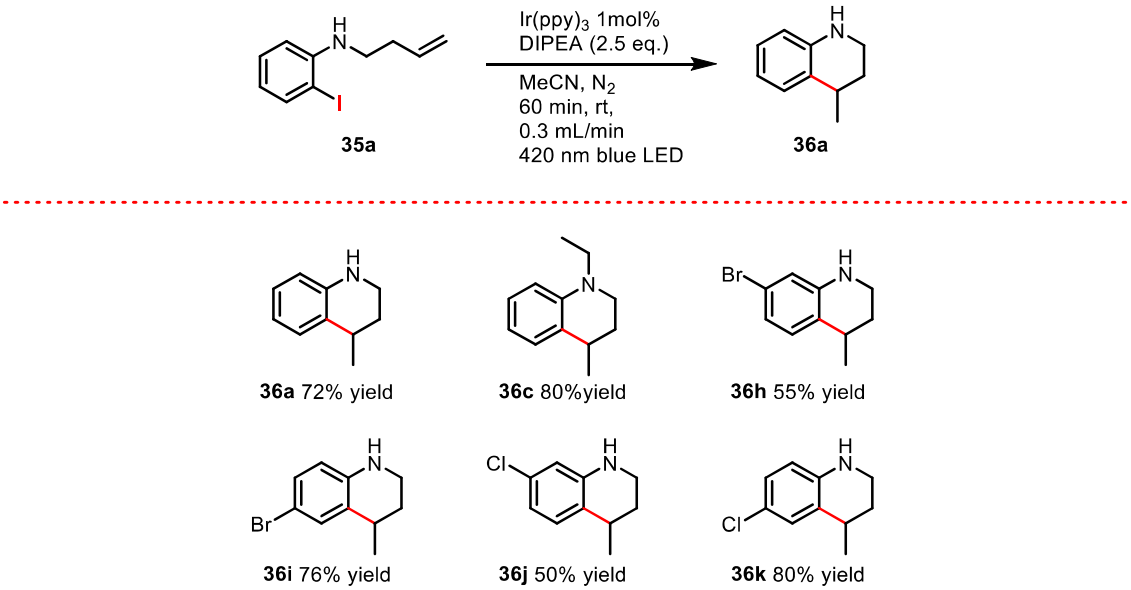

Scheme 51: Scope of the photocatalyzed synthesis of tetrahydroquinolines under flow conditions

A mechanistic framework for the photocatalytic transformation was developed, based on previous literature[152,155], and our experiments. As above described, blue LEDs irradiation, photocatalyst $Ir(ppy)_3$, and a DIPEA revealed themselves necessary for the product achievement, since no reaction occurred when one of them was removed from the reaction conditions. Moreover, Stern Volmer experiments were performed to verify the effective quencher of the catalyst excited species. These experiments indicate that whereas the DIPEA does not affect the excited state of Ir(ppy)3, 2-iodoaniline **35a** effectively quenches the emission of the photocatalyst, with a Stern-Vomer constant of Ksv = 34.6 M^{-1}.

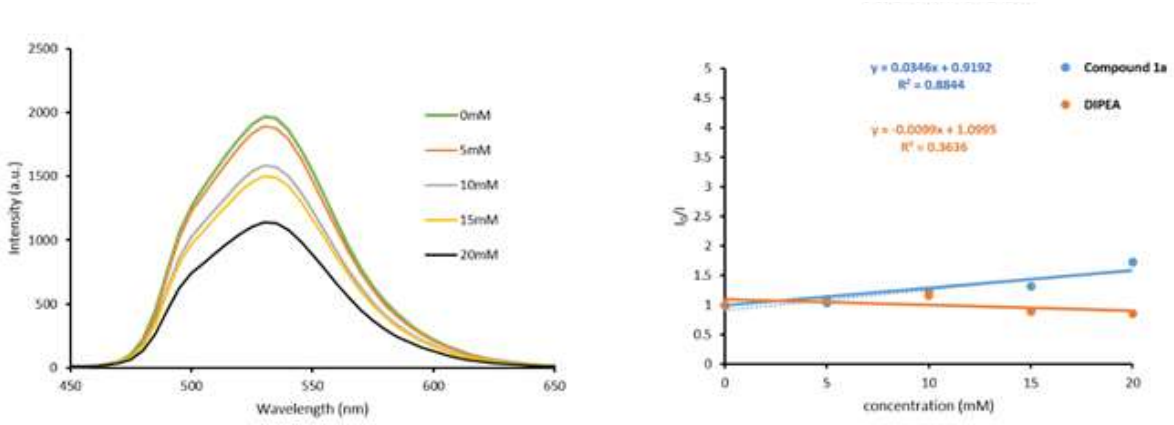

Figure 29: Stern Volmer experiments

The hypothesized mechanism is shown in Scheme 52 (Scheme 52).[151,152] Starting aniline **35a** is reduced by the excited $Ir^{(III)*}$ species to form radical **G** and the oxidized $Ir^{(IV)}$ species. Successively, **G** reacts in an intramolecular 6-*exo*-trig-radical cyclization to form radical **H**. Finally, radical **H** is subjected to a hydrogen atom transfer process (HAT) to obtain product **36**. Simultaneously, the mentioned oxidized species $Ir^{(IV)}$ is reduced by DIPEA to regenerate the catalyst original form $Ir^{(III)}$ and close the catalytic cycle. It is not clear the source of the HAT process, it could be due to both the oxidized base ($DIPEA^{\bullet+}$) or the acetonitrile solvent. It has to be outlined that a sacrificial agent is involved to restore the photocatalytic cycle. Indeed, here DIPEA acts both as a sacrificial agent and as a base, this is the reason we need 2 equivalents of it in the reaction optimized conditions.

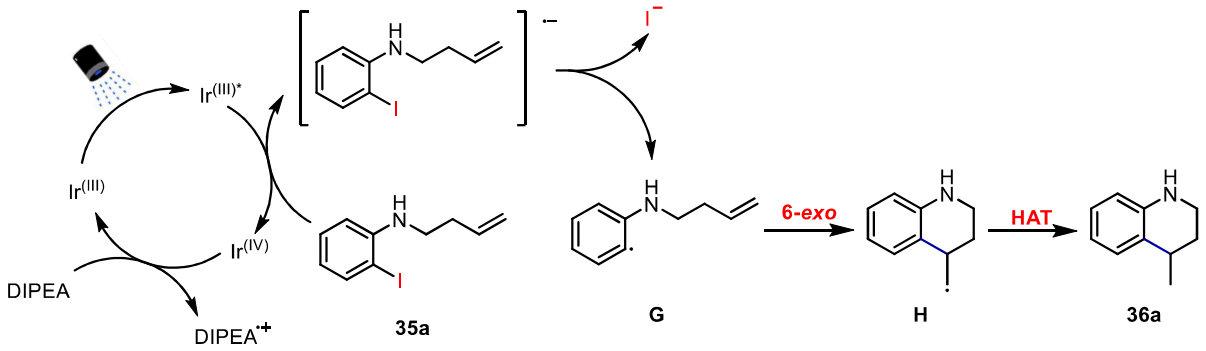

Scheme 52: Hypothesized mechanism

Conclusion

In conclusion, an effective method for the cyclization of ortho-iodo homoallylic anilines **35** to tetrahydroquinolines **36**. The developed transformation has been applied in both batch and flow conditions.

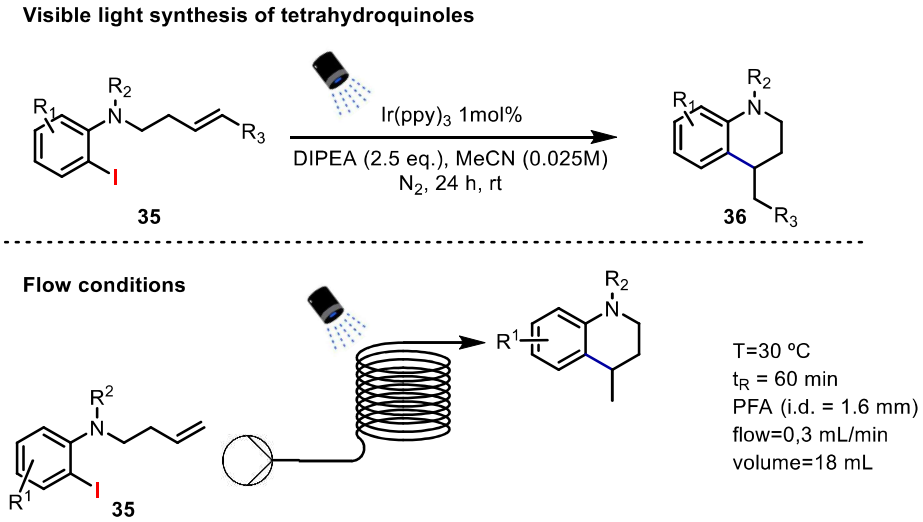

Scheme 53: Optimized conditions for the photocatalytic synthesis of tetrahydroquinolines in Batch and Flow conditions

This methodology constitutes an alternative to the classic methods that use toxic reagents and more energetic conditions. In addition, the strategy does not need the use of nitrogen protecting groups. It can be applied to various 2-iodoaniline derivatives with different substituents on the aromatic ring. Worst results were observed utilizing substrates containing substituted carbon-carbon double bond. Although one of the limitations is the 24-hour reaction times in batch conditions, the use of flow conditions allows to obtain the products in just one hour. At last, a mechanistic hypothesis has been presented based on experimental data and literatures.[144,151,152]

General Procedures and Products Characterization

Materials and methods

NMR spectra were acquired on a BRUKER AVANCE 300 or 500 MHz spectrometer running at 300 MHz for 1H, 75 or 126 MHz for 13C, 282 MHz for 19F, and are internally referenced to residual solvent signals (CDCl3 referenced at δ 7.26 ppm for 1H-NMR and δ 77.2 ppm for 13C-NMR). Data for 1H-NMR are reported as follows: chemical shift (δ ppm), multiplicity (s = singlet,d = doublet, t = triplet, q = quartet, p = quintuplet, hept = heptuplet, m = multiplet, br = broad), coupling constant (Hz) and integration. Data for 13C and 19F, are reported in terms of chemical shift. High-Resolution Mass Spectra (HRMS) were obtained on an Agilent Technologies 6120 Quadrupole LC/MS coupled with an SFC Agilent Technologies 1260 Infinity Series instrument for the MS (ESI) (Electrospray Ionization). MassWorks software version 4.0.0.0 (Cerno Bioscience) was

used for the formula identification. MassWorks is an MS calibration software which calibrates isotope profiles to achieve high mass accuracy and enables elemental composition determination on conventional mass spectrometers of unit mass resolution allowing highly accurate comparisons between calibrated and theoretical spectra. Emission spectra were recorded on a JASCO spectrofluorometer FP-8600 equipped with a TC-815 Peltier thermostatted single-cell holder (water-cooled) controlled by Spectra Manager version 2.10.01. HPLC grade deoxygenated CH3CN solvent and a 10 × 10 mm2 light path quartz Suprasil cuvette equipped with a silicone/poly(tetrafluoroethylene) (PTFE) septum were used for all measurements. Emission spectra of the light sources used for the photochemical reactions were recorded on an optical spectrometer StellarNet model Blue-Wave UV-NB50. All reagents and materials were purchased from commercial sources and used without further purification, whereas anhydrous solvents were taken from an SPS solvent dispenser or purchased from commercial sources. Chromatographic purification of products was accomplished by: i) preparative TLC (PTLC) using pre-coated glass-backed plates (Merck PLC Silicagel 60 F254, 0.5 mm) and visualizing by ultraviolet irradiation, or ii) flash chromatography using silica gel (Merck Geduran® Si 60) or porous silica gel (LSI Medience Corporation Iatrobeads 6RS-8060).

Light systems for performing the photocatalytic reactions

For the photocatalytic reactions in batch, a custom-made "light box" with 5 strips of blue LEDs (15 W) attached around a test tube rack was used, with a fan for keeping the reaction mixture at room temperature (Figure).

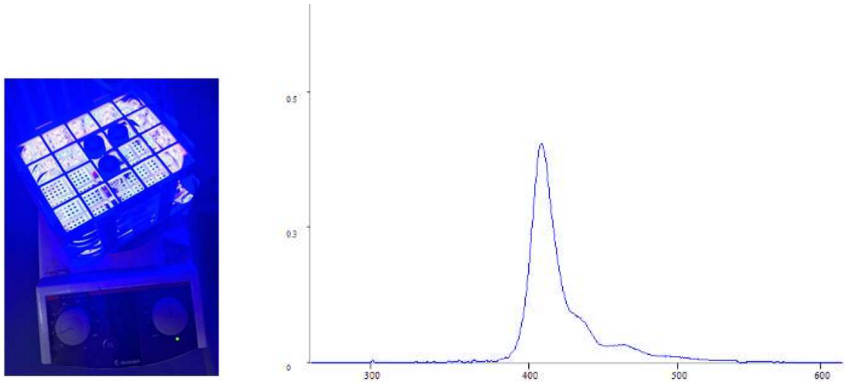

Photocatalytic system for batch reactions (left). Emission spectrum of Blue LED custom-made "light box" (right).

For the photocatalytic reactions in flow, a blue LED spot (Kessil A160WE; 40W) was used. A fan (90 mm diameter) was set at the top of the system to dissipate heat generated by the light.

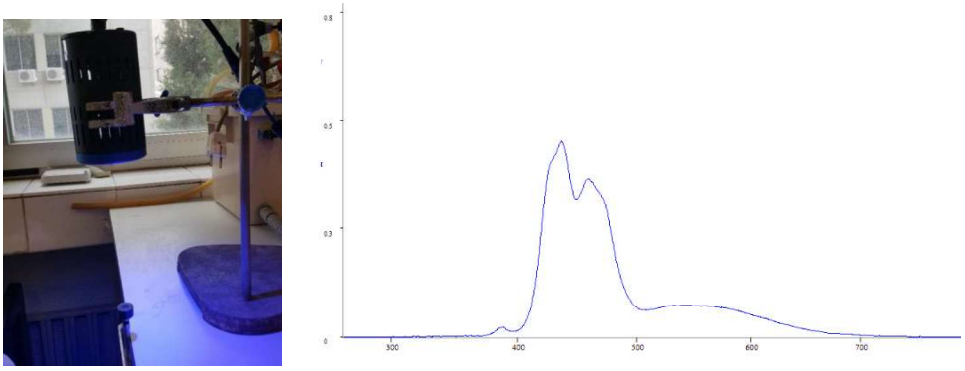

Photocatalytic system for flow reactions (left). Emission spectrum of blue LED spot Kessil A160WE

Stern-Volmer quenching studies

Emission intensities were recorded on a JASCO Spectrofluorometer FP-8600 equipped with a TC-815 Peltier thermostated single cell holder (water-cooled) controlled by Spectra Manager Version 2.10.01. CH_3CN was used for all luminescence quenching experiments (Figure S3, left). All $Ir(ppy)_3$ solutions were excited at 420 nm, observing the maximum emission peak at 530 nm. The appropriate amount of quencher (DIPEA or compound **1a**) was added to the CH_3CN solution of $Ir(ppy)_3$ (30 µM) in a Teflon-top 10x10 mm precision cell made of Quartz SUPRASIL®. After degassing with Ar for 2 min, the emission spectra of the samples were collected. The Stern-Volmer plot displayed in Figure S3 (right) shows a linear correlation between the concentration of quencher [Q] and the intensities of the emission (I) according to the equation $I_0/I = K_{SV} \cdot [Q] + 1$. These results clarify that, the excited state of the $Ir(ppy)_3$ is quenched only by compound **1a**.

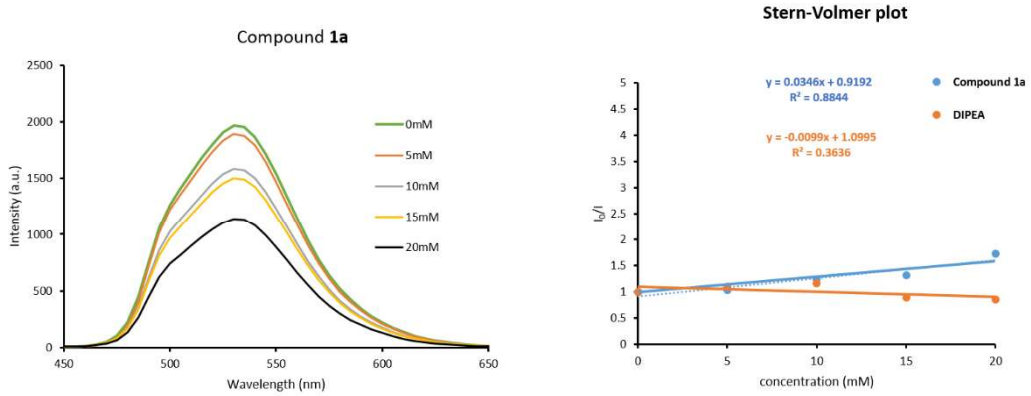

Quenching emission of compound **35a** with $Ir(ppy)_3$ (left). Stern-Volmer plot of compound **35a** and DIPEA with $Ir(ppy)_3$ (right).

Synthesis of 10-phenylphenothiazine (PTH)[157]

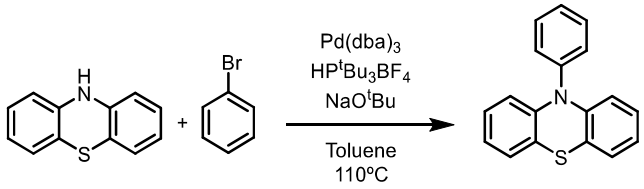

Phenothiazine (1.83 g, 10 mmol), 1-bromobenzene (1.15 mL, 11 mmol), $Pd_2(dba)_3$ (275 mg) and $HP^tBu_3BF_4$ (145 mg) were added to a sealed tube. Then 11 mL of toluene was added, and the mixture was stirred for 15 min. Finally, NaO^tBu (1.11 g) was added and the reaction mixture was stirred at 110 ºC for 48 h. After cooling to rt, the resulting mixture was diluted with DCM (20 mL) and filtered through a pad of celite®. The celite pad was washed with DCM (4 x 10 mL). The combined of organic solvents were evaporated under reduced pressure and the crude was purified by flash chromatography (silica, 99:1 cyclohexane:EtOAc). PTH was obtained as a white solid (2.40 g, 87% yield).

^{1}H-NMR (300 MHz, $CDCl_3$): δ 7.55 – 7.65 (m, 2H), 7.45 – 7.50 (m, 1H), 7.35 – 7.42 (m, 2H), 7.00 – 7.05 (m, 2H), 6.75 – 6.90 (m, 4H), 6.15 – 6.25 (m, 2H).

Synthesis of 2-iodoaryl derivatives 35

General procedure A. Synthesis of **35a**, **35e**, **35h-p**

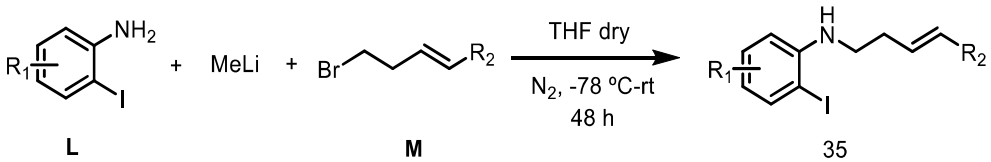

To an oven-dried round-bottomed flask were added the corresponding 2-iodoaniline (**L**) (4.57 mmol, 1 equiv.) and 20 mL of dry THF under N_2 atmosphere. Then, the reaction was cooled to -78 ºC and a 1.6 M methyl lithium solution in THF (3.6 mL, 4.57 mmol, 1 equiv.) was added dropwise. After 30 min, **M** (6.88 mmol, 1.5 equiv.) was added, and the reaction was stirring at rt for 48 h. Then, the reaction was quenched with 20 mL of a saturated aqueous solution of NH_4Cl. The reaction mixture was extracted with Et_2O (2x30 mL) and the combined organic layers were dried over $MgSO_4$ and filtered. The reaction mixture was concentrated under reduced pressure and purified by flash column chromatography (silica gel) to provide the pure 2-iodoanilines derivatives (**35**).

***N*-(but-3-en-1-yl)-2-iodoaniline(35a)** [158]

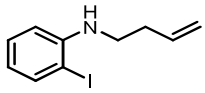

After purification by flash chromatography (silica, 99:1 cyclohexane:EtOAc), **35a** was isolated as orange liquid (555 mg, 45% yield). ^{1}H-NMR (300 MHz, $CDCl_3$): δ 7.65 (dd, *J* = 7.8, 1.5 Hz, 1H), 7.18-7.24 (m, 1H), 6.56 (dd, *J* = 8.2, 1.3 Hz, 1H), 6.44 (td, *J* = 7.6, 1.5 Hz, 1H), 5.79-5.92 (m, 1H), 5.14-5.24 (m, 2H), 4.21 (br s, 1H), 3.20-3.25 (m, 2H), 2.40-2.48 (m, 2H).

2-Iodo-*N*-(4-methylpent-3-en-1-yl)aniline (35e)

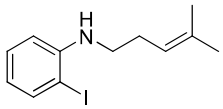

After purification by flash chromatography (silica, 80:20 cyclohexane:EtOAc), **35e** was isolated as colourless liquid (137 mg, 10% yield). ^{1}H-NMR (300 MHz, $CDCl_3$): δ 7.65 (dd, *J* = 7.8, 1.4 Hz, 1H), 7.18-7.23 (m, 1H), 6.56 (d, *J* = 8.1 Hz, 1H), 6.40–6.46 (m, 1H), 5.17 (t, *J* = 7.4 Hz, 1H), 4.20 (br s, 1H), 3.11-3.17 (m, 2H), 2.34-2.41 (m, 2H), 1.76 (s, 3H), 1.69 (s, 3H). ^{13}C-NMR (75 MHz, $CDCl_3$): δ 147.5, 139.0, 135.0, 129.4, 121.0, 118.4, 110.8, 85.5, 43.8, 27.8, 25.9, 18.0. HRMS (ESI): Calcd for $C_{12}H_{17}IN$ $[M+H]^+$: 302.0354, found: 302.0378.

***N*-(But-3-en-1-yl)-2-iodo-5-methylaniline (35h)**

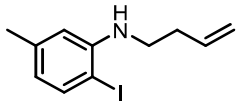

After purification by flash chromatography (silica, 99:1 cyclohexane:EtOAc), **35h** was isolated as red liquid (224 mg, 18% yield). ^{1}H-NMR (300 MHz, $CDCl_3$): δ 7.51 (d, J= 7.9 Hz, 1H), 6.40 (s, 1H), 6.28–6.39 (m, 1H), 5.82-5.91 (m, 1H), 5.14-5.24 (m, 2H), 4.13 (br s, 1H), 3.19-3.25 (m, 2H), 2.40–2.48 (m, 2H), 2.28 (s, 3H). ^{13}C-NMR (75 MHz, $CDCl_3$): δ 147.0, 139.5, 138.6, 135.4, 119.7, 117.5, 111.6, 81.5, 43.2, 33.4, 21.5. HRMS (ESI): Calcd for $C_{11}H_{15}IN$ $[M+H]^+$: 288.0244, found: 287.0280.

***N*-(But-3-en-1-yl)-2-iodo-5-(trifluoromethyl)aniline (35i)**

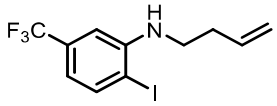

After purification by flash chromatography (silica, 100% cyclohexane), **35i** was isolated as orange liquid (250 mg, 18% yield). ^{1}H-NMR (300 MHz, $CDCl_3$): δ 7.74 (d, J= 8.0 Hz, 1H), 6.70 (s, 1H), 6.67 (d, J=8.2 Hz, 1H), 5.84-5.87 (m, 1H), 5.17-5.26 (m, 2H), 4.42 (br s, 1H), 3.22-3.28 (m, 2H), 2.43-2.50 (m, 2H). ^{13}C-NMR (75 MHz, $CDCl_3$): δ 147.5, 139.3, 135.0, 131.9 (q, $J_{C\text{-}F}$= 32.1 Hz), 124.1 (q, $J_{C\text{-}F}$ = 272.4 Hz), 118.0, 114.5 (q, $J_{C\text{-}F}$ = 3.9 Hz), 106.4 (q, $J_{C\text{-}F}$ = 3.9 Hz), 88.8, 42.9, 33.2. ^{19}F NMR (282 MHz, $CDCl_3$): δ -63.08 (s). HRMS (ESI): Calcd for $C_{11}H_{12}F_3IN$ $[M+H]^+$: 341.9961, found: 341.9986.

5-Bromo-*N*-(but-3-en-1-yl)-2-iodoaniline (35l)

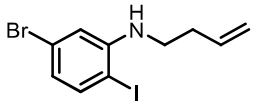

After purification by flash chromatography (silica, 98:2 cyclohexane:EtOAc), **35l** was isolated as yellow liquid (420 mg, 31% yield). ^{1}H-NMR (300 MHz, $CDCl_3$): δ 7.47 (d, J= 8.2 Hz, 1H), 6.65 (s, 1H), 6.56 (d, J= 8.3 Hz, 1H), 5.79-5.89 (m, 1H), 5.16–5.25 (m, 2H), 4.27 (br s, 1H), 3.16-3.22 (m, 2H), 2.41–2.47 (m, 2H). ^{13}C-NMR (75 MHz, $CDCl_3$): δ 148.2, 139.7, 135.1, 123.6, 121.2, 117.9, 113.3, 83.1, 43.0, 33.2. HRMS (ESI): Calcd for $C_{10}H_{12}BrIN$ $[M+H]^+$: 351.9192, found: 351.9175.

4-Bromo-*N*-(but-3-en-1-yl)-2-iodoaniline (35m)

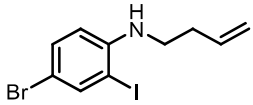

After purification by flash chromatography (silica, 100% cyclohexane), **35m** was isolated as orange liquid (350 mg, 22% yield). ^{1}H-NMR (300 MHz, $CDCl_3$): δ 7.73 (d, *J* = 2.3 Hz, 1H), 7.28 (dd, *J* = 8.7, 2.2 Hz, 1H), 6.40 (d, *J* = 8.7 Hz, 1H), 5.79-5.88 (m, 1H), 5.15–5.23 (m, 2H), 4.21 (br s, 1H), 3.15-3.22 (m, 2H), 2.39-2.46 (m, 2H). ^{13}C-NMR (75 MHz, $CDCl_3$): δ 146.4, 140.4, 135.1, 132.1, 117.8, 111.5, 108.5, 85.3, 43.2, 33.2. HRMS (ESI): Calcd for $C_{10}H_{12}BrIN$ $[M+H]^+$: 351.9192, found: 351.9220.

N-(But-3-en-1-yl)-5-chloro-2-iodoaniline (35n)

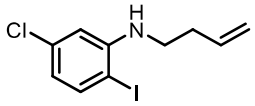

After purification by flash chromatography (silica, 98:2 cyclohexane:EtOAc), **35n** was isolated as yellow liquid (423 mg, 30% yield). ^{1}H-NMR (300 MHz, $CDCl_3$): δ 7.53 (d, *J* = 8.3 Hz, 1H), 6.51 (d, *J* = 2.3 Hz, 1H), 6.44 (dd, *J* = 8.3, 2.3 Hz, 1H), 5.80-5.89 (m, 1H), 5.16–5.25 (m, 2H), 4.28 (br s, 1H), 3.17-3.23 (m, 2H), 2.41-2.48 (m, 2H). ^{13}C-NMR (75 MHz, $CDCl_3$): δ 148.1, 139.4, 135.6, 135.1, 118.3, 117.9, 110.5, 82.2, 43.0, 33.2. HRMS (ESI): Calcd for $C_{10}H_{12}ClIN$ $[M+H]^+$: 307.9697, found: 307.9701.

N-(But-3-en-1-yl)-4-chloro-2-iodoaniline (35o)

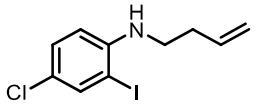

After purification by flash chromatography (silica, 100% cyclohexane), **35o** was isolated as yellow liquid (380 mg, 27% yield). ^{1}H-NMR (300 MHz, $CDCl_3$): δ 7.62 (d, *J* = 2.4 Hz, 1H), 7.17 (dd, *J* = 8.7, 2.4 Hz, 1H), 6.45 (d, *J* = 8.7 Hz, 1H), 5.78-5.91 (m, 1H), 5.15–5.24 (m, 2H), 4.20 (br s, 1H), 3.16-3.22 (m, 2H), 2.40-2.46 (m, 2H). ^{13}C-NMR (75 MHz, $CDCl_3$): δ 146.0, 137.9, 135.2, 129.2, 121.8, 117.8, 110.8, 84.7, 43.3, 33.3. HRMS (ESI): Calcd for $C_{10}H_{12}ClIN$ $[M+H]^+$: 307.9697, found: 307.9724.

N-(But-3-en-1-yl)-2-chloro-6-iodoaniline (35p)

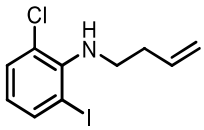

After purification by flash chromatography (silica, 100% cyclohexane), **35p** was isolated as yellow liquid (140 mg, 10% yield). ^{1}H-NMR (300 MHz, $CDCl_3$): δ 7.66 (dd, *J* = 7.9, 1.4 Hz, 1H), 7.30 (dd, *J* = 8.0, 1.4 Hz, 1H), 6.56-6-63 (m, 1H), 6.82–5.91 (m, 1H), 5.10–5.22 (m, 2H), 3.84 (br s, 1H), 3.30-3.35 (m, 2H), 2.35–2.42 (m, 2H). ^{13}C-NMR (75 MHz, $CDCl_3$): δ 146.5, 138.4, 135.6, 130.7, 125.7, 123.9, 117.2, 93.3, 47.5, 35.0. HRMS (ESI): Calcd for $C_{10}H_{12}ClIN$ $[M+H]^+$: 307.9697, found: 307.9696.

Procedure B. Synthesis of *N*-(but-3-en-1-yl)-2-iodo-*N*-methylaniline (35b) [158]

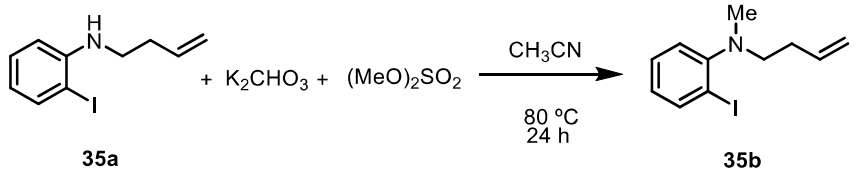

35a **35b**

N-(but-3-en-1-yl)-2-iodoaniline **35a** (145 mg, 0.53 mmol) was dissolved in 3 mL of CH_3CN. Then, K_2CO_3 (207 mg, 1.5 mmol) and dimethyl sulfate (142 □l, 1.5 mmol) were added. Then, the reaction was stirred 24 h at 80 °C. Next, the reaction was cooled to rt and diluted with EtOAc (5 mL). The organic layer was washed with water (2 x 8 mL), brine, dried over $MgSO_4$, filtered and concentrated under reduced pressure. The crude residue was purified by flash column chromatography (silica, 100% cyclohexane) to provide **35b** as colourless liquid (100 mg, 66% yield). ^{1}H-NMR (300 MHz, $CDCl_3$): δ 7.85 (dd, *J* = 7.9, 1.4 Hz, 1H), 7.28-7.34 (m, 1H), 7.09 (dd, *J* = 8.0, 1.4 Hz, 1H), 6.79 (td, *J* = 7.6, 1.5 Hz, 1H), 5.79-5.92 (m, 1H), 4.98–5.08 (m, 2H), 2.99–3.04 (m, 2H), 2.73 (s, 3H), 2.27-2.34 (m, 2H).

Procedure C. Synthesis of *N*-(but-3-en-1-yl)-*N*-ethyl-2-iodoaniline (35c)

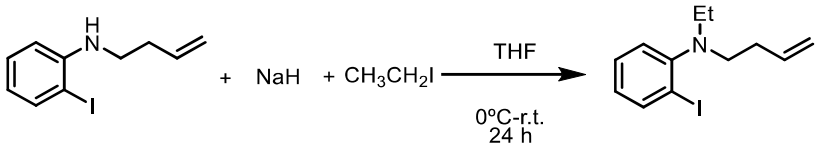

To a solution of *N*-(but-3-en-1-yl)-2-iodoaniline **35a** (137 mg, 0.5 mmol) in 5 mL of dry THF, NaH (24 mg, 1 mmol) was added. Then, the reaction was cooled to 0 °C, iodoethane (60 □l, 0.75 mmol) was added dropwise and the reaction was stirred 24 h at rt. Then, the reaction was quenched with 5 mL of saturated NH_4Cl, extracted with EtOAc (2 x 5 mL). The organic layers were washed with brine, dried over $MgSO_4$, filtered and concentrated under reduced pressure. The residue was purified by flash column chromatography (silica, 100% cyclohexane) to provide **35c** as colourless liquid (30 mg,

20% yield). ^{1}H-NMR (300 MHz, $CDCl_3$): δ 7.87 (dd, *J* = 7.9, 1.5 Hz, 1H), 7.27–7.30 (m, 1H), 7.09 (dd, *J* = 8.0, 1.5 Hz, 1H), 6.81 (td, *J* = 7.6, 1.5 Hz, 1H), 5.74-5.86 (m, 1H), 4.95-5.04 (m, 2H), 3.01–3.08 (m, 4H), 2.15-2.22 (m, 2H), 1.03 (t, *J* = 7.1 Hz, 3H). ^{13}C-NMR (75 MHz, $CDCl_3$): δ 152.0, 139.9, 136.6, 128.6, 125.8, 124.3, 115.5, 102.2, 53.0, 48.9, 31.8, 12.1. HRMS (ESI): Calcd for $C_{12}H_{17}IN$ [M+H]+: 302.0354, found: 302.0333.

Procedure D. Synthesis of *N*-(but-3-en-1-yl)-*N*-(2-iodophenyl)acetamide (35d)

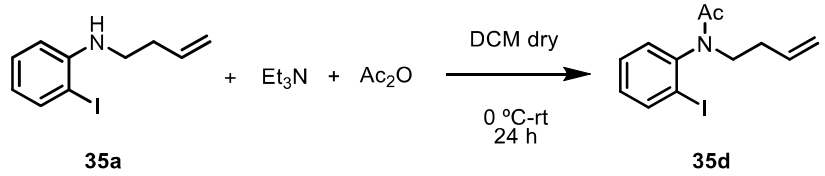

35a **35d**

N-(but-3-en-1-yl)-2-iodoaniline **35a** (200 mg, 0.73 mmol) was dissolved in 2 mL of dry DCM. After stirring for 5 min, trimethylamine (0.22 mL, 1.6 mmol) was added. Then, the reaction was cooled to 0 °C and acetic anhydride (83 □l, 0.88 mmol) was added dropwise. Afterwards, the reaction mixture was stirred for 24 h at rt. Then, the reaction was washed with water (2 x 2 mL), brine and the organic layer was dried over $MgSO_4$ and filtered. The reaction mixture was concentrated under reduced pressure, and purified by flash column chromatography (silica, 80:20 cyclohexane:EtOAc) to provide **35d** as colourless liquid (118 mg, 59% yield).

^{1}H-NMR (300 MHz, $CDCl_3$): δ 7.96 (dd, *J* = 7.9, 1.3 Hz, 1H), 7.43 (td, *J* = 7.6, 1.3 Hz, 1H), 7.23–7.28 (m, 1H), 7.09 (td, *J* = 7.7, 1.6 Hz, 1H), 5.73-5.82 (m, 1H), 5.02–5.11 (m, 2H), 4.24-4.31 (m, 1H), 3.06 –3.15 (m, 1H), 2.28–2.37 (m, 2H), 1.77 (s, 3H). ^{13}C-NMR (75 MHz, $CDCl_3$): δ 170.0, 145.0, 140.4, 135.3, 130.5, 129.8, 129.5, 116.7, 100.4, 47.4, 32.1, 22.9. HRMS (ESI): Calcd for $C_{12}H_{15}INO$ $[M+H]^+$: 316.0150, found: 316.0143.

General procedure E. Photocatalytic cyclization in batch with Ir(ppy)$_3$

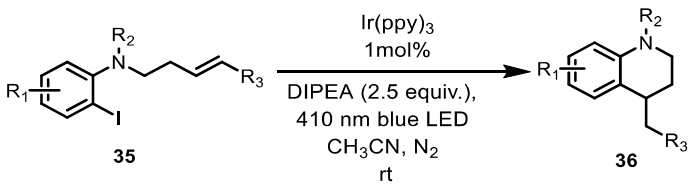

35 **36**

A dry vial containing the corresponding 2-iodoaniline derivative **35** (0.05 mmol, 1 equiv.), DIPEA (43 □l, 0.125 mmol, 2.5 equiv.), $Ir(ppy)_3$ (0.32 mg, 0.0005 mmol, 1mol%) and 2.0 mL of MeCN was sealed and degassed via freeze-pump-thaw cycling (3 x 10 min

under vacuum). Then, the reaction mixture was irradiated under 410 nm blue LED system (15W) for the corresponding time. The reaction mixture was concentrated under reduced pressure, and the conversion of the reaction was determined by ^{1}H-NMR. The yield of the reaction was determined by ^{1}H-NMR using CH_3NO_2 as internal standard.

4-Methyl-1,2,3,4-tetrahydroquinoline (36a) [159]

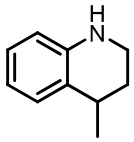

After purification by flash chromatography (silica, 95:5 cyclohexane:EtOAc), **36a** was isolated as colourless liquid (78% yield, measured by ^{1}H-NMR using CH_3NO_2 as internal standard). ^{1}H-NMR (300 MHz, $CDCl_3$): δ 7.06 (dd, J = 7.6, 1.0 Hz, 1H), 7.00–7.94 (m, 1H), 6.64 (td, J = 7.4, 1.2 Hz, 1H), 6.48 (dd, J = 7.9, 1.1 Hz, 1H), 3.87 (br s, 1H), 3.27–3.34 (m, 2H), 2.87-2.98 (m, 1H), 1.94–2.04 (m, 1H), 1.64-1.73 (m, 1H), 1.29 (t, J = 6.2 Hz, 3H).

1,4-Dimethyl-1,2,3,4-tetrahydroquinoline (36b) [158]

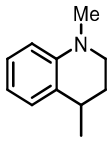

After purification by flash chromatography (silica, 98:2 cyclohexane:EtOAc), **36b** was isolated as colourless liquid (63% yield, was measured by ^{1}H-NMR using CH_3NO_2 as internal standard). ^{1}H-NMR (300 MHz, $CDCl_3$): δ 7.04–7.11 (m, 2H), 6.59-6-66 (m, 2H), 3.18–3.25 (m, 2H), 2.89 (m, 4H), 1.99-2.09 (m, 1H), 1.64-1.74 (m, 1H), 1.28 (d, J = 7.0 Hz, 3H).

1-Ethyl-4-methyl-1,2,3,4-tetrahydroquinoline (36c) [159]

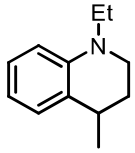

After purification by flash chromatography (silica, 80:20 cyclohexane:EtOAc), **36c** was isolated as colourless liquid (80% yield, measured by ^{1}H-NMR using CH_3NO_2 as internal standard). ^{1}H-NMR (300 MHz, $CDCl_3$): δ 7.03-7.08 (m, 2H), 6.56–6.69 (m, 2H), 3.17–3.44 (m, 4H), 2.85-2.91 (m, 1H), 1.97-2.00 (m, 1H), 1.68-1.71 (m, 1H), 1.27 (d, J = 6.9 Hz, 3H), 1.14 (t, J = 7.0 Hz, 3H).

1-(4-Methyl-3,4-dihydroquinolin-1(2H)-yl)ethan-1-one (36d)

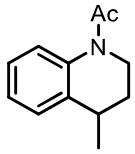

After purification by PTLC (silica, 50:50 cyclohexane:EtOAc), **36d** was isolated as colourless liquid (37% yield, measured by ^{1}H-NMR using CH_3NO_2 as internal standard). Product **36d** decomposes in the purification process. ^{1}H-NMR (300 MHz, $CDCl_3$) δ 7.22-7.24 (m, 4H), 2.65–2.82 (m, 2H), 2.56–2.64 (m, 1H), 2.09–2.17 (m, 1H), 1.86-1.98 (m, 1H), 1.86 (s, 3H), 1.32 (d, J = 6.9 Hz, 3H).

4-Isopropyl-1,2,3,4-tetrahydroquinoline/4-(prop-1-en-2-yl)-1,2,3,4-tetrahydroquinoline (36e)[160]

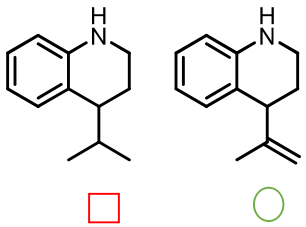

After purification by flash chromatography (silica, 98:2 cyclohexane:EtOAc), a mixture of two inseparable compounds **36e** was isolated as colourless liquid (55% yield, measured by ^{1}H-NMR using CH_3NO_2 as internal standard). ^{1}H-NMR (300 MHz, $CDCl_3$): δ 6.93-7.02 (m, 4H, □○), 6.58–6.64 (m, 2H, □○), 6.46-6.50 (m, 2H, □○), 5.01 (s, 1H, ○), 4.69 (s, 1H, ○), 3.82 (br s, 1H, □), 3.53 (t, *J*= 6.6 Hz, 1H, ○), 3.27-3.34 (m, 4H, □○), 2.54 (q, 5.6 Hz, 1H, □), 1.90–2.04 (m, 4H, □○), 1.76–1.85 (m, 1H, □), 1.71 (s, 3H, ○), 0.99 (d, *J*= 6.8 Hz, 3H, □), 0.88 (d, *J*= 6.7 Hz, 3H, □).

4,7-Dimethyl-1,2,3,4-tetrahydroquinoline (36h)

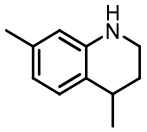

After purification by flash chromatography (silica, 95:5 cyclohexane:EtOAc) **36h** was isolated as colourless liquid (54% yield). ^{1}H-NMR (300 MHz, $CDCl_3$): δ 6.96 (d, *J*= 7.7 Hz, 1H), 6.47 (d, *J*= 7.7 Hz, 1H), 6.32 (s, 1H), 3.79 (br s, 1H), 3.21–3.36 (m, 2H), 2.83-2.94 (m, 1H), 2.22 (s, 3H), 1.93–2.01 (m, 1H), 1.61-1.71 (m, 1H), 1.28 (d, *J*= 7.0 Hz, 3H). ^{13}C-NMR (75 MHz, $CDCl_3$): δ 144.1, 136.4, 128.3, 123.9, 118.0, 114.7, 39.1, 30.2, 29.9, 22.7, 21.1. HRMS (ESI): Calcd for $C_{11}H_{16}N$ $[M+H]^+$: 162.1277, found: 162.1240.

4-Methyl-7-(trifluoromethyl)-1,2,3,4-tetrahydroquinoline (36i)

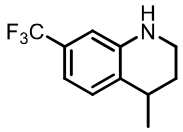

After purification by flash chromatography (silica, 95:5 cyclohexane:EtOAc) **36i** was isolated as colourless liquid (51% yield). ^{1}H-NMR (300 MHz, $CDCl_3$): δ 7.11 (d, *J*= 7.9 Hz, 1H), 6.83 (d, *J*= 7.9 Hz, 1H), 6.67 (s, 1H), 4.05 (br s, 1H), 3.31–3.37 (m, 2H), 2.88-

2.96 (m, 1H), 1.92-2.02 (m, 1H), 1.64-1.74 (m, 1H), 1.29 (d, J = 7.0 Hz, 3H). ^{13}C-NMR (126 MHz, $CDCl_3$): δ 144.3, 129.8, 129.2 (q, J = 31.8 Hz), 128.7, 124.4 (q, J = 271.9 Hz), 113.0 (q, J = 3.9 Hz), 110.3 (q, J = 3.9 Hz), 38.8, 30.3, 29.1, 22.3. ^{19}F NMR (282 MHz, $CDCl_3$): δ -62.68 (s). HRMS (ESI): Calcd for $C_{11}H_{13}F_3N$ $[M+H]^+$: 216.0923, found: 216.0951.

7-Bromo-4-methyl-1,2,3,4-tetrahydroquinoline (36l)

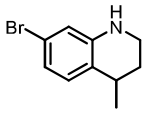

After purification by flash chromatography (silica, 95:5 cyclohexane:EtOAc) **36l** was isolated as colourless liquid (50% yield). ^{1}H-NMR (300 MHz, $CDCl_3$): δ 6.88 (d, J = 8.1 Hz, 1H), 6.71 (dd, J = 8.1, 2.0 Hz, 1H), 6.60 (d, J = 2.0 Hz, 1H), 3.92 (br s, 1H), 3.26-3.32 (m, 2H), 2.81-2.88 (m, 1H), 1.89–1.99 (m, 1H), 1.60-1.70 (m, 1H), 1.25 (d, J = 7.0 Hz, 3H). ^{13}C-NMR (75 MHz, $CDCl_3$): δ 145.5, 129.7, 125.3, 120.0, 119.5, 116.2, 38.8, 30.0, 29.4, 22.3. HRMS (ESI): Calcd for $C_{10}H_{13}BrN$ $[M+H]^+$: 225.0267, found: 225.0293.

6-Bromo-4-methyl-1,2,3,4-tetrahydroquinoline (36m) [161]

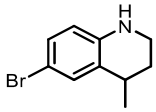

After purification by flash chromatography (silica, 95:5 cyclohexane:EtOAc), **36m** was isolated as colourless liquid (65% yield). ^{1}H-NMR (300 MHz, $CDCl_3$): δ 7.14 (d, J = 2.3 Hz, 1H), 7.03 (dd, J = 8.5, 2.2 Hz, 1H), 6.34 (d, J = 8.5 Hz, 1H), 3.87 (br s, 1H), 3.22–3.26 (m, 2H), 2.81–2.91 (m, 1H), 1.89–1.99 (m, 1H), 1.60-1.70 (m, 1H), 1.27 (d, J = 7.0 Hz, 3H).

7-Chloro-4-methyl-1,2,3,4-tetrahydroquinoline (36n)

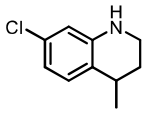

After purification by flash chromatography (silica, 95:5 cyclohexane:EtOAc), **36n** was isolated as colourless liquid (50% yield). ^{1}H-NMR (300 MHz, $CDCl_3$): δ 6.94 (d, J = 8.1 Hz, 1H), 6.57 (dd, J = 8.1, 2.0 Hz, 1H), 6.44 (d, J = 2.0 Hz, 1H), 3.93 (br s, 1H), 3.23–3.37

(m, 2H), 2.81–2.91 (m, 1H), 1.90–2.00 (m, 1H), 1.63-1.69 (m, 1H), 1.26 (d, J = 7.0 Hz, 3H). ^{13}C-NMR (75 MHz, $CDCl_3$): δ 145.2, 132.0, 129.4, 124.8, 116.6, 113.4, 38.8, 30.0, 29.5, 22.4. HRMS (ESI): Calcd for $C_{10}H_{13}ClN$ $[M+H]^+$: 182.0768, found: 182.0773.

6-Chloro-4-methyl-1,2,3,4-tetrahydroquinoline (36o)

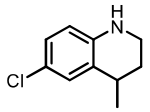

After purification by flash chromatography (silica, 95:5 cyclohexane:EtOAc), **36o** was isolated as colourless liquid (58% yield). ^{1}H-NMR (300 MHz, $CDCl_3$): δ 7.01 (d, J = 2.4 Hz, 1H), 6.90 (dd, J = 8.5, 2.4 Hz, 1H), 6.39 (d, J = 8.5 Hz, 1H), 3.87 (br s, 1H), 3.26–3.32 (m, 2H), 2.84-2.91 (m, 1H), 1.90–2.00 (m, 1H), 1.61-1.71 (m, 1H), 1.28 (d, J = 7.0 Hz, 3H). ^{13}C-NMR (75 MHz, $CDCl_3$): δ 142.8, 128.1 (2C), 126.6, 121.3, 115.1, 39.0, 30.3, 29.5, 22.3. HRMS (ESI): Calcd for $C_{10}H_{13}ClN$ $[M+H]^+$: 182.0768, found: 182.0740.

8-Chloro-4-methyl-1,2,3,4-tetrahydroquinoline (36p)

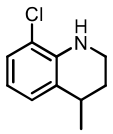

After purification by flash chromatography (silica, 95:5 cyclohexane:EtOAc), **36p** was isolated as colourless liquid (70% yield). ^{1}H-NMR (300 MHz, $CDCl_3$): δ 7.07 (d, J = 7.9 Hz, 1H), 6.96 (d, J = 7.0 Hz, 1H), 6.54 (t, J = 7.7 Hz, 1H), 4.47 (br s, 1H), 3.39-3.42 (m, 2H), 2.90-2.97 (m, 1H), 1.91-2.02 (m, 1H), 1.64–1.74 (m, 1H), 1.28 (d, J = 7.0 Hz, 3H). ^{13}C-NMR (75 MHz, $CDCl_3$): δ 140.2, 127.8, 126.7, 126.6, 117.9, 116.2, 38.6, 30.6, 29.1, 22.5. HRMS (ESI): Calcd for $C_{10}H_{13}ClN$ $[M+H]^+$: 182.0768, found: 182.0777.

General flow procedure for the photocatalytic cyclization

The corresponding amine **35** (0.0625 mmol), $Ir(ppy)_3$ (0.4 mg; 1 mol%) and DIPEA (27.2 µL; 0.16 mmol, 2.5 equiv.) were dissolved in acetonitrile (2.5 mL). The mixture was homogenized by sonication in an ultrasound bath for 10 min at 30 °C. Then, the solution was degasified via freeze-pump-thaw cycling (3 x 10 min under vacuum) in order to get an inert atmosphere. The flow system consists of a syringe pump connected to the coil reactor (18 mL) made of PFA capillary tube (1/8" OD; 1.60 mm ID; 9 m length), wrapped around a Pyrex beaker (80 mm diameter; 140 mm height). The coil was irradiated with

a blue LED spot (Kessil A160WE; 40 W) placed at the top of the setup. A fan (90 mm diameter) was set at the top of the light source to dissipate the heat generated. Starting materials solution was loaded manually to a pre-loop (3 mL). The mixture was flowed through the coil reactor by pumping acetonitrile at 0.3 mL/min flow rate and room temperature (t_R = 60 min). The outcome solution was collected in a vial, solvent was removed under reduce pressure and the residue was analysed by ^{1}H-NMR using nitromethane as internal standard.

Scale up under flow conditions for compound 36k

Amine **35k** (153.8 mg; 0.5 mmol), $Ir(ppy)_3$ (3.3 mg; 1 mol%) and DIPEA (217.7 µL; 1.25 mmol, 2.5 equiv.) were dissolved in acetonitrile (20 mL). The mixture was homogenized by sonication in an ultrasound bath for 10 min at 30 °C and was purged bubbling nitrogen during 20 minutes in order to remove oxygen. The solution was then pumped through the PFA coil reactor (18 mL) at 0.3 mL/min flow rate (t_R = 60 min). When starting materials solution runs out, the flow rate was kept constant by pumping acetonitrile at room temperature. The outcome was collected in a round-bottom flask, solvent is removed under reduced pressure and the residue was analysed by ^{1}H-NMR using nitromethane as internal standard.

A new photoredox catalyzed transformation directed to the synthesis of 2,3-dihydrofurans

Dihydrofurans are important five-membered heterocyclic compounds. These scaffolds are widely present in the scaffolds of pharmaceuticals, functional materials, and natural products. [162–166]. They are used as intermediate for the synthesis of natural products and potentially bioactive molecules. Furthermore, they are exploited for the synthesis of functionalized tetrahydrofurans[167] and fused polycyclic compounds[168].

Because of their importance, numerous syntheses of dihydrofurans have been developed over the past decades. Certainly, the most investigated strategy is the oxidative [3+2] annulation between 1,3-dicarbonyl compounds and alkenes (e.g Scheme 54).[169] Nowadays, the formation of 2,3-dihydrofurans through a radical mechanism has been deeply investigated. Early examples were reported by Desseau[170] and Nishino[171], respectively (Scheme 54). They firstly exploit the reaction between alkenes and carbonyl compounds for the synthesis of 2,3-dihydrofurans. Manganese salts were involved as catalysts.

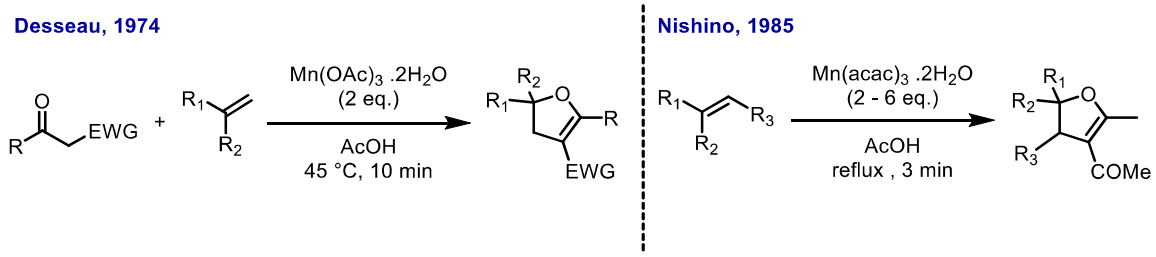

Scheme 54: Desseau, 1974; Nishino, 1985

After these pioneering reports, numerous other synthetic procedures have been developed. Some of them involve Mn(III)[172–175], others with Ce(IV)[176,177] or Cu(II)[178–182]. All of them occur with a radical process. Stoichiometric strong oxidants, transition metal salts, harsh reaction conditions, or pre-functionalized substrates are required in these reactions. Due to the existence of these limitations, it is imperative to develop a method fulfilling the demands of a more sustainable and milder chemistry.

Since the first article published by MacMillan in 2008[35], the application of photoredox catalysis in organic synthesis allowed to develop a plethora of organic transformation. Usually, mild conditions are required and hazardous chemicals or large amounts of metal additives are avoided.[39,108] Photoredox catalysis exploits the photocatalyst ability

to create active intermediate radical species from otherwise unreactive starting material. At the best of our knowledge, there are no reported photoredox catalyzed methods for the synthesis of 2,3-dihydrofurans. However, photoredox catalyzed reactions between unsaturated carbon-carbon bonds and halogenated carbonyl compounds have been recently reported. Furans[183–185] and lactones[186] have been synthesized exploiting this approach.

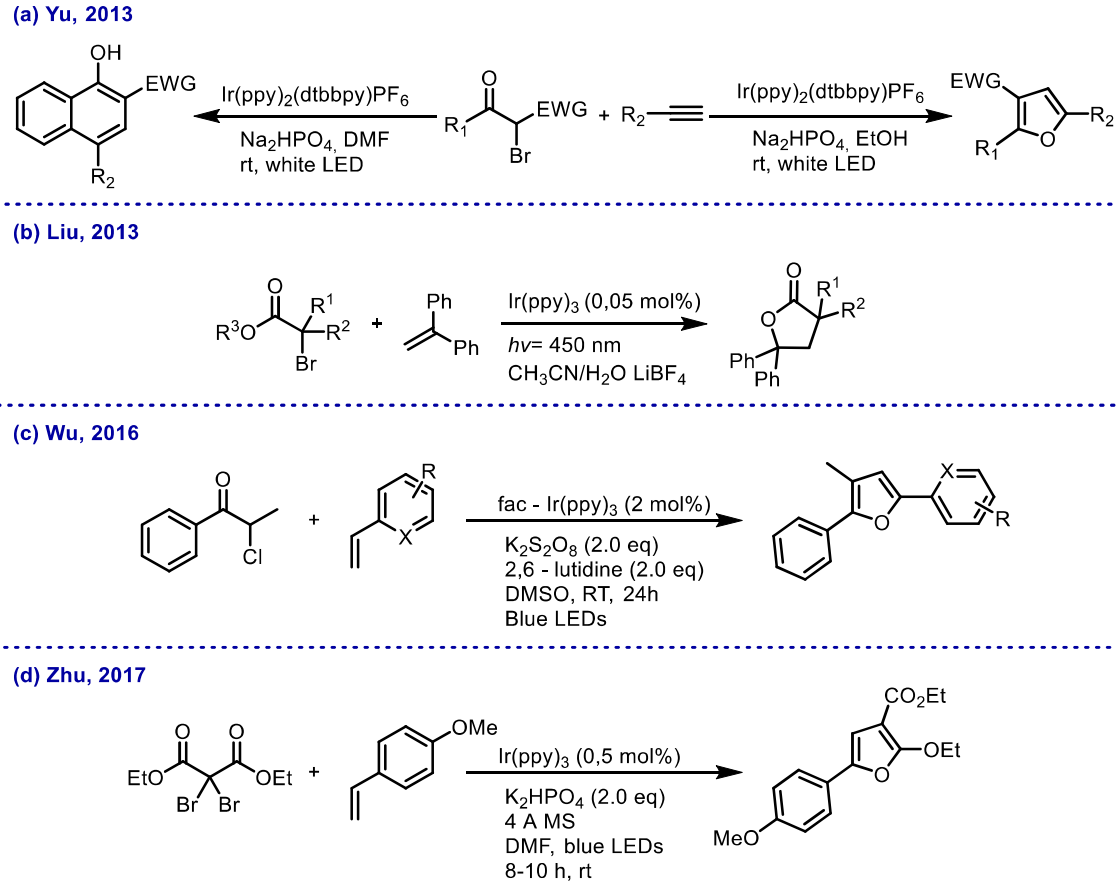

Scheme 55: (a) Yu, 2013; (b) Liu, 2013; (c) Wu, 2016; (d) Zhu, 2017

All the described examples involved the same initial step. Elecrophilic radical **XXXIX** is generated by exploiting a SET between an Ir^{3+} photocatalyst and a halogenated compound **XXXVIII**. Radical **XXXIX** subsequently reacts with the unsaturated bond of **XL** to form the desired product **XLI**.

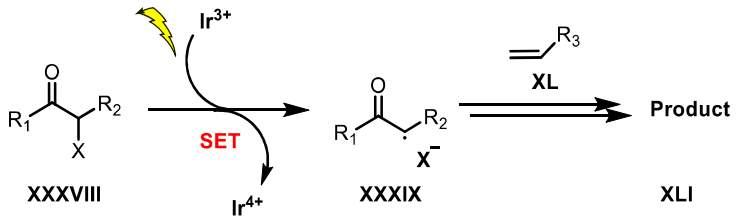

Scheme 56: SET among Ir^{3+} photocatalyst and halogenated compound **XXXVIII**

Aim of the project

Due to the wide range of applicability of 2,3-dihydrofurans,[162–166] an efficient protocol for the synthesis of 2,3-dihydrofuran is still a hot topic. Known photoredox catalysis [183–186] and Nishino's investigation[175] inspired the development of a new transformation.

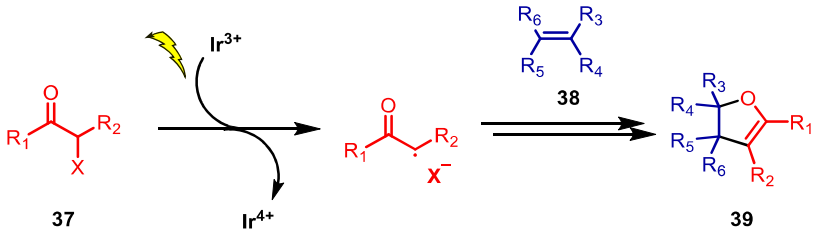

Scheme 57:Designed photoredox catalyzed transformation for the synthesis of 2,3-dihydrofurans

The 2-halogenated compound **37** and alkene **38** are the involved as starting material. Thanks to the presence of Ir^{3+}, **37** photoexcitation followed by detachment of a halide ion leads to a reactive radical intermediate able to add to **38**. The radical addition adduct is oxidize to carbocation. At last, intramolecular *O*-cyclization leads to the formation of the desired 2,3-dihydrofuran under mild reaction conditions. The application of the new methodology to diverse substrates is investigated. Finally, a mechanism is hypothesized basing on experimental data and previous pieces of literature.

Discussion and results

At first, a reaction involving $Ir(ppy)_3$ as a photocatalyst and 2,6-lutidine as a base has been performed. Acetonitrile was chosen as a solvent and the reaction has been irradiated for 24 hours using Blue LEDs. A 58% yield on product **39aa** has been detected from ^{1}H-NMR analysis on the crude reaction mixture. In addition, ß,γ-unsaturated ß-ketoester **40aa** was formed in a 15% yield.

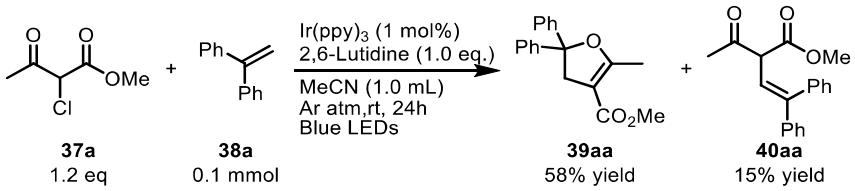

Scheme 58: Initial conditions for the photoredox catalyzed synthesis of 2,3-dihydrofurans

In the optimization process we tested various catalysts, but all failed except $Ir(ppy)_3$, demonstrated not be able to perform the desired transformation. Proving that only

$Ir(ppy)_3$ complex possesses the right potential to reduce halogenated compound **37a** (Ir(III)*/Ir(IV) = -1.73 V).[97]

Then a screening of different solvents has been carried out to find the best reaction media (Table 13)

Table 13: Solvent screening

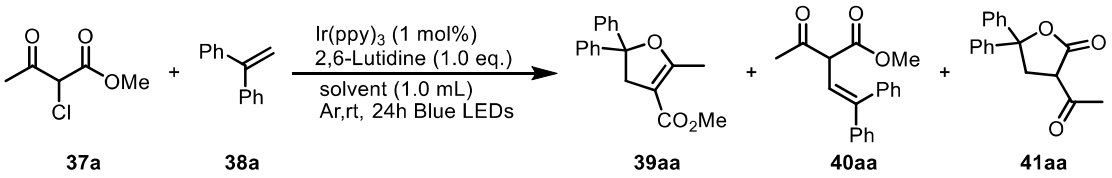

37a **38a** **39aa** **40aa** **41aa**

Entry[a]	Solvent	Conversion %[b]	Yield% 39aa[b]	Yield% 40aa[b]	Yield% 41aa[b]
1	MeCN[c]	100%	58	15	-
2	DMF[c]	100%	55	-	-
3	DMSO[c]	100%	31	-	-
4	DCM[c]	93%	44	22	-
5	THF[e]	50%	18	-	-
6	MeCN[d]	100%	56	12	-
7	DMF[d]	100%	52	8	11
8	MeOH	60%	5	10	10

[a] Reaction conditions: **37a** (0.12 mmol), **38a** (0.1 mmol), catalyst (1 mol%), 2,6-lutidine (0.1 mmol) in the corresponding solvent (1 mL), stirred at room temperature for 24h irradiated through Blue LEDs. [b] Determined through ^{1}H-NMR analysis on the crude reaction mixture involving triphenylmethane as internal standard; [c] Anhydrous solvent; [d] Not anhydrous solvent; [e] Distilled solvent.

In most of the tested solvent, complete chemoselectivity was not achieved. Even if 2,3-dihydrofuran **5aa** was obtained as the major product, other species were detected in the crude reaction mixture. Among them, **40aa** and **41aa** were identified. A complete conversion was reached with MeCN, DMF, and DMSO (dimethyl sulfoxide), but **5aa** yield never exceeded 58% (Entry 1,2,3, Table 13). An almost complete conversion was reached with DCM, but only a 44% yield on **5aa** (Entry 4. Table 13). Even in this solvent, co-product **40aa** was observed in a 22% yield. DMF proved to be the most chemoselective solvent under the selected reaction conditions (Entry 2. Table 13). However, MeCN reached a major yield in **39aa** formation even if including the formation of **40aa**. MeCN is considered less problematic from a sustainability point of view.[187] Thus, it was chosen as reaction media. Poor results were obtained performing the reaction in THF (Entry 5, Table 13) or MeOH (Entry 8, Table 13). Using not anhydrous DMF or MeOH, lactone

41aa was formed.[186] On the contrary, with not anhydrous MeCN, no substantial differences were noted compared to the anhydrous one (Entry 6, Table 13). Anhydrous MeCN was selected as a solvent for higher control over the reaction conditions.

The influence of the base amount has been then examined.

Table 14: Screening of lutidine equivalents

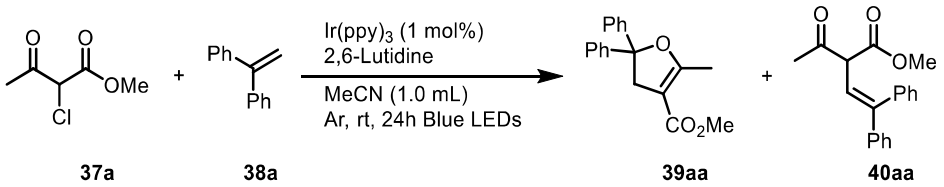

37a **38a** **39aa** **40aa**

Entry[a]	2,6-lutidine equivalents	Conversion %[b]	Yield% 39aa[b]	Yield% 40aa[b]
1	0	23%	9	-
2	0.5	88%	52	14
3	1.0	100%	59	13
4	1.2	100%	55	15
5	2.0	100%	53	8

[a] Reaction conditions: **37a** (0.12 mmol), **38a** (0.1 mmol), $Ir(ppy)_3$ (1 mol%) and the corresponding amount of 2,6-lutidine (0.1 mmol) in MeCN (1 mL), stirred at room temperature for 24h irradiated through Blue LEDs. [b] Determined through ^{1}H-NMR analysis on the crude reaction mixture involving triphenylmethane as internal standard.

A very poor yield was reached in the absence of a base (Entry 1, Table 14). With an amount of 0.5 equivalent of 2,6-lutidine the complete conversion of alkene **38a** was not achieved (Entry 2, Table 14).

At last, higher amount (1.2 eq and 2.0 eq) did not enhance **39aa** yield (55% yield and 53% yield respectively, Entry 4 and 5, Table 14). Probably, increasing the base loading favored parallel reaction pathways, indeed the crude reaction mixture resulted chaotic. Therefore, 1 equivalent of 2,6-lutidine was confirmed as the ideal amount for our purpose.

Further reaction conditions have been then evaluated. Lowering the catalytic loading to 0.05 mol% caused a drop in both conversion and yield (Entry 1, Table 15). Diluting the concentration to 0.05 M demonstrated to slightly affect the performance. 2,3-dihydrofuran was obtained in 44% yield even if the complete conversion was achieved (Entry 2, Table 14). Increasing the amount of acetoacetate **37a** slightly improved **39aa** yield (Entry 4, Table 14). However, the increasing was not large. Thus, 1.2 equivalents

of **37a** were selected as the optimized amount. At last, no enhancement was observed with a higher amount of **38a** (Entry 5, Table 14).

Table 15: Screening of miscellaneous conditions

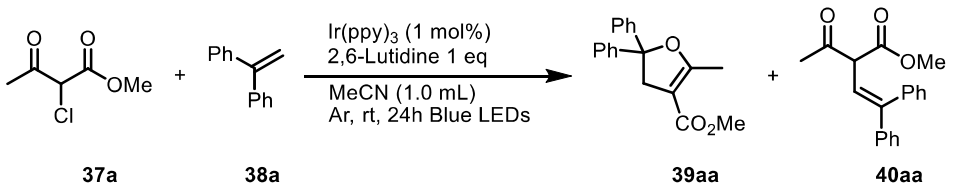

37a **38a** **39aa** **40aa**

Entry[a]	Variation from the standard conditions	Conversion %[b]	Yield% 39aa[b]	Yield% 40aa[b]
1	$Ir(ppy)_3$ 0.05 mol%	50%	10	-
2	MeCN, 2 mL	100%	44	6
3	-	100%	59	13
4	**37a** 2 eq.	100%	61	14
5	**38a** 2 eq.	90%	53	18

[a] Reaction conditions: **37a** (0.12 mmol), **38a** (0.1 mmol), $Ir(ppy)_3$ (1 mol%), 2,6-lutidine (0.1 mmol) in MeCN (1 mL), stirred at room temperature for 24h irradiated through Blue LEDs. [b] Determined through ^1H-NMR analysis on the crude reaction mixture involving triphenylmethane as internal standard.

Therefore, no changes were made in the reaction conditions. Product yield at different reaction time has been screened.

Table 16: Screening of different reaction times

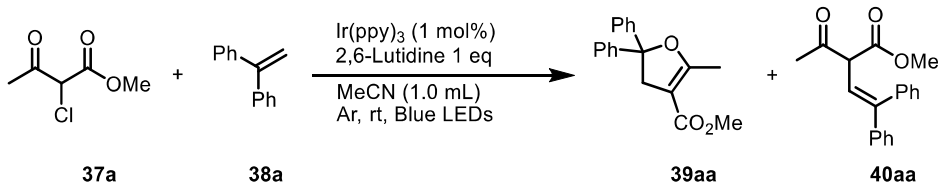

37a **38a** **39aa** **40aa**

Entry[a]	Time (h)	Conversion %[b]	Yield% 39aa[b]	Yield% 40aa[b]
1	2	40%	11	4
2	4	56%	22	9
3	6	87%	37	15
4	24	100%	59	13
5	72	100%	56	6

[a] Reaction conditions: **37a** (0.12 mmol), **38a** (0.1 mmol), $Ir(ppy)_3$ (1 mol%), 2,6-lutidine (0.1 mmol) in MeCN (1 mL), stirred at room temperature for the corresponding amount of time, irradiated through Blue LEDs. [b] Determined through ^{1}H-NMR analysis on the crude reaction mixture involving triphenylmethane as internal standard.

A good conversion was reached after 6 hours, and after 24 hours a full conversion and a higher yield were obtained (Entry 3 vs Entry 4, Table 16). Prolonging the reaction time to 72 hours, no drop was noticed in **39aa** yield (56% yield, Entry 5, Table 14), meaning that **39aa** is stable under the reaction conditions. On the contrary, **40aa** yield halved, hence proving its instability under the same conditions.

Different bases have been successively tested in this photocatalytic transformation

Table 17: Screening of diverse bases

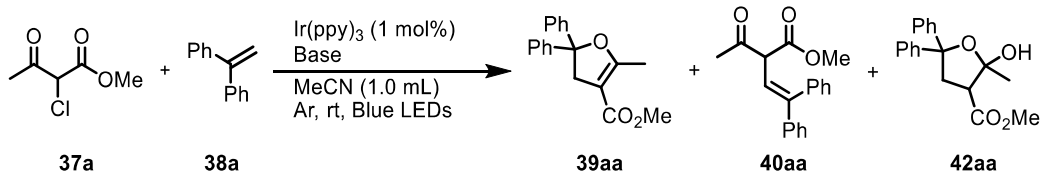

Entry[a]	Base	Conversion %[b]	Yield% 39aa[b]	Yield% 40aa[b]	Yield% 42aa[b]
1	2,6-Dicyanopyridine	28%	7	-	-
2	2,4,6-Collidine	100%	40	9	-
3	p-OMePhNPh$_2$	<5%	-	-	-
4	Imidazole	76%	23	5	-
5	2,6 - Lutidine	100%	59	13	-
6	Na_2HPO_4	85%	84	-	-
7	Na_2HPO_4[c]	100%	79	4	17
8	Na_2HPO_4[d]	68%	54	-	-

[a] Reaction conditions: **37a** (0.12 mmol), **38a** (0.1 mmol), Ir(ppy)$_3$ (1 mol%), the corresponding amount of base in MeCN (1 mL), stirred at room temperature for 24h irradiated through Blue LEDs. [b] Determined through ^{1}H-NMR analysis on the crude reaction mixture involving triphenylmethane as internal standard. [c] 2 equivalents of Na_2HPO_4 were involved; [d] The reaction was performed in 2 mL of MeCN.

2,6-Dicyanopyridine was disappointing since it gave the result obtained in the reaction without a base (Entry 1, Table 17), probably because the cyano groups on the pyridine ring highly diminish its basicity.[188] 2,4,6-Collidine, slightly more basic than 2,6-lutidine (pKa 2,4,6-collidine=7,43, pKa 2,6- lutidine=6,72), induced the formation of **39aa**, but unidentified species were observed in the crude reaction mixture (Entry 2, Table 17).[188] No reaction occurs involving 4-methoxy-*N,N*-diphenylaniline (*p*-OMePhNPh$_2$), and poor results were obtained with imidazole. (Entry 3 and 4, Table 17). We succeeded with the inorganic base Na_2HPO_4 that allowed to isolate **39aa** in 84% yield, with an 85% conversion. Na_2HPO_4 had been previously reported to participate in transformations involving photocatalyzed ß-ketoester activation.[183] At last, increasing the quantity of Na_2HPO_4 or diluting the reaction to 0.05 M did not enhance the reaction performance (Entry 7 and Entry 8, Table 17). The trend previously observed with 2,6-lutidine was so confirmed. With 2 equivalents of Na_2HPO_4 (Entry 7, Table 17), hemiketal **42aa** was isolated from the crude reaction mixture. The presence of **42aa** could be rationalized with the presence of water in the reaction mixture. Na_2HPO_4 is a hygroscopic white solid and it was not dried before use. Increasing its quantity could increase the quantity of water and different reaction pathways would consequently be promoted.

Finally, blank experiments have been conducted. With no $Ir(ppy)_3$ or irradiation, no reaction occurs (Entry 2 and 3, Table 18), confirming a photocatalyzed mechanism. Performing the reaction under air atmosphere and without degassing the solution, 44% yield on product **39aa** was detected (Entry 4, Table 18). This last experiment demonstrated that the oxygen presence affects the transformation, yet not completely suppressed it.

Table 18: Blank experiments

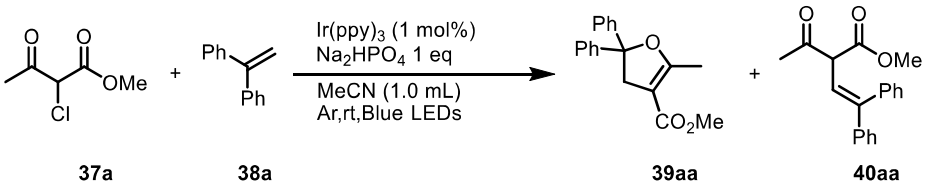

Entry[a]	Variation	Conversion %[b]	Yield% 39aa[b]	Yield% 40aa[b]
1	-	85%	84	<1
2	No catalyst	0%	-	-
3	No light	0%	-	-
4	Air atmosphere	91%	44	-

[a] Reaction conditions: **37a** (0.12 mmol), **38a** (0.1 mmol), $Ir(ppy)_3$ (1 mol%), Na_2HPO_4 (1 eq) in MeCN (1 mL), stirred at room temperature for 24h irradiated through Blue LEDs. [b] Determined through ^{1}H-NMR analysis on the crude reaction mixture involving triphenylmethane as internal standard. [c] 2 equivalents of Na_2HPO_4 were involved; [d] The reaction was performed in 2 mL of MeCN.

The optimized reaction conditions were selected at follows: alkene **38a** as a limiting reagent, 1,2 equivalents of the halogenated compound **37a**, 1 mol% of $Ir(ppy)_3$ photocatalyst, 1 equivalent of Na_2HPO_4 in MeCN 0,1 M. The reaction was stirred for 24 hours at room temperature under argon atmosphere and Blue LED irradiation. Under the selected conditions, product **39aa** was selectively obtained in 84% yield.

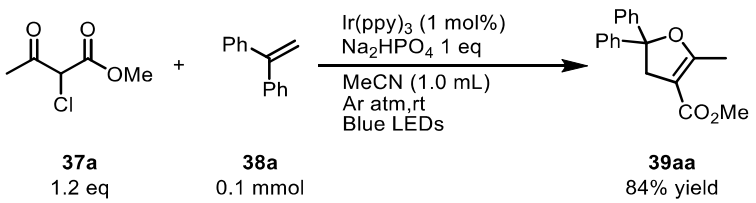

Scheme 59: Optimized reaction conditions for the photoredox catalyzed synthesis of 2,3-dihydrofuran **39**

To study the scope of the studied transformations, various alkenes **38** have been tested under the optimized reaction conditions. Initially, biaryl substituted alkenes were tested (Scheme 60).

Scheme 60: Scope of biaryl substituted alkenes

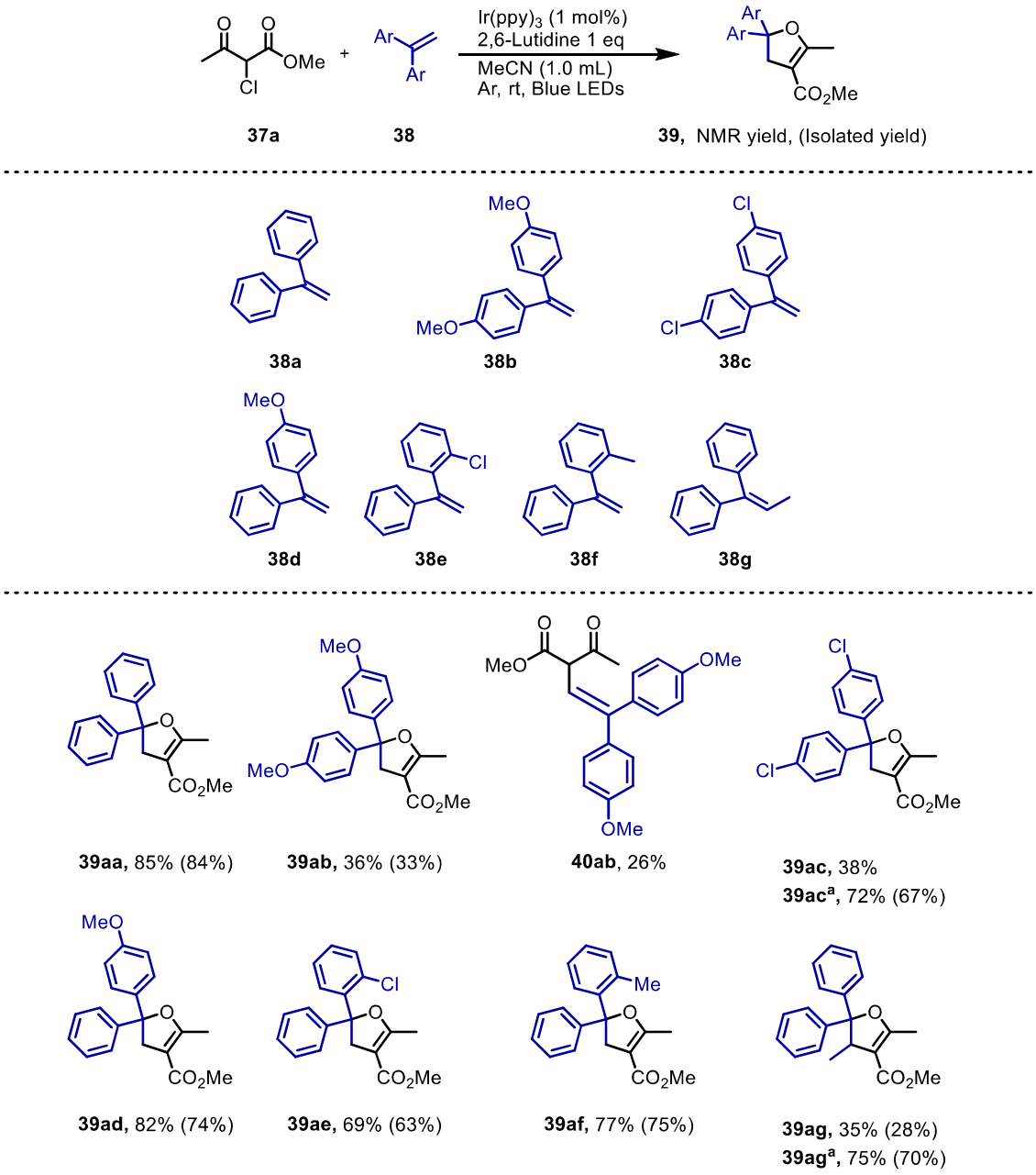

Reaction conditions: **37a** (0.12 mmol), **38a** (0.1 mmol), $Ir(ppy)_3$ (1 mol%), Na_2HPO_4 (0,1 mmol) in MeCN (1 mL), stirred at room temperature for 24h irradiated through Blue LEDs. Yield determined through ^1H-NMR analysis on the crude reaction mixture involving triphenylmethane as internal standard. Yield on the isolated product into brackets. [a] Reaction time 72 hours.

Different *para* position substituted diaryl showed divergent results. 2,3-Dihydrofuran **39ab** was obtained in 36% yield together with ß,γ-unsaturated ß-ketoester-**40ab** in 26% yield. 2,3-dihydrofuran **39ac** was formed in 38% yield in 24 hours. Performing the reaction for 72 hours, raise **39ac** yield to 72% and a complete conversion of alkene **38c** was recorded. The electron-donating methoxy group should raise the electron density on the C-C double bond, an effect much lower with the chloride substituent. A major

electron density on the carbon-carbon double bond would favor the electrophilic attack. From the experimental evidence, it resulted that **38b** reacts faster than **38c**, even if with minor selectivity towards the formation of **39ab**. On the contrary, **38c** displayed lower reactivity but high selectivity toward **39ac** formation. Notably, 82% yield was achieved in **39ad** after 24 hours utilizing the monosubstituted *p*-OMe **38d**. Both the *orto*-substituted diphenyl ethylene **38e** and **38f** allow to obtain the corresponding **39ae** and **39af** in good yields (67% and 77% yield, respectively). In this case, substitution with a weak electron donor (methyl group) brought to higher yield compared to substitution with an electron attractor (Cl). Finally, **38g** demonstrated the applicability of the methodology to trisubstituted alkenes, even if a longer reaction time was required. Indeed, 2,3-dihydrofuran **39ag** was obtained in 35% after 24 hours. Increasing the reaction time to 72 hours brought the yield up to 75%. The major steric hindrance on the alkene could justify the lower reactivity.

Secondly, the reactivity of mono aryl alkenes has been analyzed (Scheme 61).

Scheme 61: Scope of monoaryl substituted alkenes

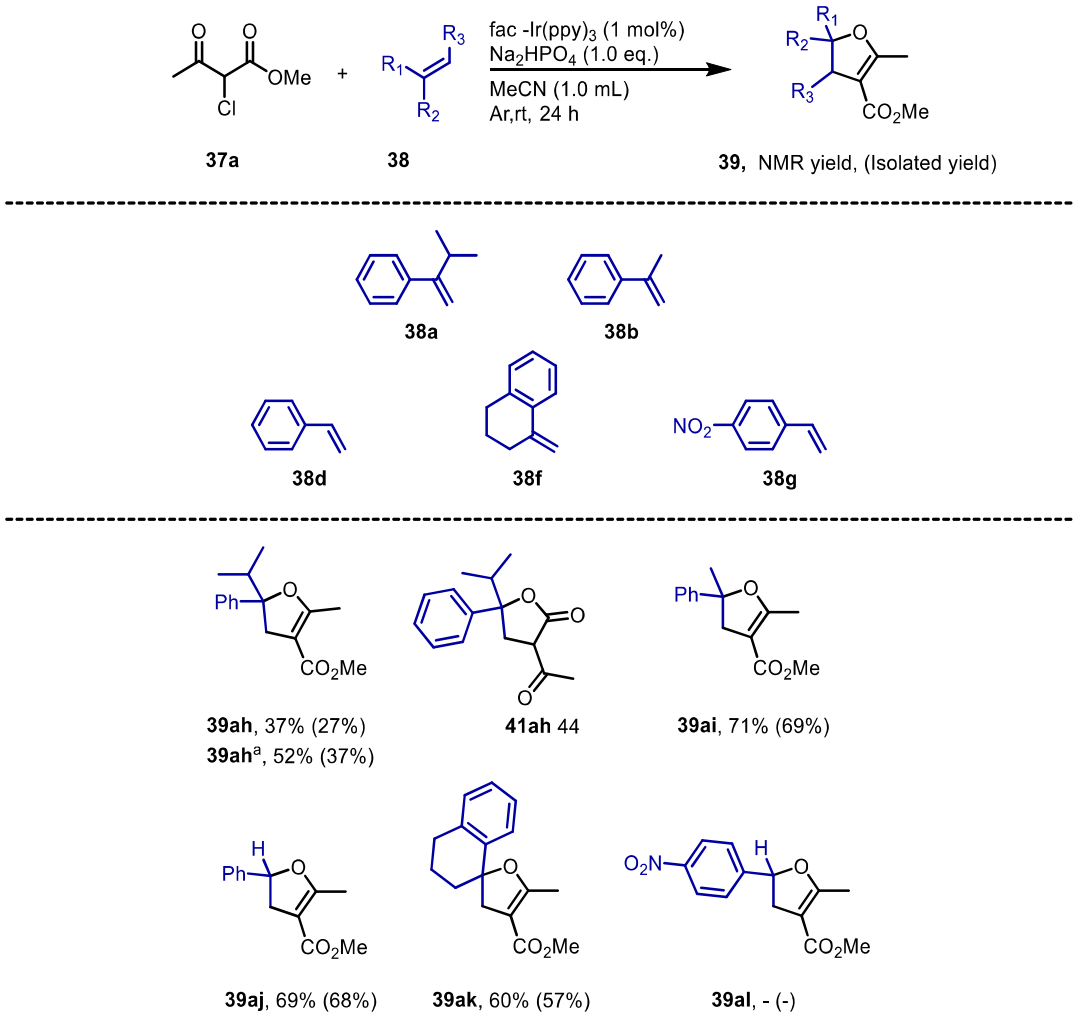

Reaction conditions: **37a** (0.12 mmol), **38a** (0.1 mmol), $Ir(ppy)_3$ (1 mol%), Na_2HPO_4 (0.1 mmol) in MeCN (1 mL), stirred at room temperature for 24h irradiated through Blue LEDs. Yield determined through ^{1}H-NMR analysis on the crude reaction mixture involving triphenylmethane as internal standard. Yield on the isolated product into brackets. [a] Reaction time 72 hours.

Using α-methyl styrene **38i**, 2,3-dihydrofuran **39ai** has been obtained in 71% yield in 24 hours. On the contrary, 72 hours were necessary to obtain product **39ah** with an acceptable yield, probably due to the major steric hindrance of the α-isopropyl styrene **38h**. Also, co-product **41ah** was isolated from the same reaction mixture. The pathway to the formation of **41ah** is still not clear. According to previously reported investigation[186], the presence of water in the reaction mixture could promote its formation. Surely, the higher steric hindrance caused by the *iso*-propyl group favors parallel reaction pathways.

A 69% yield was obtained in the reaction performed with styrene **39aj**. Meanwhile, no reaction occurred with *p*-NO_2-styrene **38l**. The nitro group (NO_2) is well known to be a

strong electron attractor. Because of its presence, the electron density on the C-C double bond could be too low to for it to react to react with the electrophilic enol radical. At last, a 60% yield was pleasantly detected in the formation of the spiro compound **39ak**.

In the end, aliphatic alkenes have been screened (Scheme 62).

Scheme 62: Scope of aliphatic alkenes

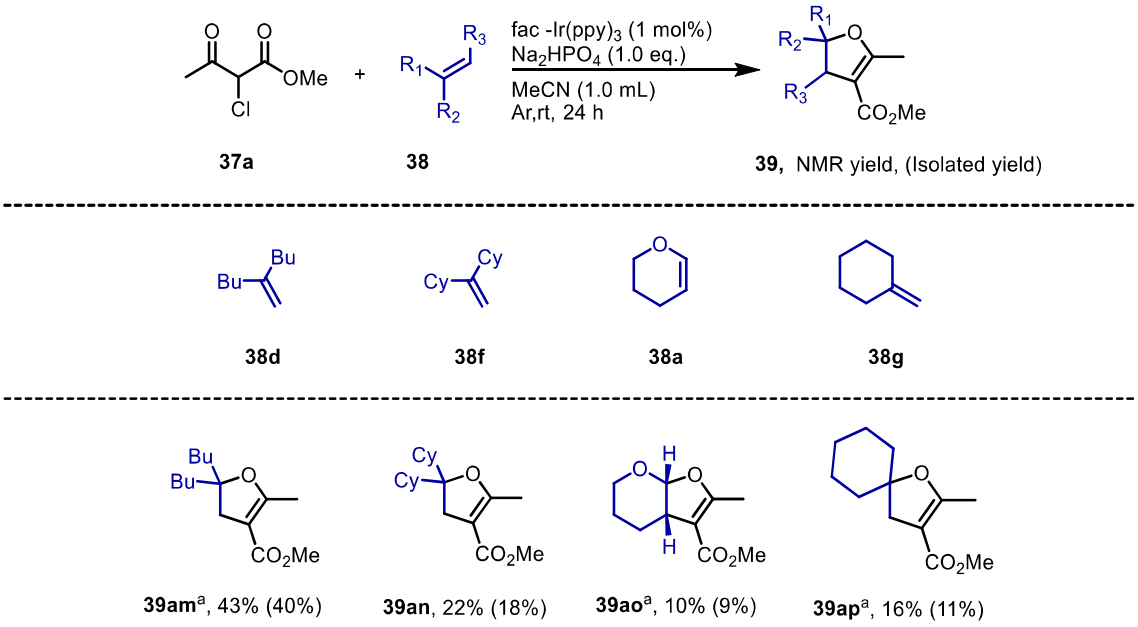

Reaction conditions: **37a** (0.12 mmol), **38a** (0.1 mmol), $Ir(ppy)_3$ (1 mol%), Na_2HPO_4 (0.1 mmol) in MeCN (1 mL), stirred at room temperature for 24h irradiated through Blue LEDs. Yield determined through ^1H-NMR analysis on the crude reaction mixture involving triphenylmethane as internal standard. Yield on the isolated product into brackets. [a] Alkene 3 equivalents.

The yields obtained with alkyl substituted alkenes resulted extremely low compared to the previously observed ones. Indeed, **39am** was achieved in a 43% yield, but 3 equivalents of **38m** were necessary.

An excess was necessary even with the other tested alkyl substituted **38**, except for di-cicloesil-ethylene **38f**. However, poor results were obtained with most of them. Alkyl substituents do not present a planar structure like the aromatic one. Therefore, the steric hindrance on the carbon-carbon double bond is increased. This could affect the reaction performance. In addition, electronic effects could influence it, since benzylic carbocations and radicals are more stabilized than the aliphatic ones.

A screening of halogenated compound has then been developed (Scheme 63).

Scheme 63: Scope of halogenated compounds

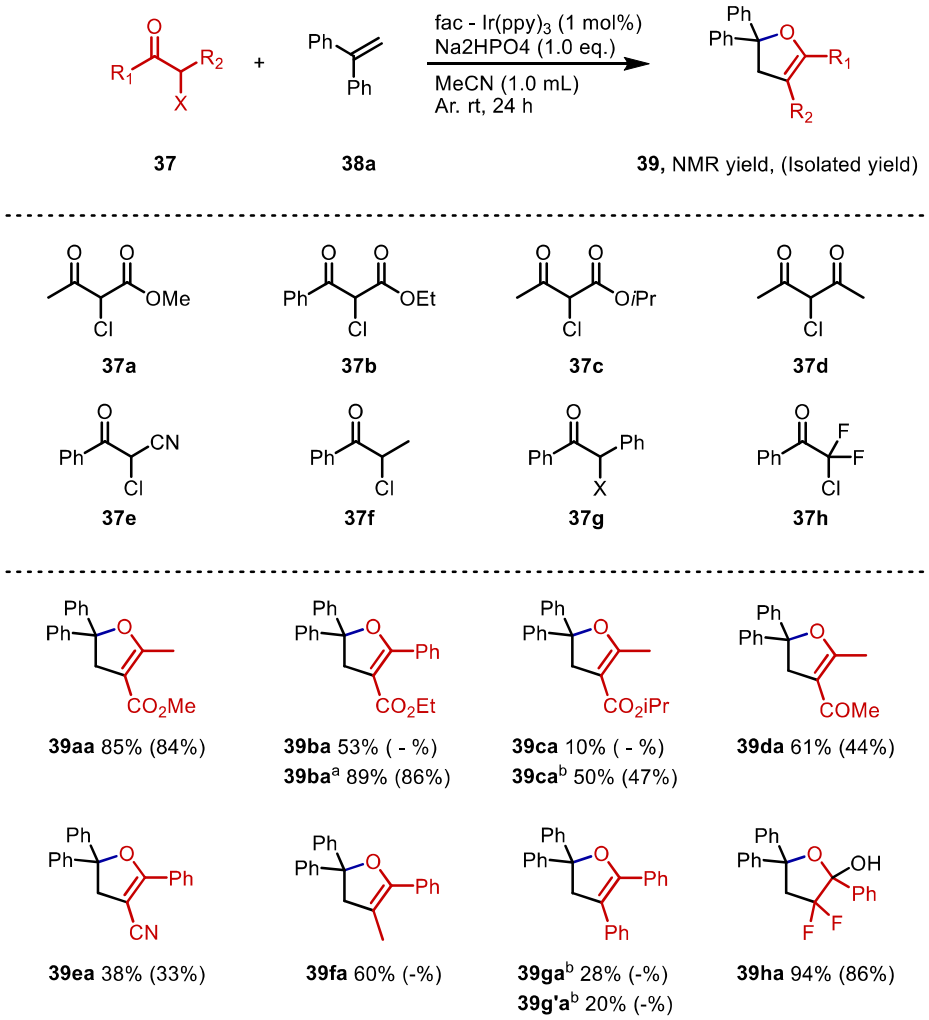

Reaction conditions: **37a** (0.12 mmol), **38a** (0.1 mmol), $Ir(ppy)_3$ (1 mol%), Na_2HPO_4 (0.1 mmol) in MeCN (1 mL), stirred at room temperature for 24h irradiated through Blue LEDs. Yield determined through ^1H-NMR analysis on the crude reaction mixture involving triphenylmethane as internal standard. Yield on the isolated product into brackets. [a] Reaction time 48 hours. [b] Reaction time 72 hours

At first, ß-ketoester **37b** and **37c** were utilized. Both required longer reaction times to give good yields. Even for these substrates, the steric effect could account for their lower performance. Good results were achieved with 3-chloropentane-2,4-dione, since 61% yield was obtained in 24 hours, proving the applicability of the process even in the absence of ester group. Interestingly, with 2-chloro-3-oxobutanenitrile **37e**, 2-3-dihydrofuran **37ea** was observed in a acceptable yield (38% yield). Numerous haloketones, both with bromine and chlorine, have been tested. Among them, two different reaction pathways could be observed, since 2,3-dihydrofuran **39** or ß-ketoester-ß,γ-unsaturated **40** were formed selectively. More in detail, chloro propiophenone **37f** brought to the formation of **39fa** in a 60% yield. On the contrary, bromo propiophenone

37f' selectively produced **40f'a** in 96% yield. Due to these contrasting experimental evidence, reactions utilizing 2-chloro-2- phenyl acetophenone **37g** and 2-bromo-2-phenyl acetophenone **37g'** were performed. Both brought to the production of 2,3-dihydrofuran **39ga** with respectively 28% and 20% yield, respectively. The poor yields detected could be derived from the high stabilization of the radical derived from **37g** and **37g'**, indeed the phenyl group on the α-carbon strongly enhances the possible delocalization reducing the reactivity. Pleasantly, the trisubstituted 2,2-difluoro-2-chloroacetophenone **37h** produced the hemiketal **42ha** in 94% yield. Due to the high substitution in the α-carbon, the formation of 2,3-dihydrofuran was not possible. With this substrate, the selectivity toward the reduction of the C-Cl bond instead of the C-F bond was demonstrated. All the other haloketones tested, selectively formed ß,γ-unsaturated ß-ketoester **40.**

Scheme 64: Scope of ß,γ-unsaturated ß-ketoester

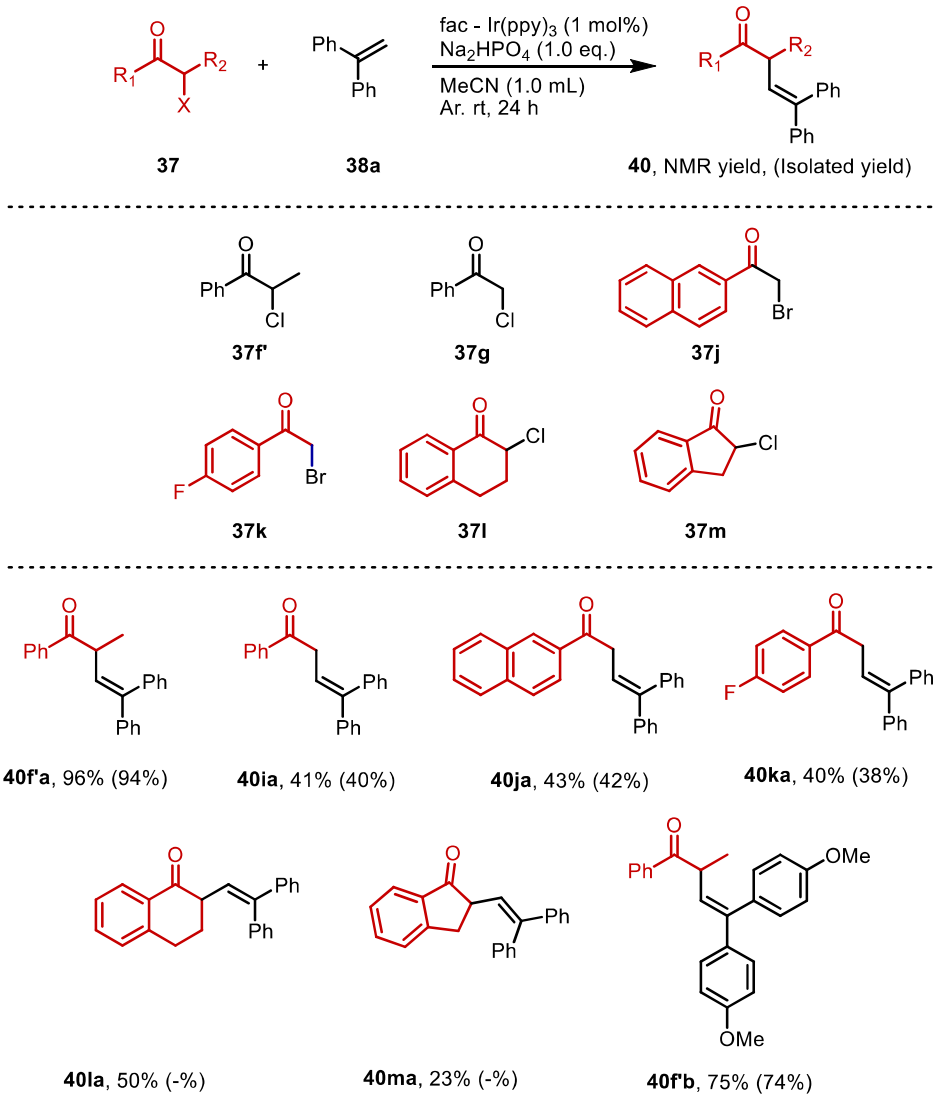

Reaction conditions: **37a** (0.12 mmol), **38a** (0.1 mmol), $Ir(ppy)_3$ (1 mol%), Na_2HPO_4 (0.1 mmol) in MeCN (1 mL), stirred at room temperature for 24h irradiated through Blue LEDs. Yield determined through ^1H-NMR analysis on the crude reaction mixture involving triphenylmethane as internal standard. Yield on the isolated product into brackets.

The experimental data so far observed outline a trend: α-substituted haloketones usually favor the cyclization pathway to **39**. Meanwhile α-unsubstituted haloketones favor the elimination toward the formation of ß-ketoester-ß,γ-unsaturated **40**. Indeed, 2,3-dihydrofurans were not detected with haloketones **37i-m**. On the other hand, products **40** were obtained in low to high yield. The different behavior of α-bromo-propriophenone **37f'** has still to be cleared. One last reaction has been performed involving **37f'** and *para*-methoxy functionalized alkene **38b**. Product **40f'b** has been obtained in a 75% yield in 24 hours reaction time. Therefore, the general applicability

of the developed transformation to the synthesis of ß,γ-unsaturated ß-ketoester **40** has for sure be further investigated. Still, the experimental data obtained are promising.

A more detailed mechanism has been hypothesized based on the experimental results and reported literature.[183,184,186] According to this mechanism, **Ir(III)** photocatalyst is excited to **Ir(III)*** (Ir(III)*/Ir(IV) = -1.73V).[100] Subsequently, a SET occurs between the excited photocatalyst and the halogenated substrate **37**. Thus the electrophilic radical **XXXIX** and **Ir(IV)** species are formed. Then, radical **37** attacks alkene **38** to give radical **L.** Now, a second SET occurs between **Ir(IV)** and radical **L**, leading to **Ir(III)** and carbocation **M**. At this point, different reaction pathways can be identified.

Pathway A leads to the formation of the desired 2,3-dihydrofuran **39**. Carbocation **M** undergo to intramolecular cyclization to form **N**. Thus, an elimination occurs to obtain 2,3-dihydrofuran **39**.

With **Pathway B**, hemiketal **42** is obtained through water addition to cation **N**. However, **42** it is not stable, slowly converging to **39**.

Pathway C brings to the formation of ß,γ-unsaturated ß-ketoester **40** *via* E1 elimination on carbocation **M**.

At last, **pathway D** leads to the production of lactone **41**. In this last case, water adds to cation **M** forming **O**[189], which eventually lactonizes to **41**.[186] This last pathway has been observed only with the high sterically hindered alkene **38h**.

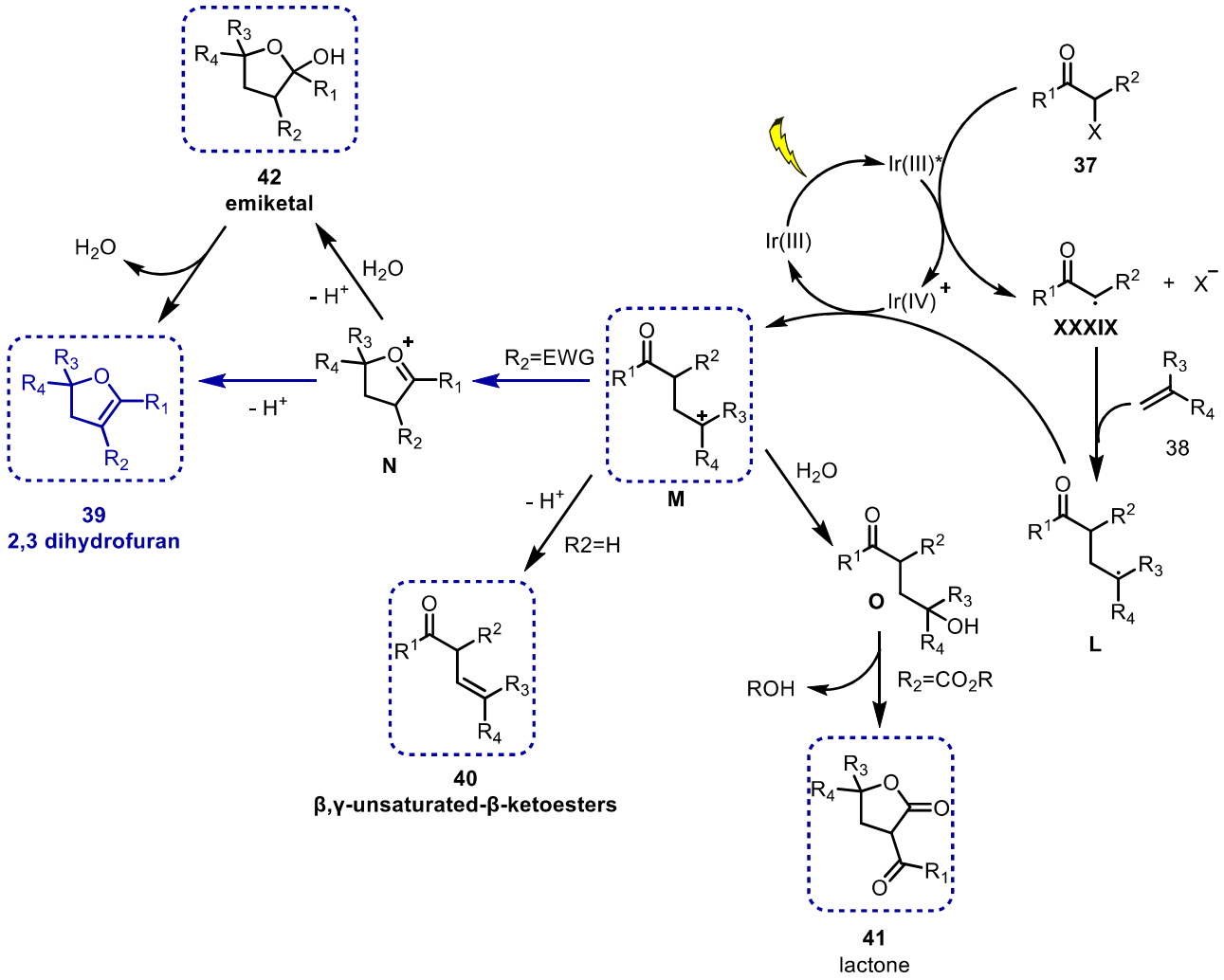

Scheme 65: Mechanism of the photocatalyzed synthesis of 2,3-dihydrofurans **39**, ß,γ-unsaturated ß-ketoester **40** and lactones **42**

To rule out the hypothesis of a radical chain pathway, light and dark tests have been performed. The reaction has been irradiated for 2 hours and kept in the dark for 1 hour, then the cycle is repeated to create a slope. From the obtained data, it resulted clear that without irradiation the reaction does not proceed. Therefore, a chain mechanism could be excluded, at least an efficient one.

Scheme 66: light and dark reaction

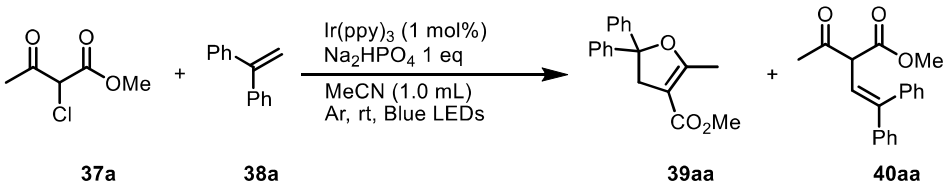

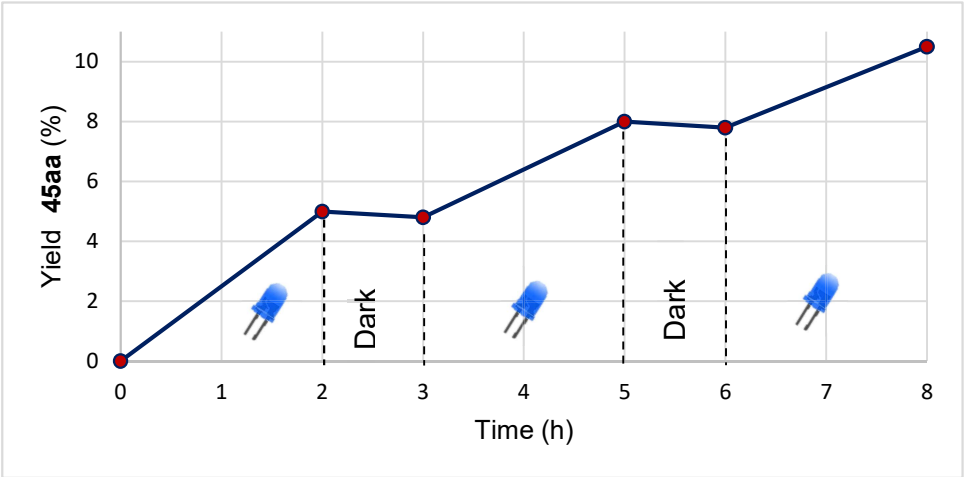

Conclusion

In conclusion, a photoredox transformation for the synthesis of 2,3-dihydrofurans has been developed. Under the optimized reaction conditions, 2,3-dihydrofuran **39** has been selectively obtained in 84% yield in 24 hours.

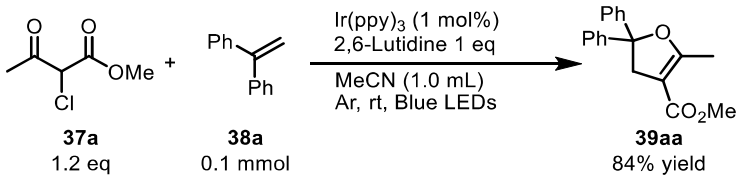

Scheme 67: Optimized photoredox catalyzed synthesis of 2,3-dihydrofuran

A library of 2,3-dihydrofuran has been constructed applying the optimized protocol to various alkenes and halogenated compounds.

During the investigation of the reaction scope, different reaction pathways emerged, leading to different products. The substrates structure results to highly influence the selectivity toward the different pathways, demonstrating the possibility to create a library of ß,γ-unsaturated-ß-ketoesters compounds **40**. More studies will be performed to rationalize the different pathways selectivity and to expand compound **40** library.

Mechanistic investigations have been performed to confirm the hypothesized reaction mechanism. From the obtained data it has been confirmed the necessity of photocatalyst and irradiation for the reaction to occurs. In addition, the possibility of a long-lived radical chain mechanism has been excluded. Theoretical calculations will be performed to confirm the hypothesized mechanism and to better understand the selectivity toward the diverse reaction pathways.

General Procedures and Products Characterization

Materials and methods

All commercial chemicals and dry solvents were purchased from Sigma Aldrich, Alfa Aesar or TCI Chemicals and used without additional purification. 1H and 13C-NMR spectra were recorded on a Varian Inova 400 NMR instrument with a 5 mm probe. All chemical shifts (δ) are referenced using deuterated solvent signals; chemical shifts are reported in ppm from TMS and coupling constants (J) are reported in Hertz. Multiplicity is reported as: s = singlet, d = doublet, t = triplet, q = quartet, hept = heptet, and m = multiplet. HPLC-MS analyses were performed using an Agilent Technologies HP1100 instrument coupled with an Agilent Technologies MSD1100 single-quadrupole mass spectrometer using a Phenomenex Gemini C18 3 µm (100 × 3 mm) column; mass spectrometric detection was performed in a full-scan mode from m/z 50 to 2500, with scan time 0.1 s in a positive ion mode, ESI spray voltage 4500 V, nitrogen gas 35 psi, drying gas flow rate 11.5 mL min−1, and fragmentor voltage 30 V. HRMS was performed using Waters Xevo G2-XS QT with, ESI+, cone voltage 40 V, Capillary 3 kV, and source temperature 120 °C. CSP-HPLC analyses were performed with an Agilent Technologies Series 1200 instrument using chiral columns. Flash chromatography purifications were carried out using VWR or Merck silica gel (40–63 µm particle size). Thin-layer chromatography was performed with Merck 60 F254 plates.

α–halo–ketons **37f**, **37h–37k** and **37m** were purchaised and used without further purifications.

methyl 2-chloro-3-oxobutanoate (37a)[190], **ethyl 2-chloro-3-oxo-3-phenylpropanoate (37b)** [191], **3-chloropentane-2,4-dione (37d)** [192,193], **2-chloro-3-oxo-3-phenylpropanenitrile (XX)**[194], **2-chloro-1-phenylpropan-1-one (37f)** [195], **2-chloro-1,2-diphenylethan-1-one (37g)**

[196], **2-bromo-1,2-diphenylethan-1-one (37g)** [197], **2-chloro-3,4-dihydronaphthalen-1(2H)-one (37l)** [198] were synthesized following previously reported procedures.

isopropyl 2-chloro-3-oxo-3-phenylpropanoate (37c)

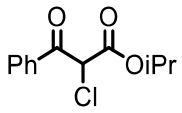

In a round bottom flask, isopropyl -3-oxo-3-phenylpropanoate (4 mmol) and DCM (8 mL, 0,5 M) are added. Then, solfonyl chloride (4 mmol) has been dropped at 0°C. The reaction is stirred for 2 hours at room temperature. Successively, water is added at 0°C. The aqueous phase is extracted with DCM and then organic solvents evaporated in vacuum. The crude reaction mixture is then purified through silica gel chromatography (Cyclohexane : DCM, 7:3). Product **37c** has been isolated as an incolour oil in a 60% yield. ^{1}H–NMR (400 MHz, $CDCl_3$) δ (ppm): 1.33 (d, J = 6.3 Hz, 6H), 2.38 (s, 3H), 4.72 (s, 1H), 5.08–5.17 (m, 1H).

Alkenes **38a, 38j** and **38o–38p** were purchaised and used without further purifications.

4,4'-(ethene-1,1-diyl)bis(methoxybenzene) (38b)[199], **4,4'-(ethene-1,1-diyl)bis(chlorobenzene)**[200] **(38c), 1-methoxy-4-(1-phenylvinyl)benzene**[201] **(38d), 1-chloro-2-(1-phenylvinyl)benzene (38e)**[202], **1-methyl-2-(1-phenylvinyl)benzene (38f)**[202], **α–isopropylstirene (38h)** [203], **α–metylstirene (38i)**[204], **1-methylene-1,2,3,4-tetrahydronaphthalene (38k)**[205,206], **p–nitro–styrene (38l)**[207], **5-methylenenonane (38m)**[208], **prop-1-ene-1,1-diyldibenzene (38g)** [209] were synthesized following previously reported procedures.

Photochemical reaction set up

A 50 cm blue LEDs strip has been used for the reaction mixture irradiation (λ_{max}= 465 nm).

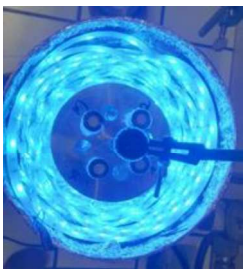

General procedure for the synthesis of 2,3-dihydrofurans 39

In a 4 mL screw-capped vial, alkene **38** (0,1 mmol), MeCN (1 mL), halogenated compound **37** (0,12 mmol), Na_2HPO_4 (0,1 mmol) and $Ir(ppy)_3$ (1% mol) are added. Freeze pump thaw (1x3 min) has been performed in the capped vial. The reaction mixture is stirred for 24 hours and irradiated with Blue LEDs for 24 hours. Then, it is filtered through a cotton filter and the solvent removed in vacuo. The reaction mixture is successively purified through a silica gel chromatographic column.

Methyl 2-methyl-5,5-diphenyl-4,5-dihydrofuran-3-carboxylate (39aa)

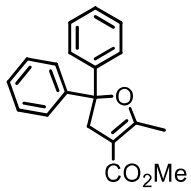

Incolor oil. Yield 84%. ^{1}H-NMR (400 MHz, $CDCl_3$) δ 7.41 – 7.36 (m, 4H), 7.38 – 7.29 (m, 4H), 7.29 – 7.24 (m, 2H), 3.69 (s, 3H), 3.60 (q, J = 1.6 Hz, 2H), 2.35 (t, J = 1.6 Hz, 3H). ^{13}C-NMR (100 MHz, $CDCl_3$) δ 166.6, 166.1, 145.1, 128.3, 127.5, 125.6, 101.5, 91.6, 50.9, 44.0, 14.2. LRMS (ESI$^+$) *m/z* 263.4 [M - OMe]$^+$, 277.4 [M – OH]$^+$, 295.4 [M + H]$^+$, 611.4 [2M + Na]$^+$.

Methyl 5,5-bis(4-methoxyphenyl)-2-methyl-4,5-dihydrofuran-3-carboxylate (39ab)[210]

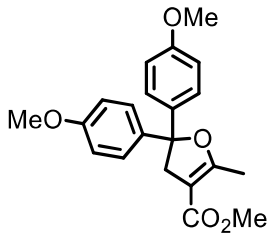

Yellowish oil. Yield 35%. ^{1}H–NMR (400 MHz, $CDCl_3$) δ (ppm):7.40 – 6.80 (m, 8H), 3.73 (s, 6H), 3.69 (s, 3H), 3.55 (q, J = 1.6 Hz, 2H), 2.31 (t, J = 1.6 Hz, 3H).

Methyl 5,5-bis(4-chlorophenyl)-2-methyl-4,5-dihydrofuran-3-carboxylate (39ac)

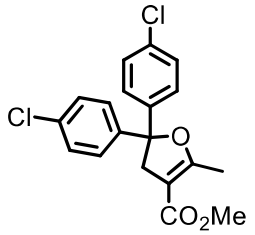

Incolor oil. Yield 67%. ^{1}H-NMR (400 MHz, $CDCl_3$) δ 7.33 – 7.26 (m, 8H), 3.70 (s, 3H), 3.53 (q, J = 1.6 Hz, 2H), 2.33 (t, J = 1.7 Hz, 3H). ^{13}C-NMR (100 MHz, $CDCl_3$) δ 166.2, 165.8, 143.1, 133.7, 128.6, 127.0, 101.6, 90.6, 51.0, 43.9, 14.1. LRMS (ESI$^+$) *m/z* 263.2 [M + H]$^+$, 280.4 [M + NH_4]$^+$.

Methyl 5-(4-methoxyphenyl)-2-methyl-5-phenyl-4,5-dihydrofuran-3-carboxylate (39ad)

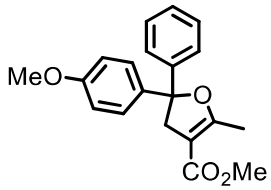

White gummy solid. Yield 74%. ^{1}H-NMR (400 MHz, $CDCl_3$) δ 7.35 – 7.28 (m, 3H), 7.28 – 7.20 (m, 4H), 6.84 – 6.78 (m, 2H), 3.75 (s, 3H), 3.65 (s, 3H), 3.57 (dq, J = 14.6, 1.7 Hz, 1H), 3.49 (dq, J = 14.6, 1.6 Hz, 1H), 2.30 (t, J = 1.6 Hz, 3H). ^{13}C-NMR (100 MHz, $CDCl_3$) δ 166.6, 166.2, 158.9, 145.4, 137.1, 128.3, 127.4, 127.1, 125.6, 113.6, 101.4, 91.5, 55.3, 50.9, 44.1, 14.2. HRMS (ESI$^+$) *m/z* 325.1441 [M + H] $^+$; 325.1434 calcd.

Methyl 5-(2-chlorophenyl)-2-methyl-5-phenyl-4,5-dihydrofuran-3-carboxylate (39ae)

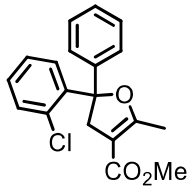

White gummy solid. Yield 63%. ^{1}H-NMR (400 MHz, $CDCl_3$) δ 7.76 (dd, J = 7.7, 1.8 Hz, 1H), 7.38 (dd, J = 7.6, 1.6 Hz, 1H), 7.34 (dd, J = 7.7, 1.6 Hz, 1H), 7.32 – 7.26 (m, 6H), 4.05 (dq, J = 15.7, 1.7 Hz, 1H), 3.73 (s, 3H), 3.44 (dq, J = 15.7, 1.8 Hz, 1H), 2.30 (t, J = 1.7 Hz, 3H). ^{13}C-NMR (100 MHz, $CDCl_3$) δ 166.1, 165.4, 142.3, 142.0, 131.1, 129.0, 128.3, 128.1, 127.1, 126.6, 126.4, 102.3, 91.0, 50.9, 42.4, 14.1. HRMS (ESI$^+$) *m/z* 329.0939 [M + H] $^+$; 329.0939 calcd.

Methyl 2-methyl-5-phenyl-5-(o-tolyl)-4,5-dihydrofuran-3-carboxylate (39af)

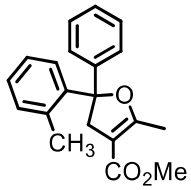

White gummy solid. Yield 74%. ^{1}H-NMR (400 MHz, $CDCl_3$) δ 7.71 – 7.62 (m, 1H), 7.36 – 7.29 (m, 3H), 7.29 – 7.24 (m, 4H), 7.21 – 7.16 (m, 1H), 3.81 (dq, J = 15.0, 1.6 Hz, 1H), 3.73 (s, 3H), 3.43 (dq, J = 14.9, 1.7 Hz, 1H), 2.33 (t, J = 1.6 Hz, 3H), 2.03 (s, 3H). ^{13}C-NMR (100 MHz, $CDCl_3$) δ 166.2, 166.0, 143.3, 142.6, 135.1, 132.1, 128.4, 127.9, 127.7, 126.1, 125.6, 125.3, 101.6, 91.8, 50.9, 42.9, 21.2, 14.2. HRMS (ESI$^+$) *m/z* 309.1487 [M + H] $^+$; 309.1485 calcd.

Methyl 2,4-dimethyl-5,5-diphenyl-4,5-dihydrofuran-3-carboxylate (39ag)

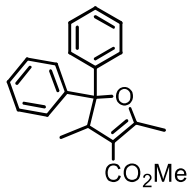

White gummy solid. Yield 70%. ^{1}H–NMR (400 MHz, $CDCl_3$) δ (ppm): 0.80 (d, J = 6.9 Hz, 3H), 2.27 (s, 3H), 3.69 (s, 3H), 3.89 (q, J = 6.9 Hz, 1H), 7.18–7.33 (m, 8H), 7.49–7.52 (m, 2H). ^{13}C-NMR (100 MHz, $CDCl_3$) δ 166.2, 166.0, 144.9, 141.2, 128.1, 127.8, 127.7, 127.0, 126.4, 126.2, 109.1, 94.9, 50.8, 44.4, 17.8, 14.7. LRMS (ESI$^+$) *m/z* HRMS (ESI$^+$) *m/z* 309.1485 [M + H] $^+$; 309.1485 calcd.

Methyl 5-isopropyl-2-methyl-5-phenyl-4,5-dihydrofuran-3-carboxylate (39ah)

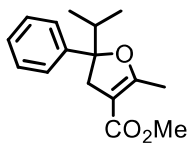

Incolour oil. Yield 37%. ^{1}H-NMR (400 MHz, $CDCl_3$) δ 7.37 – 7.29 (m, 4H), 7.26 – 7.20 (m, 1H), 3.67 (s, 3H), 3.21 (dq, J = 14.5, 1.6 Hz, 1H), 3.07 (dq, J = 14.5, 1.6 Hz, 1H), 2.27 (t, J = 1.6 Hz, 3H), 2.10 (hept, J = 6.9 Hz, 1H), 0.90 (d, J = 6.7 Hz, 3H), 0.80 (d, J = 6.8 Hz, 3H). ^{13}C-NMR (100 MHz, $CDCl_3$) δ 167.2, 166.4, 144.9, 127.9, 126.9, 125.3, 101.2,

93.6, 50.7, 40.2, 38.4, 17.3, 16.5, 14.0. LRMS (ESI+) *m/z* 243.4 [M – OH]+, 261.4 [M + H]+, 543.4 [2M + Na]+.

Methyl 2,5-dimethyl-5-phenyl-4,5-dihydrofuran-3-carboxylate (39ai)

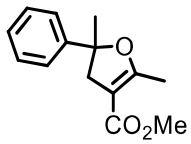

Incolour oil. Yield 37%. 70%. ^{1}H-NMR (400 MHz, $CDCl_3$) δ 7.40 – 7.32 (m, 4H), 7.31 – 7.24 (m, 1H), 3.69 (s, 3H), 3.13 (dq, J = 14.3, 1.7 Hz, 1H), 3.04 (dq, J = 14.3, 1.6 Hz, 1H), 2.30 (t, J = 1.6 Hz, 3H), 1.68 (s, 3H). ^{13}C-NMR (100 MHz, $CDCl_3$) δ 166.9, 166.5, 146.3, 128.4, 127.2, 124.2, 101.0, 88.5, 50.8, 44.3, 29.4, 14.3. LRMS (ESI+) *m/z* 215.4 [M – OH]+, 233.4 [M + H]+, 487.4 [2M + Na]+.

Methyl 2-methyl-5-phenyl-4,5-dihydrofuran-3-carboxylate (39aj)

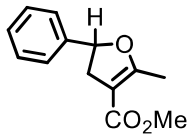

Incolour oil. Yield 37%. 68%. ^{1}H-NMR (400 MHz, $CDCl_3$) 7.41 – 7.28 (m, 1H), 5.59 (dd, J = 10.7, 8.3 Hz, 0H), 3.71 (s, 1H), 3.33 (ddq, J = 14.0, 10.7, 1.6 Hz, 0H), 2.92 (ddq, J = 14.4, 8.3, 1.6 Hz, 0H), 2.29 (t, J = 1.6 Hz, 1H). ^{13}C-NMR (100 MHz, $CDCl_3$) δ 168.0, 166.4, 141.5, 128.7, 128.1, 125.7, 101.5, 83.2, 50.9, 37.9, 14.1. LRMS (ESI+) *m/z* 219.4 [M + H]+, 260.4 [M + MeCN + H]+.

Methyl 5-methyl-3',4'-dihydro-2'H,3H-spiro[furan-2,1'-naphthalene]-4-carboxylate (39ak)

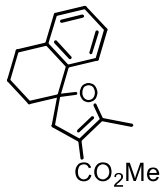

White gummy solid. Yield 57%. ^{1}H-NMR (400 MHz, $CDCl_3$) δ 7.37 – 7.31 (m, 1H), 7.22 – 7.15 (m, 2H), 7.12 – 7.03 (m, 1H), 3.71 (s, 3H), 3.15 (dq, J = 14.8, 1.7 Hz, 1H), 2.96 (dq, J = 14.8, 1.6 Hz, 1H), 2.91 – 2.68 (m, 2H), 2.25 (t, J = 1.6 Hz, 3H), 2.18 – 2.03 (m, 1H), 2.03 – 1.91 (m, 2H), 1.90 – 1.75 (m, 1H). ^{13}C-NMR (100 MHz, $CDCl_3$) δ 167.2, 166.6,

139.7, 136.4, 128.8, 127.8, 126.7, 126.3, 100.5, 87.1, 50.8, 44.9, 36.8, 29.3, 19.8, 14.4. HRMS (ESI+) *m/z* 259.1336 [M + H] +; 259.1329 calcd.

Methyl 5,5-dibutyl-2-methyl-4,5-dihydrofuran-3-carboxylate (39am)

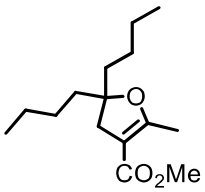

Incolour oil. Yield 40%. ^{1}H-NMR (400 MHz, $CDCl_3$) δ 3.69 (s, 3H), 2.64 (t, J = 1.6 Hz, 2H), 2.17 (t, J = 1.5 Hz, 3H), 1.69 – 1.50 (m, 4H), 1.41 – 1.16 (m, 8H), 0.90 (t, J = 6.8 Hz, 6H). ^{13}C-NMR (100 MHz, $CDCl_3$) δ 167.6, 166.9, 100.8, 90.7, 50.7, 39.2, 38.6, 25.4, 23.1, 14.2, 14.0.

Methyl 5,5-dicyclohexyl-2-methyl-4,5-dihydrofuran-3-carboxylate (39an)

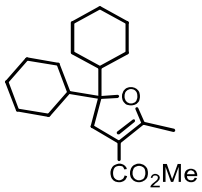

Incolour oil. Yield 18%. ^{1}H-NMR (400 MHz, $CDCl_3$) δ 3.68 (s, 3H), 2.62 (d, J = 1.9 Hz, 2H), 2.15 (t, J = 1.4 Hz, 3H), 1.82 – 1.71 (m, 4H), 1.71 – 1.55 (m, 7H), 1.38 – 1.03 (m, 9H), 1.04 – 0.84 (m, 2H). ^{13}C-NMR (100 MHz, $CDCl_3$) δ 168.4, 166.7, 101.3, 94.2, 50.7, 43.4, 33.9, 26.5, 26.4, 26.3, 25.9, 25.6, 13.7.

Methyl 2-methyl-3a,5,6,7a-tetrahydro-4H-furo[2,3-b]pyran-3-carboxylate (39ao)[211]

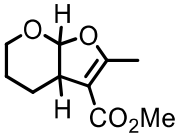

Incolour oil. Yield 18%. ^{1}H-NMR (400 MHz, $CDCl_3$) δ 1.56 – 1.67 (m, 3H), 1.92 – 1.98 (m, 1H), 2.23 (d, J = 1.4 Hz, 3H), 2.96 – 3.01 (m, 1H), 3.70 (s, 3H), 3.74 – 381 (m, 2H), 5.77 (d, J = 6.7 Hz, 1H).

Ethyl 2,5,5-triphenyl-4,5-dihydrofuran-3-carboxylate (39ba)

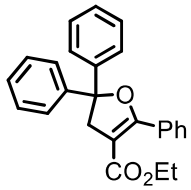

White gummy solid. Yield 86%. ^{1}H-NMR (400 MHz, $CDCl_3$) δ 7.98 – 7.87 (m, 2H), 7.55 – 7.46 (m, 4H), 7.47 – 7.41 (m, 2H), 7.39 – 7.32 (m, 4H), 7.32 – 7.27 (m, 2H), 4.14 (q, J = 7.1 Hz, 2H), 3.86 (s, 2H), 1.21 (t, J = 7.1 Hz, 3H). ^{13}C-NMR (100 MHz, $CDCl_3$) δ 164.9, 163.4, 145.2, 130.4, 129.9, 129.5, 128.4, 127.6, 127.5, 125.7, 102.2, 90.8, 59.8, 45.7, 14.2. HRMS (ESI^{+}) *m/z* 371.1647 [M + H] $^{+}$; 371.1642 calcd.

Isopropyl 2-methyl-5,5-diphenyl-4,5-dihydrofuran-3-carboxylate (39ca)[175]

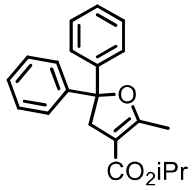

Incolour oil. Yield 47%. ^{1}H–NMR (400 MHz, $CDCl_3$) δ (ppm): 7.40 – 7.35 (m, 4H), 7.34 – 7.31 (m, 4H), 5.02 (p, *J*=6.3, 1H), 3.57 (q, *J*=1.7, 2H), 2.33 (t, *J*=1.6, 3H), 1.23 (d, *J*=6.3, 6H).

1-(2-methyl-5,5-diphenyl-4,5-dihydrofuran-3-yl)ethan-1-one (39da)

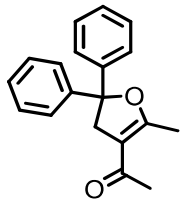

Incolour oil. Yield 44%. ^{1}H-NMR (400 MHz, $CDCl_3$) δ 7.42 – 7.30 (m, 8H), 7.30 – 7.26 (m, 2H), 3.66 (q, J = 1.5 Hz, 3H), 2.39 (t, J = 1.5 Hz, 3H), 2.23 (s, 3H). ^{13}C-NMR (100 MHz, $CDCl_3$) δ 194.1, 165.9, 144.9, 128.4, 127.6, 125.6, 112.2, 91.5, 44.8, 29.4, 15.2. LRMS (ESI^{+}) *m/z* 279.4 [M + H]$^{+}$, 579.4 [2M + Na]$^{+}$.

2,5,5-triphenyl-4,5-dihydrofuran-3-carbonitrile (39ea)

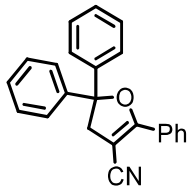

White gummy solid. Yield 33%. ^{1}H–NMR (400 MHz, $CDCl_3$) δ (ppm): ^{1}H-NMR (400 MHz, $CDCl_3$) δ 8.10 (dd, J = 7.7, 2.1 Hz, 2H), 7.50 (d, J = 7.8 Hz, 3H), 7.42 (d, J = 8.1 Hz, 4H), 7.37 (t, J = 7.5 Hz, 4H), 7.32 (d, J = 7.2 Hz, 2H), 3.78 (s, 2H). ^{13}C-NMR (100 MHz, $CDCl_3$) δ 165.3, 143.8, 131.5, 128.8, 128.6, 128.0, 127.9, 127.2, 125.6, 117.3, 92.8, 79.1, 45.6. HRMS (ESI^{+}) *m/z* 324.1381 [M + H] $^{+}$; 324.1383 calcd.

4-methyl-2,2,5-triphenyl-2,3-dihydrofuran (39fa)

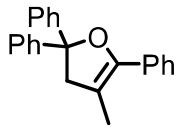

Incolour oil. Yield 58%. ^{1}H–NMR (400 MHz, $CDCl_3$) δ (ppm): 7.98 – 7.87 (m, 2H), 7.55 – 7.46 (m, 4H), 7.47 – 7.41 (m, 2H), 7.39 – 7.32 (m, 4H), 7.32 – 7.27 (m, 2H), 3.51 (q, *J*=1.5, 2H), 1.92 (t, *J*=1.5, 3H).

3,3-difluoro-2-methyl-5,5-diphenyltetrahydrofuran-2-ol (42ha)

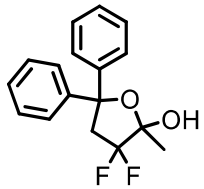

Incolour oil. Yield 86%.^{1}H-NMR (400 MHz, $CDCl_3$) δ 7.81 – 7.68 (m, 2H), 7.61 – 7.47 (m, 4H), 7.48 – 7.40 (m, 3H), 7.40 – 7.30 (m, 4H), 7.32 – 7.21 (m, 2H), 3.60 (ddd, J = 27.7, 13.7, 9.3 Hz, 1H), 3.35 (ddd, J = 16.3, 13.7, 1.2 Hz, 1H), 2.98 (brs, 1H). ^{13}C-NMR (100 MHz, $CDCl_3$) δ 147.2 , 145.5 , 136.2 (d, J = 1.5 Hz), 129.4 , 128.4 , 128.2 , 127.2 (d, J = 1.7 Hz), 127.1 , 125.5, 125.4 , 125.2 (dd, J = 265.0, 250.9 Hz), 102.0 (dd, J = 32.9, 22.8 Hz), 85.2 (d, J = 8.6 Hz), 44.5 (t, J = 22.3 Hz). ^{19}F NMR (380 MHz, $CDCl_3$) δ 105.5 (ddd, J = 229.4, 27.7, 16.3 Hz), 118.0 (dd, J = 229.2, 9.3 Hz). LRMS (ESI^{+}) *m/z* 335.4 [M - OH] $^{+}$, 375.4 [M + Na] $^{+}$.

2-methyl-1,4,4-triphenylbut-3-en-1-one (40f'a)

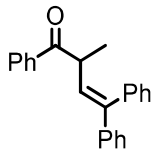

Yellowish oil. Yield 94%. ^{1}H-NMR (400 MHz, $CDCl_3$) δ 7.71 – 7.60 (m, 2H), 7.53 – 7.47 (m, 1H), 7.45 – 7.39 (m, 3H), 7.37 – 7.30 (m, 2H), 7.25 – 7.14 (m, 7H), 6.14 (d, J = 10.2 Hz, 1H), 4.27 (dq, J = 10.2, 6.7 Hz, 1H), 1.38 (d, J = 6.7 Hz, 3H). ^{13}C-NMR (100 MHz, $CDCl_3$) δ 201.7, 143.0, 141.7, 139.7, 136.2, 132.9, 129.6, 128.9, 128.5, 128.4, 128.4, 128.1, 127.6, 127.4, 127.3, 42.1, 18.3. LRMS (ESI$^+$) *m/z* 313.4 $[M + H]^+$, 335.4 $[M + Na]^+$, 647.8 [2M + Na].

1,4,4-triphenylbut-3-en-1-one (40ia)

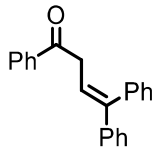

Yellowish oil. Yield 40%. ^{1}H-NMR (400 MHz, $CDCl_3$) δ: 7.71 – 7.60 (m, 2H), 7.53 – 7.47 (m, 1H), 7.45 – 7.39 (m, 3H), 7.37 – 7.30 (m, 2H), 7.25 – 7.14 (m, 7H), 6.14 (d, J = 10.2 Hz, 2H), 4.20 (d, J = 10.2, 2H).

1-(naphthalen-2-yl)-4,4-diphenylbut-3-en-1-one (40ja)

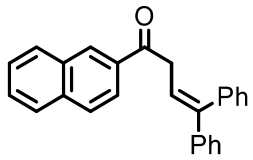

Incolour oil. Yield 42%.^{1}H-NMR (400 MHz, $CDCl_3$) δ: 8.54 – 8.50 (m, 1H), 7.97 – 7.81 (m, 3H), 7.59 – 7.48 (m, 4H), 7.44 – 7.29 (m, 14H), 6.43 (t, *J*=6.2, 1H), 3.94 (d, *J*=6.2, 3H).

1-(4-fluorophenyl)-4,4-diphenylbut-3-en-1-one (40ka)

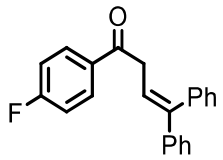

Incolour oil. Yield 38%.^{1}H-NMR (400 MHz, $CDCl_3$) δ: 7.88 – 7.76 (m, 4H), 7.58 (t, *J*=7.5, 1H), 7.47 (t, *J*=7.3, 2H), 7.37 (dt, *J*=14.4, 6.9, 4H), 7.21 – 7.17 (m, 2H), 7.06 (t, *J*=8.6, 1H), 6.38 (t, *J*=7.1, 1H), 3.77 (d, *J*=7.1, 2H).

4,4-bis(4-methoxyphenyl)-2-methyl-1-phenylbut-3-en-1-one (40f'b)

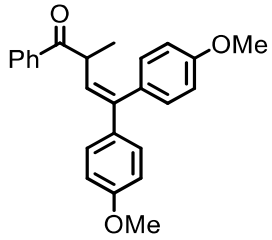

Yellowish oil. Yield 74%.^{1}H-NMR (400 MHz, $CDCl_3$) δ 7.68 (d, J = 7.0 Hz, 2H), 7.49 (t, J = 7.4 Hz, 1H), 7.34 (t, J = 7.7 Hz, 2H), 7.11 (dd, J = 10.2, 8.7 Hz, 4H), 6.96 (d, J = 8.6 Hz, 2H), 6.76 (d, J = 8.8 Hz, 2H), 5.97 (d, J = 10.3 Hz, 1H), 4.28 (dq, 10.1, 6.7 Hz, 1H), 3.88 (s, 3H), 3.77 (s, 3H),1.38 (d, J = 6.7 Hz, 3H). ^{13}C-NMR (100 MHz, $CDCl_3$) δ 201.9, 159.1, 159.0, 142.2, 136.3, 134.8, 132.8, 132.2, 130.8, 128.5, 128.4, 128.3, 127.0, 113.9, 113.4, 55.3, 55.3, 42.2, 18.3. LRMS (ESI^{+}) *m/z* 373.4 $[M + H]^{+}$.

A novel photoredox catalyzed transformation for the synthesis of 2-aminofurans

Introduction

Furans have a wide presence in natural compounds and bioactive molecules.[212,213] For example, 2-amino furans are used as intermediates for the synthesis of bioactive molecules, such as some inhibitors of various kinase proteins[214,215] or bacterial RNA.[216]

Because of their importance, numerous different approach for the synthesis of 2-amino furans has been developed. [217–221] Usually, high temperatures, stoichiometric additives, and metals are required. In addition, functionalized starting materials are often necessary for the reported methodologies. Therefore, the development of an efficient and smooth methodology is still an issue nowadays.

Among the developed methodologies, metal-catalyzed cycloisomerization of allenes demonstrated to be an efficient approach for the obtainment of amino furan. Procedures involving Au[222,223], In[224], and Pd[225,226] as catalysts were reported. In all of them, the metal catalyst activates the allene toward an intramolecular cyclization.

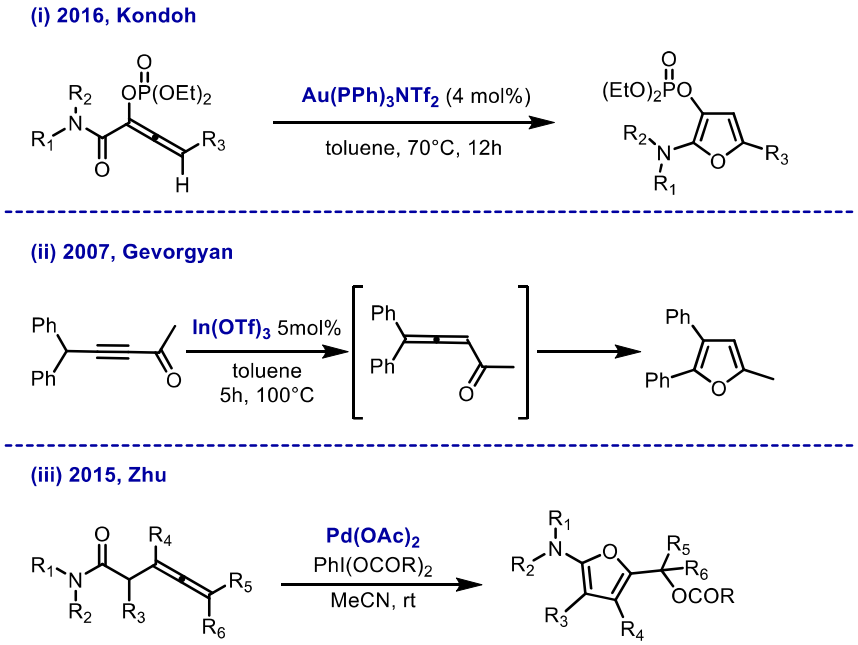

Figure 30: (i) Synthesis of 2,3-allenylamides utilizing [1,2]-phospha-Brook rearrangement and their application to gold-catalyzed cycloisomerization providing 2-aminofuran derivatives;[222] (ii) Metal-Catalyzed [1,2]-Alkyl Shift in Allenyl Ketones: Synthesis of Multisubstituted Furans;[227] (iii) Palladium-catalyzed cycloisomerization and aerobic oxidative cycloisomerization of homoallenyl amides: A facile and divergent approach to 2-aminofurans.[228]

Allenes are widely used as a building blocks in the synthesis of important compounds.[229] In particular, allenamines present a peculiar reactivity. Indeed, the electron density on the C_α-C_β double bond is enhanced by the nitrogen lone pair donation. The major electron density leads to increased nucleophilicity of the allene ß-carbon. Consequently, the regioselectivity toward electrophilic addition on the ß-carbon respect to the γ-carbon is increased (Scheme 68).

Allenamines are usually considered more reactive than allenes.[230,231] However, the enhanced electron density on the C_α-C_β double bond lowers their stability. For this reason, the use of allenamines in organic synthesis is limited. To avoid the stability problem, allenamides are often used instead of allenamines. The amide moiety diminishes the nitrogen lone pair electron-donation to the double bonds. By this way, more stable but still reactive compounds are formed.

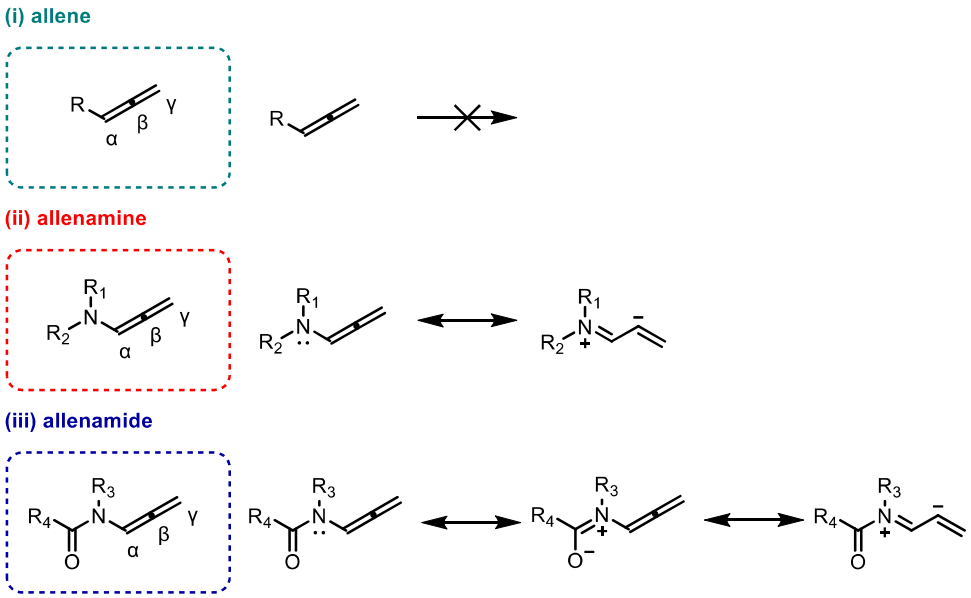

Scheme 68: (i) allene; (ii) allenamine; (iii) allenamide

In the last years, allenes reactivity in photoredox catalysis has been investigated.[232–235] In detail, Kimber reported *N*-acyliminium **XLIII** formation through photoredox catalyzed intermolecular radical electrophilic addition to allenamides **XLII**.[236]

In this reaction, an electrophilic radical $\mathbf{R_2}^\bullet$ is generated through SET transformation with a Ir complex photocatalyst. Successively, $\mathbf{R_2}^\bullet$ selectively attacks the allene **XLII** ß carbon to form radical **XLIV.** Then, a SET occurs and iminium carbocation **XLV** is formed. At this point, a nucleophilic species $\mathbf{Nu}^-$ attacks the carbocation to generate product **XLIII.**

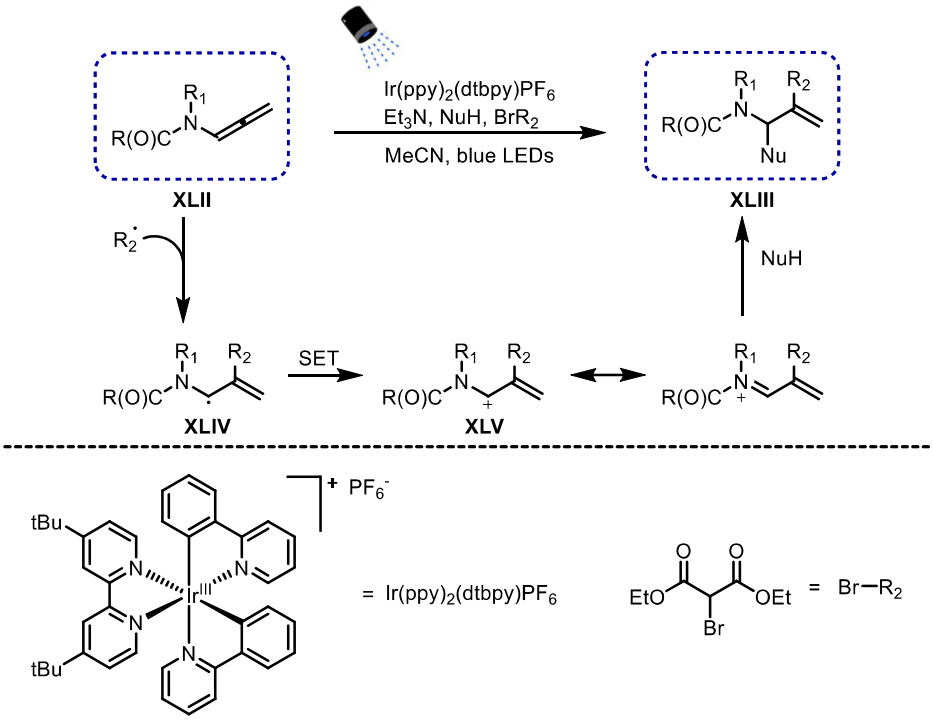

Scheme 69: N-acyliminium formation through photoredox catalyzed intermolecular radical electrophilic addition to allenamides[237]

To the best of our knowledge, this is the first example of photoredox catalysis involving allenamides. However, Kimber's work highlighted the potential of allenamides substrates in the photocatalytic field.

Aim of the project

Considering the importance of 2-amino furans, a new photoredox catalyzed synthetic methodologies is investigated. Inspired by classical synthetic methodologies[222,223,225–227] and Kimber's recent work[236], allenamides are selected as starting material.

The designed transformation involves the intermolecular reaction between an allenamide **43** and a halogenated compound **44** under photoredox catalyzed conditions. Subsequently, an intramolecular cyclization produces 2-aminofuran **45**.

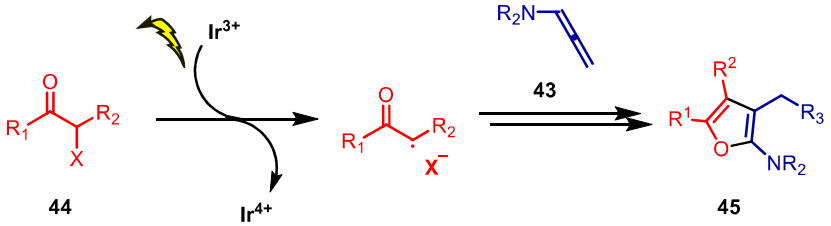

Scheme 70: Photoredox catalyzed synthesis of 2-aminofurans

Once optimized the reaction conditions, the reaction mechanism is investigated to shed some light on it. Moreover, the scope of the reaction is explored to test the applicability of the developed methodology. At the end, its applicability under flow conditions is studied to verify the practicability of a future scale-up.

Discussion and results

Initially, allenamide[238] **43a** and chlorophenyl acetoacetate[191] **44a** have been synthesized following reported procedures. A first catalystic test has been run based on previously reported literature[184,186,232,236,239]. Therefore, $Ir(ppy)_3$ was chosen as a catalyst, acetonitrile (MeCN) as a solvent, and 2,6-lutidine as a base. The reaction mixture has been stirred for 24 hours at room temperature and irradiated with blue LEDs. Pleasantly, a 78% yield on product **45aa** was detected from ^{1}H-NMR analysis on the crude reaction mixture. (Scheme 71)

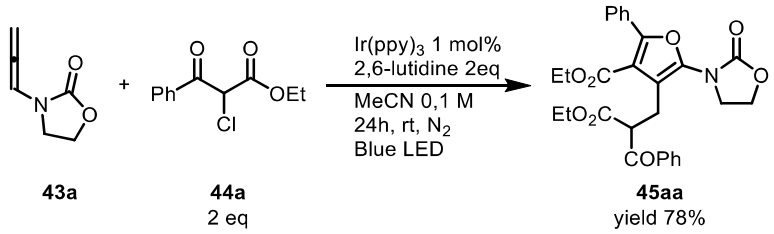

Scheme 71: First catalytic test for the synthesis of **45**

Product **45aa** resulted in a double attack of halogenated compound **44a** to allenamide **43a**. After this promising result, different reaction conditions were analyzed.

At first different catalysts have been tested. No reaction was observed with neither one of them, confirming $Ir(ppy)_3$ as a catalyst for this transformation.

Successively, different solvents were investigated.

Table 19: Solvents screening

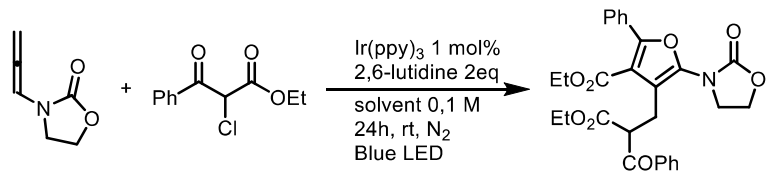

43a **44a** 2 eq **45aa**

Entry [a]	Solvent	Yield % [b]
1	MeCN anhydrous	78
2	THF	27
3	DCM	58
4	MeCN:H_2O 4:1	-
5	DMF	40
6	MeCN	73
7	DMSO	36

[a] Reactions conditions: **43a (**0.1 mmol), **44a (**0.12 mmol), 2,6-lutidine (0.2 mmol) and $Ir(ppy)_3$ (0.001 mmol) in 1 mL of the corresponding solvent for 24h at room temperature irradiated with blue LEDs ; [b] Calculated using Ph_3CH as internal standard from ^{1}H-NMR on the crude mixture.

Tetrahydrofuran (THF), dimethyl sulfoxide (DMSO), dichloromethane (DCM), and dimethylformamide (DMF) were tested in the same reaction conditions of acetonitrile (MeCN). Acetonitrile appeared to be the most suitable solvent for this transformation (Entry 1, Table 19). No high yields were obtained with all the other solvents, even if no allene was detected after 24h of reaction. Probably due to the formation of different byproducts or decomposition of the **43a**. Noteworthily, no products derived from an addition of **44a** on the γ-carbon of **43a** were observed.

The influence of water was investigated as well. No substantial difference was detected between the reactions performed with dry MeCN (78% yield, Entry 1, Table 19) and not dry one (73% yield, Entry 6, Table 19). In contrast, when a mixture of MeCN and water (4:1) was used, no trace of **45aa** was detected (Entry 4, Table 19). Trace amounts of water does not dramatically affect the studied transformation, but a substantial amount completely inhibits it. Anyway, dry MeCN was chosen as the reaction solvent to achieve good control over the reaction conditions.

Some organic and inorganic bases have been tested.[184,240] No improvements were observed with all the examined bases. Therefore 2,6-lutidine was selected for the desired

transformation. Also, changing the amount of base did not increase **45aa** yield. thus 2 eq of base were consequently chosen for the optimized conditions. Finally, an excess of **44a** resulted in a lower **45aa** yield.

The reaction concentration was investigated. Due to the poor solubility of the catalyst $Ir(ppy)_3$, a low concentration is necessary to obtain a homogeneous reaction mixture. Indeed, increasing the molarity to 0.2 M decreased **45aa** yield (50% yield, Entry 2, Table 20). Even lowering the concentration slightly affects it (72% yield, Entry 20). Therefore, 0.1 M was confirmed for the optimized reaction conditions.

Table 20: Screening of concentrations

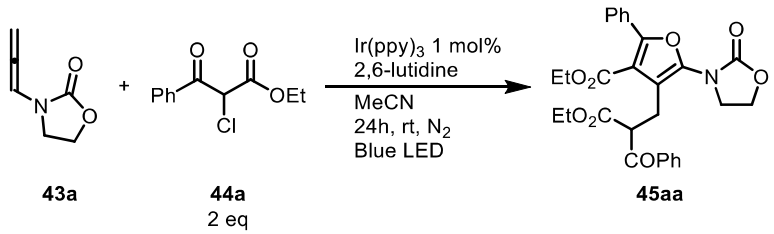

43a **44a** 2 eq **45aa**

Entry[a]	Concentration (M)	MeCN (mL)	Yield %[b]
1	0.1	1	78
2	0.2	0.5	50
3	0.05	2	72

[a] Reactions conditions: **43a** (0.1 mmol), **44a** (0.12 mmol), 2,6-lutidine (0.2 mmol) and $Ir(ppy)_3$ (0.001 mmol) in the corresponding amount of MeCN for 24h at room temperature irradiated with blue LEDs ; [b] Calculated using Ph_3CH as internal standard from ^1H-NMR on the crude mixture.

The influence of the catalytic loading (mol %) on the transformation performance has been analyzed. A catalytic loading of 0,1 mol% had been used in all previous reactions. Both increasing and decreasing it, sightly diminished reaction performance (Entry 2 and 3, Table 21). It is noteworthy that no consistent decrease in the product yield was revealed with 0,05 mol% of $Ir(ppy)_3$. However, a catalytic amount of 1 mol% led to the higher yield, therefore it has been chosen for the optimized reaction conditions.

Table 21: Catalyst loading screening

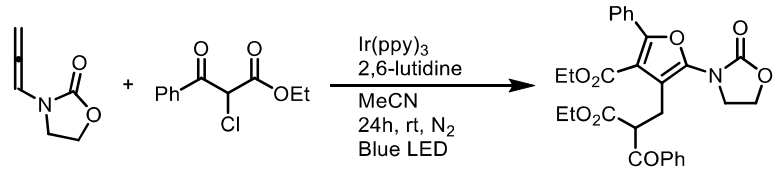

43a 44a 2 eq 45aa

Entry[a]	Ir(ppy)$_3$ mol %	Yield %[b]
1	1	78
2	2	73
3	0.05	72

[a] Reactions conditions: **43a** (0.1 mmol), **44a** (0.12 mmol), 2,6-lutidine (0.2 mmol) and the corresponding amount of Ir(ppy)$_3$ in 1 mL of MeCN for 24h at room temperature irradiated with blue LEDs ; [b] Calculated using Ph_3CH as internal standard from ^{1}H-NMR on the crude mixture.

At last, the reaction time has been investigated. After 2 hours, an 89% conversion and a 57% yield were obtained (Entry 3, Table 22). Six hours were sufficient to reach a complete conversion and a 72% yield (Entry 2, Table 22).

Table 22: Reaction time screening

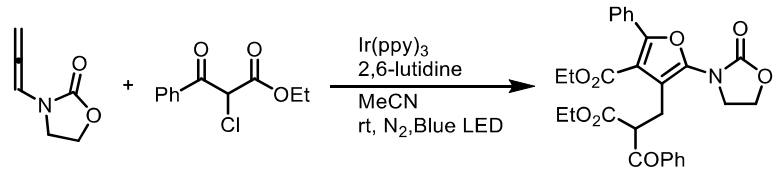

43a 44a 2 eq 45aa

Entry	Time	Conversion (%)[a]	Resa (%)[a]
1	24 h	100	78
2	6 h	100	72
3	2 h	89	57

[a] Reactions conditions: **43a** (0.1 mmol), **44a** (0.12 mmol), 2,6-lutidine (0.2 mmol) and Ir(ppy)$_3$ (0.001 mmol) in 1 mL of MeCN for the corresponding time at room temperature irradiated with blue LEDs ; [b] Calculated using Ph_3CH as internal standard from ^{1}H-NMR on the crude mixture.

Under the optimized reaction conditions, **45aa** has been obtained in 78% yield in 24h. (Scheme 71) No excess of chloride **44a** or 2,6-lutidine was used. The 1 mol% catalytic loading was confirmed. A relatively high concentration (0.1 M) was tolerated, diminishing the required volume of solvent.

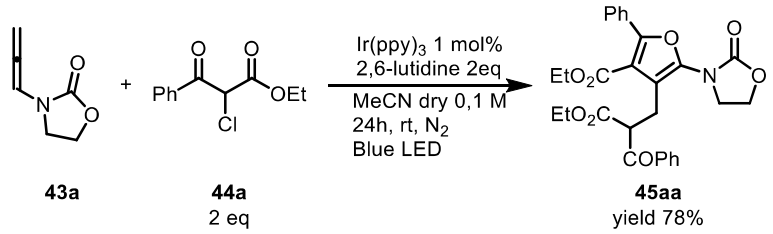

Scheme 72: Optimized conditions for the photocatalyzed synthesis of 2-aminofurans

Various allenes **43** and halogenated compounds **44** have been examined to verify the applicability of the developed transformation (Scheme 73 and 74).

Allenes **43b-h** were synthesized according to literature procedures.[235,238] Enantiopure allenamide **43b** reacted to produce 2-aminofuran **45ba** in a 1:1 diastereomeric mixture with a 60% yield. No stereoinduction was achieved in the formation of the newly formed chiral center. Allenamides **43a** and **43b** were also tested. Compared to **43a,** their nitrogen lone pair is more delocalized and the ability to donate is reduced.[241,242] However, product **45ca** was achieved with a 55% yield. On the contrary, a 20% yield was reach on product **45ad**. If we suppose that the size ring of the lactam should influence the nitrogen donation to the allene moiety, a larger and more flexible lactam ring will increase the delocalization of the nitrogen lone pair into the carbonyl moiety, thereby diminishing the ability to push electron density to the allene moiety.[241,243] On the other hand, the major is the electron richness of C_α-C_β, the minor is **2** stability.[238] From our investigation, a larger lactam ring seems to favor the photocatalyzed transformation. This could derive from the major stability of **43c** compare to **43d** under the reaction conditions, increasing the chemoselectivity towards **45** formation. However, no residual allene was detected in both reactions with **43c** and **43d**. More lactam derived allenamides needs to be tested to define a reactivity trend. The electron poor allene **43e** led to a 22% yield on product **45ea** after 48 hours. Due to the double carbonyl moiety, the nitrogen lone pair is strongly delocalized, and the allenamide reactivity is negatively affected. Even in 48 hours, a poor **45ea** yield was achieved. Three N-allenes substantially dissimilar from the previous ones have been then tested under the optimized reaction conditions.

Scheme 73: Scope of different allenes **43**

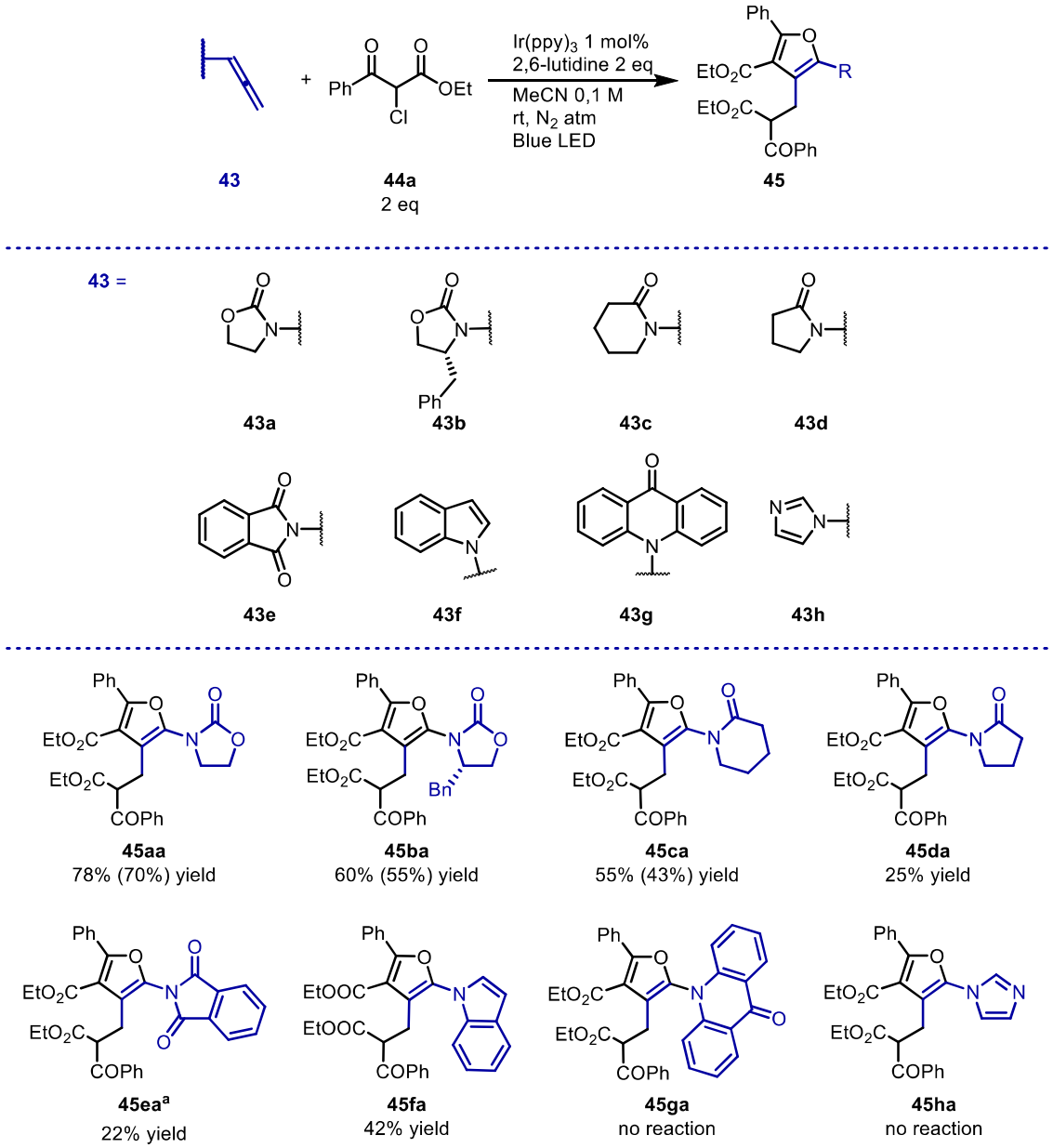

Reaction conditions: **43a** (0,1 mmol), **44a** (0,2 mmol), $Ir(ppy)_3$ (1 mol%), 2,6-lutidine (0,2 mmol) in MeCN (1 mL), stirred at room temperature for 24h irradiated through Blue LEDs. Yield determined through ^{1}H-NMR analysis on the crude reaction mixture involving triphenylmethane as internal standard. Yield on the isolated product into brackets. [a] Reaction time 48 hours.

With *N*-allenyl indole **43f,** product **43fa** was obtained in an acceptable 42% yield. Even in this case, no **43f** persisted after 24 hours. Some parallel decomposition pathways could affect product **45fa** formation. At last, no reaction was observed with both *N*-allenyl acrididdone **43g** and *N*-allenyl imidazole **43h**. *N*-allenyl acrididdone **43g** is known to have the nitrogen lone pair strongly delocalized in the acrididdone moiety. No reactivity was expected.[241] Concerning the *N*-allenyl imidazole **43h,** there is no

information about his reactivity. However, he proved not to be suitable for this project purpose.

At last, diverse halogenated compounds were investigated. 35% yield was obtained with the aliphatic ß-keto ester **44b.** It shows a scarce reactivity compared to the aromatic one **44a**. A first limitation of the developed reaction was outlined by ß-keto ester **44g**. Probably the high steric hindrance of the isopropyl group strongly impedes the product formation.

Medium to high yields were obtained with 2-halogenated ketones **44c-44e'**. At first, they were all tested under the reaction conditions optimized for ß-keto ester **44a**. 2-bromoacetophenone **44c** led to product **45ac** with a 52% yield. Also, doubling the catalyst loading (2 mol% $Ir(ppy)_3$), permits to reach an 82% yield in **45ac**. On the other hand, with 2-chloroacetophenone **44c[1]** only a 25% yield was ontained. Whit 2-bromoacetonaphtalene **44d**, a 30% yield and a 43% yields in **44ad** were obtained using 1 mol% and 2 mol% $Ir(ppy)_3$, respectively. The different reactivity between ketones **44c** and **44d** could be attributed to both the greater steric hindrance of **44d** and diverse electronic potentials. A second limitation is represented by 2'-methyl-2-bromoacetophenone **44h**. The corresponding *in situ* formed radical could undergo a 1,5-radical shift. This could cause low reactivity. At last, 2-bromopropriophenone **44e** and 2-chloropropriophenone **44e[1]** have been tested. Again, a difference between chlorinated and brominated precursors results (40% yield in **44e** and 75% yield in **44e[1]**). Unexpectedly, performing the reaction with **44e** as a starting material and DMF as a solvent, a 75% yield of **45ae** was obtained. The third limitation is evidenced with the use of α-chloroketone **44f**. Less than 10% yield was obtained for product **45af**. Two effects could explain this lack of reactivity. First, the steric hindrance around the site of the generation of the radical[184]. Second, the high stabilization of the **44f** derived radical. From the obtained results, the investigated halogenated compounds possess diverse reactivity. The data collected until now, are not sufficient to rationalize a trend. The exploration of more halogenated compounds is in progress.

Scheme 74: Scope of the halogenated compounds **44**

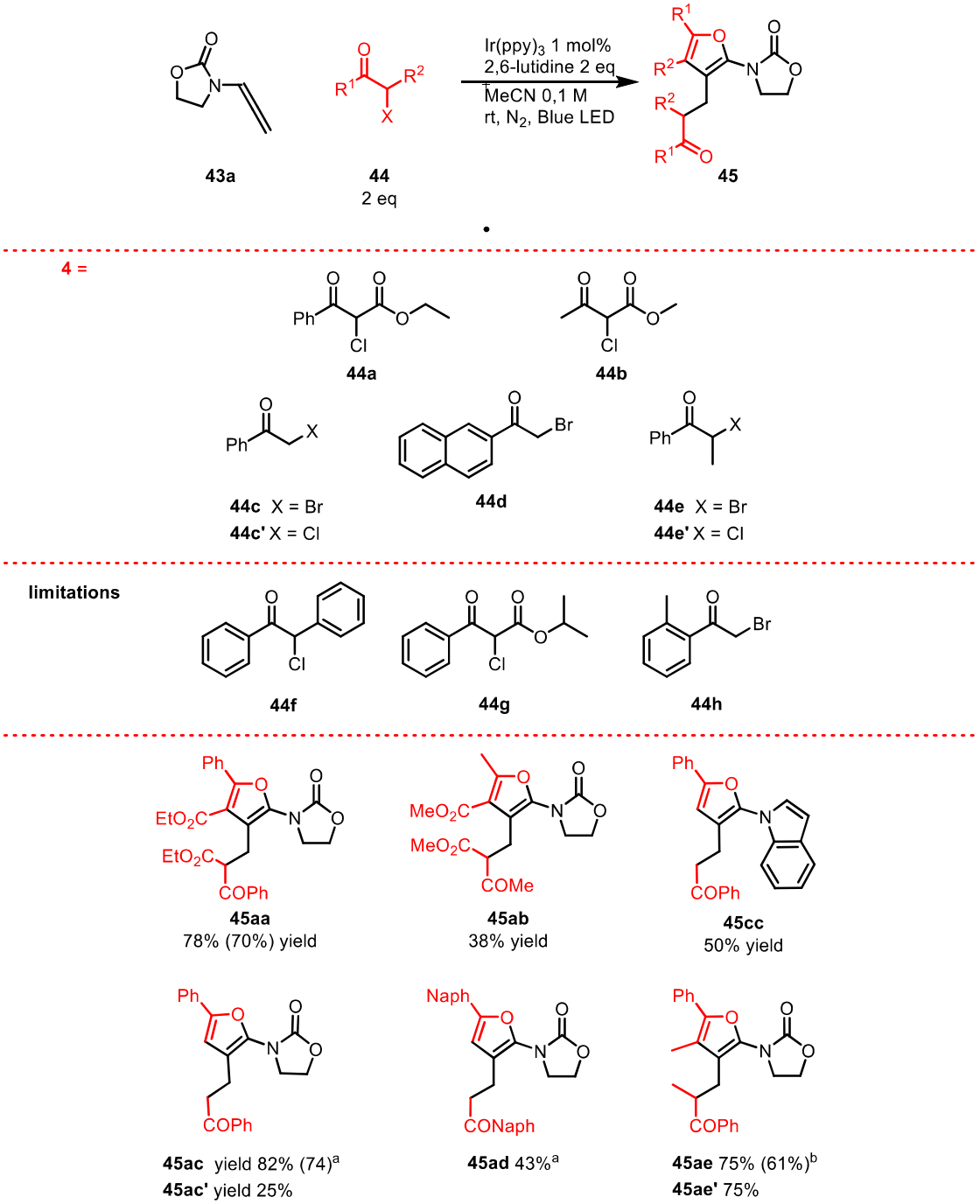

Reaction conditions: **43a** (0,1 mmol), **44a** (0,2 mmol), $Ir(ppy)_3$ (1 mol%), 2,6-lutidine (0,2 mmol) in MeCN (1 mL), stirred at room temperature for 24h irradiated through Blue LEDs. Yield determined through ^1H-NMR analysis on the crude reaction mixture involving triphenylmethane as internal standard. Yield on the isolated product into brackets. [a] Reaction performed with 2 mol% catalytic loading. [a] Reaction performed in DMF.

Based on literature data, a mechanism has been hypothesized for the developed transformation (Scheme 74). It includes two subsequential photoredox cycles catalyzed by $Ir(ppy)_3$.

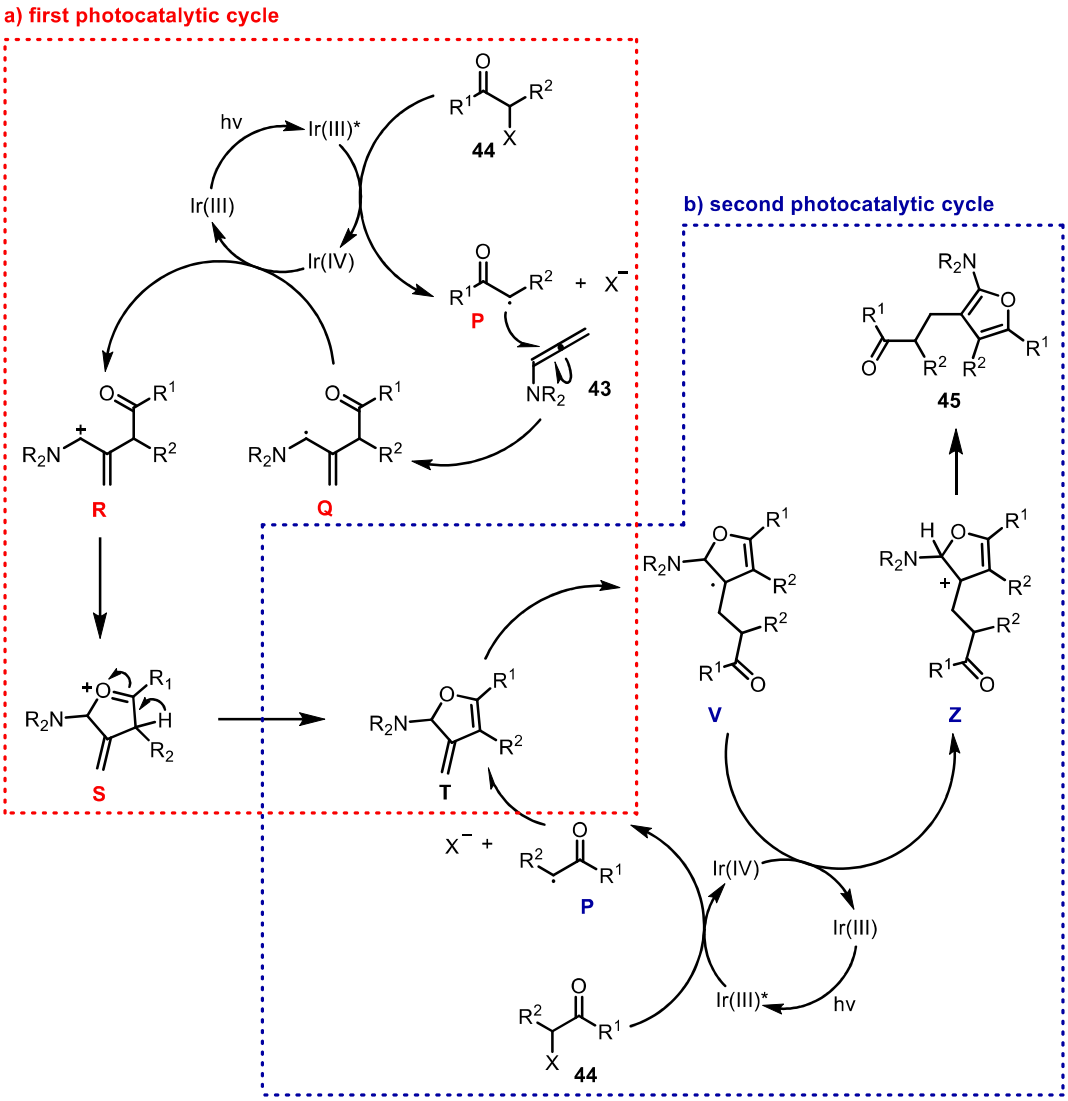

Scheme 75: Hypothesized mechanism for the photocatalyzed synthesis of 2-aminofurans

In the first one (Scheme 74, red), **Ir(ppy)$_3$^{III}** is photoexcited to **Ir(ppy)$_3$***. A SET occurs among **Ir(ppy)$_3$*** and **44**. Through way, electrophilic radical **P** is generated along with **Ir(ppy)$_3$^{IV}**. Radical **P** attacks the ß-carbon of **43**, and α-amidoallyl carbon radical **Q** is formed. A second SET from radical **Q** to **Ir^{IV}(ppy)$_3$**, restores **Ir^{III}(ppy)$_3$**, and forms the α-aminoallyl carbocation **R**. Intramolecular cyclization and elimination lead to 2,3-dihydrofuran **T**. **T** presents an exocyclic electron rich carbon-carbon double bond. This double bond is rapidly subjected to an electrophilic attack performed by radical **P**.

A second photocatalytic cycle is triggered by radical **P** (Scheme 74, blue), formed as previously described, that attacks **T** to create carbon radical **V**. At this point a SET between **V** and **Ir^{IV}(ppy)$_3$** occurs. The iridium photocatalyst returns to his original form (**Ir^{III}(ppy)$_3$**), and carbocation **Z** is created. In the end, product **45** is generated *via* elimination, which is thermodynamically favored by the consequent aromatization.

To confirm the hypothesized mechanism, some reactions have been run.

Table 23: Mechanistic investigations

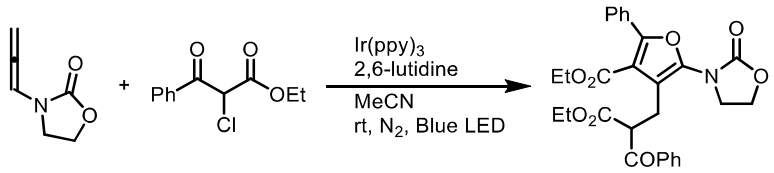

43a **44a** 2 eq **45aa**

Entry[a]	Variation from optimized conditions	Conversion (%)[b]	Yield (%)[b] 5aa
1	No $Ir(ppy)_3$	15	-
2	No light	32	-
3	2 h light – 22 h dark	80	51
4	air atmosphere	-	45

[a] Reactions conditions: **43a** (0.1 mmol), **44a** (0.12 mmol), 2,6-lutidine (0.2 mmol) and $Ir(ppy)_3$ (0.001 mmol) in 1 mL of MeCN for the corresponding time at room temperature irradiated with blue LEDs; [b] Calculated using Ph_3CH as internal standard from ^{1}H-NMR on the crude mixture.

No product **45aa** was obtained with no photocatalyst (Entry 1, Table 23)) or no Blue LEDs (Entry 2, Table 23). Thus, the photocatalytic pathway of the reaction was confirmed. 51% yield on **45aa** was obtained with 2 hours of irradiation and 22 hours of dark (Entry 3, Table 23). This value is comparable with the one obtained in 2 hours reaction time (Entry 4, Table 23). Thus, a radical propagation pathway could be discarded.[239] At last, one reaction has been performed under air and without degassing the solvent. The obtainment of a 45% yield on **45aa** proved a slight tolerance toward the presence of oxygen. Even if reduced, a significant amount of product was observed. The oxygen could quench the excited state of the catalyst, favor different reaction pathways, or even participate in the degradation of the allenamide **43a**. It has been proved that **43a** could be stored for a long time under an inert atmosphere. However, it degrades rapidly when exposed to air. Notably, no reaction intermediate has never been observed or isolated. This could be due to a higher reactivity toward radical electrophilic addition of **T** respect to **43.**

Considering the importance of developing a scalable procedure, preliminary tests on the applicability of the developed methodology under flow chemistry have been performed.

Scheme 76: Flow chemistry apparatus

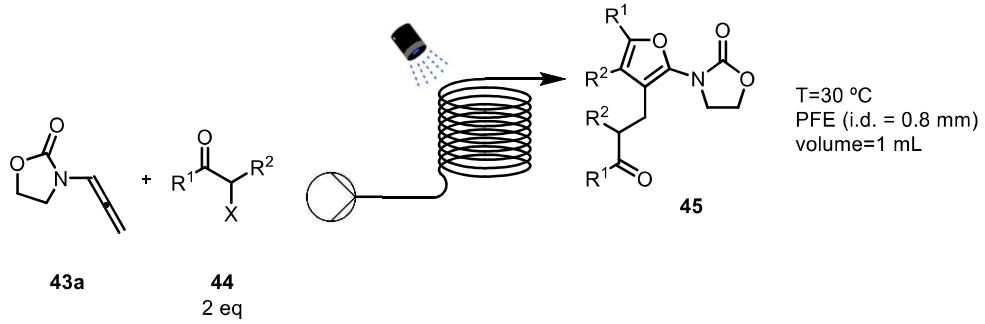

The manufactured flow apparatus was composed of a 5 mL plastic syringe connected with a FEP tube (Ǿ 0,8 x 1,6 mm) wrapped around an aluminum paper covered becker. The coiled reactor (1 mL total volume) was located in the center of a handmade photoreactor

To be able to transfer a bath reaction to flow technology, a homogeneous reaction mixture is mandatory. Therefore, the concentration of the reaction was lowered to 0.05 M to completely solubilize the $Ir(ppy)_3$ photocatalyst.

A first test has been conducted, product **45aa** was obtained with an average of 40% yield after one hour reaction time (Entry 1, Table 24). Doubling residence time increased the detected yield (average of 51%, Entry 2, Table 24). Successively, the effect of lower concentration was investigated. Reducing it to 0.03 M increase **45aa** yield to an average of 50% in 1 hour residence time (Entry 4, Table 24). A further lowering revealed itself as damaging (Entry 5, Table 24). Increasing the concentration was not possible with 1 mol% of catalytic loading. Therefore, a test with 0.05 mol% of $Ir(ppy)_3$ and 0.1 M concentration has been done (Entry 3, Table 24). Unfortunately, no improvements were observed. On the involved reaction scale, the results reached did not show a big advantage of the flow technology compared to the batch one. Further optimization screenings need to be planned, as well as the apparatus settings and reaction conditions need to be optimized. In any case, the applicability of flow conditions has been demonstrated. The results obtained in the preliminary tests were really promising. It is worth considering, that the transformation in question is rather complex being composed of two sequential photoredox catalyzed intermolecular reactions and one intramolecular cyclization.

Table 24: Optimization of the reaction under flow chemistry conditions

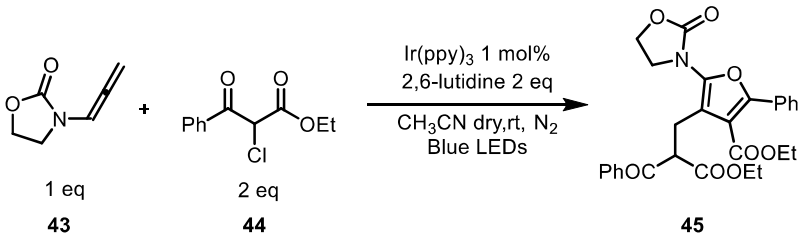

Entry[a]	Residence time	Concentration (M)	$Ir(ppy)_3$ mol %	NMR Yield % [b]
1	1h	0.05	1	37[c], 40[d], 40[e], 41[f]
2	2h	0.05	1	52[c], 50[d]
3	1h	0.1	0.5	32[c], 35[d]
4	1h	0.0333	1	41[c], 47[d], 50[e], 52[f]
5	1h	0.025	1	22[c], 25[d]

[a] Reaction conditions of the continuous flow experiment: **43a** (0.3 mmol), **44a** (0.36 mmol), 2,6-lutidine (0.6 mmol) and with the corresponding amount of $Ir(ppy)_3$ and MeCN at room temperature irradiated with blue LEDs; [b] Calculated using Ph_3CH as internal standard from ^1H-NMR on the crude mixture. [c] 1st reactor volume; [d] 2nd volume; [e] 3rd volume; [f] 4th volume.

Conclusion

A new photoredox transformation exploiting allenamides for the synthesis of 2-aminofurans has been developed. Under the optimized reaction condition, 2-amino furan **45** has been obtained with a 78% yield in 6 hours reaction time. No excess of reactant or additives were required.

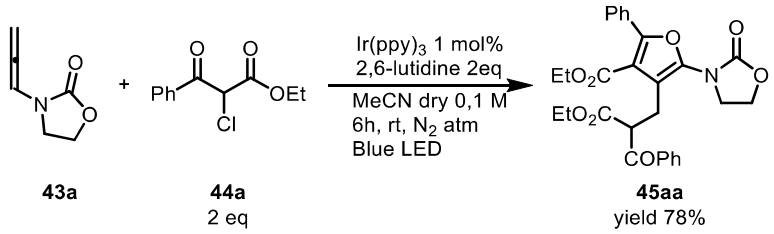

Scheme 77: Photoredox transformation for the synthesis of 2-aminofurans **45** under Batch conditions

Expanding reaction time to 24 hours allowed to obtain a library of 2-aminofurans in decent to good yields. The applicability of the methodology to diversely functionalized allenes and halogenated compounds has to be further explored. However, the results obtained until now are promising. A mechanism has been hypothesized and confirmed by experimental data. Moreover, the transformation has been applied in flow photochemistry. From the reactions performed, the applicability of the flow conditions has been proved. Product **45** was obtained in 50% in 2 hours of residence time. In the

future, more experiments will be performed to optimize the synthesis under flow conditions.

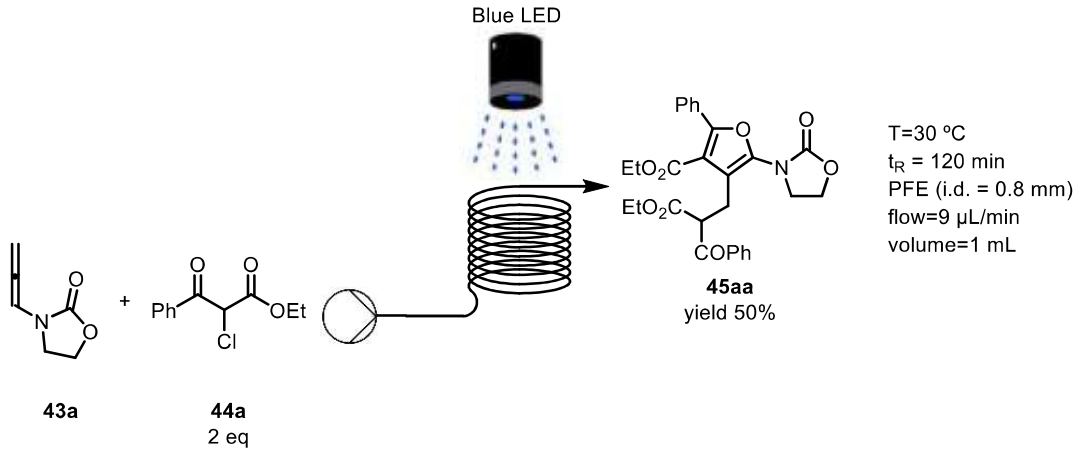

Scheme 78: Photoredox transformation for the synthesis of 2-aminofurans **45** under Batch conditions

General Procedures and Products Characterization

Materials and methods

All commercial chemicals and dry solvents were purchased from Sigma Aldrich, Alfa Aesar or TCI Chemicals and used without additional purification. 1H and 13C-NMR spectra were recorded on a Varian Inova 400 NMR instrument with a 5 mm probe. All chemical shifts (δ) are referenced using deuterated solvent signals; chemical shifts are reported in ppm from TMS and coupling constants (J) are reported in Hertz. Multiplicity is reported as: s = singlet, d = doublet, t = triplet, q = quartet, hept = heptet, and m = multiplet. HPLC-MS analyses were performed using an Agilent Technologies HP1100 instrument coupled with an Agilent Technologies MSD1100 single-quadrupole mass spectrometer using a Phenomenex Gemini C18 3 µm (100 × 3 mm) column; mass spectrometric detection was performed in a full-scan mode from m/z 50 to 2500, with scan time 0.1 s in a positive ion mode, ESI spray voltage 4500 V, nitrogen gas 35 psi, drying gas flow rate 11.5 mL min−1, and fragmentor voltage 30 V. HRMS was performed using Waters Xevo G2-XS QT with, ESI+, cone voltage 40 V, Capillary 3 kV, and source temperature 120 °C. CSP-HPLC analyses were performed with an Agilent Technologies Series 1200 instrument using chiral columns. Flash chromatography purifications were carried out using VWR or Merck silica gel (40–63 µm particle size). Thin-layer chromatography was performed with Merck 60 F254 plates

3-(propa-1,2-dien-1-yl)oxazolidin-2-one[238], **1-(propa-1,2-dien-1-yl)piperidin-2-one (43d), 1-(propa-1,2-dien-1-yl)pyrrolidin-2-one (43f), 1-(propa-1,2-dien-1-yl)-1H-imidazole (43g), 10-(propa-1,2-dien-1-yl)acridin-9(10H)-one (43h)** have been synthesized according to a reported literature procedure.[238]

(S)-4-benzyl-3-(propa-1,2-dien-1-yl)oxazolidin-2-one (43b) has been synthesized according to a reported literature procedure. [244]

1-(propa-1,2-dien-1-yl)-1H-indole (43c) have been synthesized following a reported procedure. [235]

2-(propa-1,2-dien-1-yl)isoindoline-1,3-dione (43e)[245] have been synthesized following a reported procedure.α-haloketones **44b**, **44b**[I], **44c**, **44d** e **44h** were used as bought, without any further purification.

ethyl 2-chloro-3-oxo-3-phenylpropanoate (44a) has been synthesized following a reported procedure. [191]

Syhntesis of 2-chloro-1-phenylpropan-1-one (44c[I]):

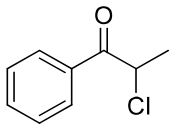

In a round bottom flask, propriophenone (5 mmol) and DCM (10 mL, 0.5 M) are added. Successively, solforil chloride (6 mmol) is dropped at 0°C. The reaction mixture is stirred for 3 hours at room temperature. Water is then added to the reaction mixture at 0°C, and the aqueous phase are extracted three times with DCM. Organic phases are then dried with Na_2SO_4 and the solvents evaporated in vacuo. The crude mixture is purified by means of flash chromatography (Cyclohexane: DCM, 7:3). The product is obtained as colorless oil with 70% yield. ^{1}H–NMR (400 MHz, CDCl3) δ (ppm): 1.75 (d, J = 6.7 Hz, 3H), 5.26 (q, J = 6.7 Hz, 1H), 7.47 – 7.53 (m, 2H), 7.58 – 7.63 (m, 1H), 7.99 – 8.05 (m, 2H).

Synthesys of methyl 2-chloro-3-oxobutanoate (44d)

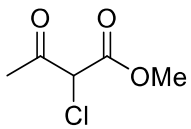

In a round bottom flask, methyl 3 – oxobutanoate (10 mmol) and DCM (10 mL, 1 M) are added. Successively, solforil chloride (10 mmol) is dropped at 0°C. The reaction mixture is stirred for 2 hours at room temperature. Water is then added to the reaction mixture

at 0°C, and the aqueous phase are extracted three times with DCM. Organic phases are then dried with Na_2SO_4 and the solvents evaporated in vacuo. The product is obtained as yellowish oil with 92% yield.

^{1}H–NMR (400 MHz, $CDCl_3$) δ (ppm): 2.39 (s, 3H), 3.85 (s, 3H), 4.78 (s, 1H)

Synthesis of 2-chloro-1,2-diphenylethan-1-one (44f):

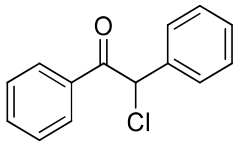

To a solution of 2-hydroxy-1,2-di(phenyl)ethenone (5 mmol) and DCM (10 mL, 0,5 M), $SOCl_2$ (20 mmol) is added at 0°C. The reaction mixture is stirred at room temperature for 1 hours. Water is then added to the reaction mixture at 0°C, and the aqueous phase are extracted three times with DCM. Organic phases are then dried with Na_2SO_4 and the solvents evaporated in vacuo. The crude mixture is purified by means of flash chromatography (Cyclohexane: AcOEt, 9:1). The product is obtained as white solid with 84% yield. ^{1}H–NMR (400 MHz, CDCl3) δ (ppm): 6.31 (s, 1H), 7.31 – 7.51 (m, 7H), 7.55 (t, J = 7.3 Hz, 1H), 7.95 (d, J = 7.7 Hz, 2H).

Synthesis of isopropyl 2-chloro-3-oxo-3-phenylpropanoate (44g)

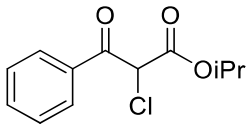

In a round bottom flask, ispropyl 3-oxobutanoate (4 mmol) and DCM (8 mL, 0.5 M) are added. Successively, solforil chloride (4 mmol) is dropped at 0°C. The reaction mixture is stirred for 2 hours at room temperature. Water is then added to the reaction mixture at 0°C, and the aqueous phase are extracted three times with DCM. Organic phases are then dried with Na_2SO_4 and the solvents evaporated in vacuo. The crude mixture is purified by means of flash chromatography (Cyclohexane: DCM, 7:3). The product is obtained as colorless oil with 60% yield. ^{1}H–NMR (400 MHz, CDCl3) δ (ppm): 1.33 (d, J = 6.3 Hz, 6H), 2.38 (s, 3H), 4.72 (s, 1H), 5.08 – 5.17 (m, 1H).

General procedure for the synthesis of 2-amino furans 45

In a septum capped vial, are added in sequence halogenate compound **44** (0,2 mmol), MeCN (1 mL, 0,1 M), 2-6 lutidine (0,2 mmol), allene **43** (0,1 mmol) and $Ir(ppy)_3$ (0,001 mmol). The reaction mixture is degased through freeze-pump-thaw cycles (3x10

minutes). The reaction is stirred for 24 hours at room temperature under Blue LEDs irradiation (λ= 465 nm). The crude is then evaporated in vacuum, and the product isolated by means of flash chromatography. If necessary, 0,1 mmol of triphenylmethane is added into the reaction vial to determine the ^{1}H-NMR yield.

Ethyl 4-(2-benzoyl-3-ethoxy-3-oxopropyl)-5-(2-oxooxazolidin-3-yl)-2-phenylfuran-3-carboxylate (45aa):

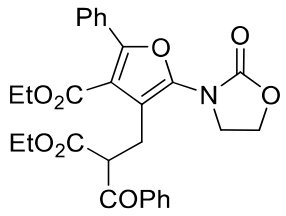

Product **45aa** has been isolated as yellowish oil by means of silica flash chromatography (Cy : AcOEt, 9:1 to 6:4) with 73% yield. ^{1}H-NMR (400 MHz, $CDCl_3$) δ 8.01 (d, *J*= 7.1 Hz, 2H), 7.67 – 7.60 (m, 2H), 7.60 – 7.53 (m, 1H), 7.46 (t, *J*= 7.6 Hz, 2H), 7.41 – 7.35 (m, 3H), 5.03 (dd, *J*= 8.0, 6.6 Hz, 1H), 4.57 (td, *J*= 8.8, 7.3 Hz, 1H), 4.49 (td, *J*= 8.6, 6.8 Hz, 1H), 4.27 (qd, *J*= 7.1, 4.9 Hz, 2H), 4.12 (qd, *J*= 7.1, 1.4 Hz, 2H), 4.03 – 3.92 (m, 2H), 3.35 (qd, *J*= 14.4, 7.3 Hz, 2H), 1.22 (t, *J*= 7.1 Hz, 3H), 1.13 (t, *J*= 7.1 Hz, 3H). ^{13}C-NMR (100 MHz, $CDCl_3$) δ 195.1, 169.3, 163.4, 156.0, 155.3, 140.9, 136.2, 133.58, 129.6, 128.8, 127.9, 117.2, 114.1, 63.1, 61.5, 60.8, 53.3, 46.2, 23.6, 13.9, 13.9. LC-MS (ESI) m/z 506 [M+H^{+}]

^{1}H-^{1}H-COSY (400 MHz, $CDCl_3$):

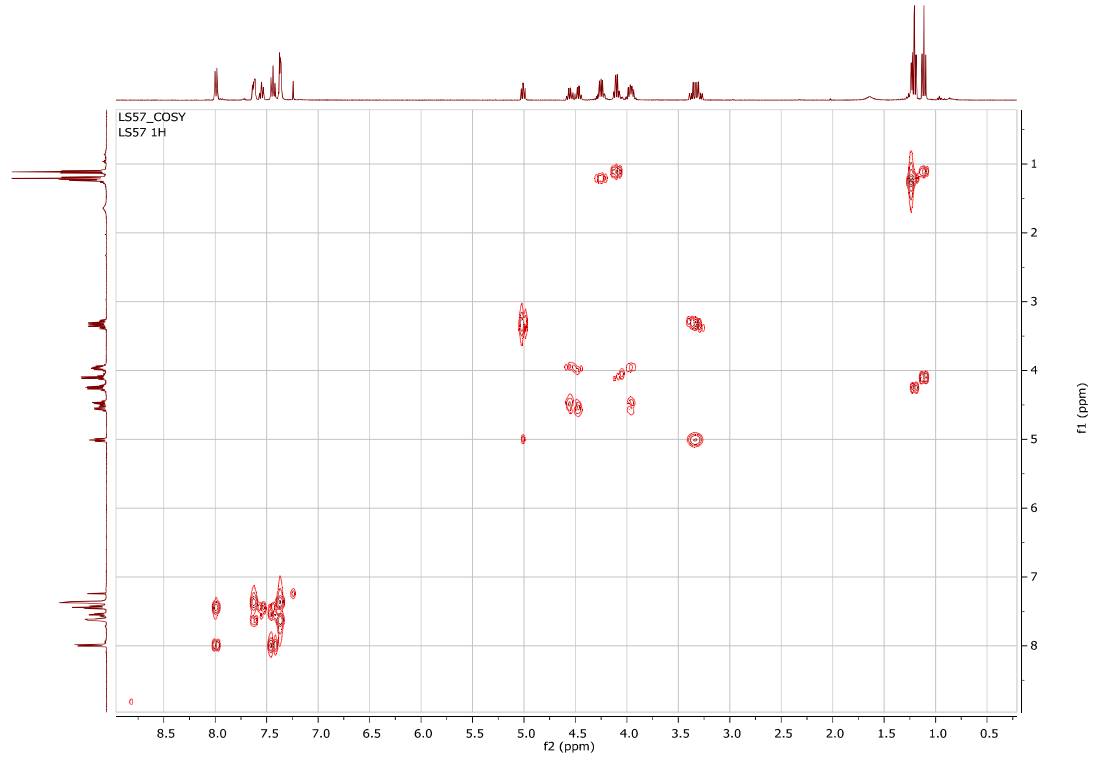

^{1}H-^{13}C-HSQC (400 MHz, $CDCl_3$)

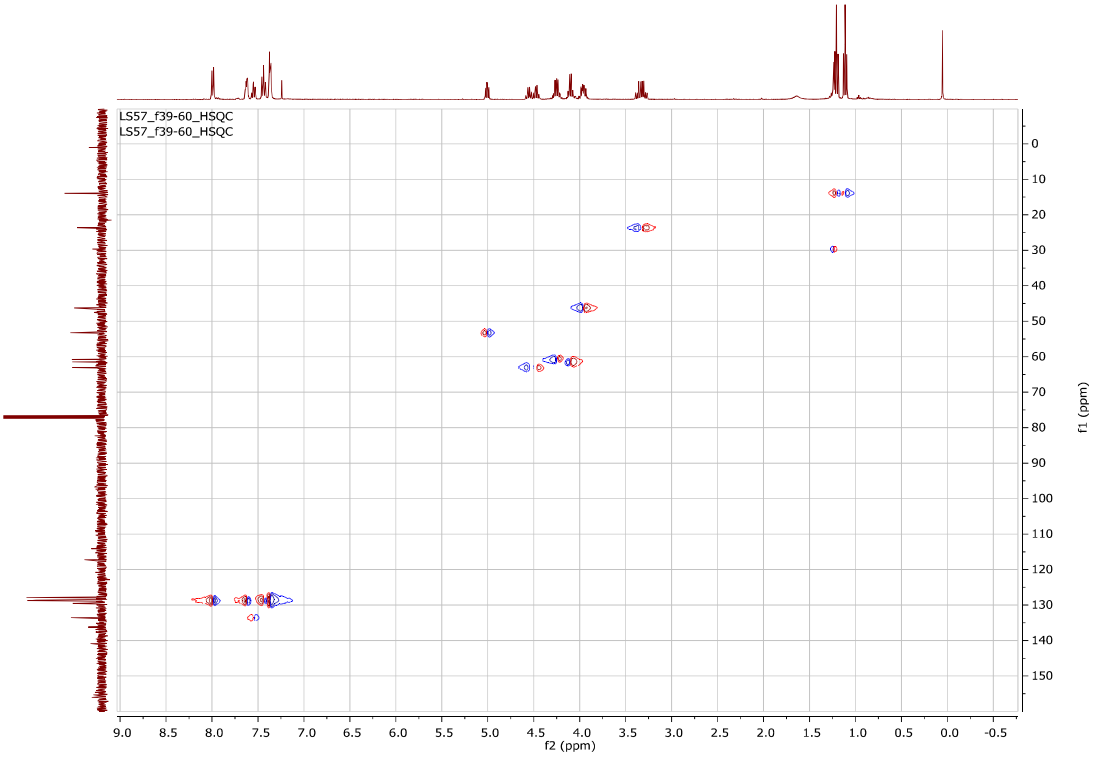

3-(3-(3-oxo-3-phenylpropyl)-5-phenylfuran-2-yl)oxazolidin-2-one (45ab):

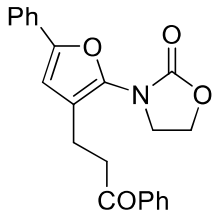

Product **5aa** has been isolated as yellowish oil by means of silica flash chromatography (Cy : AcOEt, 9:1 to 6:4) with 74% yield.

T_m(°C) = 143,3-145,8. Rf = 0,24 (Cy : AcOEt, 7:3); ^{1}H-NMR (400 MHz, $CDCl_3$) δ 8.03 – 7.92 (m, 2H), 7.63 – 7.51 (m, 3H), 7.46 (t, *J* = 7.6 Hz, 2H), 7.35 (t, *J* = 7.7 Hz, 2H), 7.29 – 7.20 (m, 1H), 6.59 (s, 1H), 4.53 (t, *J* = 8.4, 7.7 Hz, 2H), 4.05 (t, *J* = 8.5, 8.0 Hz, 2H), 3.35 (t, *J* = 7.2 Hz, 2H), 2.86 (t, *J* = 7.2 Hz, 2H). ^{13}C-NMR (101 MHz, Chloroform-*d*) δ 199.2, 156.2, 150.7, 139.0, 136.8, 133.1, 130.2, 128.6, 128.6, 128.1, 127.7, 123.6, 119.5, 107.4, 62.8, 46.6, 38.3, 18.9. LC-MS (ESI) m/z 362 [M+H$^+$].

3-(4-methyl-3-(2-methyl-3-oxo-3-phenylpropyl)-5-phenylfuran-2-yl)oxazolidin-2-one (45ac):

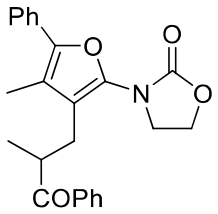

Product **45ac** has been isolated as gummy yellowish solid by means of silica flash chromatography (Cy : AcOEt, 9:1 to 6:4) with 61% yield.

^{1}H-NMR (400 MHz, $CDCl_3$) δ 7.96 (dd, *J* = 8.2, 1.4 Hz, 2H), 7.59 – 7.43 (m, 5H), 7.38 (t, *J* = 7.7 Hz, 2H), 7.26 (t, *J* = 8.8, 7.5 Hz, 1H), 4.48 (td, *J* = 8.8, 6.7 Hz, 1H), 4.19 (td, *J* = 8.8, 7.0 Hz, 1H), 3.96 – 3.84 (m, 2H), 3.82 – 3.73 (m, 1H), 3.00 (dd, *J* = 14.8, 8.4 Hz, 1H), 2.59 (dd, *J* = 14.8, 5.8 Hz, 1H), 2.22 (s, 3H), 1.27 (d, *J* = 7.1 Hz, 3H). ^{13}C-NMR (100 MHz, $CDCl_3$) δ 203.1, 156.3, 146.1, 138.6, 136.2, 133.1, 131.1, 128.8, 128.5, 128.2, 127.1, 125.8, 118.7, 117.4, 62.7, 46.4, 39.9, 26.9, 18.5, 10.3. MS (ESI) m/z 390 [M+H$^+$], m/z 412 [M+Na$^+$], m/z 428 [M+K$^+$].

Methyl 4-(2-(methoxycarbonyl)-3-oxobutyl)-2-methyl-5-(2-oxooxazolidin-3-yl)furan-3-carboxylate (45ad):

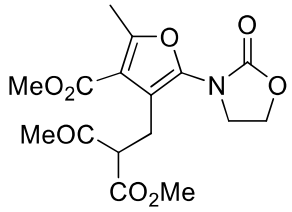

Product **5aa** has been isolated as yellowish oil by means of silica flash chromatography (Cy : AcOEt, 9:1 to 6:4) with 30% yield.

^{1}H-NMR (400 MHz, $CDCl_3$) δ 4.55 (t, *J*= 8.4, 7.8 Hz, 2H), 4.02 (dd, *J*= 7.9, 6.3 Hz, 1H), 3.97 (t, *J*= 8.2, 7.3 Hz, 2H), 3.84 (s, 3H), 3.69 (s, 3H), 3.08 (qd, *J*= 14.2, 7.1 Hz, 2H), 2.51 (s, 3H), 2.25 (s, 3H). ^{13}C-NMR (100 MHz, $CDCl_3$) δ 202.8, 169.7, 164.1, 157.8, 156.3, 116.4, 113.3, 110.0, 63.0, 58.6, 52.5, 51.4, 46.4, 29.6, 22.5, 14.5. LC-MS (ESI) m/z 354,4 [$M+H^+$], m/z 371,4 [$M+NH_4^+$].

3-(5-(naphthalen-2-yl)-3-(3-(naphthalen-2-yl)-3-oxopropyl)furan-2-yl)oxazolidin-2-one (45ae)

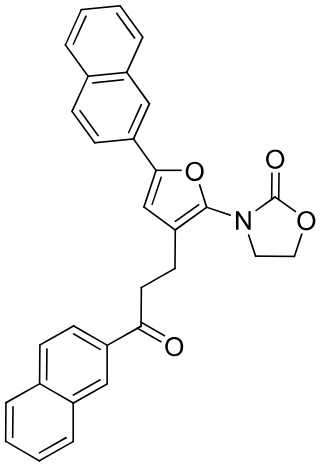

^{1}H-NMR (400 MHz, $CDCl_3$) δ 8.57 – 8.50 (m, 1H), 8.09 – 8.04 (m, 2H), 7.97 (d, *J*= 8.1 Hz, 1H), 7.93 – 7.76 (m, 6H), 7.69 (dd, *J*= 8.6, 1.8 Hz, 1H), 7.57 (m, Hz, 2H), 7.51 – 7.42 (m, 2H), 4.56 (t, *J*= 8.3, 7.7 Hz, 2H), 4.11 (t, *J*= 8.5 Hz, 2H), 3.52 (t, *J*= 7.2 Hz, 2H), 2.95 (t, *J*= 7.2 Hz, 2H).

Ethyl 4-(2-benzoyl-3-ethoxy-3-oxopropyl)-5-((R)-4-benzyl-2-oxooxazolidin-3-yl)-2-phenylfuran-3-carboxylate (45ba)

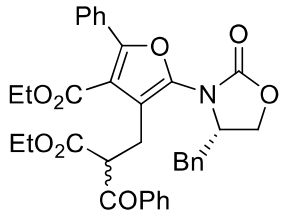

Product **5aa** has been isolated in a diastereomeric mixture as colorless oil by means of silica flash chromatography (Cy : AcOEt, 9:1 to 6:4) with 55% yield.

^{1}H-NMR (400 MHz, $CDCl_3$) δ 8.06 (d, *J* = 7.7 Hz, 1H), 8.00 (d, *J* = 7.8 Hz, 1H), 7.69 – 7.61 (m, 2H), 7.60 – 7.52 (1, 1H), 7.45 (t, *J* = 7.7 Hz, 2H), 7.42 – 7.34 (m, 3H), 7.31 – 7.10 (m,5H), 5.07 (q, *J* = 7.7 Hz, 1H), 4.70 – 4.47 (m, 1,5H), 4.43 (t, *J* = 8.4 Hz, 0,5H), 4.33 – 4.04 (m, 5H), 3.33 (qd, *J* = 14.6, 7.3 Hz, 2H), 3.12 – 3.01 (m, 1H), 2.89 (ddd, *J* = 15.0, 9.2, 7.0 Hz, 1H), 1.22 (dt, *J* = 10.8, 7.1 Hz, 3H), 1.13 (td, *J* = 7.1, 3.8 Hz, 3H). ^{13}C-NMR (101 MHz, $CDCl_3$) δ 195.3 e 195.0, 169.5 e 169.2, 163.4, 155.9 e 155.9, 155.8, 155.5, 140.3 e 140.2, 136.3 e 136.0, 135.1 e 135.1, 133.6 e 133.6, 129.5, 129.4, 129.4, 128.98, 128.95, 128.88, 128.80, 128.78, 128.75, 128.68, 128.6, 127.9, 127.1 e 127.1, 118.6 e 118.5, 114.3 e 114.2, 68.2 e 67.9, 61.7 e 61.4, 60.8 e 60.7, 58.6 e 58.5, 53.2 e 53.0, 39.4 e 39.2 , 23.6, 13.9, 13.91, 13.89. LC-MS (ESI) m/z 596,6 [M+H$^+$].

Ethyl-4-(2-benzoyl-3-ethoxy-3-oxopropyl)-5-(1H-indol-1-yl)-2-phenylfuran-3-carboxylate (45ca)

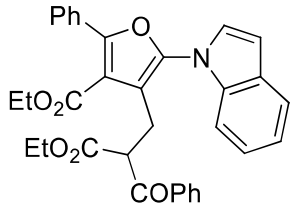

Product **45aa** has been isolated as brown oil by means of neutral alumine flash chromatography (Cy) with 40% yield.

^{1}H-NMR (400 MHz, Chloroform-*d*) δ 7.83 – 7.72 (m, 4H), 7.64 (d, *J* = 7.7 Hz, 1H), 7.51 (t, *J* = 7.2 Hz, 1H), 7.45 – 7.31 (m, 6H), 7.23 – 7.14 (m, 3H), 4.71 (t, *J* = 7.4 Hz, 1H), 4.32 (qd, *J* = 7.2, 2.9 Hz, 2H), 3.95 – 3.79 (m, 1H), 3.77 – 3.60 (m, 1H), 3.33 (d, *J* = 7.4 Hz, 2H), 1.26 (t, *J* = 7.5, 7.0 Hz, 3H), 0.87 (t, *J* = 7.1 Hz, 3H). LC-MS m/z 536,6 [M+H$^+$], m/z 553, 6 [M+NH_4^+]

Ethyl 4-(2-benzoyl-3-ethoxy-3-oxopropyl)-5-(2-oxopiperidin-1-yl)-2-phenylfuran-3-carboxylate (45da)

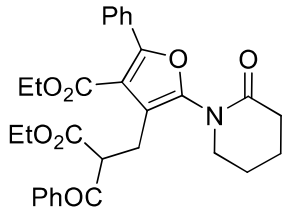

Product **45aa** has been isolated as yellowish oil by means of silica flash chromatography (Cy : AcOEt, 9:1 to 6:4) with 43% yield.

^{1}H-NMR (400 MHz, $CDCl_3$) δ 8.05 – 7.94 (m, 2H), 7.70 – 7.61 (m, 2H), 7.60 – 7.50 (m, 1H), 7.44 (dd, *J* = 8.3, 7.0 Hz, 2H), 7.37 (dd, *J* = 5.1, 1.8 Hz, 3H), 4.98 (t, *J* = 7.1 Hz, 1H), 4.34 – 4.17 (m, 2H), 4.11 (qd, *J* = 7.2, 1.5 Hz, 2H), 3.60 (dt, *J* = 11.3, 5.6 Hz, 1H), 3.54 – 3.41 (m, 1H), 3.26 (dd, *J* = 7.1, 1.1 Hz, 2H), 2.55 (m, 2H), 2.06 – 1.85 (m, 4H), 1.21 (t, *J* = 7.1 Hz, 3H), 1.12 (t, *J* = 7.1 Hz, 3H).

^{13}C-NMR (100 MHz, $CDCl_3$) δ 195.3, 170.8, 169.5, 163.7, 154.9, 145.4, 136.3, 33.4, 129.8, 129.2, 128.8, 128.8, 128.6, 127.8, 115.5, 114.1, 61.4, 60.6, 53.2, 50.4, 32.7, 23.8, 22.9, 21.0, 14.0, 13.9. LC-MS (ESI) m/z 518,6 [$M+H^+$]

Ethyl 4-(2-benzoyl-3-ethoxy-3-oxopropyl)-5-(1,3-dioxoisoindolin-2-yl)-2-phenylfuran-3-carboxylate (45ea)

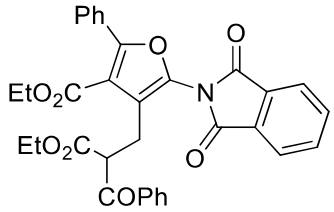

^{1}H-NMR (400 MHz, $CDCl_3$) δ 8.02 – 7.95 (m, 4H), 7.83 (dd, *J* = 5.5, 3.0 Hz, 2H), 7.72 (ddd, *J* = 5.5, 3.0, 1.6 Hz, 2H), 7.56 – 7.49 (m, 1H), 7.41 – 7.36 (m, 5H), 4.92 (t, *J* = 7.0 Hz, 1H), 4.34 – 4.21 (m, 2H), 4.10 – 4.00 (m, 2H), 3.40 – 3.24 (m, 2H), 1.23 (t, *J* = 7.2 Hz, 3H), 1.07 (t, *J* = 7.1 Hz, 3H); LC-MS (ESI) m/z 566,6 [$M+H^+$].

Ethyl-4-(2-benzoyl-3-ethoxy-3-oxopropyl)-5-(2-oxopyrrolidin-1-yl)-2-phenylfuran-3-carboxylate (45fa):

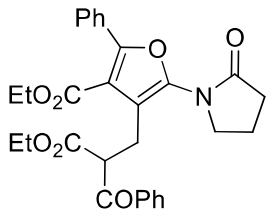

LC-MS (ESI) m/z 504,6 [M+H$^+$]

3-(2-(1H-indol-1-yl)-5-phenylfuran-3-yl)-1-phenylpropan-1-one (45cb)

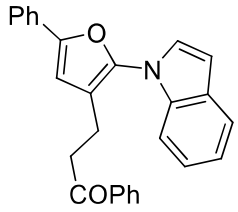

Product **45aa** has been isolated as brown oil by means of neutral alumina flash chromatography (Cy) with 42% yield.

^{1}H-NMR (400 MHz, $CDCl_3$) δ 7.87 – 7.76 (m, 2H), 7.74 – 7.61 (m, 3H), 7.58 – 7.48 (m, 1H), 7.44 – 7.32 (m, 5H), 7.30 – 7.17 (m, 4H), 6.75 (s, 1H), 6.70 (d, J = 3.3 Hz, 1H), 3.13 (t, J = 7.4 Hz, 2H), 2.84 (t, J = 7.4 Hz, 2H). ^{13}C-NMR (100 MHz, $CDCl_3$) δ 198.63, 150.55, 140.93, 137.69, 136.53, 133.08, 130.17, 128.72, 128.69, 128.57, 128.53, 128.50, 128.47, 127.92, 127.65, 123.60, 122.96, 121.00, 120.9, 118.20, 110.76, 107.39, 104.52, 38.23, 18.86. LC-MS (ESI) m/z 392,4 [M+H$^+$]

Stern-Volmer quenching studies

Excited state lifetime measurements were performed using a spectrofluorimeter Edinburgh Analytical Instruments FLS920, equipped with a time-correlated single-photon counting device, which is able to measure lifetimes in a range between 0.5 ns and 30 μs.

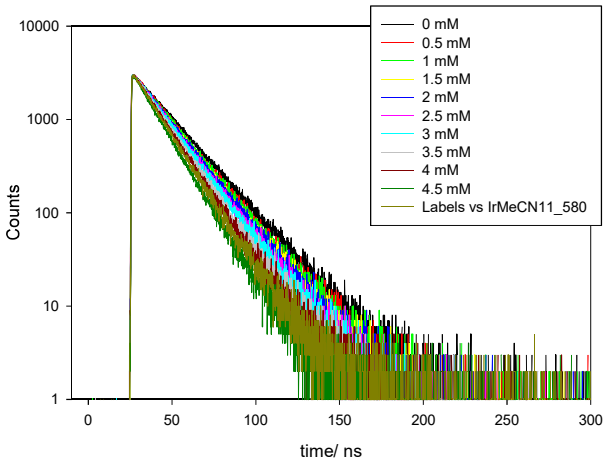

Lifetime of compound *Ir(ppy)*$_3$ with **37a**.

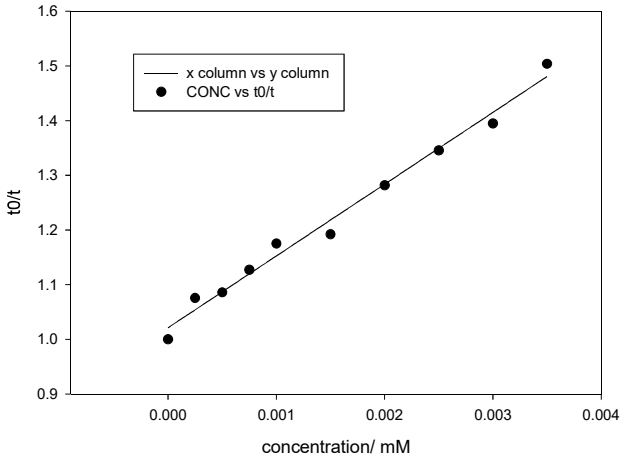

Stern-Volmer plot of compound **37a** with *Ir(ppy)*$_3$.

The Stern-Volmer plot displayed shows a linear correlation between the concentration of quencher **37a** and the lifetime of Ir(ppy)$_3$*. The quenching constant is calculated according to the equation **Kq= a/t0.**

The terms **a** is calculated from the line equation **y= y0+ax.** Where y0= 1.018 and R= 0.995. Consequently, **a** value is 133.55.

Theerefore, **Kq**= a/t0 = **6.26x10^9**.

Apparatus for flow photocatalysis

In order to achieve a more scalable process, a continuous flow microreactor was assembled. The flow system consisted of a syringe pump connected to a coil reactor (1 mL) made of fluorinated ethylene propylene (FEP) capillary tubing (1/16" OD; 0.80 mm ID), wrapped around an alluminium paper covered Pyrex beaker (70 mm diameter).

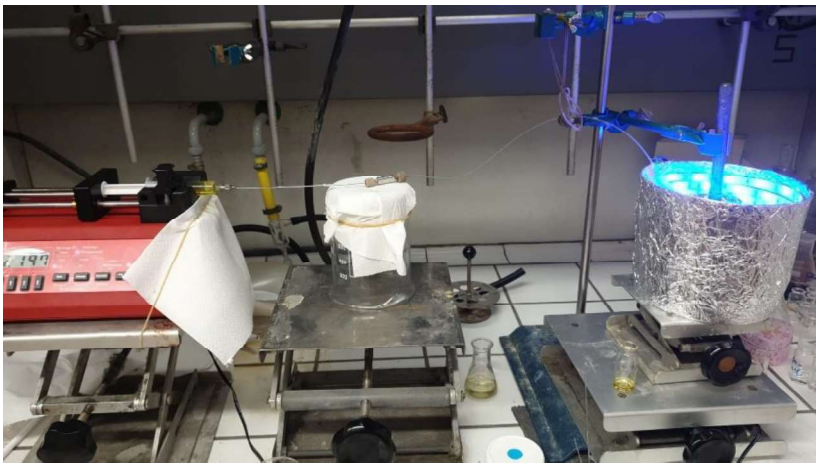

The coiled reactor (1 mL total volume) was located in the center of a handmade photoreactor. The reaction mixture has been degassed through pump-freeze-thaw cycles and then aspirated with the plastic syringe. Subsequently it has been pumped in the FEP photoreactor through a syringe pump. The reliability of the manufactured apparatus has been proved by repeating several times each catalytic test.

Bibliography

1 D. W. C. MacMillan, *Nature*, 2008, **455**, 304–308.

2 F. Gomollón-Bel, *Chem. Int.*, 2020, **42**, 3–9.

3 G. Lelais and D. W. C. Macmillan, *New Front. Asymmetric Catal.*, 2006, 313–358.

4 T. Fulgheri, F. Della Penna, A. Baschieri and A. Carlone, *Curr. Opin. Green Sustain. Chem.*, 2020, **25**, 100387.

5 M. Lombardo, A. Quintavalla, M. Chiarucci and C. Trombini, *Synlett*, 2010, 1746–1765.

6 M. Lombardo and C. Trombini, *ChemCatChem*, 2010, **2**, 135–145.

7 A. Puglisi, M. Benaglia, R. Porta and F. Coccia, *Curr. Organocatalysis*, 2015, **2**, 79–101.

8 H. Pracejus, *Justus Liebigs Ann. Chem.*, 1960, **634**, 9–22.

9 Z. G. Hajos and D. R. Parrish, *J. Org. Chem.*, 1974, **39**, 1615–1621.

10 E. J. Corey and M. J. Grogan, *Org. Lett.*, 1999, **1**, 157–160.

11 M. S. Sigman and E. N. Jacobsen, *J. Am. Chem. Soc.*, 1998, **120**, 4901–4902.

12 B. List, R. A. Lerner and C. F. Barbas, *J. Am. Chem. Soc.*, 2000, **122**, 2395–2396.

13 K. A. Ahrendt, C. J. Borths and D. W. C. MacMillan, *J. Am. Chem. Soc.*, 2000, **122**, 4243–4244.

14 P. I. Dalko and L. Moisan, *Angew. Chem. Int. Ed.*, 2004, **43**, 5138–5175.

15 P. Melchiorre, M. Marigo, A. Carlone and G. Bartoli, *Angew. Chem. Int. Ed.*, 2008, **47**, 6138–6171.

16 M. J. Gaunt, C. C. C. Johansson, A. McNally and N. T. Vo, *Drug Discov. Today*, 2007, **12**, 8–27.

17 Y. Hayashi, H. Gotoh, T. Hayashi and M. Shoji, *Angew. Chem. Int. Ed.*, 2005, **44**, 4212–4215.

18 S. Brandau, A. Landa, J. Franzén, M. Marigo and K. A. Jørgensen, *Angew. Chem. Int. Ed.*, 2006, **45**, 4305–4309.

19 S. Mukherjee, J. W. Yang, S. Hoffmann and B. List, *Chem. Rev.*, 2007, **107**, 5471–5569.

20 J. Franzén, M. Marigo, D. Fielenbach, T. C. Wabnitz, A. Kjærsgaard and K. A. Jørgensen, *J. Am. Chem. Soc.*, 2005, **127**, 18296–18304.

21 A. Erkkilä, I. Majander and P. M. Pihko, *Chem. Rev.*, 2007, **107**, 5416–5470.

22 T. Tebeka and A. Abera, *Int. Res. J. Sci. Technol.*, 2019, **1**, 6–12.

23 D. Myers, *Surfactant Sci. Technol.*, 2020, 1–16.

24 K. Kacprzak and J. Gawroński, *Synthesis (Stuttg).*, , DOI:10.1055/s-2001-14560.

25 L. Bernardi, M. Fochi, R. Carbone, A. Martinelli, M. E. Fox, C. J. Cobley, B. Kandagatla, S. Oruganti, V. H. Dahanukar and A. Carlone, *Chem. Eur. J.*, 2015, **21**, 19208–19222.

26 T. Ooi, M. Kameda and K. Maruoka, *J. Am. Chem. Soc.*, 1999, **121**, 6519–6520.

27 J. Tan and N. Yasuda, *Org. Process Res. Dev.*, 2015, **19**, 1731–1746.

28 A. G. Doyle and E. N. Jacobsen, *Chem. Rev.*, 2007, **107**, 5713–5743.

29 A. G. Wenzel and E. N. Jacobsen, *J. Am. Chem. Soc.*, 2002, **124**, 12964–12965.

30 J. P. Malerich, K. Hagihara and V. H. Rawal, *J. Am. Chem. Soc.*, 2008, **130**, 14416–14417.

31 V. H. Rawal, A. N. Thadani, A. K. Unni and Y. Huang, *Nature*, 2003, **424**, 146.

32 S. Cha, B. Marekha, M. Wagner and J. Hunger, *Chem. Eur. J.*, 2019, **25**, 9984–9990.

33 S. J. Connon, *Angew. Chem. Int. Ed.*, 2006, **45**, 3909–3912.

34 J.-B. H. Teresa D. Beeson, Anthony Mastracchio and G. A. Kate Ashton, 1, 2 David W. C. MacMillan, Borges, *Science*, 2007, **316**, 582–585.

35 D. A. Nicewicz and D. W. C. MacMillan, *Science*, 2008, **322**, 77–80.

36 H. Kim and D. W. C. MacMillan, *J. Am. Chem. Soc.*, 2008, **130**, 398–399.

37 H. Y. Jang, J. B. Hong and D. W. C. MacMillan, *J. Am. Chem. Soc.*, 2007, **129**, 7004–7005.

38 V. Balzani, G. Bergamini and P. Ceroni, *Angew. Chem. Int. Ed.*, 2015, **54**, 11320–11337.

39 B. König, *Chemical photocatalysis*, 2013.

40 J. G. Hernández and E. Juaristi, *Chem. Commun.*, 2012, **48**, 5396–5409.

41 M. Gruttadauria, F. Giacalone and R. Noto, *Chem. Soc. Rev.*, 2008, **37**, 1666–1688.

42 E. Alza, X. C. Cambeiro, C. Jimenez and M. A. Pericàs, *Org. Lett.*, 2007, **9**, 3717–3720.

43 I. Atodiresei, C. Vila and M. Rueping, *ACS Catal.*, 2015, **5**, 1972–1985.

44 E. Alza, S. Sayalero, P. Kasaplar, D. Almaşi and M. A. Pericàs, *Chem. Eur. J.*, 2011, **17**, 11585–11595.

45 C. Rosso, M. G. Emma, A. Martinelli, M. Lombardo, A. Quintavalla, C. Trombini, Z. Syrgiannis and M. Prato, *Adv. Synth. Catal.*, 2019, **361**, 2936–2944.

46 T. Kano, H. Mii and K. Maruoka, *J. Am. Chem. Soc.*, 2009, **131**, 3450–3451.

47 M. Shimogaki, H. Maruyama, S. Tsuji, C. Homma, T. Kano and K. Maruoka, *J. Org. Chem.*, 2017, **82**, 12928–12932.

48 H. A. Beejapur, V. Campisciano, F. Giacalone and M. Gruttadauria, *Adv. Synth. Catal.*, 2015, **357**, 51–58.

49 J. M. Andrés, M. González, A. Maestro, D. Naharro and R. Pedrosa, *European J. Org. Chem.*, 2017, **2017**, 2683–2691.

50 D. D. Chronopoulos, M. Tsakos, N. Karousis, C. G. Kokotos and N. Tagmatarchis, *Mater. Lett.*, 2014, **137**, 343–346.

51 X. Duan, H. Sun and S. Wang, *Acc. Chem. Res.*, 2018, **51**, 678–687.

52 D. S. Su, G. Wen, S. Wu, F. Peng and R. Schlögl, *Angew. Chem. Int. Ed.*, 2017, **56**, 936–964.

53 S. Navalon, A. Dhakshinamoorthy, M. Alvaro and H. Garcia, *Chem. Rev.*, 2014, **114**, 6179–6212.

54 T. Kano, F. Shirozu and K. Maruoka, *Org. Lett.*, 2014, **16**, 1530–1532.

55 M. G. Emma, A. Tamburrini, A. Martinelli, M. Lombardo, A. Quintavalla and C. Trombini, *Catalysts*, 2020, **10**, 1–22.

56 C. Capello, U. Fischer and K. Hungerbühler, *Green Chem.*, 2007, **9**, 927–93.

57 N. Kaur and D. Kishore, *Synth. Commun.*, 2014, **44**, 1375–1413.

58 D. E. Ward and V. Jheengut, *Tetrahedron Lett.*, 2004, **45**, 8347–8350.

59 Y. S. Wu, Y. Chen, D. S. Deng and J. Cai, *Synlett*, 2005, 1627–1629.

60 Y. Zhou and Z. Shan, *J. Org. Chem.*, 2006, **71**, 9510–9512.

61 Y. Zhou and Z. Shan, *Tetrahedron Asymmetry*, 2006, **17**, 1671–1677.

62 Ö. Reis, S. Eymur, B. Reis and A. S. Demir, *Chem. Commun.*, 2009, 1088–1090.

63 N. Ei-Hamdouni, X. Companyó, R. Rios and A. Moyano, *Chem. Eur. J.*, 2010, **16**, 1142–1148.

64 A. S. Demir and S. Basceken, *Tetrahedron Asymmetry*, 2013, **24**, 515–525.

65 M. Lombardo, M. Chiarucci, A. Quintavalla and C. Trombini, *Adv. Synth. Catal.*, 2009, **351**, 2801–2806.

66 D. E. Siyutkin, A. S. Kucherenko and S. G. Zlotin, *Tetrahedron*, 2010, **66**, 513–518.

67 S. K. Ghosh, K. Dhungana, A. D. Headley and B. Ni, *Org. Biomol. Chem.*, 2012, **10**, 8322–8325.

68 E. Montroni, M. Lombardo, A. Quintavalla, C. Trombini, M. Gruttadauria and F. Giacalone, *ChemCatChem*, 2012, **4**, 1000–1006.

69 A. M. P. Salvo, F. Giacalone, R. Noto and M. Gruttadauria, *Chempluschem*, 2014, **79**, 857–862.

70 M. Lombardo, S. Easwar, F. Pasi and C. Trombinia, *Adv. Synth. Catal.*, 2009, **351**,

276–282.

71 N. Bernhard and S. Wolfgang, *Angew. Chemie Int. Ed. English*, 1978, **17**, 522–524.

72 I. Fleischer and A. Pfaltz, *Chem. Eur. J.*, 2010, **16**, 95–99.

73 O. V. Maltsev, A. S. Kucherenko and S. G. Zlotin, *European J. Org. Chem.*, 2009, 5134–5137.

74 M. M. S. Chauhan and S. Singh, *J. Mol. Catal. A Chem.*, 2015, **398**, 184–189.

75 A. Ma, S. Zhu and D. Ma, *Tetrahedron Lett.*, 2008, **49**, 3075–3077.

76 Y. Suzuki, *Mini. Rev. Org. Chem.*, 2017, **15**, 236–245.

77 R. S. Tukhvatshin, A. S. Kucherenko, Y. V. Nelyubina and S. G. Zlotin, *ACS Catal.*, 2017, **7**, 2981–2989.

78 K. S. Feu, A. M. Deobald, S. Narayanaperumal, A. G. Corrêa and M. Weber Paixão, *European J. Org. Chem.*, 2013, 5917–5922.

79 H. Sato, F. Nagashima and T. Oriyama, *Chem. Lett.*, 2010, **39**, 379–381.

80 S. Zhu, S. Yu and D. Ma, *Angew. Chem. Int. Ed.*, 2008, **47**, 545–548.

81 H. Erdmann, F. An, P. Mayer, A. R. Ofial, S. Lakhdar and H. Mayr, *J. Am. Chem. Soc.*, 2014, **136**, 14263–14269.

82 F. An, B. Maji, E. Min, A. R. Ofial and H. Mayr, *J. Am. Chem. Soc.*, 2020, **142**, 1526–1547.

83 G. E. M. Crisenza and P. Melchiorre, *Nat. Commun.*, 2020, **11**, 8–11.

84 L. Buzzetti, G. E. M. Crisenza and P. Melchiorre, *Angew. Chem. Int. Ed.*, 2019, **58**, 3730–3747.

85 M. A. Ischay, M. E. Anzovino, J. Du and T. P. Yoon, *J. Am. Chem. Soc.*, 2008, **130**, 12886–12887.

86 M. H. Shaw, J. Twilton and D. W. C. MacMillan, *J. Org. Chem.*, 2016, **81**, 6898–6926.

87 R. C. McAtee, E. J. McClain and C. R. J. Stephenson, *Trends Chem.*, 2019, **1**, 111–125.

88 R. Brimioulle, D. Lenhart, M. M. Maturi and T. Bach, *Angew. Chem. Int. Ed.*, 2015, **54**, 3872–3890.

89 D. A. N. U. T. A. Frackowiak, *J. Photochem. Photobiol.*, 1988, **2**, 399–401.

90 F. Strieth-Kalthoff, M. J. James, M. Teders, L. Pitzer and F. Glorius, *Chem. Soc. Rev.*, 2018, **47**, 7190–7202.

91 P. N. Off, V. Relaxation, I. Conversion, I. Crossing, T. Scale and O. Links, 2011, 1–7.

92 Jones Garth A. and Bradshaw David S., *Front. Phys.*, 2019, **7**, 1–19.

93 D. L. Dexter, *J. Chem. Phys.*, 1953, **21**, 836–850.

94 R. E. Transfer, *Princ. Fluoresc. Spectrosc.*, 2006, 331–351.

95 L. Capaldo and D. Ravelli, *European J. Org. Chem.*, 2017, **2017**, 2056–2071.

96 S. Protti, M. Fagnoni and D. Ravelli, *ChemCatChem*, 2015, **7**, 1516–1523.

97 D. M. Arias-Rotondo and J. K. McCusker, *Chem. Soc. Rev.*, 2016, **45**, 5803–5820.

98 C. K. Prier, D. A. Rankic, D. W. C. MacMillan, Chem. Rev., 2013, **113**, 5322-5363

99 J. W. Tucker and C. R. J. Stephenson, *J. Org. Chem.*, 2012, **77**, 1617–1622.

100 A. B. Tamayo, B. D. Alleyne, P. I. Djurovich, S. Lamansky, I. Tsyba, N. N. Ho, R. Bau and M. E. Thompson, *J. Am. Chem. Soc.*, 2003, **125**, 7377–7387.

101 M. S. Lowry, J. I. Goldsmith, J. D. Slinker, R. Rohl, R. A. Pascal, G. G. Malliaras and S. Bernhard, *Chem. Mater.*, 2005, **17**, 5712–5719.

102 K. R. Campos, P. J. Coleman, J. C. Alvarez, S. D. Dreher, R. M. Garbaccio, N. K. Terrett, R. D. Tillyer, M. D. Truppo and E. R. Parmee, *Science*, **363**, 244-252

103 M. Di Filippo, C. Bracken and M. Baumann, *Molecules*, **25**, 356-369

104 M. B. Plutschack, B. Pieber, K. Gilmore and P. H. Seeberger, *Chem. Rev.*, 2017, **117**, 11796–11893.

105 Y. Su, N. J. W. Straathof, V. Hessel and T. Noël, *Chem. Eur. J.*, 2014, **20**, 10562–10589.

106 D. Cambié and T. Noël, *Top. Curr. Chem.*, 2018, **376**, 1–27.

107 J. W. Tucker, Y. Zhang, T. F. Jamison and C. R. J. Stephenson, *Angew. Chem. Int. Ed.*, 2012, **51**, 4144–4147.

108 C. R. J. Stephenson, T. P. Yoon and D. W. C. MacMillan, *Visible Light Photocatalysis in Organic Chemistry*, Wiley, 2018.

109 D. Dallinger and C. O. Kappe, *Curr. Opin. Green Sustain. Chem.*, 2017, **7**, 6–12.

110 A. Gualandi, F. Calogero, A. Martinelli, A. Quintavalla, M. Marchini, P. Ceroni, M. Lombardo and P. G. Cozzi, *Dalt. Trans.*, 2020, **49**, 14497–14505.

111 A. Gualandi, M. Marchini, L. Mengozzi, M. Natali, M. Lucarini, P. Ceroni and P. G. Cozzi, *ACS Catal.*, 2015, **5**, 5927–5931.

112 M. Cherevatskaya, M. Neumann, S. Füldner, C. Harlander, S. Kümmel, S. Dankesreiter, A. Pfitzner, K. Zeitler and B. König, *Angew. Chem. Int. Ed.*, 2012, **51**, 4062–4066.

113 P. Riente, A. Matas Adams, J. Albero, E. Palomares and M. A. Pericàs, *Angew. Chem. Int. Ed.*, 2014, **53**, 9613–9616.

114 M. Neumann, S. Füldner, B. König and K. Zeitler, *Angew. Chem. Int. Ed.*, 2011, **50**, 951–954.

115 A. Bahamonde and P. Melchiorre, *J. Am. Chem. Soc.*, 2016, **138**, 8019–8030.

116 H. Mayr, S. Lakhdar, B. Maji and A. R. Ofial, *Beilstein J. Org. Chem.*, 2012, **8**, 1458–1478.

117 S. Lakhdar, B. Maji and H. Mayr, *Angew. Chem. Int. Ed.*, 2012, **51**, 5739–5742.

118 T. Rigotti, A. Casado-Sánchez, S. Cabrera, R. Pérez-Ruiz, M. Liras, V. A. De La Peña O'Shea and J. Alemán, *ACS Catal.*, 2018, **8**, 5928–5940.

119 Z. Xun, T. Yu, Y. Zeng, J. Chen, X. Zhang, G. Yang and Y. Li, *J. Mater. Chem. A*, 2015, **3**, 12965–12971.

120 T. Mede, M. Jäger and U. S. Schubert, *Chem. Soc. Rev.*, 2018, **47**, 7577–7627.

121 S. Pagoti, D. Dutta and J. Dash, *Adv. Synth. Catal.*, 2013, **355**, 3532–3538.

122 K. Du, C. Lu, Z. Chen, J. Nie and G. Yang, *Catal. Letters*, 2016, **146**, 1107–1112.

123 I. P. Date, .

124 J. D. Slinker, A. A. Gorodetsky, M. S. Lowry, J. Wang, S. Parker, R. Rohl, S. Bernhard and G. G. Malliaras, *J. Am. Chem. Soc.*, 2004, **126**, 2763–2767.

125 M. Silvi, E. Arceo, I. D. Jurberg, C. Cassani and P. Melchiorre, *J. Am. Chem. Soc.*, 2015, **137**, 6120–6123.

126 T. Kano, H. Maruyama, C. Homma and K. Maruoka, *Chem. Commun.*, 2017, **54**, 176–179.

127 M. A. Cismesia and T. P. Yoon, *Chem. Sci.*, 2015, **6**, 5426–5434.

128 T. Schnitzer, J. S. Möhler and H. Wennemers, *Chem. Sci.*, 2020, **11**, 1943–1947.

129 A. Gualandi, M. Marchini, L. Mengozzi, H. T. Kidanu, A. Franc, P. Ceroni and P. G. Cozzi, *European J. Org. Chem.*, 2020, **2020**, 1486–1490.

130 D. A. Nagib, M. E. Scott and D. W. C. MacMillan, *J. Am. Chem. Soc.*, 2009, **131**, 10875–10877.

131 H. W. Shih, M. N. Vander Wal, R. L. Grange and D. W. C. MacMillan, *J. Am. Chem. Soc.*, 2010, **132**, 13600–13603.

132 G. Cecere, C. M. König, J. L. Alleva and D. W. C. MacMillan, *J. Am. Chem. Soc.*, 2013, **135**, 11521–11524.

133 Y. Li, D. Wang, L. Zhang and S. Luo, *J. Org. Chem.*, 2019, **84**, 12071–12090.

134 D. González-Muñoz, J. L. Nova-Fernández, A. Martinelli, G. Pascual-Coca, S. Cabrera and J. Alemán, *European J. Org. Chem.*, 2020, **37**, 5995-5999.

135 I. Muthukrishnan, V. Sridharan and J. C. Menéndez, *Chem. Rev.*, 2019, **119**, 5057–5191.

136 B. Nammalwar and R. A. Bunce, *Molecules*, 2014, **19**, 204–232.

137 S. G. Davies, A. M. Fletcher, P. M. Roberts and J. E. Thomson, *European J. Org. Chem.*, 2019, **2019**, 5093–5119.

138 J. S. Bello Forero, J. Jones Joel and F. M. da Silva, *ChemInform*, 2016, **47**, 157–175.

139 L. M. Bedoya, M. J. Abad, E. Calonge, L. A. Saavedra, M. Gutierrez C., V. V. Kouznetsov, J. Alcami and P. Bermejo, *Antiviral Res.*, 2010, **87**, 338–344.

140 S. Wu, C. Liu, G. Luo, Z. Jin, P. Zheng and Y. R. Chi, *Angew. Chem. Int. Ed.*, 2019, **58**, 18410–18413.

141 A. R. Romero Bohórquez, V. V. Kouznetsov and S. A. Zacchino, *Univ. Sci.*, 2015, **20**, 177–189.

142 X. F. Wang, S. B. Wang, E. Ohkoshi, L. T. Wang, E. Hamel, K. Qian, S. L. Morris-Natschke, K. H. Lee and L. Xie, *Eur. J. Med. Chem.*, 2013, **67**, 196–207.

143 M. Abdollahi and S. Mostafalou, *Encycl. Toxicol.*, 2014, **4**, 838.

144 L. E. Peisino and A. B. Pierini, *J. Org. Chem.*, 2013, **78**, 4719–4729.

145 D. B. Guthrie, S. J. Geib and D. P. Curran, *J. Am. Chem. Soc.*, 2009, **131**, 15492–15500.

146 H. Zhang, E. Ben Hay, S. J. Geib and D. P. Curran, *J. Am. Chem. Soc.*, 2013, **135**, 16610–16617.

147 T. P. Nicholls, G. E. Constable, J. C. Robertson, M. G. Gardiner and A. C. Bissember, *ACS Catal.*, 2016, **6**, 451–457.

148 X. L. Yang, J. D. Guo, T. Lei, B. Chen, C. H. Tung and L. Z. Wu, *Org. Lett.*, 2018, **20**, 2916–2920.

149 A. J. Clark, K. Jones, C. McCarthy and J. M. D. Storey, *Tetrahedron Lett.*, 1991, **32**, 2829–2832.

150 J. D. Nguyen, E. M. D'Amato, J. M. R. Narayanam and C. R. J. Stephenson, *Nat. Chem.*, 2012, **4**, 854–859.

151 H. Kim and C. Lee, *Angew. Chem. Int. Ed.*, 2012, **51**, 12303–12306.

152 J. D. Nguyen, E. M. D'Amato, J. M. R. Narayanam and C. R. J. Stephenson, *Nat. Chem.*, 2012, **4**, 854–859.

153 E. H. Discekici, N. J. Treat, S. O. Poelma, K. M. Mattson, Z. M. Hudson, Y. Luo, C. J. Hawker and J. R. De Alaniz, *Chem. Commun.*, 2015, **51**, 11705–11708.

154 A. J. Fry and R. L. Krieger, *J. Org. Chem.*, 1976, **41**, 54–57.

155 H. Kim and C. Lee, *Angew. Chemie*, 2012, **124**, 12469–12472.

156 R. Ciriminna, R. Delisi, Y. J. Xu and M. Pagliaro, *Org. Process Res. Dev.*, 2016, **20**, 403–408.

157 D. Rombach and H. A. Wagenknecht, *ChemCatChem*, 2018, **10**, 2955–2961.

158 U. Martínez-Estíbalez, O. García-Calvo, V. Ortiz-De-Elguea, N. Sotomayor and E. Lete, *European J. Org. Chem.*, 2013, 3013–3022.

159 B. Abarca, R. Adam and R. Ballesteros, *Org. Biomol. Chem.*, 2012, **10**, 1826–1833.

160 D. Wang, Z. Wang, Z. Liu, M. Huang, J. Hu and P. Yu, *Org. Lett.*, 2019, **21**, 4459–4463.

161 T. O. Vieira and H. Alper, *Chem. Commun.*, 2007, 2710–2711.

162 Y. Zhang, H. Zhong, T. Wang, D. Geng, M. Zhang and K. Li, *Eur. J. Med. Chem.*, 2012, **48**, 69–80.

163 W. B. Mors, M. C. do Nascimento, J. Parente, M. H. da Silva, P. A. Melo and G. Suarez-Kurtz, *Toxicon*, 1989, **27**, 1003–1009.

164 K. Sugimoto, K. Tamura, N. Ohta, C. Tohda, N. Toyooka, H. Nemoto and Y. Matsuya, *Bioorganic Med. Chem. Lett.*, 2012, **22**, 449–452.

165 M. J. Somerville, P. L. Katavic, L. K. Lambert, G. K. Pierens, J. T. Blanchfield, G. Cimino, E. Mollo, M. Gavagnin, M. G. Banwell and M. J. Garson, *J. Nat. Prod.*, 2012, **75**, 1618–1624.

166 B. H. Lipshutz, *Chem. Rev.*, 1986, **86**, 795–819.

167 M. Pohmakotr, A. Issaree, L. Sampaongoen, P. Tuchinda and V. Reutrakul, *Tetrahedron Lett.*, 2003, **44**, 7937–7940.

168 H. Tsuji and E. Nakamura, *Acc. Chem. Res.*, 2017, **50**, 396–406.

169 M. Xiong, X. Liang, X. Liang, Y. Pan and A. Lei, *ChemElectroChem*, 2019, **6**, 3383–3386.

170 E. I. Heiba and R. M. Dessau, *J. Org. Chem.*, 1974, **39**, 3456–3457.

171 H. Nishino, *Bull. Chem. Soc. Jpn.*, 1985, **58**, 1922–1927.

172 E. Biçer and M. Yilmaz, *Arkivoc*, 2013, 304–316.

173 M. Yilmaz, N. Uzunalioglu and A. T. Pekel, *Tetrahedron*, 2005, **61**, 8860–8867.

174 M. Yilmaz and A. Tarik Pekel, *Synth. Commun.*, 2001, **31**, 2189–2194.

175 R. Matsumoto and H. Nishino, *Synth. Commun.*, 2015, **45**, 1807–1816.

176 E. Baciocchi and R. Ruzziconi, *J. Org. Chem.*, 1991, **56**, 4772–4778.

177 M. Yilmaz, *Helv. Chim. Acta*, 2011, **94**, 1335–1342.

178 T. Naveen, R. Kancherla and D. Maiti, *Org. Lett.*, 2014, **16**, 5446–5449.

179 F. L. Zhu, Y. H. Wang, D. Y. Zhang, J. Xu and X. P. Hu, *Angew. Chem. Int. Ed.*, 2014, **53**, 10223–10227.

180 Y. F. Chen, H. F. Wang, Y. Wang, Y. C. Luo, H. L. Zhu and P. F. Xu, *Adv. Synth. Catal.*, 2010, **352**, 1163–1168.

181 H. Yi, Z. Liao, G. Zhang, G. Zhang, C. Fan, X. Zhang, E. E. Bunel, C. W. Pao, J. F. Lee and A. Lei, *Chem. Eur. J.*, 2015, **21**, 18925–18929.

182 T. Y. Ko and S. W. Youn, *Adv. Synth. Catal.*, 2016, **358**, 1934–1941.

183 H. Jiang, Y. Cheng, Y. Zhang and S. Yu, *Org. Lett.*, 2013, **15**, 4884–4887.

184 S. Wang, W. L. Jia, L. Wang, Q. Liu and L. Z. Wu, *Chem. Eur. J.*, 2016, **22**, 13794–13798.

185 J. Cheng, Y. Cheng, J. Xie and C. Zhu, *Org. Lett.*, 2017, **19**, 6452–6455.

186 X. J. Wei, D. T. Yang, L. Wang, T. Song, L. Z. Wu and Q. Liu, *Org. Lett.*, 2013, **15**, 6054–6057.

187 D. Prat, A. Wells, J. Hayler, H. Sneddon, C. R. McElroy, S. Abou-Shehada and P.

J. Dunn, *Green Chem.*, 2015, **18**, 288–296.

188 E. F. V. Scriven and R. Murugan, *Kirk-Othmer Encyclopedia of Chemical Technology*, 2005, **20**, 1-33.

189 E. Speckmeier, P. J. W. Fuchs and K. Zeitler, *Chem. Sci.*, 2018, **9**, 7096–7103.

190 N. De Kimpe, D. C. Wim and N. Schamp, *Synth. Commun.*

191 M. Altuna-Urquijo, A. Gehre, S. P. Stanforth and B. Tarbit, *Tetrahedron*, 2009, **65**, 975–984.

192 R. R. Fraser and F. Kong, *Synth. Commun.*, 1988, **18**, 1071–1077.

193 M. Tanaka, T. Shono and K. Shinra, *Bull. Chem. Soc. Jpn.*, 1969, **42**, 3190–3194.

194 A. G. Sams, G. K. Mikkelsen, M. Larsen, L. Torup, L. T. Brennum, T. J. Schrøder and B. Bang-Andersen, *Bioorganic Med. Chem. Lett.*, 2010, **20**, 5241–5244.

195 J. S. Grossert, S. Sotheeswaran, H. R. W. Dharmaratne and T. S. Cameron, *Can. J. Chem.*, 1988, **66**, 2870–2879.

196 A. Kamal, M. Balakrishna, V. L. Nayak, T. B. Shaik, S. Faazil and V. D. Nimbarte, *ChemMedChem*, 2014, **9**, 2766–2780.

197 I. Moreno, I. Tellitu, E. Domínguez and R. SanMartín, *European J. Org. Chem.*, 2002, 2126–2135.

198 Y. Mei, P. A. Bentley and J. Du, *Tetrahedron Lett.*, 2008, **49**, 3802–3804.

199 T. W. Liwosz and S. R. Chemler, *Chem. Eur. J.*, 2013, **19**, 12771–12777.

200 G. Zhang, R. Bai, C. Li, C. Feng and G. Lin, *Tetrahedron*, 2019, **75**, 1658–1662.

201 T. Vom Stein, M. Peréz, R. Dobrovetsky, D. Winkelhaus, C. B. Caputo and D. W. Stephan, *Angew. Chem. Int. Ed.*, 2015, **54**, 10178–10182.

202 S. Zhang, Z. Shen and H. Jian, *J. Org. Chem.*, 2020, **85**, 6143–6150.

203 K. Bert, T. Noël, W. Kimpe, J. L. Goeman and J. Van Der Eycken, *Org. Biomol. Chem.*, 2012, **10**, 8539–8550.

204 M. Y. Han, H. Pan, P. Li and L. Wang, *J. Org. Chem.*, 2020, **85**, 5825–5837.

205 C. R. Larsen and D. B. Grotjahn, *J. Am. Chem. Soc.*, 2012, **134**, 10357–10360.

206 V. C. Purohit, S. P. Allwein and R. P. Bakale, 2013, 6–9.

207 C. J. Thomson, Q. Zhang, N. Al-Maharik, M. Bühl, D. B. Cordes, A. M. Z. Slawin and D. O'Hagan, *Chem. Commun.*, 2018, **54**, 8415–8418.

208 F. L. Wu, B. P. Ross and R. P. McGeary, *European J. Org. Chem.*, 2010, 1989–1998.

209 J. Li, Q. Liu, H. Shen, R. Huang, X. Zhang, Y. Xiong and C. Chen, *RSC Adv.*, 2015, **5**, 85291–85295.

210 H. Nishino and K. Kurosawa, 1997, 81–86.

211 P. Müller, G. Bernardinelli, Y. F. Allenbach, M. Ferri and S. Grass, *Synlett*, 2005, 1397–1400.

212 D. Biplab, S. Sandip and T. S. Easwari, *Asian J. Res. Chem.*, 2015, **8**, 428–438.

213 Z. Batool, D. Xu, X. Zhang, X. Li, Y. Li, Z. Chen, B. Li and L. Li, *Crit. Rev. Food Sci. Nutr.*, 2020, **0**, 1–12.

214 J. M. Axten, J. R. Medina, Y. Feng, A. Shu, S. P. Romeril, S. W. Grant, W. H. H. Li, D. A. Heerding, E. Minthorn, T. Mencken, C. Atkins, Q. Liu, S. Rabindran, R. Kumar, X. Hong, A. Goetz, T. Stanley, J. D. Taylor, S. D. Sigethy, G. H. Tomberlin, A. M. Hassell, K. M. Kahler, L. M. Shewchuk and R. T. Gampe, *J. Med. Chem.*, 2012, **55**, 7193–7207.

215 H. Y. Shiao, M. S. Coumar, C. W. Chang, Y. Y. Ke, Y. H. Chi, C. Y. Chu, H. Y. Sun, C. H. Chen, W. H. Lin, K. S. Fung, P. C. Kuo, C. T. Huang, K. Y. Chang, C. T. Lu, J. T. A. Hsu, C. T. Chen, W. T. Jiaang, Y. S. Chao and H. P. Hsieh, *J. Med. Chem.*, 2013, **56**, 5247–5260.

216 W. A. M. Elgaher, M. Fruth, M. Groh, J. Haupenthal and R. W. Hartmann, *RSC Adv.*, 2014, **4**, 2177–2194.

217 H. Synthesis, *Molecules*, 2003, **8**, 793–865.

218 D. Somashekar, A. M. Reddy, J. S. Yadav and B. Sridhar, *Synthesis (Stuttg).*, 2010, 2069.

219 P. Liu, M. Lei, L. Ma and L. Hu, *Synlett*, 2011, 1133–1136.

220 D. A. Links, *Chem. commun.*, 2012, **48**, 7200–7202.

221 S. Wang, Z. Ni, X. Huang, J. Wang and Y. Pan, *Org. Lett.*, 2014, **16**, 5648–5651.

222 A. Kondoh, S. Ishikawa, T. Aoki and M. Terada, *Chem. Commun.*, 2016, **52**, 12513–12516.

223 A. W. Sromek, M. Rubina and V. Gevorgyan, *J. Am. Chem. Soc.*, 2005, **127**, 10500–10501.

224 A. S. Dudnik and V. Gevorgyan, *Angew. Chem. Int. Ed.*, 2007, **46**, 5195–5197.

225 J. Zhang, M. Wu, W. Lu, S. Wang, Y. Zhang, C. Cheng and G. Zhu, *J. Org. Chem.*, 2017, **82**, 11134–11140.

226 C. Cheng, S. Liu and G. Zhu, *J. Org. Chem.*, 2015, **80**, 7604–7612.

227 A. S. Dudnik and V. Gevorgyan, *Angew. Chemie*, 2007, **119**, 5287–5289.

228 C. Cheng, S. Liu and G. Zhu, *Org. Lett.*, 2015, **17**, 1581–1584.

229 L. L. Wei, H. Xiong and R. P. Hsung, *Acc. Chem. Res.*, 2003, **36**, 773–782.

230 L. Wei, H. U. I. Xiong and R. P. Hsung, *Acc. Chem. Res*, 2003, **36**, 773–782.

231 T. Lu, Z. Lu, Z. Ma, Y. Zhang and R. P. Hsung, *Chem. Rev.*, 2013, **113**, 4862–4904.

232 R. Tomita, T. Koike and M. Akita, *Chem. Commun.*, 2017, **53**, 4681–4684.

233 O. K. Koleoso, M. Turner, F. Plasser and M. C. Kimber, *Beilstein J. Org. Chem.*, 2020, **16**, 1983–1990.

234 Y. Cai, W. Zhao, S. Wang, Y. Liang and Z. J. Yao, *Org. Lett.*, 2019, **21**, 9836–9840.

235 O. A. Storozhenko, A. A. Festa, G. I. Detistova, V. B. Rybakov, A. V. Varlamov, E. V. Van Der Eycken and L. G. Voskressensky, *J. Org. Chem.*, 2020, **85**, 2250–2259.

236 O. K. Koleoso, M. Turner, F. Plasser and M. C. Kimber, *Beilstein J. Org. Chem.*, 2020, **16**, 1983–1990.

237 O. K. Koleoso, M. Turner, F. Plasser and M. C. Kimber, *Beilstein J. Org. Chem.*, 2020, **16**, 1983–1990.

238 T. W. Bousfield and M. C. Kimber, *Tetrahedron Lett.*, 2015, **56**, 350–352.

239 C. J. Wallentin, J. D. Nguyen, P. Finkbeiner and C. R. J. Stephenson, *J. Am. Chem. Soc.*, 2012, **134**, 8875–8884.

240 M. Weitman, K. Lerman, A. Nudelman, D. T. Major, A. Hizi and A. Herschhorn, *Eur. J. Med. Chem.*, 2011, **46**, 447–467.

241 L. Shen and R. P. Hsung, *Org. Lett.*, 2005, **7**, 775–778.

242 Y. Liu, A. Cerveri, A. De Nisi, M. Monari, O. Nieto Faza, C. S. Lopez and M. Bandini, *Org. Chem. Front.*, 2018, **5**, 3231–3239.

243 O. K. Koleoso, M. Turner, F. Plasser and M. C. Kimber, *Beilstein J. Org. Chem.*, 2020, **16**, 1983–1990.

244 L. L. Wei, J. A. Mulder, H. Xiong, C. A. Zificsak, C. J. Douglas and R. P. Hsung, *Tetrahedron*, 2001, **57**, 459–466.

245 K. Spielmann, M. Xiang, L. A. Schwartz and M. J. Krische, *J. Am. Chem. Soc.*, 2019, **141**, 14136–14141.